THE UNIVERSITY
of EDINBURGH

Reductive metalation of the uranyl oxo-groups with main Group-, d- and f-block metals

Markus Zegke

The University of Edinburgh

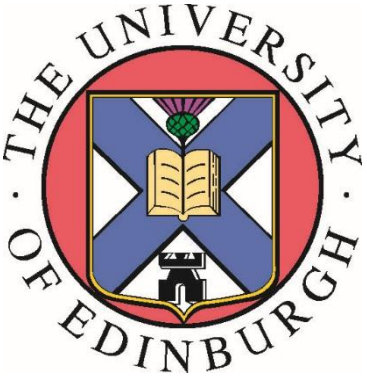

Submitted for the degree of

Doctor of Philosophy

Edinburgh

2015

Declaration

The work described in this thesis is entirely my own, except where named reference is given. I confirm that appropriate credit has been given where reference has been made to the work of others. This work has not been submitted for any other degree.

Signature: Date:

Markus Zegke

Acknowledgments

First of all I would like to thank my supervisor Prof. Dr. Polly L. Arnold for giving me the opportunity and the privilege to pursue the chemistry of my "favourite" element. Thank you for having confidence in me, and thank you for letting me go to such exceptional places like the Institute for Transuranium Elements (ITU) (twice!), and handle the "hot stuff". The transuranics were definitely a challenging, "exotic" and – at least within this thesis – one of the most exciting experiences a chemist can come across.

I also gratefully acknowledge the help and guidance of Dr. Jason B. Love who very often pointed me in the right direction when my own view was blurred.

A big big thank you goes out to the good spirit of the crystals, Dr. Gary S. Nichol, whose help was tremendous. You have kind of become my personal hero by picking up the tiniest and most sensitive crystals, and by letting me constantly pester you with my crystallographic problems and questions. This thesis would be only half as thick without your help!

I would like to express my thanks to Lucy N. Platts and James R. Pankhurst. We had a great little project together and I really enjoyed working with you both.

My thank goes out to Michał Dutkiewicz at the ITU, Karlsruhe, Germany, for producing a lot of nuclear waste (sonicator in neptunium box), for disposing of 50 mSv of plutonium, for exceptional chemistry and for taking me inside the "matrix".

Thank you to the co-workers around the world: Xiaobin Zhang and Prof. Dr. Georg Schreckenbach at the University of Manitoba, Canada, for their calculations and explanations, Dr. Alessandro Prescimone (now University of Basel, Switzerland) and Dr. Nicola Magnani (ITU) for collecting, analysing and interpreting SQUID data. The help of Dr. Christos Apostolidis and Dr. Olaf Walter at the ITU with additional data collection (NIR, XRD) on the highly radioactive transuranium materials is greatly acknowledged.

Thank you to Dr. Joy H. Farnaby for the walks and the talks, the hugs and the philosophy.

Thank you to Jamie McKinven for the laughs, the fun and the postcards, Max McMullon for using his broken phone to take pictures of my samples, Dr. Johann A. Hlina for climbing and titanium chemistry. For help with syntheses, analyses, crystallography and proof-reading thank you to Dr. Daniel Betz, Dr. Thomas Cadenbach, Dr. Stephen M. Mansell, Dr. Guy M. Jones and Dr. Charlotte J. Stevens.

One person who deserves my special thanks is Dr. Rianne M. Lord. You have not only inspired me, you also brought back motivation to me, resulting in beautiful crystals, nice structures and great excitement. You have made the last months of my stay very enjoyable, and I am very happy about how things have developed. And I hope it will continue :)

Finally: My ladies, mum and sis. I dedicate this to you:

Big love and wOrm hugs!

This thesis was funded by the Engineering and Physical Sciences Research Council (EPSRC) which is gratefully acknowledged. The stays at the ITU were granted by the EU Actinet-I3-AC3-JRP-02 and Talisman-JRPL-C02-07 programs which the author is most thankful to.

“If I have seen further, it is by standing on the shoulders of giants”

Sir Isaac Newton, in a letter to Robert Hooke (1676)[1]

Lay summary

The present document describes the chemistry of novel uranium compounds, with a primary focus on the reactivity and modification of the usually unreactive uranyl dication. These experiments target the synthesis of model systems for nuclear waste characterisation. Given their comparatively low radioactivity, the synthesised compounds can be used to predict the properties of highly radioactive irradiated nuclear fuel. Furthermore, these complexes are being used to study fundamental electronic and magnetic properties of the elements of the actinide series. These experiments address the current interest in the development of molecular magnets and also focus on the facile chemical modification of uranyl containing systems. The described new compounds consist of a variety of different metals from across the periodic table, allowing for a systematic and comparative description of these new materials.

Abstract

This thesis describes the reductive functionalisation of the uranyl(VI) dication by metalation of the uranyl oxo-groups ($O=U^{VI}=O$), using reductants from Group I, Group II, Group IV, Group XII and Group XIII as well as from the lanthanide and actinide series of the periodic table.

Chapter 1 introduces uranium and nuclear waste, and gives an introduction into uranium(V) chemistry. It further compares the chemistry of uranyl(V) to neptunyl(V), with a specific focus on solid state interactions. The chemistry of the Pacman calixpyrroles is briefly introduced. These macrocyclic ligands form the basis for the synthesis of uranyl Pacman, which represents the major uranyl complex investigated in this thesis.

Chapter 2 describes the reductive and catalytic uranyl oxo-group metalation using Group XIII and Group I reagents. It presents the reductive uranyl alumination using di-(*iso*-butyl)-aluminium hydride and Tebbe's reagent to form the first Al(III)-uranyl(V) oxo complexes (Al^{III}-O-U^{V}=O). The chapter shows how the transmetalation of these aluminated uranyl(V) complexes with alkali metal hydrides and alkyls leads to the formation of mono-metalated alkali metal uranyl(V) complexes (M^{I}-O-U^{V}=O). The combination of these two reactions is developed into a catalytic synthesis of the latter. The use of elemental alkali metals is described as another pathway of accessing alkali metal uranyl(V) complexes, carried out in collaboration with Dr. Rianne M. Lord.

Chapter 3 describes the synthesis of the first Group IV uranyl(V) complexes, using low-valent titanium and zirconium starting materials. The chapter includes magnetic measurements on the first Ti(III)-uranyl(V) complex and a comparison of computational results regarding a selection of uranyl(V) complexes from this thesis. The magnetic measurements were carried out by Dr. Alessandro Prescimone, University of Edinburgh, and analysed by Dr. Nicola Magnani, Institute for Transuranium Elements, Karlsruhe, Germany. Theoretical calculations were carried out by Xiaobin Zhang and Prof. Dr. Georg Schreckenbach, University of Manitoba,

Canada. The chapter further describes the reductive metalation of uranyl using elemental Mg, Ca and Zn and their respective metal halides.

Chapter 4 describes the uranyl functionalisation using f-elements and their complexes. It describes the attempted mono-metalation using lanthanides and the formation of a Sm(III)-bis(uranyl(V)) complex. It further describes the uranyl reduction using actinides and the synthesis of the first U(IV)-uranyl(V) complex. The chapter further describes the first Np(IV)-uranyl(V) complex and the attempted synthesis of a Pu(IV)-uranyl(V) complex. These syntheses were performed in collaboration with Michał S. Dutkiewicz at the Institute for Transuranium Elements (ITU) in Karlsruhe, Germany. This work was carried out with the help of Dr. Christos Apostolidis and Dr. Olaf Walter and supervised by Prof. Dr Roberto Caciuffo.

Chapter 5 describes the reductive uranyl functionalisation in a redox-active dipyrromethene ligand, collaboratively carried out with James R. Pankhurst and Lucy N. Platts. The synthetic work and analyses were performed jointly with Lucy N. Platts (master student under the supervision of the author); UV-vis spectra and cyclic voltammograms were recorded by James R. Pankhurst and Lucy N. Platts. The chapter presents the synthesis of a new uranyl(VI) complex and its two-electron reduction to uranium(IV) using a titanium(III) reductant. Additionally the chapter describes the reductive uranyl silylation in a dipyrromethane complex of which the ligand was designed by Dr. Daniel Betz.

Section 6 describes the synthetic procedures.

Section 7 gives references to the work of others.

Section 8 shows the publication related to this thesis.

Section 9 is a table of the complexes described in this thesis.

Abbreviations

18C6	–	18-Crown-6
AIM	–	Atoms-in-Molecules
An	–	element(s) of the actinide series
a.u.	–	atomic units
BCP	–	bond critical point
COSY	–	correlation (nuclear magnetic resonance) spectroscopy
Cp	–	cyclopentadienyl
Cp’	–	methyl cyclopentadienyl
Cp*	–	pentamethyl cyclopentadienyl
CV	–	cyclic voltammetry
Dbm	–	dibenzoyl methanate
DIBAL	–	di(*iso*-butyl)aluminium hydride
dme	–	dimethoxyethane
DMSO	–	dimethyl sulfoxide
DOSY	–	diffusion ordered (nuclear magnetic resonance) spectroscopy
Fc/Fc^{+}	–	ferrocene/ferrocenium
H	–	total electronic energy density
^{i}Bu	–	*iso*-butyl
Ln	–	element(s) of the lanthanides series
$\nabla^2\rho$	–	Laplacian of electron density
N''	–	hexamethyldisilylamide
NMR	–	nuclear magnetic resonance
ODtbp	–	2,6-di-*tert*-butyl phenolate
OTf	–	triflate

Ph	–	phenyl
py	–	pyridine
QTAIM	–	Quantum Theory of Atoms in Molecules
ρ	–	electron density
solv	–	solvent
TEMPO	–	2,2,6,6-tetramethylpiperidine-*N*-oxyl
^{t}Bu	–	*tert*-butyl
THF	–	tetrahydrofuran
TMS	–	trimethylsilyl
Ur	–	uranyl group
XRD	–	X-ray diffraction

Table of Contents

1 Introduction

1.1 Uranium and nuclear waste

As the major component of the nuclear fuel cycle uranium has become the most important member of the actinide series, but in addition to that it is also a very widespread naturally occurring element. The amount of uranium in the earth's crust sums up to about 3 mg/kg, forming more than 160 mineral species which account for 5% of all known minerals.[2] Despite its usage as a nuclear material depleted uranium is still used for civilian applications, such as for counterweights in aeroplane wings or due to its density as a radiation shield both in medical equipment as well as for the transport of high level radioactive material.[3] Moreover, in the 21st century uranium chemistry has seen rapid growth, resulting in diverse research activities concerning uranium magnetism studies,[4] uranium bearing hybrid materials such as uranium metal organic frameworks (U-MOFs) and coordination polymers (CPs),[5] uranium nanotubes,[6][7] uranyl hydroxide nanowires,[8] C-H bond activation[9] and catalytic applications such as Michael reactions and ring opening polymerisations.[10]

However, since the advent of nuclear energy production scientists are concerned with the problems of nuclear waste disposal and the reprocessing of nuclear fuel.[11] Spent nuclear fuel is a highly complex mixture consisting of 96 % uranium dioxide, 3 % fission products and 1 % transuranium elements, of which the latter two create the majority of the radioactivity and decay heat.[12] The long-term storage of high-level radioactive waste has long been an issue, and research is being carried out regarding partitioning and transmutation strategies.[13] It includes the chemical separation of irradiated spent nuclear fuel (partitioning) and the subsequent physical conversion of highly radioactive isotopes such as plutonium to low-level fission products (transmutation). This can help to physically decrease the amount of high level nuclear waste.[14] However, relatively little is known about the actual behaviour of uranium and the transuranium elements in nuclear waste, leading to concerns about the inherent safety of long-term geologic disposal sites.[15,16] In order to ensure the efficiency of nuclear waste disposal it is crucial to determine all relevant chemical aspects which are necessary to employ a proper treatment of these hazardous materials.

While uranium itself shows a comparatively low radioactivity of 12.44 kBq/g (based on ^{238}U), the transuranium elements which are formed as side products due to neutron capture and β-decay reactions make up most of the radioactivity of nuclear waste. These elements possess isotopes which are several million times more radioactive than uranium and can reach levels of up to 2.99 TBq/g for specific nuclides such as ^{244}Cm. This makes nuclear fuel reprocessing techniques a demanding task that requires an in-depth understanding of actinide interactions in nuclear waste.[17]

The following graph (Figure 1) demonstrates the radiotoxicity of nuclear waste:[18]

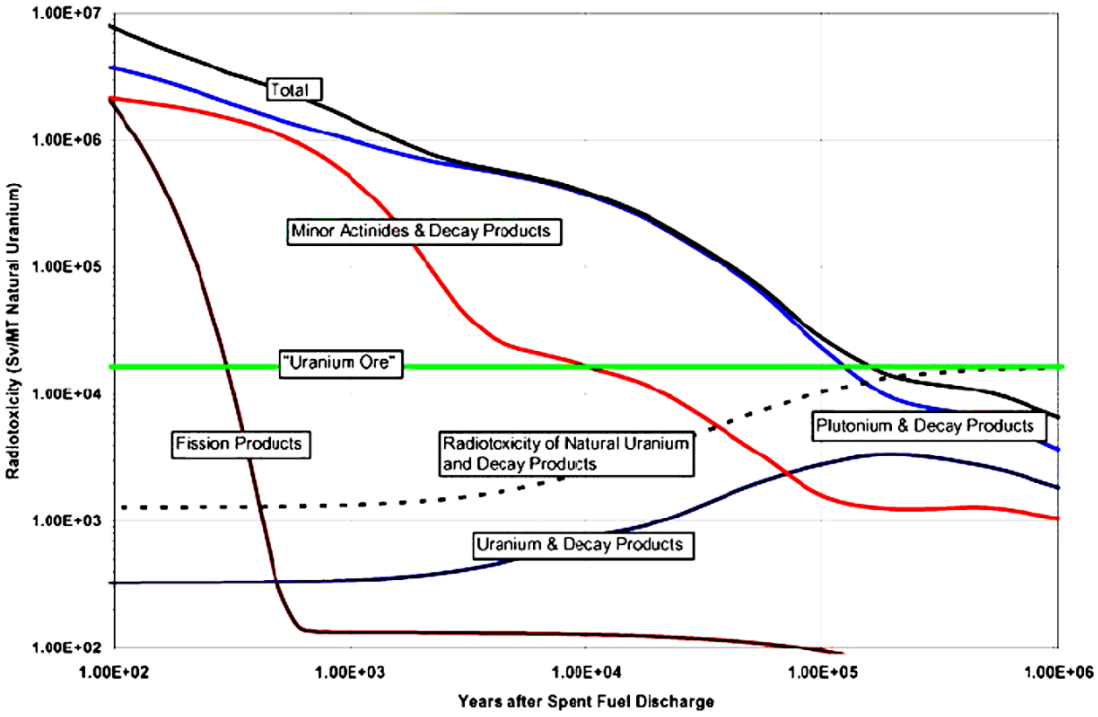

Figure 1 Dependency of the radiotoxicity of nuclear waste on time.[18]

The graph shows that any produced fission products occurring in nuclear waste (**dark red**) have already decayed after 500 years to reach a level of radioactivity similar to naturally occurring uranium ore (**green**). In geological terms this time is relatively short, compared to the behaviour of the minor actinides and their decay products (**red**) and in particular plutonium and its decay products (**blue**). These strong alpha emitting transuranic elements pose a threat to mankind for 10 000 to 100 000 years before reaching the level of natural uranium ore. It is therefore essential to

understand their chemical behaviour in order to provide secure long term storage as well as to handle them efficiently.

In addition to nuclear waste disposal it is still necessary to investigate the behaviour of nuclear material in different chemical and biological environments[19][20] and under reducing and/or oxidising conditions to accurately determine in which ways they affect ecological systems.[21] The impact of nuclear accidents[22] such as reactor core meltdowns as seen in Fukushima-Daiichi in Japan in 2011 or at Chernobyl Nuclear Power Plant in Ukraine in 1986[23] are severe and leave affected areas heavily contaminated for years (Figure 2).

Figure 2 The sarcophagus covering the destroyed reactor block IV of the Chernobyl Nuclear Power Plant in 2013 providing provisional protection from the highly radioactive material inside.

Also non-nuclear accidents which released highly radioactive material to the environment as happened in Mayak ("*Kyschtym disaster"*) in Russia in 1957[24] pose a wide range of threats to the environment and people[25][26] and generate inherently complex systems which are difficult to model and cause demanding scientific investigations.[27]

1.2 Uranyl(V) chemistry

1.2.1 Uranyl(VI) reduction and functionalisation

Uranium, the last naturally occurring element of the periodic system, possesses a wide range of different chemical oxidation states and complex reactivity behaviour both in aqueous and non-aqueous media, as well as in oxidising and non-oxidising environments. These oxidation states range from the recently discovered +II oxidation state (f^4),[28–30]over the strongly reducing +III (f^3)[31,32] to the relatively stable +IV (f^2),[33] followed by +V (f^1)[34,35] and +VI (f^0),[36] of which the two latter tend to form the oxo ("-yl") cations $U^{V}O_2^{+}$ (uranyl(V) monocation) and $U^{VI}O_2^{2+}$ (uranyl(VI) dication).

Of the above, the uranyl dication UO_2^{2+} with its linear *trans*-oxo arrangement[37] is the most prevalent uranium species, highly soluble in water[38] and relatively chemically inert, showing usually only significant reactivity in its equatorial coordination sphere.[39] This *trans*-oxo arrangement is common in actinides, but uncommon in d-block metals. Among the d-metals only the osmyl dication OsO_2^{2+} resembles this linear oxo-group configuration, for example in $K_2OsO_2Cl_4$, but the corresponding aqua ion is unknown.[40] In contrast, molybdyl MoO_2^{2+}, which has no accessible f-orbitals, shows a bent geometry to maximise the π-interaction with the t_{2g}-orbitals.[41–43] The uranyl dication is very stable with respect to its strong oxygen bonding and it possesses a bond dissociation energy for the U-O bond of ΔH_{diss} = 761 kJ/mol. This is even higher than the bond dissociation energy of the C-O bonds in CO_2 (ΔH_{diss} = 749 kJ/mol).[44] Studies on the exchange rate of the uranyl oxygen atoms by Gordon and Taube using 1 M solutions of $UO_2(ClO_4)_2$ in 1 M $HClO_4$ in the presence of ^{18}O-enriched water followed by mass spectrometric analysis have further shown that this reaction proceeds with a half-life of 36 000 hours (= 4.1 years).[45] This results, as Denning has shown, from a nominal bond order of three for the U-O bonds in $O=U^{VI}=O$ and demonstrates the high stability of uranyl(VI) (Figure 2).[46]

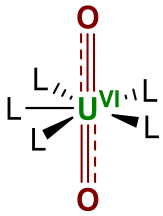

Figure 3 Nominal bond order of 3 for the uranyl(VI) (L = ligand).

These uranyl(VI) oxo-groups show a very small Lewis basicity, which is greatly enhanced upon reduction to uranyl(V). This is supported by quantum chemical calculations by Vallet *et al.* for the singly reduced $UO_2^+(H_2O)_5$ in the gas phase, who report an effective charge on the uranium atom of +2.19 and for the oxygen atoms of -0.66. In contrast, the uranyl(VI) dication $UO_2^{2+}(H_2O)_5$ exhibits an effective charge of +2.43 for the uranium atom and -0.21 for the oxygen atoms resulting from the strong covalent U=O bond in uranyl(VI).[47] This enhanced Lewis-basicity of the uranyl(V) oxo-groups is reflected in their solid state structures, of which a dominant feature is the presence of cation-cation interactions (CCIs).[48] These interactions occur when an axial Lewis-basic actinyl oxygen atom coordinates to a Lewis acidic metal centre. This effect was first observed in actinides by Sullivan *et al.* as a "specific interaction" between neptunyl(V) and uranyl(VI) in aqueous acidic media.[49] CCIs are very well known for the more basic neptunyl(V) NpO_2^+ complexes,[50] and have also been observed for plutonyl(V) PuO_2^+,[51] but remain very rare for uranyl(VI) UO_2^{2+} complexes.[52–55] CCIs in uranium(V) compounds are as such a direct effect invoked by the increased Lewis basicity of the "-yl" oxygen atoms in UO_2^+, and can show different binding motifs depending on the nature of the ligand and the presence of available cations. In aqueous and biological systems CCIs may be a key aspect of the reduction of uranyl(VI) and the disproportionation of uranyl(V).[56,57] Figure 4 shows different CCIs known to form in actinyl complexes.

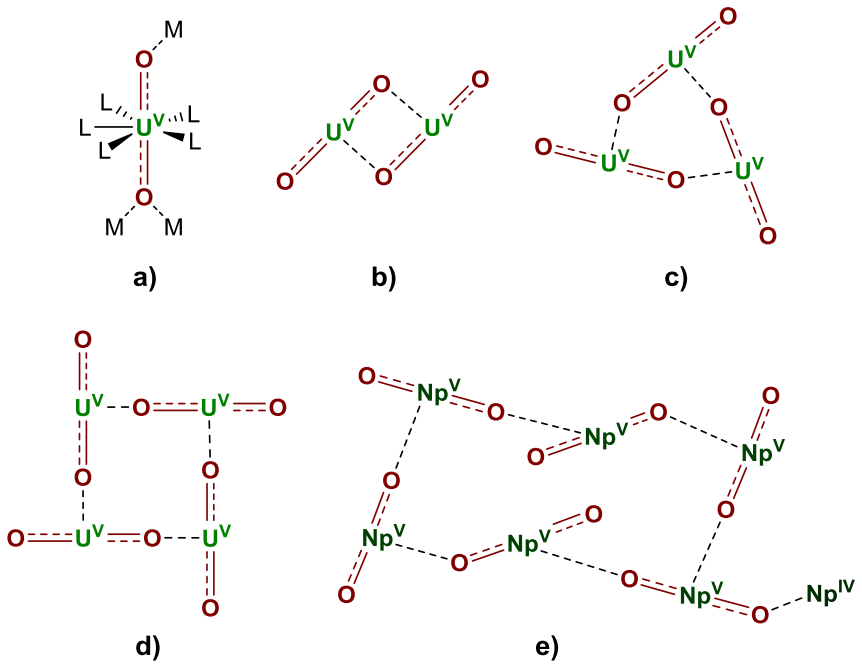

Figure 4 Cation-cation interactions in actinyl(V) complexes (For clarity, no equatorial ligands are shown except for a)). a) monomeric CCI (M = metal cation, L = ligand)[58] b) dimeric diamond-shaped CCI[59,60] c) trimeric CCI[61] d) tetrameric T-shaped CCI[62,63] e) hexameric neptunyl(V) CCI with additional Np(IV) coordination.[64]

Figure 4 shows that the formation of multimetallic CCI complexes occurs when both oxo-groups of the uranyl are allowed to take part in the interaction. In fact, the steric bulk and shape of the ligand strongly influences which kind of complex forms. Hence, the formation of mono uranyl CCI complexes is rather rarely observed because most ligands like salen (*N*,*N*'-ethylenebis(salicylimine)),[65,66] acnac (acetyl-*N*-acetonate)[67,68] and dbm (dibenzoylmethanate)[69,70] solely coordinate the equatorial plane of the uranyl, leaving both oxo-groups unprotected for reductive metalation.

The reduction of uranyl(VI) to uranyl(V) can be carried out both in anhydrous and in aqueous media and results in the formation of the uranyl(V) monocation UO_2^+.[71] However, this is usually unstable with respect to disproportionation, and no isolated hydrated uranyl(V) complexes have been reported to date.[72] For instance, if a $U^{VI}O_2(NO_3)_2$ solution in dimethyl sulfoxide is electrochemically reduced to uranyl(V) the resulting UO_2^+ monocation exhibits a half-life of one hour.[73] This half-life can be significantly increased in aqueous media by the choice of an appropriate ligand (Scheme 1), so that a reduced uranyl acetylacetonate ($UO_2(acac)_2$) complex shows a

half-life of 1.5 hours and a similar tetraketonate (UO_2(T), T = *m*-bis(2,4-dioxo-l-pentyl)benzene)[74] complex has a half-life of 3.7 hours.[75]

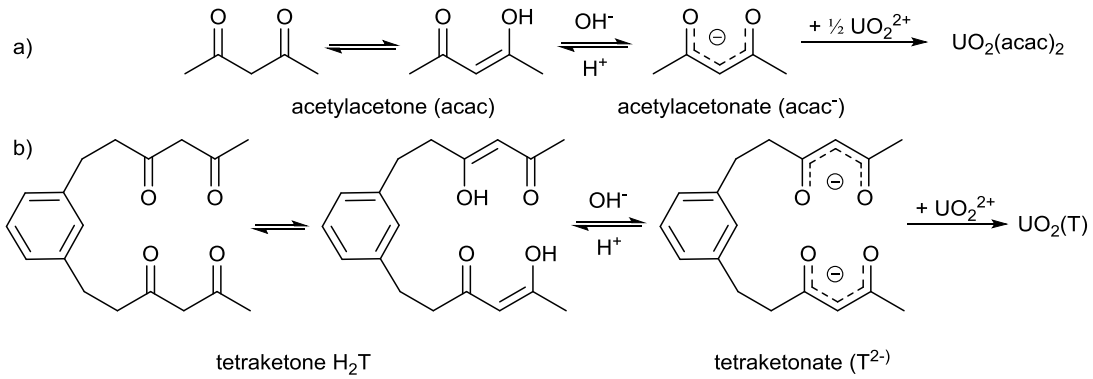

Scheme 1 Keto-enol tautomerism in *β*-diketonate ligands and formation of uranyl(VI) acetylacetonate (a) and uranyl(VI) tetraketonate (b).

Uranyl(V) disproportionates with a ΔG of -142 kJ/mol according to the following scheme to uranyl(VI) and uranium(IV):[77]

$$2\ U^{V}O_2(H_2O)_5^{+}{}_{(aq)} + 2\ H_2O_{(l)} \longrightarrow U^{VI}O_2(OH)(H_2O)_4^{+}{}_{(aq)} + U^{IV}(OH)_3(H_2O)_4^{+}{}_{(aq)}$$

Scheme 2 Disproportionation of uranyl(V) to uranyl(VI) and uranium(IV) in aqueous media.

The electrochemical potentials of the uranyl(VI) reduction both to uranyl(V) and uranium(IV) have been reported by Grenthe *et al.* and are given below.[78]

$$U^{VI}O_2^{2+}{}_{(aq)} + e^- \underset{}{\overset{0.0878\ V}{\rightleftharpoons}} U^{V}O_2^{+}{}_{(aq)}$$

$$U^{VI}O_2^{2+}{}_{(aq)} + 4\ H^{+}{}_{(aq)} + 2\ e^- \overset{0.2673\ V}{\rightleftharpoons} U^{4+}{}_{(aq)} + 2\ H_2O_{(l)}$$

Scheme 3 Electrochemical potentials of the uranyl(VI) reduction to uranyl(V) and uranium(IV).

Steele and Taylor used Density Functional Theory to show that the U(V) disproportionation in water proceeds via the formation of a dimeric cation-cation complex followed by two consecutive protonation reactions of the axial uranyl oxygen atoms.[79] This process is assumed to be an inner sphere electron transfer. Bühl and Schreckenbach carried out computational studies on the oxygen exchange reactions in tetrahydroxouranylate(VI) complexes ($[UO_2(OH)_4]^{2-}$) and have found that the exchange can proceed *via* two non-classical molecular pathways (Scheme 4).[80]

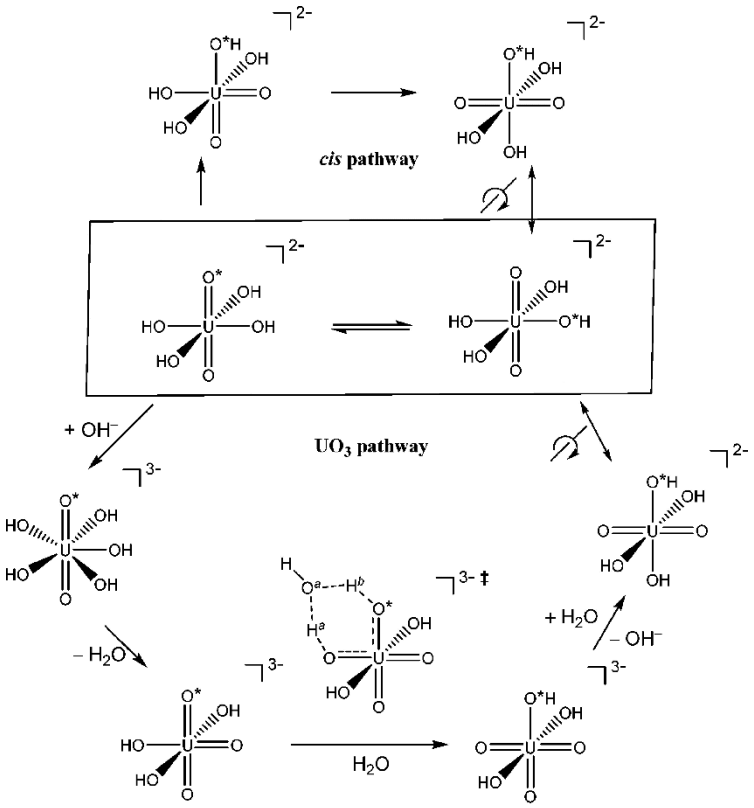

Scheme 4 Oxygen exchange in tetrahydroxouranylate(VI) with two possible mechanistic pathways. *Cis* pathway (top) and T-shaped UO_3 pathway (bottom) (Identical complexes in different orientation are connected by rotation signs).[80]

The authors give evidence that a *cis* pathway employing a *cis*-$[UO_2(OH)_4]^{2-}$ moiety as well as a T-shaped trisoxo uranium pathway with an intermediate $[UO_3(OH)_3]^{3-}$ moiety can be involved in the transfer of the "-yl" oxygens. In addition to this, Szabó and Grenthe have investigated the mechanism of uranyl oxygen exchange using ^{17}O-NMR spectroscopy.[81] They observe the formation of a $[UO_2(OH)_5]^{3-}$ which is in a dynamic equilibrium with $[UO_2(OH)_4]^{2-}$, proposing a mechanism that involves the ion pair $[UO_2(OH)_5]^{3-}/[UO_2(OH)_4]^{2-}$. The Gibbs energy of activation at 320 K derived from this system is $\Delta G^{\ddagger} = 60.8 \pm 2.4$ kJ/mol and is in good agreement with the values calculated by Bühl and Schreckenbach of $\Delta G^{\ddagger} = 52.3 \pm 5.4$ kJ/mol.[80] This suggests that the proposed mechanism by Bühl and Schreckenbach may also proceed via a binuclear pathway. The difference in the two results may therefore be explained because the computational approach is based on an "infinite" dilute system, whereas the ^{17}O-NMR studies were carried out at rather high concentrations.

Similarly, organic acids such as benzoic acid facilitate the disproportionation of uranyl(V) in non-aqueous media such as pyridine to a hexanuclear U(IV) benzoate cluster and a uranyl bis-benzoate complex and water.[82] The provision of a multidentate ligand and the exclusion of H^+ ions is thus a means of stabilising uranyl(V) successfully in order to explore its chemical and physical properties.[83]

This chemistry is of high significance with respect to nuclear waste disposal. In order to accurately predict the long-term behaviour of nuclear waste it is crucial to understand all the processes encountered in complex mixtures of actinides and their fission products. However, many of the redox-reactions regarding the reduction of U(VI), the oxidation of U(IV) or the disproportionation of U(V) are not yet fully understood on a molecular level. Also the occurrence of these oxidation states side by side is an important factor in the light of the presence of plutonium in nuclear waste. Burns *et al.* claim for instance that the crystal-chemical requirements of Pu^{4+} and U^{4+} are very similar, so that it is likely that Pu(IV) ions can substitute U(IV) ions in ianthinite-type crystal phases of nuclear waste, thus being immobilised.[84] Burns and co-workers have also demonstrated that sodium-substituted metaschoepite with the approximate formula $Na[(UO_2)_4O_2(OH)_5](H_2O)_5$ (the prefix '*meta*' indicating partial dehydration) is capable of incorporating groundwater soluble Np^{5+};[85] and similarly synthetic soddyite $(UO_2)_2(SiO_4)(H_2O)_2$ shows increased substitution of Np^{5+} for U^{6+} at pH 4.[86] However, little is known on a molecular level regarding the structural identity and the chemical and physicochemical aspects of formation of these materials, which render uranyl(V) materials ideal model systems for neptunyl(V).

Even though uranyl(V) seems to be an important intermediate in uranyl(VI) reduction and a key to understand anaerobic transformation of nuclear waste crystal phases, to date, there is only one naturally occurring uranium(V) mineral known – wyartite I $(CaU^{5+}(UO_2)_2(CO_3)O_4(OH)(H_2O)_7)$[87] and its dehydration product wyartite II $(CaU^{5+}(UO_2)_2(CO_3)O_4(OH)(H_2O)_3)$.[88] However, no uranyl(V) mineral as such has yet been observed in nature and even wyartite itself does not exhibit a uranyl(V) moiety but a uranium atom with a formal charge of +5.

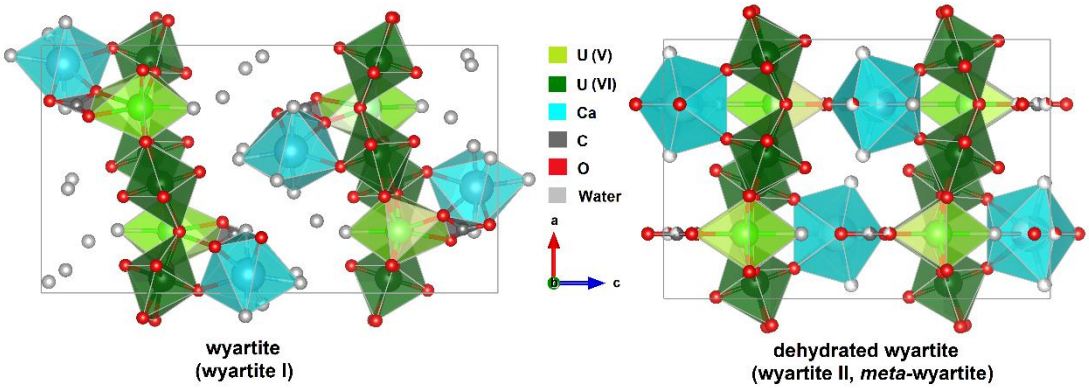

Figure 5 Depiction of the unit cells of wyartite (left) and dehydrated wyartite (right) in the direction of the crystallographic *b*-axis. The light green polyhedra represent the uranium(V) sites.

Joan Clark mentions in her studies in 1960 that crystals of wyartite undergo alteration in the laboratory within the course of two years, however, she was not able to accurately determine the product of alteration.[89] Hawthorne and co-workers noted a yellow mottling on the surface of purple wyartite II crystals and suggest a partial oxidation similar to that of ianthinite.[88] In contrast to wyartite I the structure of wyartite II contains less water and carbonate and shows significant disorder. In Wyartite I the Ca^{2+} cation coordinates to both the uranyl(VI) and the uranium(V) site in a chain of uranium polyhedra. The disordered Ca^{2+} cation in wyartite II however links a uranyl(VI) site in one chain with a uranium(V) site in the opposite chain. Quite uncommon for uranyl(VI) cations the structures of both wyartite I and wyartite II show a cation-cation interaction of the Ca^{2+} cation to the uranyl(VI) oxygen atom with $Ca\cdots O{=}U^{VI}{=}O$ separations of 2.52 Å (wyartite I) to 2.42 Å (wyartite II).

The behaviour of the “classic” uranyl(VI) in wyartite is contrasted by the unique uranium(V) site, of which the coordination environment is shown in Figure 6.

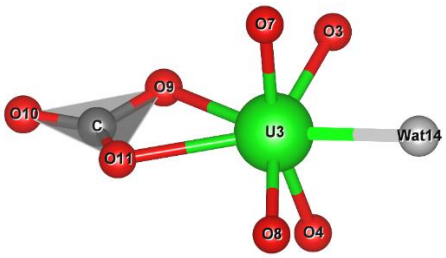

Figure 6 Coordination environment of the pentagonal bipyramidal uranium(V) in wyartite. Selected bond lengths (Å): U3-Wat14 2.47(1), U3-O4 2.09(2), U3-O8 2.06(2), U3-O11 2.48(2), U3-O9 2.44(2), U3-O7 2.07(2), U3-O3 2.14(2). Bond angles O7-U3-O4: 167.0(9)°, O8-U3-O3: 155.2(9)°.

Even though the coordination environment for the uranium(V) atom in wyartite is pentagonal bipyramidal it contrasts the "classic" behaviour of the uranyl(VI) cations found in the same structure. The U-O distances range from 2.06 to 2.48 Å and are significantly longer than the average U=O distance of 1.78 Å. The O-U-O bond angles with O7-U3-O4 167.0(9)° and O8-U3-O3 155.2(9)° deviate significantly from the almost linear uranyl(VI) dication with angles between 174.1(7)° and 176.7(0)°. The bond valence parameter calculated for the uranium atom at the U3 site in wyartite is 5.07 valence units and confirms the U^{5+} oxidation state.

In spite of this it was only in 2003 when for the first time the infra-red shift of a uranyl(V) *N*,*N*′-disalicylidene-*o*-phenylenediaminate (saloph) complex had been reported (Figure 7).

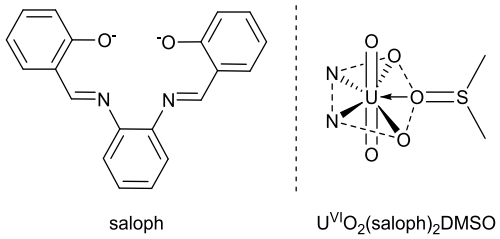

Figure 7 *N*,*N*′-disalicylidene-*o*-phenylenediaminate (saloph) and the corresponding uranyl(VI) complex as the DMSO adduct.[90]

By electrochemical reduction of uranyl(VI) in a thin layer electrode IR cell in DMSO, a shift in the U=O asymmetric stretching frequency was observed from 895 cm^{-1} in uranyl(VI) to 770 cm^{-1} in uranyl(V), corresponding to a redox couple at -1.73 V vs. Fc/Fc^{+} (Scheme 5).[90]

$$U^{VI}O_2(saloph)DMSO + e^- \underset{}{\overset{-1.73\ V}{\rightleftharpoons}} [U^{V}O_2(saloph)DMSO]^-$$

Scheme 5 Electrochemical reduction of the uranyl(VI) to uranyl(V).

This results from both ligand effects in the equatorial plane as well as from the chemical reduction, which weakens the U=O bonds, thus increasing the U=O distance. This effect hence results in asymmetric stretching modes at significantly lower wavenumbers compared to the free UO_2^{2+} which has an absorption at 962 cm^{-1}.[91] In the same year Berthet, Nierlich and Ephritikhine were able to isolate the first uranyl(V)

complex $[U^{V}O_2(OPPh_3)_4](OTf)$ which was crystallographically characterised (Figure 8). In an attempt to recrystallise $[U^{VI}O_2(OPPh_3)_4](OTf)_2$ the authors serendipitously observed the formation of a small quantity of small red-orange cube-shaped crystals of $[U^{V}O_2(OPPh_3)_4](OTf)$ along with yellow crystals of the parent uranyl(VI) complex.[92]

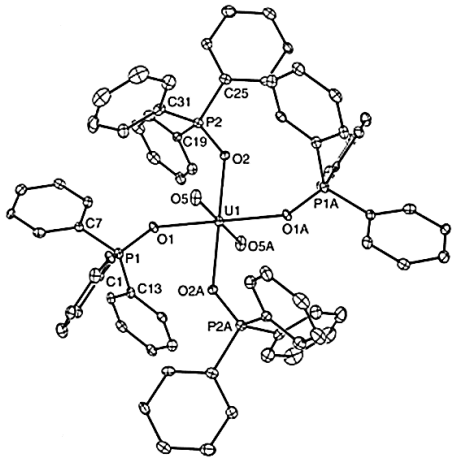

Figure 8 Solid state structure of the first uranyl(V) complex, representing one of the two crystallographically independent $[U^{V}O_2(OPPh_3)_4]^{+}$ ions (displacement ellipsoids drawn at 30 % probability). 'A' indicates symmetry related atoms. Selected bond lengths (Å): U1-O5 1.821(6), U1-O5A 1.817(6).[92]

Berthet *et al.* failed to repeat this first uranyl(V) structure, however, uranyl(V) chemistry has since seen rapid growth,[93] and – an air- and moisture-free environment provided - different methods of obtaining stable uranyl(V) complexes such as polymeric $\{[UO_2(Py)_5][KI_2(py)_2]\}_{\infty}$ have since been developed.[94,95]

In 2004 Sarsfield and Helliwell reported the synthesis of a uranyl complex that acts as a Lewis base, showing an unusual coordination to the highly Lewis acidic tris(pentafluorophenyl) borane $B(C_6F_5)_3$ to one of its oxygen atoms and a significantly longer U-O_{coord} bond length of 1.898(3) Å than compared to the uncoordinated U-$O_{uncoord}$ bond of 1.770(3) Å (Scheme 6).[96]

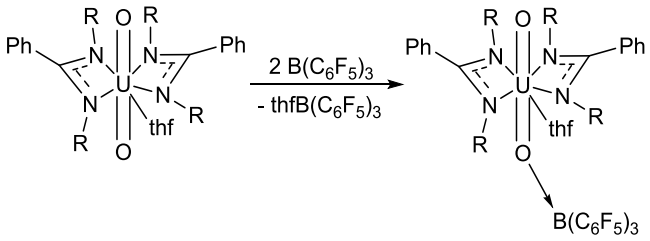

Scheme 6 Uranyl acts as a Lewis base towards $B(C_6F_5)_3$, yielding a O=U=O·$B(C_6F_5)_3$ motif.

Recently Mazzanti and co-workers have been able to show that U(IV) is capable of promoting the disproportionation of U(V) in Salophen-^{t}Bu$_2$H$_2$ (Salophen-^{t}Bu$_2$H$_2$ = *N,N′*-phenylene-bis-(3,5-di-tert-butylsalicylideneimine) and mesaldienH$_2$ (mesaldien-H$_2$ = *N,N′*-(2-aminomethyl)diethylenebis(salicylimine)) ligands leading to linear {[UO_2(mesaldien)-(U(mesaldien)]$_2$(μ-O)} and pentanuclear {[UO_2(salen)][U(salophen-^{t}Bu$_2$)]$_2$[(U(salen)]$_2$(μ-O)$_3$(μ$_3$-O)} oxo clusters containing $UO_2^{+}\cdots U^{4+}$ cation-cation interactions (Figure 9).[97]

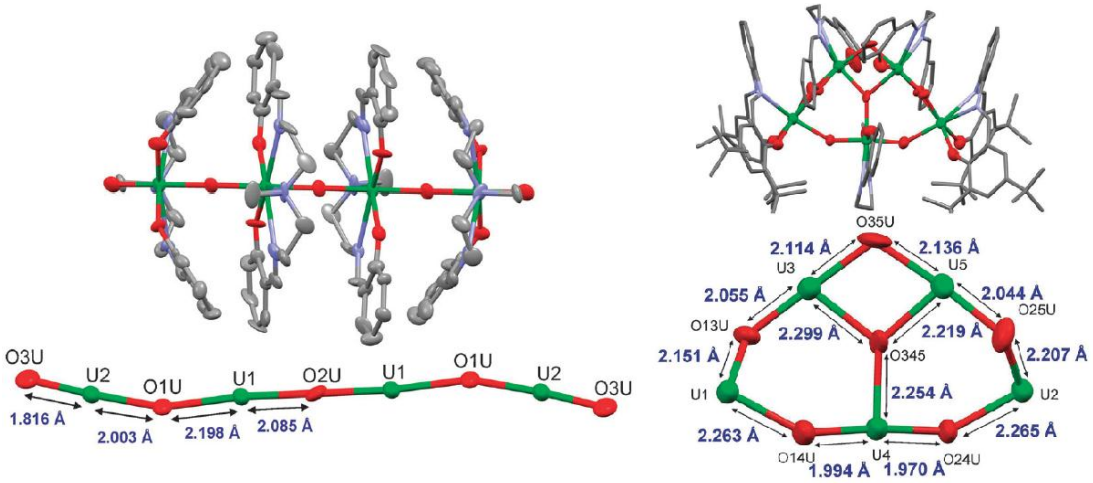

Figure 9 Depictions of solid state linear (left) and pentanuclear (right) $UO_2^{+}\cdots U^{4+}$ interactions (displacement ellipsoids drawn at 50% probability; O = red, U = green).[97]

Uranyl(V) complexes have recently also gained attention as potential candidates for single molecule magnets (SMMs). This is due to the paramagnetism of the uranyl(V) monocation, created by its f^1 electron and its ability to coordinate Lewis acidic metal cations via cation-cation interactions in the direction of its axial oxygen atoms which generate a pathway for magnetic superexchange.[98]

Recently Mazzanti and co-workers have reported the first homometallic trimeric uranyl(V) β-diketiminate complex $[UO_2L]_3$ (L = 2-(4-Tolyl)-1,3-bis(quinolyl)malon-diiminate) with a blocking temperature of 12 K[61] as well as a Mn(II)-uranyl(V) $[U_{12}Mn_6]$ wheel-shaped cluster with a blocking temperature of 4 K (Figure 10).[99]

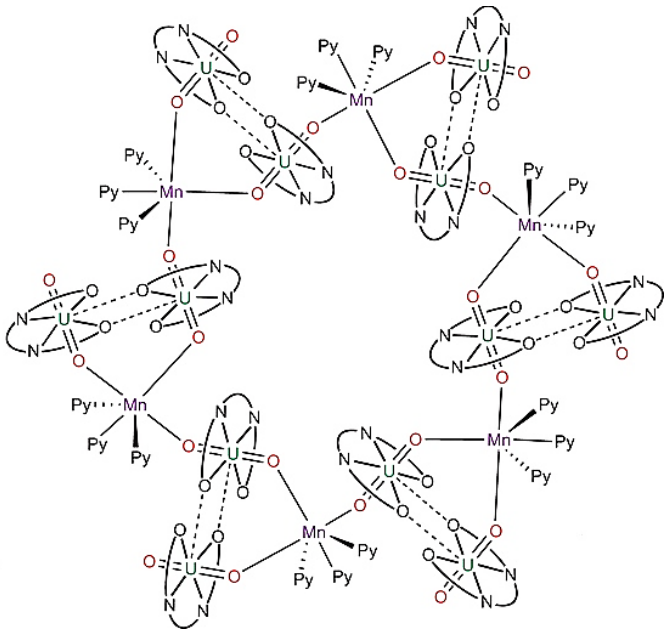

Figure 10 The dodecanuclear uranyl(V) complex $[\{[UO_2(salen)]_2Mn(Py)_3\}_6]$ with six Mn(II) centres.

Another prominent aspect of the reduction of uranyl(VI) is the reductive silylation (Scheme 7), particularly within the Schiff-base polypyrrolic "Pacman" macrocycle, which provides reduction and selective oxo-group silylation upon bond homolysis in the Si-N bonds of the used silylamide metal complexes.[100] This reaction is particularly favoured when the lower macrocyclic pocket is occupied by a metal which shows a $U{=}O_{endo}\cdots M$ interaction, thus significantly enhancing the Lewis basicity of the exogenous uranyl oxo-group $U{=}O_{exo}$. This reductive oxo-metalation depends strongly on the metal amide used in the synthesis. In particular lithium, magnesium and zinc silylamides interact strongly with the lower macrocyclic pocket, thus enhancing the basicity and oxidative strength of the uranyl(VI). Specifically magnesium bis(hexamethyldisilylamide) $Mg(N(SiMe_3)_2)_2$ shows a strong Lewis acidic behaviour, allowing for an endogenous $U{=}O_{endo}\cdots Mg$ interaction, followed by a dative exogenous interaction $U{=}O_{exo}\cdots Mg$ that concomitantly reduces *via* Mg-N bond cleavage to form a Mg(II)-uranyl(V) complex with a $U\text{-}O_{exo}\text{-}Mg$ bonding motif.

In contrast the softer zinc chloride hexamethyldisilylamide $ZnClN(SiMe_3)_2$ forms a dative exogenous $U{=}O_{exo}\cdots Zn$ interaction, that subsequently results in reductive silylation by bond homolysis of the Si-N bond to form the $U\text{-}O_{exo}\text{-}Si$ motif (Scheme 7).[100]

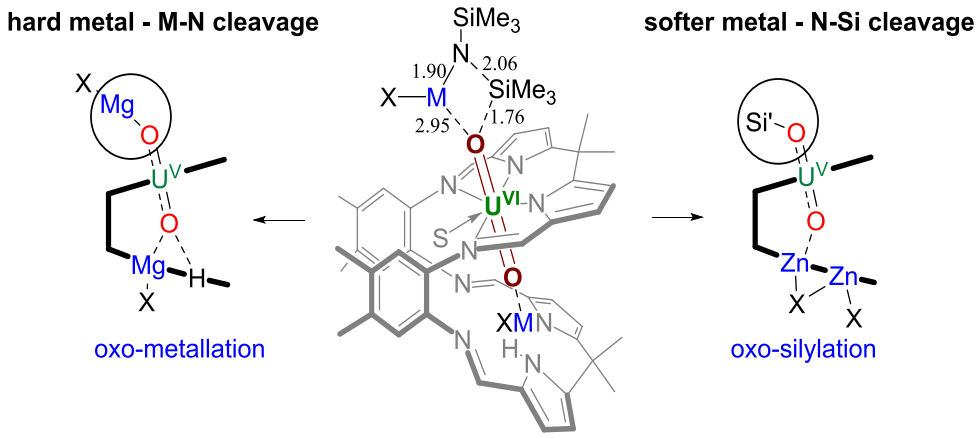

Scheme 7 Bond homolysis in Si-E bonds resulting in reductive uranyl oxo-metalation or oxo-silylation depending on the softness of the metal.[100]

This mechanism has also led to the synthesis of a chemically inert and air-stable butterfly-shaped bimetallic uranium(V) dioxo complex in which the *trans* uranyl oxo, due to its steric congestion, is rearranged into a mutually *cis* position, being the first example of its kind (Figure 4).[101][102]

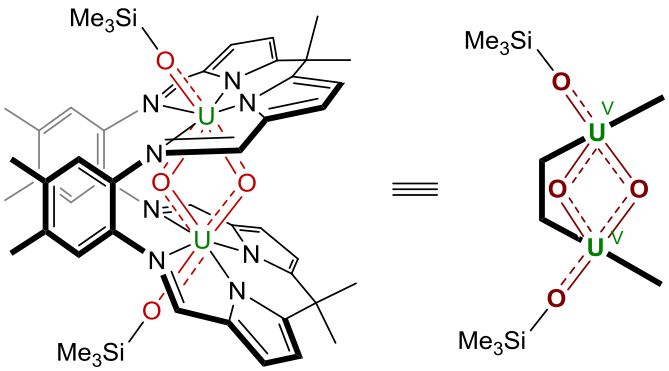

Figure 11 Bimetallic uranyl(V) Pacman complex with mutual *cis*-*trans*-uranyl motif.

Computational studies on the tetrahydroxouranylate ion $[(UO_2)(OH)_4]^{2-}$ have shown that the synthesis of a *cis*-conformer of the *trans* uranyl should be feasible, although the *cis* motif is 75 - 79 kJ/mol higher in energy.[103]

Reductive uranyl silylation has since become a prominent feature of uranyl(V) chemistry. For instance Hayton *et al.* have recently reported a borane assisted silylation and shown that the equatorial ligand environment of the uranyl significantly influences its oxo-reactivity.[70]

In addition to this Hayton and co-workers have shown that also iodotrimethylsilane Me_3SiI is able to reduce uranyl(VI) to uranyl(V), claiming that the weak oxidation potential of the uranyl(VI) dication is greatly enhanced by coordination of the Me_3Si^+ moiety to the uranyl oxygen, in addition to the thermodynamic driving force of Si-O (ΔH_{diss} = 514 kJ/mol) bond formation *versus* Si-I (ΔH_{diss} = 322 kJ/mol) bond homolysis, finally stating the possibility of a subsequent deoxygenation of the uranyl to U(IV) complexes upon addition of excess Me_3SiI (Scheme 8).[104]

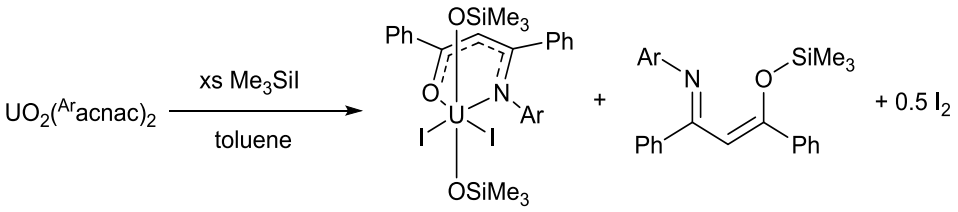

Scheme 8 Reductive silylation of uranyl(VI) using TMSI.[104]

This is in concordance with the results of Berthet *et al*, who observed that $UO_2I_2(thf)_3$ or $UO_2(OTf)_2$ are easily reduced in acetonitrile by Me_3SiX (X = Cl, Br, I) yielding the tetravalent $UX_4(MeCN)_4$ complexes. However these studies have not led to the isolation of a silylated uranyl(V) intermediate or the expected bis-silyl ether.[105]

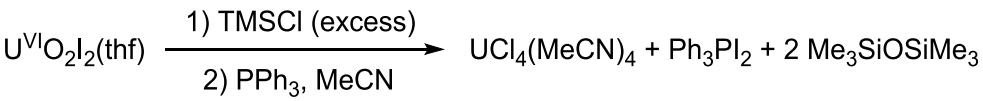

Scheme 9 Uranyl(VI) reduction using TMSCl to yield uranium(IV) and the bis-silyl ether.[104,105]

In contrast, the reduction of uranium either in oxidation state +4 or +6 with metallic reductants such as elemental alkali metals is known to reduce uranium to the element.[106] In fact, the first preparation of elemental uranium in 1841 by Péligot was carried out by heating a mixture of UCl_4 with metallic K.[107] The synthesis of highly reactive and finely dispersed uranium metal (Rieke-uranium) can be achieved by reducing UCl_4 with sodium-potassium alloy in dimethoxyethane.[108] It has been

shown that K can reduce UCl_4 to uranium(III), forming K_2UCl_5.[109] However, no controlled reduction of high oxidation state uranium using elemental alkali metals has been reported to date.

1.2.2 Uranyl(V) *vs.* neptunyl(V)

The reduced uranyl(V) monocation UO_2^+ is also a useful model for the more radioactive transuranium element neptunium (26.04 MBq/g based on ^{237}Np).[110] The neptunyl(V) monocation NpO_2^+ represents the most stable oxidation state of neptunium and behaves – because of its two f-electrons and its subsequently increased Lewis basicity on the neptunyl oxygens – chemically very similar to uranyl(V). As previously described for uranyl(V) the decreased overall charge on the metal atom results in the "-yl" oxygens to become more Lewis basic, and they are therefore more likely to form covalent interactions with other metal ions. The bond strength of Np-O is weakened and the bond dissociation enthalpy is, compared to uranyl(VI), reduced by 41 kJ/mol to 720 kJ/mol. Neptunyl(V) itself is also more likely to form cation-cation interactions in a self-recognising pattern, coordinating one neptunyl oxygen to an adjacent Np atom in its equatorial plane.[111] This motif is known for 50 % of all Np(V) structures.[112]

For example, Mazzanti and co-workers have shown that neptunyl(V) salen complexes $[K(18C6)py]_2[\{NpO_2(salen)\}_4(\mu_8\text{-}K)_2]$ can form similar cation-cation complexes in comparison to analogous uranyl(V) material $[K(18C6)py]_2[\{UO_2(salen)\}_4(\mu_8\text{-}K)_2]$ (Figure 5).[65]

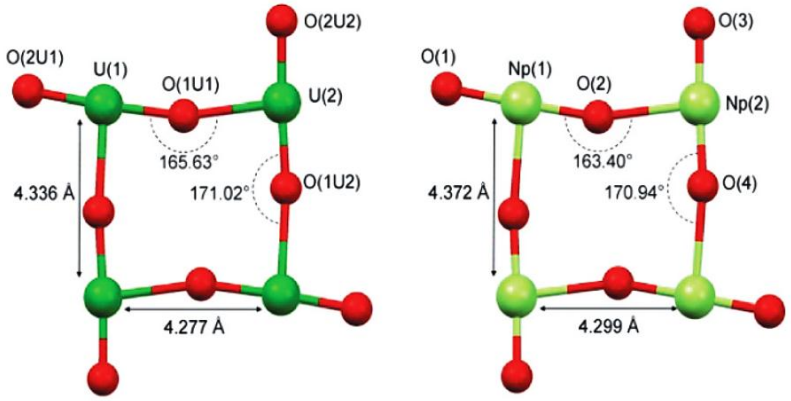

Figure 12 Comparison between the tetrameric uranyl(V) $[\{UO_2(salen)\}_4(\mu_8\text{-}K)_2][K(18C6)Py]_2$ (left) and the tetrameric neptunyl(V) $[\{NpO_2(salen)\}_4(\mu_8\text{-}K)_2][K(18C6)Py]_2$ (right) by Mazzanti *et al.*[65]

In these systems a potassium coordinated uranyl(V) salen complex forms a tetrameric uranyl(V) motif with uranyl-uranyl interactions by coordination of a uranyl oxygen to the equatorial plane of an adjacent uranyl. This motif was verified by synthesising the analogous NpO_2^+ compound which leads to a similar binding motif, with neptunyl oxygen atoms coordinating to the equatorial plane of an adjacent neptunyl. Although the overall characteristics of the two tetrameric complexes are similar with respect to geometry, binding motif and bond angles, slight deviations can be found regarding the Np-O bond distances as well as the neptunyl-neptunyl distances. The two An=O distances found in the neptunium complex ($Np\text{-}O_{bound}$ = 1.877(2) Å and $Np\text{-}O_{unbound}$ = 1.830(2) Å) are slightly shorter than those in the uranium complex ($U\text{-}O_{bound}$ = 1.933(5) Å and $U\text{-}O_{unbound}$ = 1.840(7) Å), mainly because of the differences in ionic radii (0.09 Å).

Similar CCIs have hence also been reported by Burns *et al.* on neptunyl(V), showing a rare two-dimensional side-on interaction. This neptunyl(V) complex $K[(Np^VO_2)(OH)_2]\cdot 2\,H_2O$ thus gives a direct comparison between uranyl(V) and neptunyl(V) (Figure 6).[113]

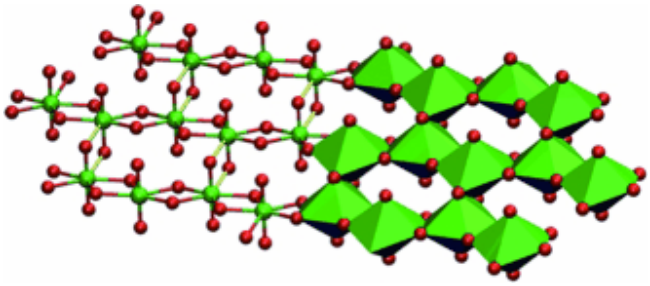

Figure 13 Ball-and-stick and polyhedral representations of the X-ray structure of $K[(Np^{V}O_2)(OH)_2]\cdot 2\,H_2O$ (CCIs = yellow, Np = green, O = red).[113]

However, even though uranium and neptunium are neighbours in the periodic table, the much stronger radioactivity of the transuranium elements very often inhibits more extensive systematic research regarding periodic trends in Th, U, Np and Pu compounds.[114] While the activity of the most stable isotope ^{237}Np is still about a 1000 times higher than that of ^{238}U,[115] structural studies comparing U, Np and Pu suggest that even though the actinides show many similarities it is not advisable to only use substitutes or surrogates but also to work with the actual element in question.[116–118] In general though, access to transuranium elements is very limited and cost intensive[119] and quite often the focus lies on uranium and plutonium because of their importance for nuclear fission. This has brought neptunium the reputation of being the "stepchild" of transuranium chemistry,[120] although it is the element that is considered to possess the most hazardous potential because it will remain in nuclear waste from 10 000 to 30 million years.[121] It is therefore crucial to investigate this first transuranium element in greater detail.

1.3 Chemistry of the Pacman calixpyrroles

Calixpyrroles (gr. κάλυξ = chalice, goblet) are cyclic pyrrole compounds which are, due to their chemical structure, able to fold and form wedge-shaped molecules.

The calixpyrrole macrocycle used in this work is the so called "Pacman" ligand, first reported independently by Love[122] and Sessler.[123] Its structure and preparation is shown in (Scheme 10):

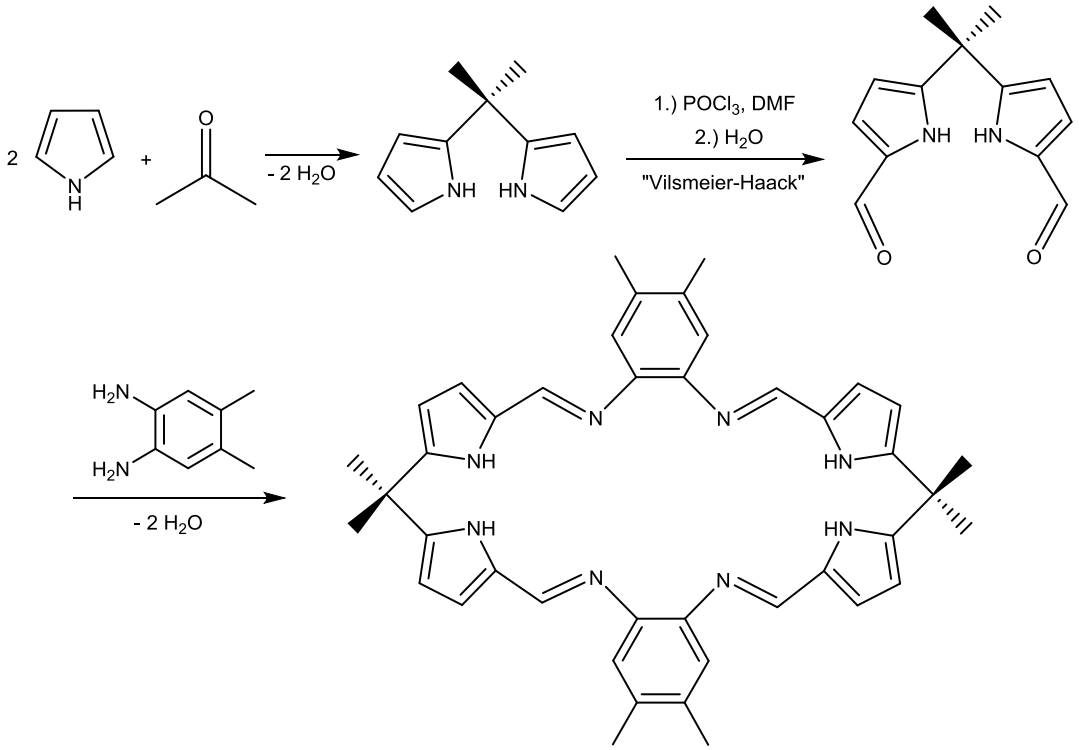

Scheme 10 Preparation of the Pacman calixpyrrole ligand.

These macrocycles are known to complex a variety of different metals, such as Pd, Ni, Cu, Fe and Co, resulting usually in bimetallic complexes due to its two N_4-donor pockets.[124] However, the uranyl dication is one of the two examples which mainly forms a monometallic complex, prepared as shown in Scheme 11.[125] The only other monometallic Pacman complex of this kind is the dimethyl tin(IV) complex $[SnMe_2(H_2L)]$.[126]

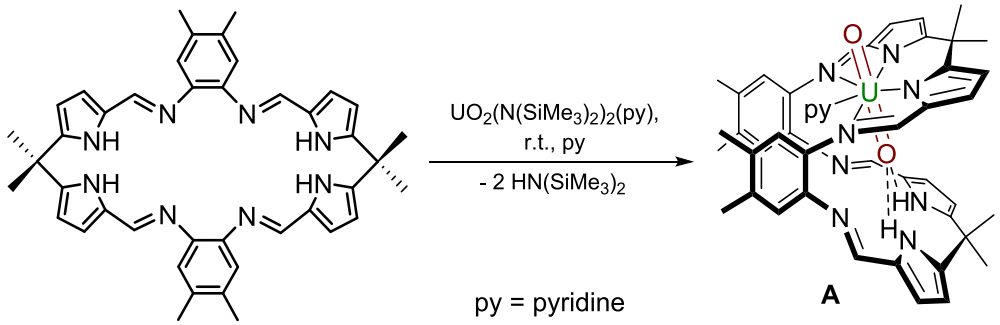

Scheme 11 Synthesis of uranyl(VI) Pacman **A**.

1.4 Aims of this thesis

The aims of this project were to synthetically investigate the reactivity of the uranyl oxygen atoms by uranyl(VI) reduction and subsequent oxo-functionalisation through metal coordination. The first aim is to synthesise novel uranyl(V) complexes with cation-cation interactions to a variety of metal cations from across the periodic table. These will be carried out using the Pacman macrocycle to confine the uranyl(VI) and to constrain its oxo-metalation to only one oxo-group.

At first the reactivity of organometallic aluminium reagents on uranyl(VI) shall be investigated. This will be followed by reactivity studies with alkali metal hydrides and alkyls. Secondly the single electron reduction of uranyl(VI) by elemental alkali metals shall be explored.

Furthermore, the synthesis of novel uranyl(V) complexes coordinated by a *d*-metal *via* single electron reduction using low-valent organometallic Group(IV) reagents will be explored. In addition to this, reactions will be undertaken with uranyl Pacman and divalent Group II and Group XII elements to determine their reductive potential and aim to obtain exclusively mono-oxo metalated M(II)-uranyl(V) complexes.

Moreover, uranyl reduction shall be tested by utilisation of low-valent or metallic reductants from the lanthanides series, to target *f-f* electron correlations through a bridging uranyl oxygen.

Another aspect will be a collaboration with the Institute for Transuranium Elements (ITU) in Karlsruhe, Germany, to investigate the reactivity of low-valent organo-metallic neptunium and plutonium compounds as possible one-electron-reductants to form actinide-uranyl(V) cation-cation interactions.

Finally, newly developed redox-active dipyrromethane and dipyrromethene ligands will also be used to investigate the two-electron reduction of uranyl(VI), targeting the synthesis and characterisation of novel, bis-oxo metalated uranium(IV) complexes.

This research focuses will focus on the solid state characterisation of novel uranyl(V) complexes by single crystal X-ray diffraction. Nuclear magnetic resonance spectroscopy will be used as an important tool to determine the paramagnetically shifted resonances resulting from the single electron reduction of uranyl(VI) to

uranyl(V) in solution. For selected complexes computational studies will be undertaken to correctly assign the oxidation state and hydrogen bonding interactions with the macrocycle. This will be supported by magnetic and cyclic voltammetry studies as well as UV-vis spectroscopy. The relevance of these materials as potential model systems for nuclear waste, their catalytic applications and their role as potential candidates for single molecule magnets will be discussed.

.

2 Reductive and catalytic uranyl metalation with Group XIII and Group I reagents

2.1 Uranyl functionalisation using organometallic aluminium(III) reagents

Targeting the reductive mono-oxo uranyl functionalisation by oxophilic Lewis-acids it was envisaged to test a variety of organoaluminium reagents, of which Tebbe's reagent and di-(*iso*-butyl)aluminium hydride (DIBAL) have proven most useful. The resulting Al(III)-uranyl(V) complexes [(py)(Me_2AlOUO)(py)(H_2L)] **1** and [(py)$^{i}Bu_2$AlOUO(py)(H_2L)] **2** have hence been used as precursor materials for the synthesis of novel, exclusively exo-oxo coordinated alkali metal uranyl(V) complexes in multi-step synthesis as well as in a catalytic one-pot reaction.

2.1.1 Uranyl functionalisation using Tebbe's reagent

Scheme 12 illustrates the two reductive metalation reactions which are further described below.

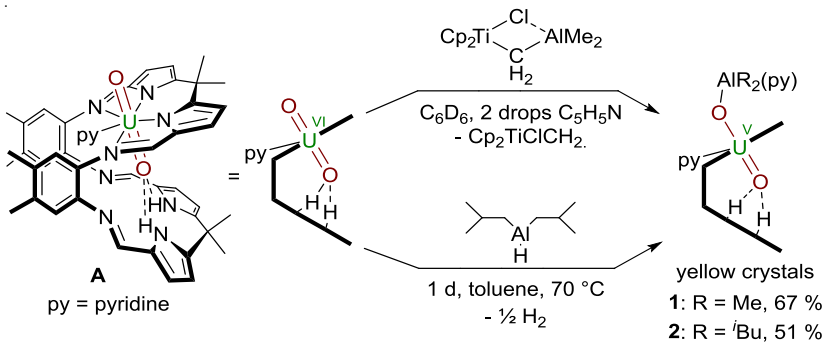

Scheme 12 Reductive alumination of [(UO_2)(py)(H_2L)] **A** by Tebbe's reagent or DIBAL.

The combination of benzene solutions of equimolar quantities of **A** and [Cp_2Ti(μ-Cl)(μ-CH_2)$AlMe_2$], and two drops of pyridine at room temperature results in a clear orange solution from which yellow crystals form upon standing, and are characterised as [(py)(Me_2AlOUO)(py)(H_2L)] **1**, isolated in 67 % yield. The solid state structure of **1** was determined and shows the expected wedge-shaped Pacman geometry of the parent complex with *exo*-oxo aluminium coordination (Figure 14).

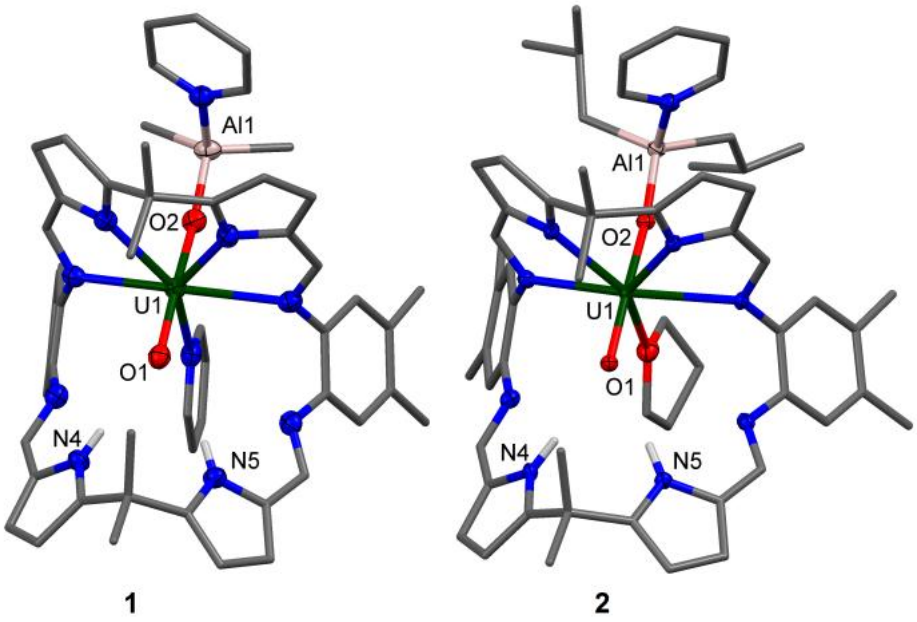

Figure 14 Solid state structures of **1** and **2**, front view. For clarity, all hydrogen atoms except the pyrrole NHs and all solvent molecules are omitted (displacement ellipsoids are drawn at 50% probability). Selected bond lengths (Å) for **1**: U1-O1 1.857(3), U1-O2 1.962(3), O1-N4 2.964(5), O1-N5 3.068(5). O1-U1-O2 bond angle: 174.3(1)°. Selected bond lengths for **2**: U1-O1 1.855(2), U1-O2 1.962(2), O1-N4 3.033(4), O1-N5 3.027(4). O1-U1-O2 bond angle: 175.1(1)°.

1 crystallises in a monoclinic crystal system, and the structural solution was performed in space group $P2_1/c$ with four molecules in the unit cell. The uranyl oxo-groups adopt a *trans* geometry, with an O1-U1-O2 angle of 174.3(1)° and U1-O1 and U1-O2 bond lengths elongated to 1.857(3) Å and 1.962(3) Å respectively, compared to the $O=U^{VI}=O$ bonds of 1.793(6) Å and 1.773(6) Å for **A**.[125] This significant lengthening of these bonds is indicative of a decrease in the uranyl bond order and is similar to related experimental and calculated systems in which an increase of 0.151 - 0.242 Å in U-O bond lengths upon reduction of $O=U^{VI}=O$ to $O=U^{V}$-O-M is seen.[127] Furthermore, the hydrogen-bonding interactions between the *endo*-oxo O1 and the two pyrrole protons in the vacant macrocyclic pocket, shown by O1···N1 2.964(5) Å and O1···N2 3.068(5) Å are slightly shorter than those in **A** (3.111(7) Å and 3.146(7) Å) and supports the enhanced oxo basicity of the f^1 cation. To our knowledge, this is the first reaction in which Tebbe's reagent is used as a source of aluminium.

2.1.2 Uranyl functionalisation using DIBAL

A more atom-economic route to these heterobimetallic complexes is through the reaction between **A** and di(*iso*-butyl)aluminium hydride (DIBAL) in toluene at 70 °C for 24 h which results in the formation of yellow [(py)^{i}Bu$_2$AlOUO(py)(H$_2$L)] **2** in 51 % yield. The compound crystallises in a monoclinic crystal system and the structural solution was carried out in space group $P2_1/n$ with four molecules in the unit cell. The solid state structure of **2** is shown in Figure 14 and is very similar to **1**, with a bond length for U1-O1 of 1.855(2) Å and for U1-O2 of 1.962(2) Å. Also the O1-N$_{pyrrole}$ interactions show similar values, with an O1-N4 length of 3.033(4) Å and an O1-N5 length of 3.027(4) Å. The elongation of the U1-O1 and U1-O2 bond distances thus exemplifies once more the formal U^{V} oxidation state. Mechanistically, it is likely that **1** and **2** are formed through Al-ligand bond homolysis (Al-H or Al-C) which provides the reducing electron. This process is similar to that suggested by us previously to be responsible for uranyl(VI) reduction in the formation of lithium-functionalised [(LiOUO)(py)(Li$_3$L)] and lanthanide-functionalised [UO$_2$(py)(Ln{N(SiMe$_3$)$_2$}(L)]$_2$ that result from C-H[128] or Ln-N bond homolysis (Scheme 13).[60] The latter is also known as a sterically induced reduction, which commonly occurs in congested trivalent lanthanide complexes.[129]

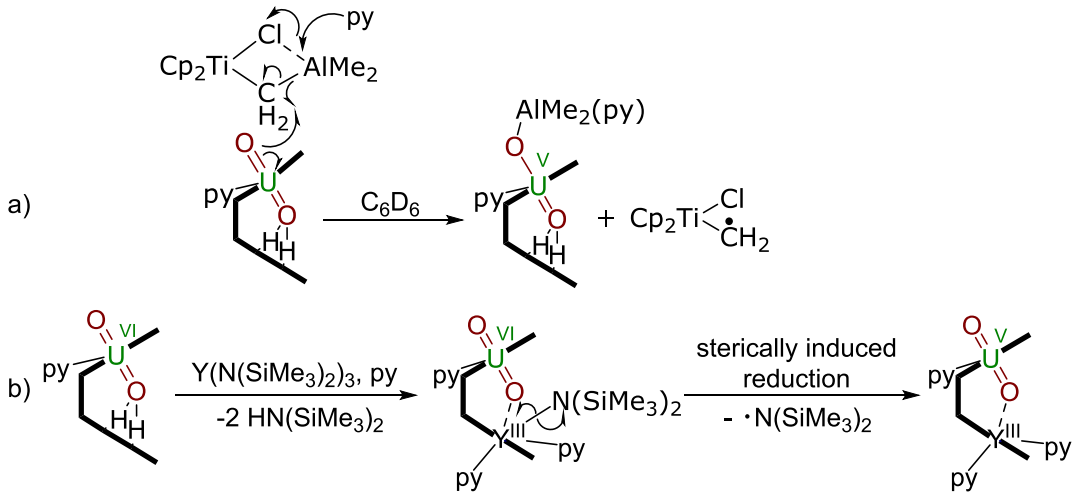

Scheme 13 Bond homolysis in the Al-CH$_2$ bond (a) forming **1** and a Cp$_2$Ti(Cl)CH$_2$· radical and sterically induced reduction in Y-substituted uranyl Pacman complexes forming uranyl(V) and a ·N(SiMe$_3$)$_2$ radical[60]

The ^{1}H-^{1}H-COSY (Figure 15) spectrum of **2** shows paramagnetically shifted and broadened resonances between –6 and +70 ppm due to the paramagnetism of the f^{1} centre. Even so, the ^{i}Bu methyl hydrogens can be identified at 6.10 ppm and 6.67 ppm with $^{3}J_{H\text{-}H}$ coupling of 8 Hz, and the methine proton is a broad resonance at 11.31 ppm that couples with the methylene protons at 16.35 ppm and 16.81 ppm. The most contact-shifted resonance at +69 ppm is assigned to the pyrrole N-H protons.

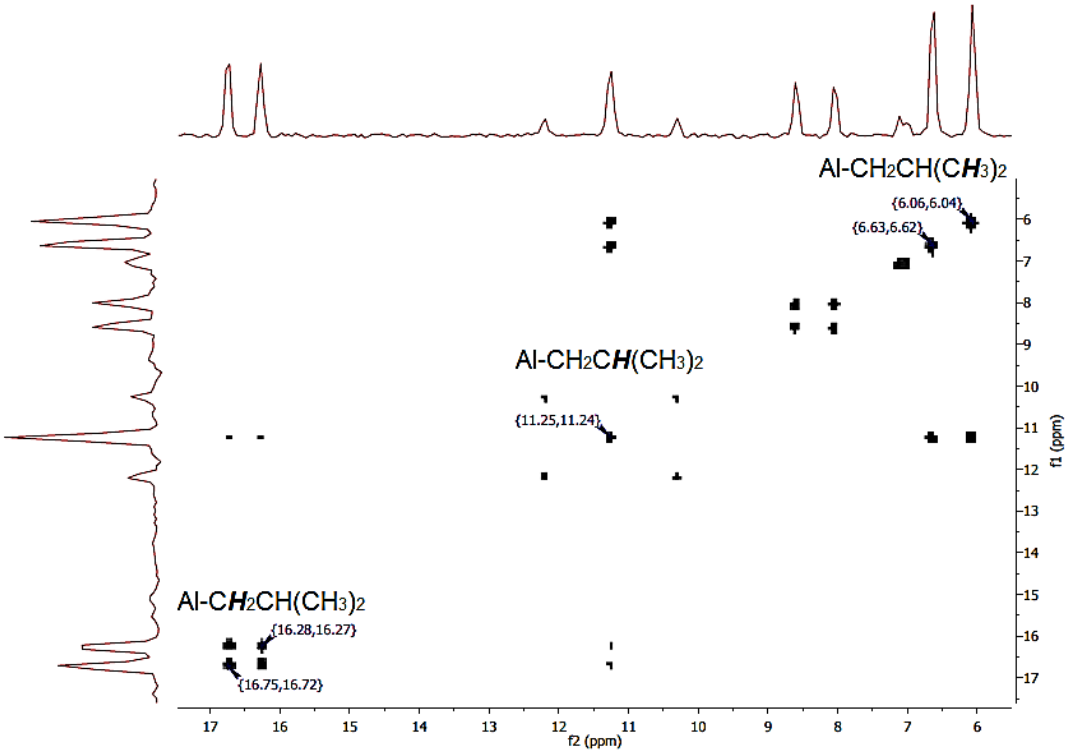

Figure 15 ^{1}H-^{1}H-COSY of **2** in C_6D_6 covering the range of 18 ppm to 5 ppm showing the coupling of the *iso*-butyl groups.

These resonances can also be identified in the ^{1}H-NMR of **2** which is shown in Figure 16.

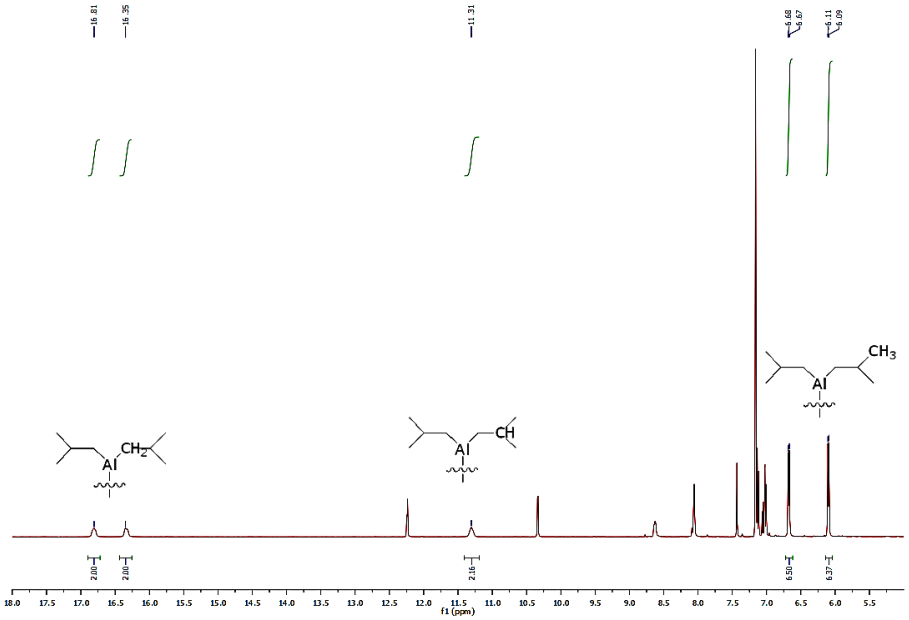

Figure 16 ^{1}H-NMR spectrum of **2** in C_6D_6 covering the range of 18 ppm to 5 ppm showing the coupling of the *iso*-butyl groups.

Both $U^{V}O_2$-Al^{III} compounds **1** and **2** are stable in THF, pyridine and non-coordinating solvents. A study of the redox chemistry of **2** by cyclic voltammetry in THF with 0.1 M [NBu_4][PF_6] as a supporting electrolyte at 500 mV/s reveals a quasi-reversible reduction at $E_{1/2}$ = -1.42 V (vs. Fc/Fc^{+}) which is ascribed to a uranyl(V)/uranium(IV) redox couple (Figure 17). A pre-reduction wave is also seen at E_{pc} = -1.45 V, implying that the redox chemistry of **1** and **2** is not straightforward; as such, the chemical reduction of complex **1** or **2** has not yet been successful.

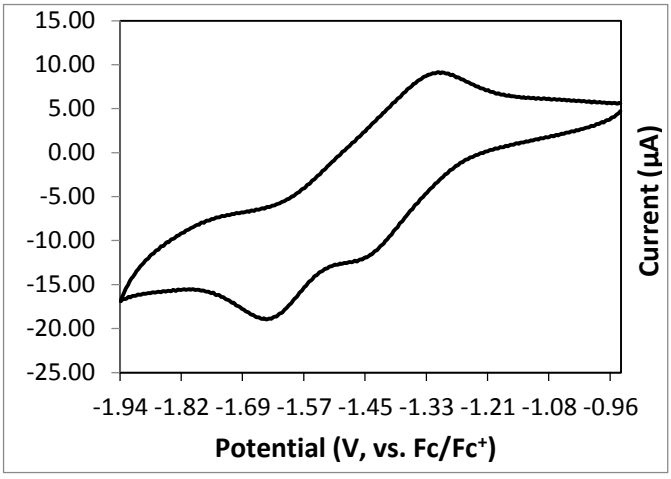

Figure 17 Room temperature cyclic voltammogram of **2** (5 mM) in THF at 500 mV/s (*vs.* Fc/Fc^{+}, 0.1 M [NBu_4][PF_6] as supporting electrolyte) $i_{p/c}$ = -1.65 V; $i_{p/a}$ = -1.31 V; $E_{1/2}$ = -1.42 V.

An attempt to further reduce **1** or **2**, respectively, by addition of rubidium metal to form a potential uranium(IV) complex remained unsuccessful (Scheme 14). Prolonged heating at 80 °C of a benzene solution of either **1** or **2**, subsequent addition of naphthalene to form naphthalenide *in situ* and the addition of tetrahydrofuran as a donor solvent to help solubilise the alkali metal had no effect and no change in the ^{1}H-NMR spectrum was observed.

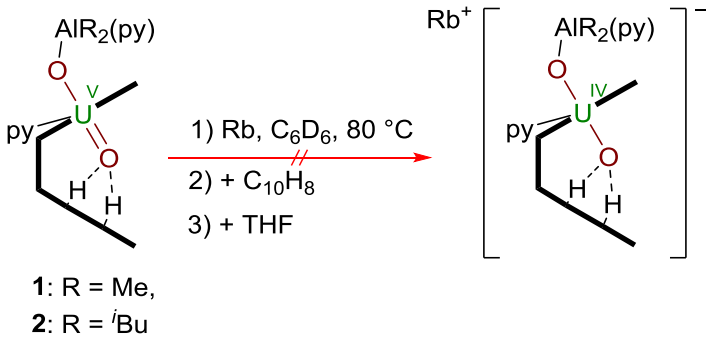

Scheme 14 Attempted reduction of **1** and **2** using Rb metal.

However, we have found that the AlR_2 group is readily substituted by a Group 1 metal cation by reaction with an alkyl or hydride reagent such as MeLi, NaH or KH; these experiments had been anticipated to deprotonate the two, likely acidic, pyrrole NHs in **1** and **2**. The following Section 2.1.3 gives an overview over these reaction.

2.1.3 Substitution reactions on Al(III)-uranyl(V) complexes

Reactions between benzene solutions of **1** with either one or two equivalents of the strong base LiMe affords solely [{(OUO)Li(py)(H_2L)}$_2$] **3** in moderate isolated yield (40 %), which remains U^V and doubly NH protonated (Scheme 15).

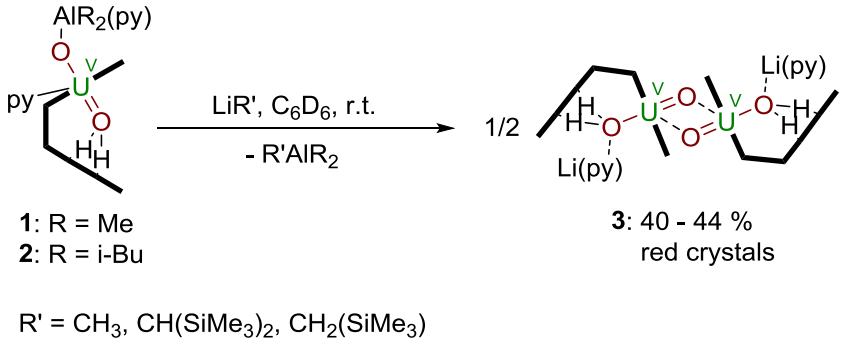

Scheme 15 Transmetalation of **1** and **2** using lithium alkyls.

This contrasts with the reactions of the uranyl(VI) Pacman complex $[UO_2(py)(H_2L)]$ **A** with single equivalents of LiR (R = H, NH_2, N^iPr_2, $N(SiMe_3)_2$, CPh_3, C_5H_5) that simply result in pyrrole deprotonation to afford the uranyl(VI) complex $[(UO_2)(py)(LiHL)]$,[130] and suggests that the hydrogen-bonding interaction between the f^1 uranyl oxo-group and the pyrrole protons is significant enough to attenuate deprotonation. The X-ray crystal structure of **3** is shown in Figure 18.

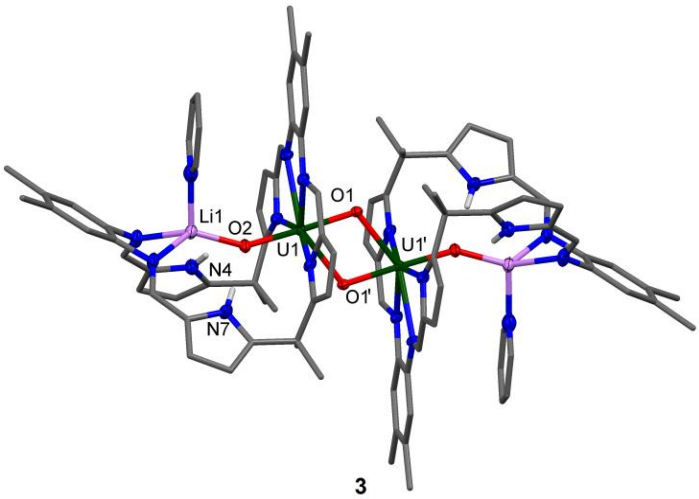

Figure 18 Solid state structure of **3**. For clarity, all hydrogen atoms except pyrrole NH and all solvent molecules are omitted (displacement ellipsoids are drawn at 50% probability). Selected bond lengths (Å): U1-O1 1.908(2), U1-O2 1.891(2), U1-O1' 2.372(3), N4-O2 3.269(4), N7-O2 3.198(5). O1-U1-O2 bond angle: 177.7(1)°. U1···U1': 3.5199(9) Å.

Compound **3** crystallises in a triclinic crystal system, and the structural solution was performed in space group *P*-1 with one molecule in the unit cell. The solid state structure shows that the lithium cation is coordinated by the imine groups of the macrocycle and that the uranium centre has migrated from its usual N_4 donor pocket to an alternative pyrrole-imine-imine-pyrrole motif. This results in the macrocycle folding at the *meso*-carbons and not the aryl groups, so resulting in a 'bowl-shaped' geometry.[124,131,132] As above, the U1-O1 and U1-O2 bond lengths of 1.891(2) and 1.908(2) Å are elongated compared to **A**, supporting a U^V oxidation state, and the oxo-groups are arranged in a *trans* disposition. The Li cation is thus sited within the cavity of the macrocycle, bound to the uranyl *endo*-oxo atom, the two imine groups, and a molecule of pyridine. As in the other complexes the uranyl is five-coordinate in the equatorial plane but the site which was occupied by the donor solvent is now filled by

the *exo*-oxo-group of its counterpart in the dimer, resulting in a diamond-shaped U_2O_4-cation-cation interaction.[41,133,134] The uranium-uranium separation in this dimer is short at 3.5199(9) Å, but similar to other complexes previously reported by us, for example 3.4487(4) Å in the uranyl(V) yttrium dimer [{$UO_2Y(py)_2(L)$}$_2$].[60]

Treatment of **2** with one equivalent of $LiCH_2SiMe_3$ or $LiCH(SiMe_3)_2$ in benzene also yielded **3** as verified by ^{1}H-NMR spectroscopy and crystal structure analysis (unit cell check).

In contrast, reactions between **1** or **2** and an excess of LiH in the donor solvent pyridine at 40 °C results in the formation of the known, triply lithiated, uranyl(V) complex [$(py)_3$(LiOUO)(py)({Li(py)}$_2$L)] $\mathbf{A^{3Li}}$ (Scheme 16).[128]

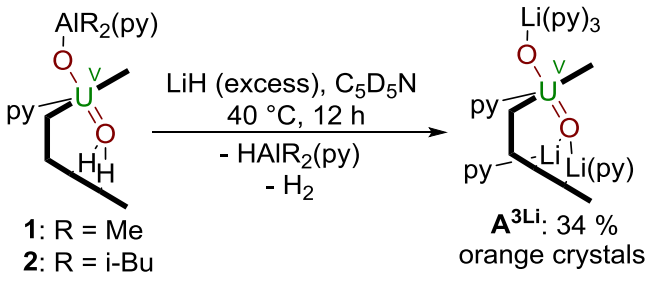

Scheme 16 Formation of triply lithiated uranyl(V) Pacman $\mathbf{A^{3Li}}$ upon treatment of **1** or **2** with excess LiH in pyridine at 40 °C for 12 h.

The difference in ability of the two types of Li reagents (LiR *vs*. LiH) to effect N-H deprotonation is likely due to the nature of the reaction solvent. The use of pyridine stabilises the exogenous coordination of the Li cation to the uranyl oxo-group, whereas in benzene, the reorganization of the uranyl coordination pocket allows for maximum interaction of the Li cation with the macrocycle. In support of this, the addition of pyridine to a benzene solution of **3** shows a rearrangement from the bowl-shaped structure to [$(py)_3$(LiOUO)(py)(H_2L)] **4**, possessing the classical Pacman structure (Scheme 17). This suggests that the bowl-shaped structure is only favoured in a non-coordinating solvent.

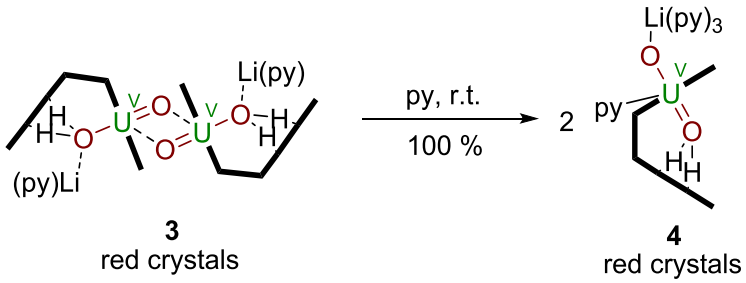

Scheme 17 Addition of pyridine to **3** results in the complete conversion to **4**.

Exogenous coordination of a Li cation was also seen in the cleavage products of the heterobimetallic lanthanide-uranyl(V) dimers [{(UO_2)Ln $(py)_2$(L)}$_2$] (Ln = Sc, Y, Ce, Sm, Eu, Gd, Dy, Er, Yb, Lu) to yield [$(py)_3$(LiOUO)Ln$(py)_2$(L)].[135]

The synthesis of **4** completes the series of previously reported lithiated uranyl Pacman complexes,[128] where syntheses using LiH, Li silyl amides and Li alkyls have yielded the complexes [($OU^{VI}O$)(py)({Li(py)}HL)] $\mathbf{A^{Li}}$, [$(py)_3$($LiOU^{V}O$)(py)({Li(py)}HL)] $\mathbf{A^{2Li}}$ and [$(py)_3$($LiOU^{V}O$)(py)({Li(py)}$_2$L)] $\mathbf{A^{3Li}}$. A comparison of the characteristic bond distances and angles of the named complexes is given in Table 1.

The bond distances for these complexes are the same within the standard deviation, except for the uranyl(VI) complex $\mathbf{A^{Li}}$, which shows the short bond distance known for the uranyl(VI) moiety.[125]

Table 1 Comparison of characteristic bond distances an angles in Li uranyl Pacman complexes

Entry	Li-O-U^{V}=O **4**	O=U^{VI}=O···Li $\mathbf{A^{Li}}$	Li-O-U^{V}=O···Li $\mathbf{A^{2Li}}$	Li-O-U^{V}=O···$(Li)_2$ $\mathbf{A^{3Li}}$
U1=O1 (Å)	1.853(6)	1.794(4)	1.835(4)	1.859(3)
O2-U1 (Å)	1.884(7)	1.768(4)	1.879(4)	1.894(3)
Li-O2 (Å)	1.95(2)	---	1.93(1)	1.91(1)
O1···Li (Å)	---	2.06(1)	1.94(2)	1.980(9)/1.977(8)
O2-U1-O1 (°)	173.8(3)	176.1(2)	174.8(2)	174.2(1)
Li-O2-U1 (°)	166.6(8)	---	167.3(4)	169.2(3)

Treatment of **1** or **2** with NaH or KH in pyridine at room temperature results exclusively in the exchange of the aluminium cation for the respective alkali metal to yield $[(py)_3(NaOUO)(py)(H_2L)]$ **5** and $[(py)_3(KOUO)(py)(H_2L)]$ **6** (Na: 69 %, K: 65 %); in both of these cases, the lower pocket remains protonated (Scheme 18).

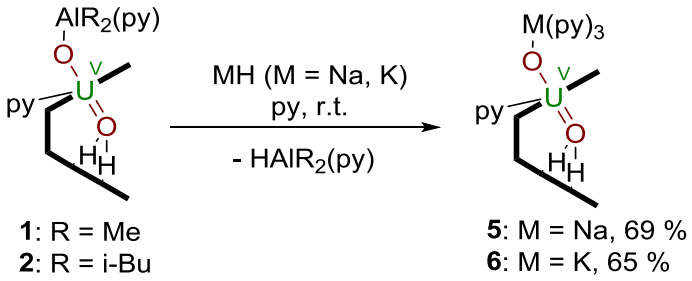

Scheme 18 Transmetalation of **1** and **2** using MH (M = Na, K) to yield **5** (Na) and **6** (K).

Compounds **4** – **6** were dissolved in pyridine. The solutions were allowed to stand, and upon slow solvent evaporation gave red crystals suitable for X-ray diffraction. Single crystalline material of **4** is shown in Figure 19.

Figure 19 Single crystals of $[(py)_3(LiOUO)(py)(H_2L)]$ **4**. Dimensions of the largest crystal (front): 3 mm × 2 mm × 2 mm. (Photo: Jamie McKinven)

The solid state structures of **4** – **6** are very similar and in contrast to **3** show the classic uranyl Pacman geometry (Figure 20). **4** and **5** are isostructural. Both compounds crystallise in a monoclinic crystal system and their structural solution was performed in space group *Cc* with four molecules per unit cell. **6** crystallises in an orthorhombic cell with space group $P2_12_12_1$ and four molecules per unit cell.

The main difference between the structures of **4**, **5** and **6** is that the U1-O2-M1 angle is nearly linear for the Li (**4**) (173.8(3)°) and Na (**5**) (174.7(6)°) complexes whereas the U1-O2-K1 angle is considerably bent (116.0(1)°). This is caused by a η^5-interaction between K and a U-bound pyrrolide ring due to the softness and size of K^+ (169 pm) compared to Na^+ (112 pm) and Li^+ (0.73 pm).[136] The uranyl bond

distances are for all three complexes in within the same region, showing values for U1-O1 of 1.853(6) Å (**4**), 1.844(5) Å (**5**) and 1.871(2) Å (**6**). Similarly the U1-O2 bond distances show values of 1.884(7) Å (**4**), 1.756(7) Å (**5**) and 1.837(2) Å (**6**). These values all represent the +5 oxidation state of the uranyl. Also the uranyl bond angle O1-U1-O2 remains practically linear for all three complexes 173.8(3)° (**4**), 174.2(3)° (**5**) and 176.1(1)° (**6**).

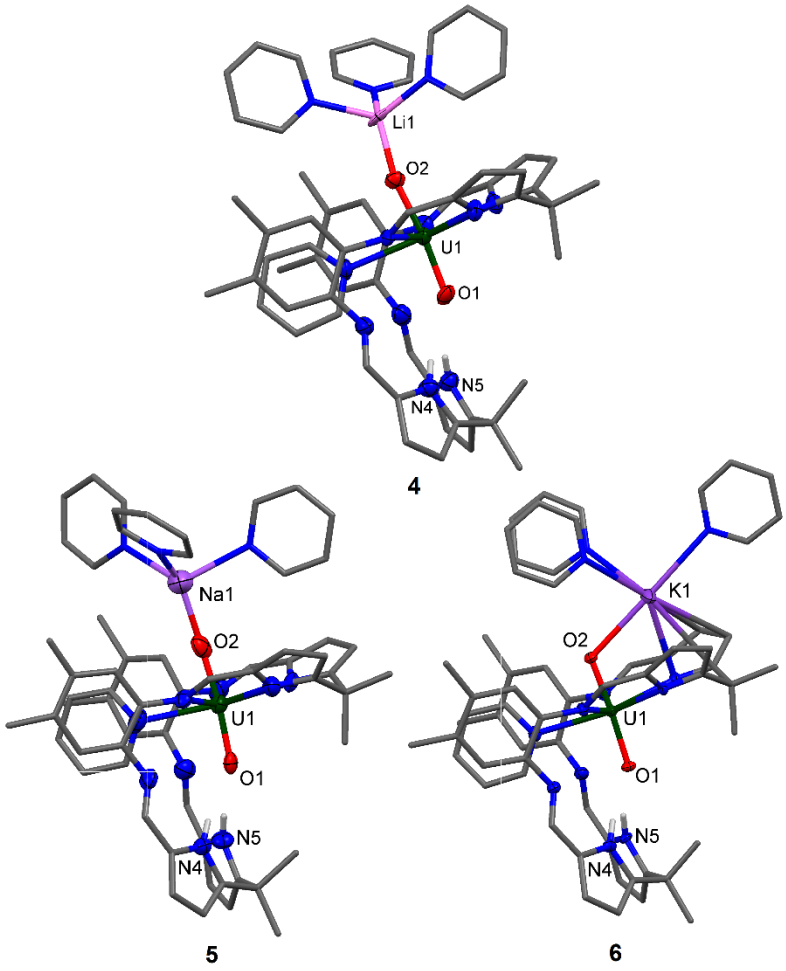

Figure 20 Solid state structures of **4, 5** and **6**. For clarity, all hydrogen atoms except pyrrole NHs and all solvent molecules are omitted (displacement ellipsoids are drawn at 50% probability). Selected bond lengths (Å) for **4**: U1-O1 1.853(6), U1-O2 1.884(7), O1-N4 3.09(1), O1-N5 3.10(1). O1-U1-O2 bond angle: 173.8(3)°. Selected bond lengths (Å) for **5**: U1-O1 1.844(5), U1-O2 1.856(7), O1-N4 3.010(9), O1-N5 2.988(8). O1-U1-O2 bond angle: 174.2(3)°. Selected bond lengths (Å) for **6**: U1-O1 1.871(2), U1-O2 1.837(2), O1-N4 2.898(4), O1-N5 2.932(4). O1-U1-O2 bond angle: 176.1(1)°.

The most prominent feature which distinguishes complexes **4** – **6** is the shift of the NH protons of the lower macrocyclic pocket to high frequencies. The ^{1}H-NMR

resonances of **4**, **5** and **6** in deuterated pyridine are successively shifted with increasing size of the alkali metal cation to 85.48 ppm (**4**), 91.11 ppm (**5**) and 93.06 (**6**). Additionally the ^{7}Li-NMR of **4** shows only one resonance at 88.48 ppm, confirming the exogenous mono-Li coordination. In contrast, the endogenous Li coordination reported for uranyl(VI) Pacman complex [$OU^{VI}O$(thf){Li(thf)}(HL)] has an NMR resonance for the Li^{+} at 0.66 ppm.[128]

A study of the redox chemistry of **6** by cyclic voltammetry in THF with 0.2 M [NBu_4][PF_6] as a supporting electrolyte at scan rates between 100 and 500 mV/s reveals a quasi-reversible reduction at $E_{1/2}$ = -1.31 V (*vs*. Fc/Fc^{+}) which is ascribed to a uranyl(V)/uranyl(VI) redox couple (Figure 21).

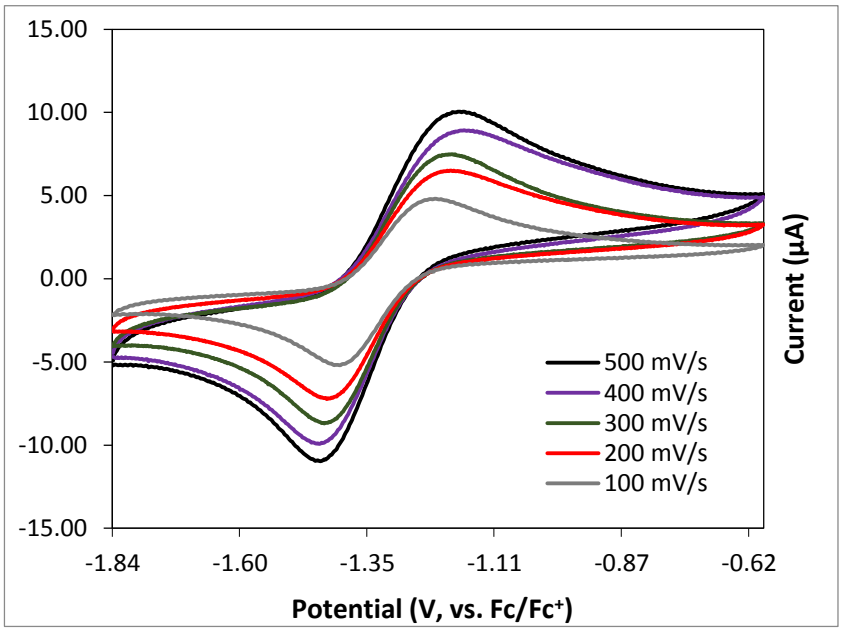

Figure 21 Room temperature cyclic voltammogram of **6** (3.2 mM) in THF at scan rates from 500 to 100 mV/s (*vs*. Fc/Fc^{+}); $E_{1/2}$ = -1.31 V.

The uranyl complexes given in Table 2 show that the observed redox couple of -1.31 V lies within the values of previously observed uranyl(VI)/uranyl(V) couples.

The reductive potentials of the alkali metals in non-aqueous solvents are not well reported. A review by Connelly and Geiger reports reductive potentials for K (in NH_3) at -2.38 V and for Na (in THF) at -3.04 V.[137]

Table 2 Comparison of reported $U^{VI}O_2/U^{V}O_2$ redox couples

Complex	Solvent	$E_{1/2}$ in V (*vs.* Fc/Fc$^+$)	Reference
6	THF	-1.31	This thesis
[(K)UO_2(salan-^{t}Bu$_2$)(py)]$_n$	pyridine	-1.74	[138]
$U^{VI}O_2$(saldien)	DMSO	-1.58	[139]
$U^{VI}O_2$(gha)	DMSO	-1.20	[140]
$U^{VI}O_2$(^{t}Buacnac)$_2$	CH_2Cl_2	-1.46	[141]
$U^{VI}O_2$(^{ArMe}acnac)$_2$	CH_2Cl_2	-1.52	[142]
$U^{VI}O_2$(^{ArBu}acnac)$_2$	CH_2Cl_2	-1.35	[142]
$U^{VI}O_2$(dbm)$_2$(thf)	CH_2Cl_2	-1.19	[70]

Ligands: salan-^{t}Bu = *N*,*N*′-bis(2-hydroxybenzyl-3,5-di-*tert*-butyl; saldien = *N*,*N*'-disalicylidenedi-ethylenetriaminate; gha = glyoxal bis(2-hydroxanil)ate; ^{t}Buacnac = ^{t}Bu-*N*C(Ph)CHC(Ph)*O*; ^{ArMe}acnac = 2,4,6-Me$_3$C$_6$H$_2$-*N*C(Ph)CHC(Ph)*O*; ^{ArBu}acnac = 3,5-^{t}Bu$_2$C$_6$H$_3$-*N*C(Ph)CHC(Ph)*O*; dbm = *O*C(Ph)CHC(Ph)*O*

As a consequence it had been tried to use transition metal hydrides in a similar manner in order to easily synthesise transition metal uranyl(V) complexes, however, the available hydrides such as [PPh_3CuH]$_6$ and Cp_2ZrHCl did not react and showed no transmetalation similar to the alkali metal hydrides. An orange-red solution of **1** and [PPh_3CuH]$_6$ in pyridine did not react after three days at room temperature and **1** was recovered as yellow crystals. To a mixture of Cp_2ZrHCl and **1** benzene was added, however, the poor solubility of the zirconium reagent inhibited any reaction. Addition of THF had no effect. Carrying out this reaction in pyridine was not possible because of the known strong interaction with Cp_2ZrHCl, forming a highly stable 18-electron complex Cp_2ZrHCl·py.[143]

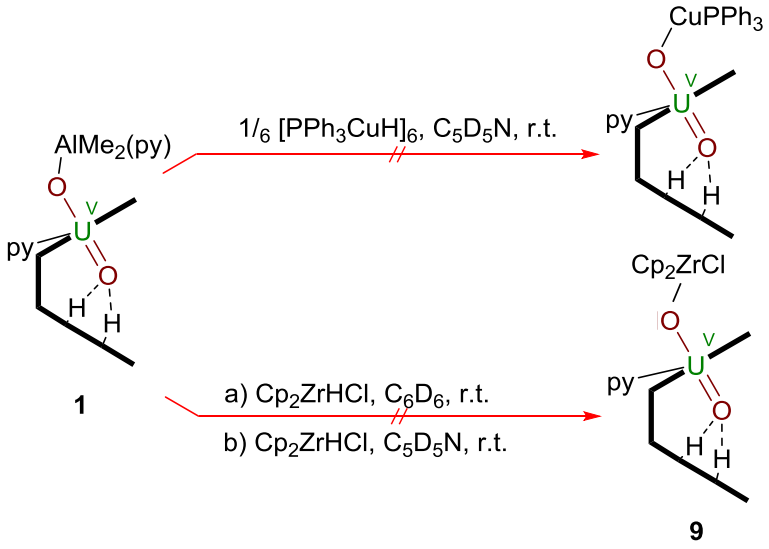

Figure 22 Attempted transmetalation reactions of **1** with transition metal hydrides.

In the light of previously reported boryl-mediated silylation of uranyl complexes[144][68] it was envisaged to further modify complexes **1** and **2** with the boron reagents $BH_3{\cdot}SMe_2$ and $BHCl_2{\cdot}thf$ in order to either substitute the coordinated aluminium for boron or to remove the uranyl oxygen completely *via* formation of R'$_3$B-O-AlR"$_2$(py) motifs, however, none of these reactions resulted in the formation of isolable material (Scheme 19).

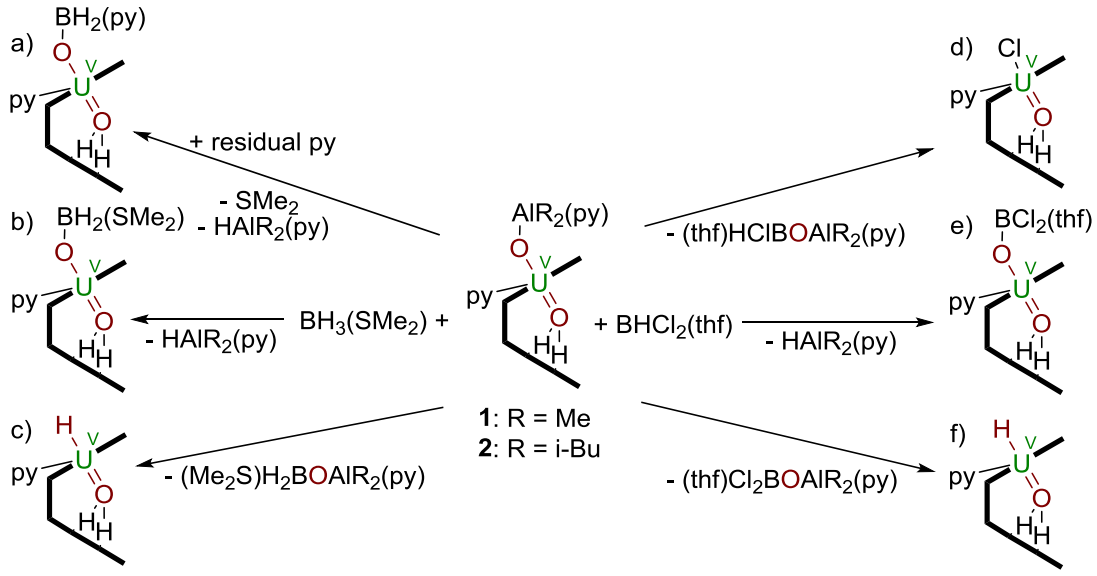

Scheme 19 Anticipated substitution reactions of **1** and **2** with $BH_3{\cdot}SMe_2$ and $BHCl_2{\cdot}thf$.

Attempted reactions using **1** using $BH_3{\cdot}SMe_2$ as well as treatment of **1** with $BHCl_2{\cdot}thf$ in C_6D_6 have produced inconclusive results. The addition of $BH_3{\cdot}SMe_2$ showed the formation of new paramagnetically shifted NMR resonances which can be attributed to a uranyl(V) complex (Figure 23), whereas the addition of $BHCl_2{\cdot}thf$ has led to complete decomposition.

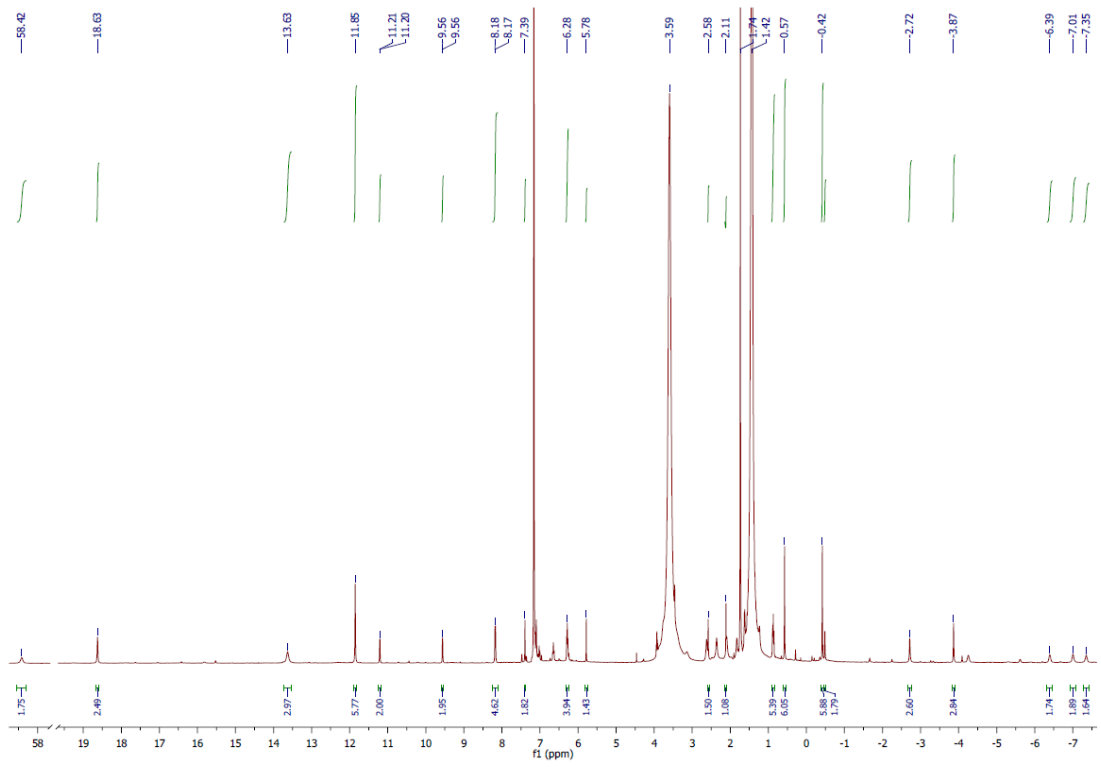

Figure 23 ^{1}H-NMR spectrum after treatment of **1** with $BH_3{\cdot}SMe_2$ (high frequency resonances omitted for clarity).

The spectrum shows resonances attributable to the methyl groups of the macrocyclic backbone (-0.42 ppm, 0.57 ppm) as well as resonances attributable to the methyl groups of the dimethyl dipyrromethane part of the macrocycle (-3.87 ppm, -2.72 ppm, 13.63 ppm, 18.63 ppm). The spectrum also features a resonance at 58.42 ppm attributable to the pyrrole N-H atoms and shows the sharp singlet of free dimethyl sulphide at 1.74 ppm, indicating the coordination of the boron atom to another donor, most likely the uranyl oxygen. However, any attempt to isolate this material was unsuccessful. Removal of all volatiles under vacuum resulted in the formation of a brown powder which was characterised as **A**.

The addition of one equivalent of Meerwein salt (Me_3OBF_4) in order to either remove Me-O-AlR_2 or to form Me-O-U^V=O led instantly to decomposition (Scheme 20). A similar reaction was observed using methyl triflate. The addition of one equivalent of HCl in diethyl ether afforded only the partly reformation of **A**.

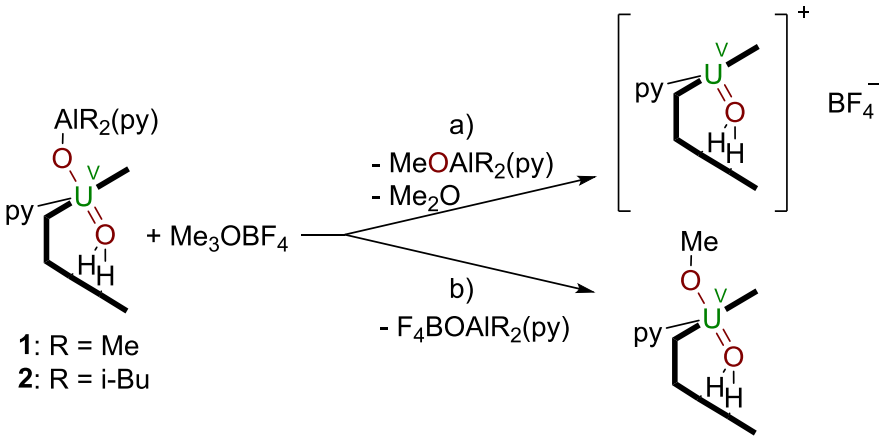

Scheme 20 Anticipated reactions of **1** and **2** with Meerwein salt Me_3OBF_4.

Since it could be proven that Li coordinates to the exogenous uranyl oxygen it was also tried to add LiCl to **1** in pyridine at 80 °C in the hope of removing $LiOAlR_2$ and generating a Cl-U=O motif (Scheme 21). This was unsuccessful and besides the reformation of uranyl(VI) Pacman **A** only minor amounts of indeterminable decomposition products were observed. Alternatively the formation of **4** could have been expected, but no resonances of that material were detected in the ^{1}H-NMR spectrum.

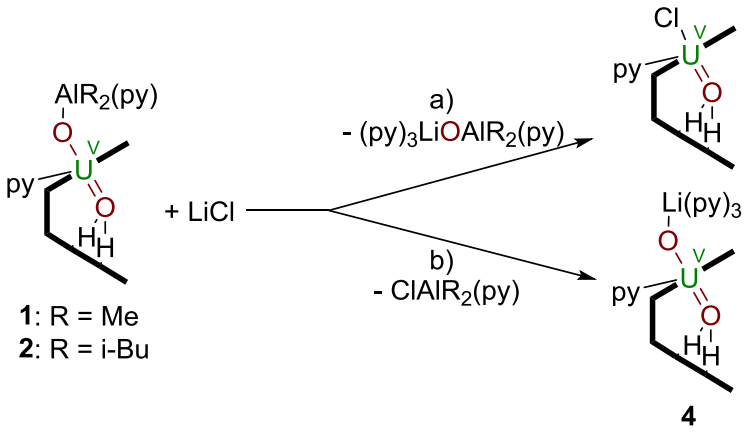

Scheme 21 Anticipated reactions of **1** and **2** with LiCl in pyridine.

It had also been tried to use $LiNEt_2$ to either substitute the AlR_2 group for Li, or remove $LiOAlR_2(py)$ in order to form an $Et_2N\text{-}O\text{-}U^{V}{=}O$ motif (Scheme 22). An equimolar mixture of **1** and $LiNEt_2$ which was heated to 80 °C in C_6D_6 showed in the ^{1}H-NMR spectrum resonances of **1**, **A** (relative ration 1 : 0.75) and a variety of paramagnetic resonances at low frequencies below -6 ppm as well as four individual resonances at high frequencies (39.02, 50.79, 64.43 and 68.51 ppm) with differing integral heights, indicating the probable formation of a mixture of mono- and doubly deprotonated species.

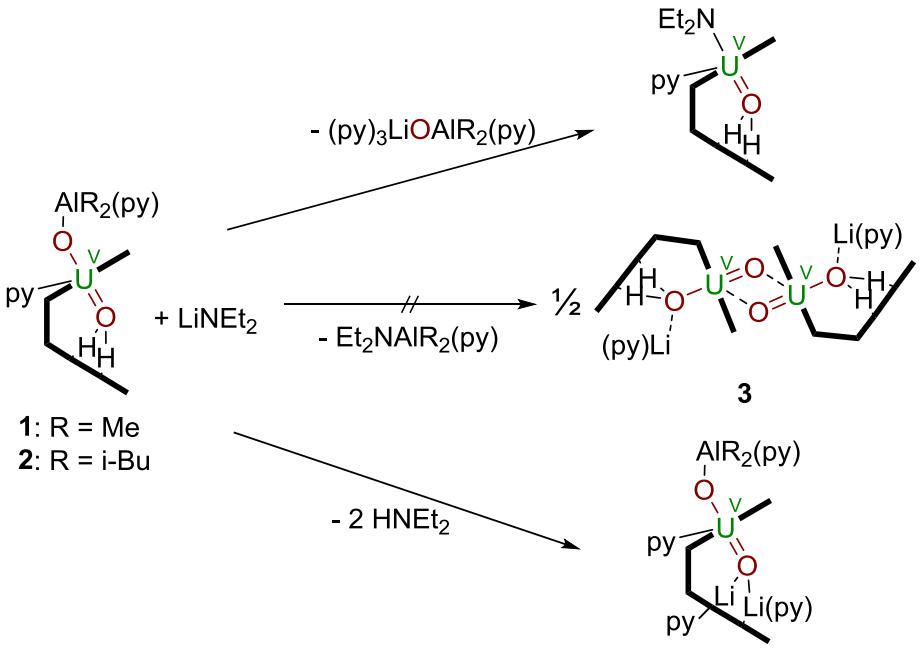

Scheme 22 Anticipated products of the reaction of **1** or **2** with $LiNEt_2$.

2.1.4 Catalytic functionalisation

It is clear from the above transmetalation reactions that the aluminium by-product is the alane or aluminium hydride. As such it was envisaged that formation of the reduced, alkali-metalated uranyl complexes **4** – **6** from **A** should be achievable using MH (M = Li, Na, K) and a catalytic amount of $AlH(^{i}Bu)_2$, as this latter reagent should be regenerated during the transmetalation step. As such, reactions using 10 mol% of DIBAL and an excess of MH in toluene at 70 °C for 72 to 96 hours (Table 1) were carried out and were found to cleanly generate **4**, **5** or **6** in essentially quantitative yields (Scheme 23).

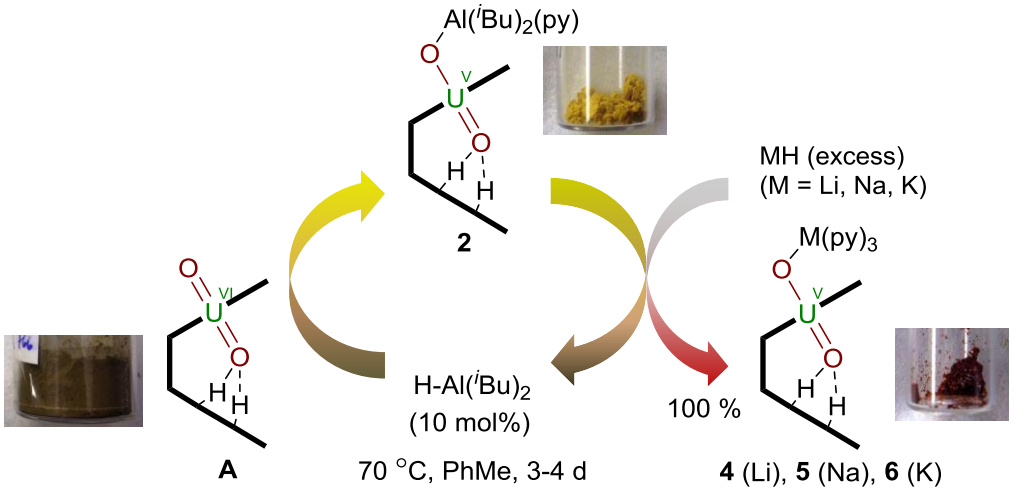

Scheme 23 Catalytic reduction of **A** using 10 mol% DIBAL to yield **4** – **6** in essentially quantitative yield. (Photos: Max McMullon)

To verify that the above reactions are indeed under catalytic control, reactions using KH were carried out using different amounts of DIBAL (Table 3). The reactions were heated at 70 °C from 24 to 240 hours and analysed by determining the ratios of the ^{1}H-NMR resonances of **6** to **A**. With no aluminium reagent 50% of **6** formed after 96 hours, and increasing the reaction time up to ten days afforded a 4:1 mixture of **6** and **A**. Treatment of **A** with 5 mol% of DIBAL only gave 20 % of **6** with 80 % of the starting material still present, even after a prolonged reaction time. As such, reactions that incorporate 10 mol% DIBAL are significantly accelerated.

Table 3 Control reactions for the HAl(*i*-Bu)$_2$-catalyzed reduction of A with KH

Entry	Mol% HAl(*i*-Bu)$_2$	Time/h	Ratio **6**/**A**
1	5	24	20/80
2	5	60	20/80
3	10	96	100/0
4	0	96	50/50
5	0	240	80/20

Reaction conditions: 70 °C, toluene, 5 equivalents KH

2.2 Reductive uranyl metalation using elemental alkali metals

Since the above reactions with aluminium reagents and alkali metal hydrides have shown the facile reduction of uranyl(VI) and the straightforward substitution of Al^{3+} for Li^+ (**4**), Na^+ (**5**) and K^+ (**6**) it was anticipated that mono-metalated uranyl(V) complexes should also form with the heavier alkali metal homologues Rb and Cs. Due to the fact that no hydride salts of Rb nor Cs exist it was envisaged that the treatment of a pyridine suspension of uranyl(VI) Pacman **A** with just the elemental alkali metal should result in the formation of the mono-metalated uranyl(V) complexes. The following section describes both the reductive uranyl metalation with elemental Rb (carried out in collaboration with Dr. Rianne M. Lord) and Cs. An attempt has been made to transfer this reactivity onto Ga metal as a possible reductant.

2.2.1 Reductive uranyl metalation using Rb

In order to extend the series of uranyl(V) alkali metal complexes we have treated a pyridine suspension of **A** with one equivalent of rubidium metal to generate the mono-metalated rubidium complex $[(py)_3(RbOUO)(py)(H_2L)]$ **7** (Scheme 24).

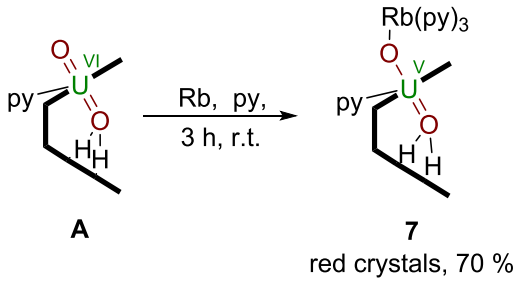

A **7**

red crystals, 70 %

Scheme 24 Reductive metalation of **A** by addition of one equivalent of metallic Rb forming **7**.

Stirring a brown solution of **A** in pyridine at room temperature in the presence of elemental rubidium results after three hours in the formation of a dark cherry red solution. Filtration and subsequent evaporation of the solvent resulted in the formation of intensely dark red prismatic crystals of $[(py)_3(RbOUO)(py)(H_2L)]$ **7** (Figure 24).

Figure 24 Single crystals of **7**. Dimensions: 5 mm × 3 mm × 2.5 mm (left, on Young's NMR tube cap); 1.5 mm × 1.5 mm × 0.8 mm (right, seen through microscope). (Photos: Rianne Lord)

The solid state structure of **7** is shown in Figure 25. **7** crystallises in an orthorhombic cell. The structural solution was performed in space group $P2_12_12_1$ and four molecules per unit cell.

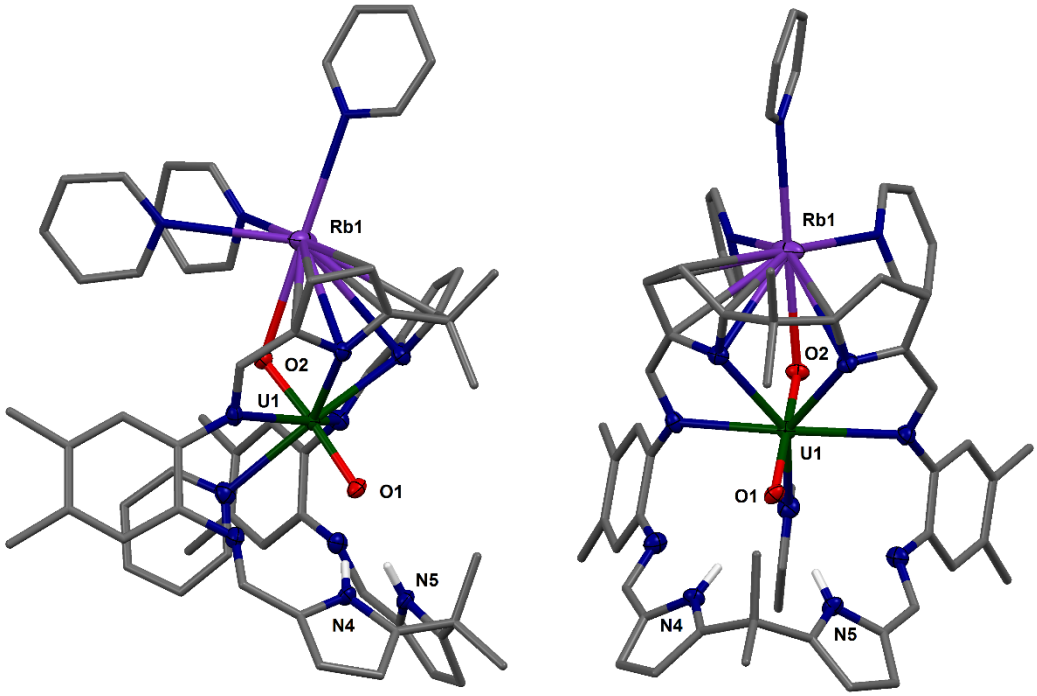

Figure 25 Solid state structure of **7**. For clarity, all hydrogen atoms except pyrrole NHs and all solvent molecules are omitted (displacement ellipsoids are drawn at 50% probability). Selected bond lengths (Å): U1-O1 1.871(3), U1-O2 1.837(3), O1-N4 2.940(5), O1-N5 2.906(5). O1-U1-O2 bond angle: 175.6(1)°.

The compound represents to our knowledge the first mono-metalated uranyl(V) rubidium complex. As seen in the complexes **4** – **6** compound **7** exhibits once more cation-cation interaction from the alkali metal to the exogenous uranyl oxygen. All

other uranyl complexes that contain rubidium cations exhibit only the uranyl(VI) dication and show no Rb-oxo interaction. In contrast, they form layers of uranyl(VI) polyhedra bridged by polyoxo anions like selenate in $Rb_2[(UO_2)(SeO_4)_2(H_2O)](H_2O)$,[145] molybdate in $Rb_6[(UO_2)(MoO_4)_4]$[146] or borate in $Rb_2[(UO_2)_2B_{13}O_{20}(OH)_5]$[147] with the Rb^+ cation occupying the interstitial layer.

The bond distances and angles of complex **7** are similar to those obtained for the potassium complex **6**. The most dominating feature of the crystal structure of **7** is the coordination of the Rb^+ cation to the two pyrrole rings of the macrocycle, coordinating to one ring with an η^5-interaction and to the other ring with an η^2-interaction, resulting from the size of the Rb^+ cation of 186 pm.[136] This leads to a bond angle of 115.8(1)° for the Rb1-O2-U1 coordination which is similar to the one observed for the K complex **6** (116.0(1)°). The bond distances for U1-O1 and U1-O2 show similar values to **6** as well as the distances of the endogenous oxygen O1 to the lower macrocyclic pocket. Table 4 shows a comparison of the main characteristics of the solid state structures of the alkali metal uranyl(V) complexes **4** – **7**.

Table 4 Comparison of bond distances and angles of alkali metal uranyl(V) complexes 4 – 7

Entry	Li-O-U^V=O **4**	Na-O-U^V=O **5**	K-O-U^V=O **6**	Rb-O-U^V=O **7**
U1-O1 (Å)	1.853(6)	1.844(5)	1.871(2)	1.871(3)
U1-O2 (Å)	1.884(7)	1.856(7)	1.837(2)	1.837(3)
O1-N4 (Å)	3.09(1)	3.010(9)	2.898(4)	2.940(5)
O1-N5 (Å)	3.10(1)	2.988(8)	2.932(4)	2.906(5)
M1-O2 (Å)	1.95(2)	2.176	2.707(3)	2.838(3)
O1-U1-O2 (°)	173.8(3)	174.2(3)	176.1(1)	175.6(1)
M1-O2-U1 (°)	166.6(8)	176.5(2)	116.0(1)	115.8(1)

Most significantly the uranyl(V) oxygen bond lengths decrease slightly with increasing size of the alkali metal. In particular the exogenous oxygen O2, which directly coordinates the Group I cation, is predominantly affected by this and decreases

from 1.884(7) Å in **4** (Li) to 1.837(3) Å in **7** (Rb). This tendency can also be seen in the hydrogen bond interaction of the endogenous oxygen O1 with the pyrrole protons of the lower macrocyclic pocket, which are the longest for **4** with 3.10 Å and shortest in **6** and **7** with 2.898(4) Å and 2.906(5) Å respectively. However, within standard deviation the bond distances of **5**, **6** and **7** are very similar, which can be seen in the similarities of the U1-O1 bond distances. Specifically **6** and **7** are very similar, with all bond angles and distances being statistically indistinguishable.

This similarity can also be observed spectroscopically in the ^{1}H-NMR shift for the pyrrole NH protons as well as in the IR data for the uranyl(V) asymmetric bond stretch (Table 5).

Table 5 Comparison of ^{1}H-NMR shifts and IR stretches of alkali metal uranyl(V) complexes 4 – 7

Entry	Li-O-U^{V}=O **4**	Na-O-U^{V}=O **5**	K-O-U^{V}=O **6**	Rb-O-U^{V}=O **7**
δ_H (NH, C_5D_5N) (ppm)	85.48	91.11	93.06	92.37
ν (O-U^{V}=O)$_{asym}$ (cm^{-1})	891	891	894	892

The NH protons are significantly shifted to higher frequencies with increasing alkali metal cation size, however, the shift of **6** (K) is practically identical to the one of **7** (Rb). The uranyl(V) asymmetric stretches are all observed at similar wavenumbers, and are shifted strongly from the parent uranyl(VI) complex **A** (958 cm^{-1}).

Even though the synthesis of complex **7** was carried out in pyridine it had been found that the material is unstable in this solvent. A single crystal of **7** was dissolved in pyridine-d_5 and its ^{1}H-NMR spectrum was recorded after three, seven, nine, eleven and 17 days. **7** reacts back to the starting material uranyl(VI) Pacman **A**. After three days in pyridine the percentage of **7** drops already to 25 %. After 17 days only 3% of the uranyl(V) complex remains. Table 6 lists the percentage of **7** *versus* **A** over time. However, it cannot be fully excluded that the deuterated pyridine used for this

experiment was contaminated with trace amounts of moisture or air which could have ultimately led to the disintegration of the complex.

Table 6 Relative ratio of 7 to A over time

Time (d)	**7** (%)	**A** (%)
0	100	0
3	25	75
7	17	83
9	14	86
11	10	90
17	3	97

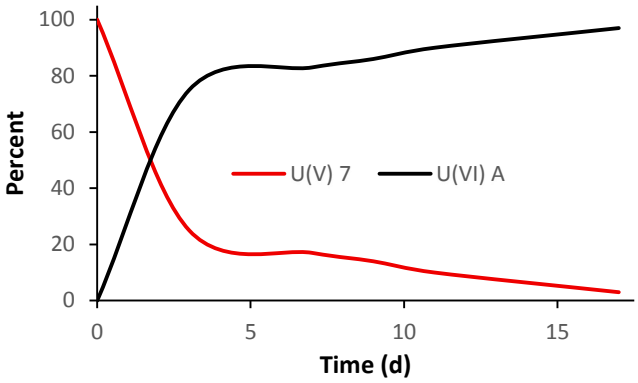

Complex **7** was additionally examined using variable temperature (VT) ^{1}H-NMR spectroscopy.

The VT-NMR measurements were carried out between 240 K and 340 K on a single crystal which was dissolved in pyridine-d_5. Unfortunately this analysis was scheduled to a time when the amount of **7** was already decreased to 10%, and due to lack of starting material could not be repeated on a freshly prepared sample. However, the resonances of the impurity only affected the chemical shifts between 0 and 10 ppm, in which **7** shows only three resonances at 0.84 (s, 6H, Ph-CH_3), 5.20 (s, 2H), 5.38 (s, 2H). An initial spectrum was recorded at 300 K, after which the compound was cooled to 240 K and heated stepwise in increments of 10 K to 300 K, followed by two heating steps in increments of 20 K. The compound showed no signs of degradation at 340 K and gave after cooling to 300 K a ^{1}H-NMR spectrum identical to the one initially recorded. To our surprise the paramagnetic resonances of **7** showed no signs of splitting at low temperature nor of coalescence at elevated temperature. All resonances above 10 ppm however were shifted to higher frequencies with decreasing temperature while all resonances below 0 ppm were shifted to lower frequencies with decreasing temperature. Figure 26 shows the spectra recorded for **7** from 240 K to 340 K in the range of 17.5 ppm to -12 ppm. For clarity, the spectrum was cut between 9.80 – 5.20 ppm and 3.20 – 0.20 ppm to eliminate the resonances of **A**.

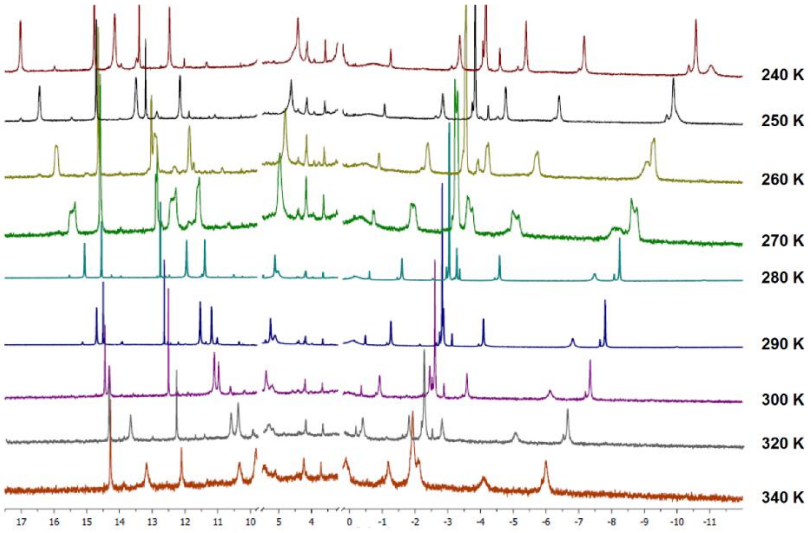

Figure 26 Variable temperature 1H-NMR spectra of **7** from 240 K to 340 K.

The chemical shift of the pyrrole protons of the lower macrocyclic pocket could also be determined. Although their resonance is very broad and weak in intensity the respective shifts from 240 K to 340 K could be assigned. Their values are given in Table 7 and show a shift to lower frequencies of about 3 to 6 ppm with every temperature increase of 10 K.

Table 7 Shift of the ^{1}H-NMR resonances of the pyrrole NH protons of 7 in dependency of the temperature

Temperature in K	N-H shift in ppm
240	119.2
250	113.5
260	108.5
270	103.3
280	99.9
290	96.1
300	92.3
320	86.2
340	80.5

Furthermore DOSY (Diffusion Ordered SpectroscopY) was applied in order to obtain the diffusion coefficient of uranyl(VI) Pacman **A** (83 %)and **6** (17 %). Its spectrum is given in Figure 27, but unfortunately the resonances of **A** and **7** overlap so that no difference in diffusion rates could be obtained. Besides this only the presence of the solvent pyridine is visible in the DOSY spectrum.

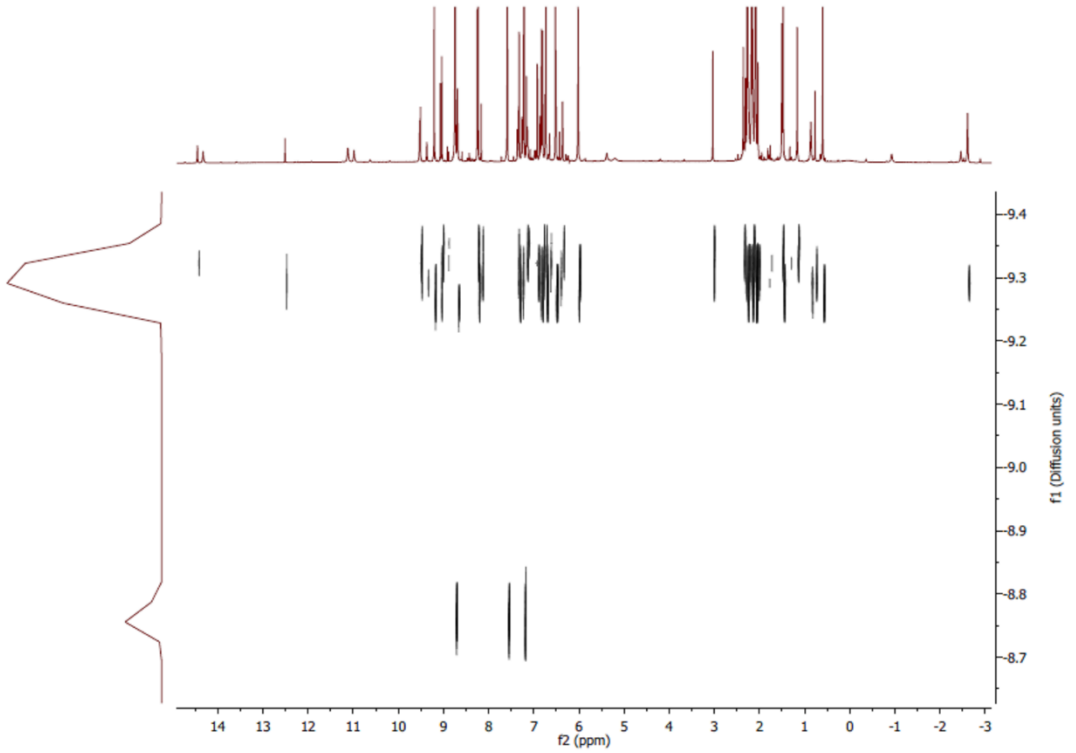

Figure 27 DOSY spectrum of the mixture of **7** and **A** in pyridine.

It was attempted to further substitute the pyrrole NH protons of the lower macrocyclic pocket by reacting **A** with an excess of Rb metal. The brown suspension reacted upon sonication instantly to form an orange-red precipitate which was isolated by centrifugation. The ^{1}H-NMR showed paramagnetically shifted resonances which compare to the spectra of the previously described uranyl(V) alkali metal complexes. As expected, no resonances are found at high frequencies between 60 and 90 ppm, indicating that the pyrrole N-H atoms are replaced by the alkali metal.

From these data it seems very likely that the uranyl(V) complex $[(py)_3(RbOUO)(py)(\{Rb(py)\}_2L)]$ has formed in this reaction (Scheme 25). However, no crystals suitable for X-ray crystallography could be grown from this material.

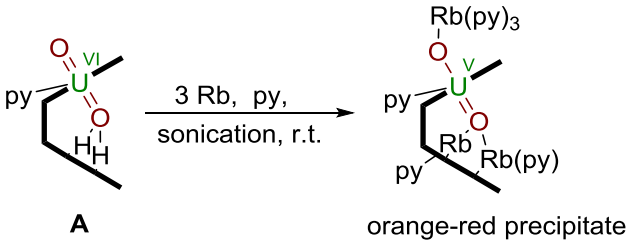

Scheme 25 Reductive metalation of **A** by addition of three equivalents of metallic Rb with deprotonation of the lower pocket of the macrocycle.

2.2.2 Reductive uranyl metalation using Cs

To complete the series of mono-metalated uranyl(V) alkali metal complexes a brown suspension of **A** was treated with one equivalent of metallic caesium in pyridine, and after 30 minutes yielded a dark red solution. The solution was filtered and allowed to crystallise by solvent evaporation to give small rectangular crystals of the first mono-metalated caesium uranyl(V) complex $[(CsOUO)(py)(H_2L)]_6$ **8** (Scheme 26).

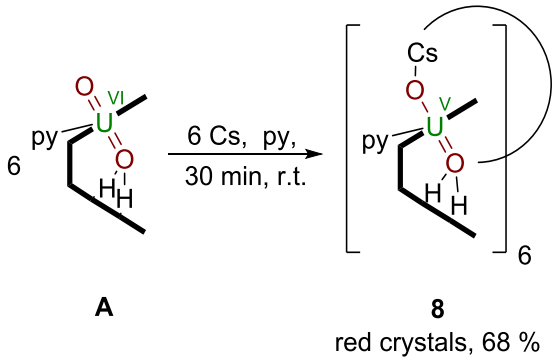

Scheme 26 Reductive metalation of **A** by addition of one equivalents of metallic Cs forming **8**.

The complex crystallises in very small, red, translucent crystals. Figure 28 shows a crystal of **8** mounted on the goniometer head MicroLoop™ for X-ray diffraction studies. The size of the depicted crystal is 0.05 mm × 0.04 mm × 0.03 mm.

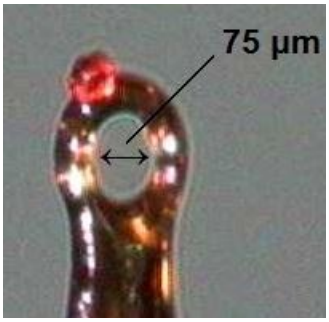

Figure 28 Single crystal of **8** mounted on the goniometer head MicroLoop™ for X-ray diffraction studies. Size of the crystal: 0.05 mm × 0.04 mm × 0.03 mm.

Complex **8** crystallises in a trigonal cell, and the structural solution was performed in space group *R*-3. The unit cell contains three formula units and has a large volume of 23880.5(8) $Å^3$. The solid state structure of the complex is shown in Figure 29.

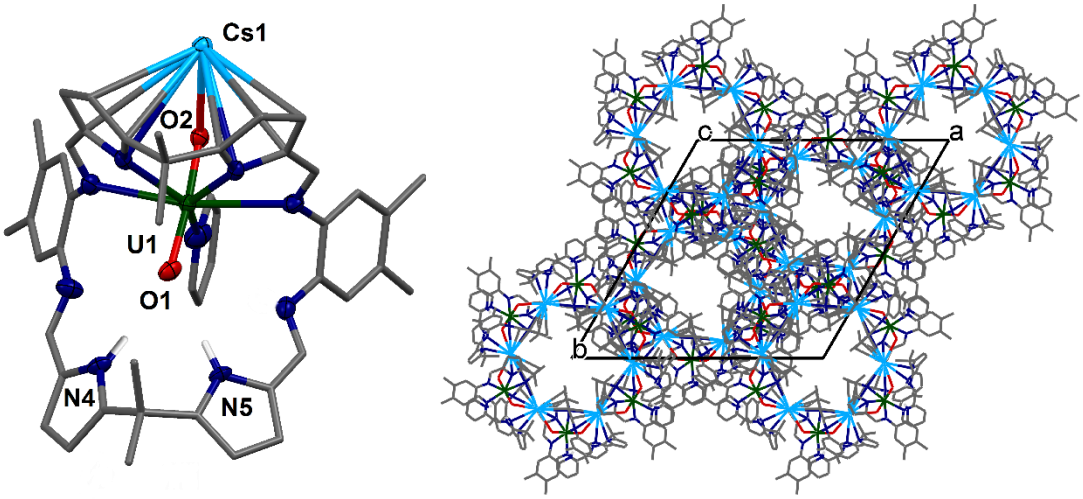

Figure 29 Solid state structure of **8**, depicting the asymmetric unit (left) and the crystal packing in the direction of the crystallographic *c*-axis (right). For clarity, all hydrogen atoms except pyrrole NHs and all solvent molecules are omitted (displacement ellipsoids are drawn at 50% probability). Selected bond lengths (Å): U1-O1 1.857(6), U1-O2 1.833(6), O1-N4 3.01(1), O1-N5 2.92(1). Bond angles: O1-U1-O2: 175.2(3)°, Cs1-O2-U1 117.6(3)°.

In contrast to the lighter homologues of the alkali metal uranyl(V) complexes **4** (Li), **5** (Na), **6** (K) and **7** (Rb) which all show a monomeric complex with a triply solvated alkali metal, complex **8** crystallises as a ring of six metalated uranyl Pacman complexes, linked by the large Cs^+ cation *via* oxo coordination to the exogenous uranyl oxygen of one uranyl moiety to the endogenous oxygen of another (Figure 30).

The uranyl oxo distances U1-O1 and U1-O2 of 1.857(6) Å and 1.833(6) Å are similar to those reported above for the mono-metalated alkali metal uranyl(V) complexes **4** – **7** and represent the U(V) oxidation state. The Cs1-O2 distance of 2.976(9) Å results from the large ionic radius of the Cs^+ cation (202 pm).[136] The bond distance of the Cs^+ to the adjacent uranyl moiety is slightly longer with a Cs1-O1' distance of 3.440(8) Å. The uranyl bond angle O1-U1-O2 is essentially linear with 175.2(3)°, whereas the Cs1-O2-U1 and Cs1-O1'-U1' bond angles are bent, with values of 117.6(3)° and 104.0(3)°, respectively. The O2-Cs1-O1' moiety has an angle of 122.2(2)°, and is also bent out of the plane.

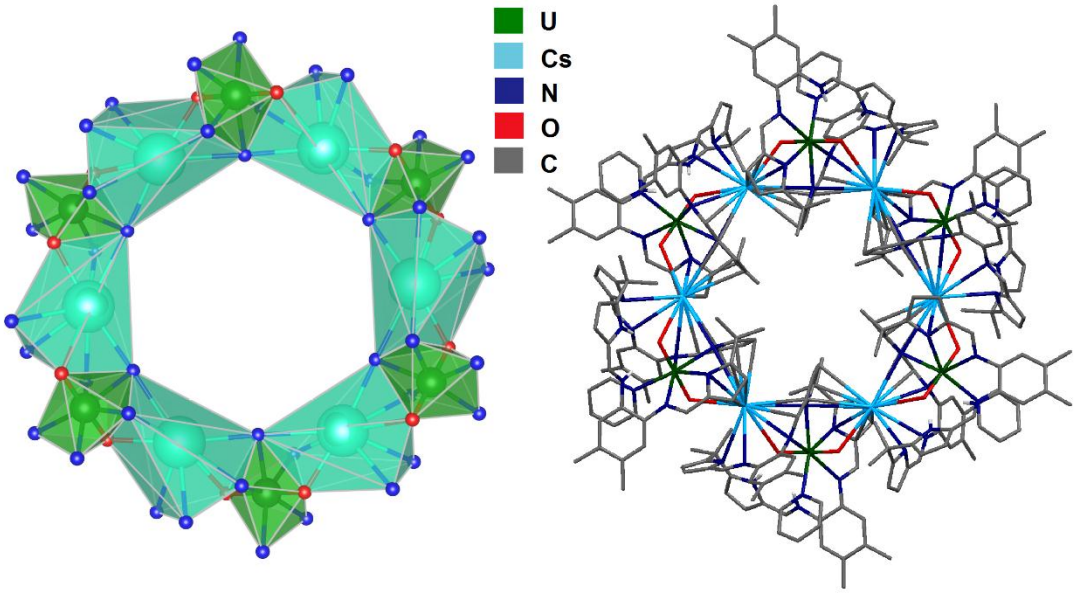

Figure 30 Depiction of the six-membered Cs(I)-uranyl(V) ring with coordination polyhedra (left) and within the macrocyclic Pacman framework (right).

The coordination polyhedra of **8** represent a regular hexagon and the capped stick model shows that the $[Cs(OUO)]_6$ motif resembles the shape of a crown, known from the crown ether 18-Crown-6 (Figure 30).[148,149] Along the essentially linear uranyl moiety between two adjacent Cs atoms the torsion angle Cs1'-O1(U1)O2-Cs1 is 68.4(3)°, which is close to the torsion angles for the three individual -O-CH_2-CH_2-O- moieties in 18-Crown-6 which are 67.6°, 75.4° and 79.7°, respectively. Similarly, the torsion angles along U1-O2-Cs1-O1' (173.8(3)°) and U1-O1-Cs'-O2' (166.7(3)°) resemble the -CH_2-CH_2-O-CH_2- torsion angles in 18-Crown-6 (155.2° and 165.8°, respectively).[149] However, the Cs1-Cs1''' separation across the cavity measures

13.4807(9) Å (= 1.35 nm), and the U1-U1''' distance is even bigger (16.518(1) Å), yet this distance is not "free" as it is obstructed by equatorial nitrogen coordination. The cavity itself is empty. A pyridine solvent molecule is located outside the ring. This cavity has a volume of 648 $Å^3$, and suggest that this complex could function as a uranium based host-guest complex.[150] A candidate for this could possibly be Buckminsterfullerene C_{60}, which has a diameter of 700 pm (7 Å).[151]

Robert Mulvey *et al.* have shown that heterobimetallic Group I and Group II metal amide complexes are able to interact in a similar way to form so called "inverse crown ethers" (ICEs). The term "inverse" indicates the interchanged Lewis acidic/Lewis basic positions compared to the classic organic ether: A Lewis acidic metal in an ICE occupies the space of a Lewis basic oxygen atom in an ether and *vice versa*.[152–155]

Recently the chemistry of uranium nano-materials has seen new impact, and novel hybrid materials such as uranium metal-organic nanotubes (UMONs) have been reported. Forbes *et al.* report the complexation of uranyl(VI) with an iminodiacetate ligand and the synthesis of a UMON showing the inclusion of highly ordered water molecules with a thermal reversibility at 37 °C (Figure 31).[156]

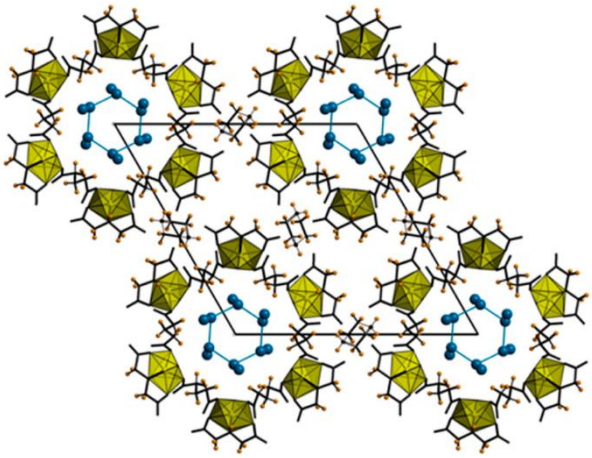

Figure 31 UMON with inclusion of highly ordered H_2O molecules.[156]

A wheel-shaped cation-cation complex featuring uranyl(V) and uranium(IV) in the Pacman macrocycle had previously been synthesised unintentionally in our research group (Figure 32).[157]

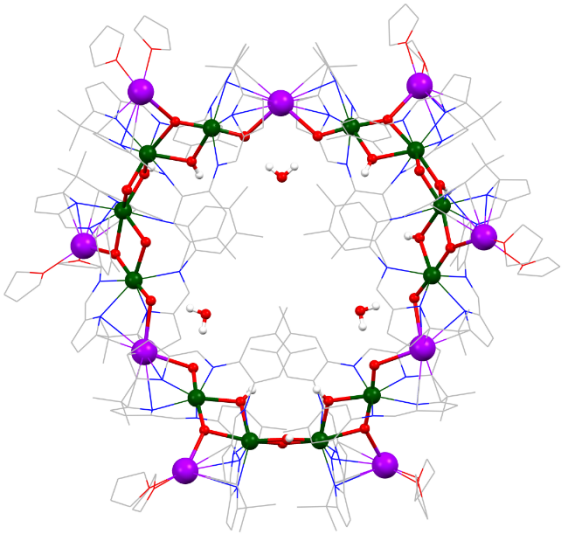

Figure 32 Wheel of $[K_9(U^VO_2)_6U^{IV}{}_6O_6(OH)_6(L)_6(THF)_{12}]\cdot 3H_2O$ held together by CCI.

This compound was accidentally synthesised as a binuclear uranyl Pacman complex $K_2[(Me_3SiOUO)_2(L)]$ was exposed to air and moisture for one month. It features six binuclear uranyl Pacman molecules each in a diamond-shaped U_2O_4 arrangement. The major motif is a binuclear U^{IV}/U^V Pacman moiety that assembles *via* K coordination at the U^V oxo atoms and *via* a μ-O and a μ-OH bridging ligand from one U^{IV} to the adjacent U^{IV}. No other such uranium Pacman complex is known to date.

Complex **8** is of great interest in the understanding of nuclear waste behaviour. For example, as a major component of nuclear fission, Cs is constantly being generated in nuclear reactors, and during the Chernobyl accident about 8.5×10^{16} Bq of ^{137}Cs were released into the environment. This amount represented 33 % of the total amount of ^{137}Cs which was present at that time in the reactor core.[158] With a half-life of 30.1 years[159] it emits β-radiation and decays to ^{137m}Ba, which in turn decays to the stable ^{137}Ba within 2.6 minutes, releasing strong γ-radiation with an energy of 0.66 MeV.[160] Ultimately, the water soluble Cs^+ cation can relatively easily replace K^+ ions in biological systems.[161] Its biological half-life varies from species to species and remains in lichen for 4.5 years, in fish 70 to 300 days, in children 57 days, in women 84 days and in men 105 days.[162] Thus, Cs released from nuclear waste streams or in nuclear accidents poses a strong environmental hazard and it is crucial to understand its behaviour in those systems.

Studies have shown that uranium(VI) compounds exist which contain Cs^+ cations, but to date no such complex has been investigated under reducing conditions. Thuéry and Masci report the coordination of Cs^+ to uranyl(VI) in calixarene[163] and pyrazine-2,3-dicarboxylic acid[164] complexes. Babo and Albrecht-Schmitt have shown that the high temperature synthesis of $Cs_2(UO_2)_2Si_8O_{19}$ (Figure 33) and $Rb_2(UO_2)_2Si_5O_{13}$ yields three-dimensional networks of uranyl(VI) forming six-ring voids and ten-ring channels in both compounds which are occupied by Cs^+ ions.[165]

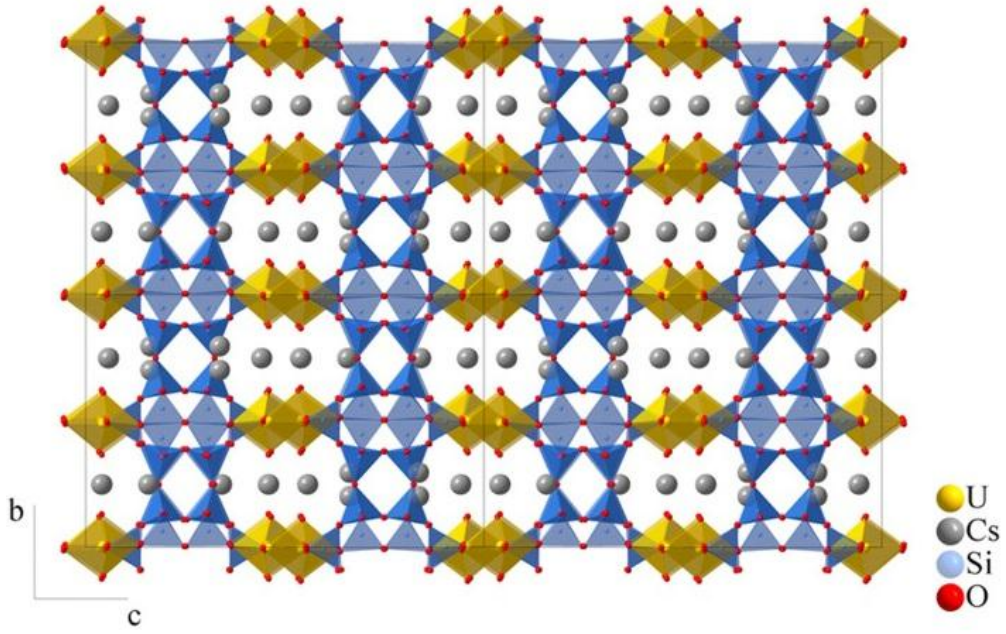

Figure 33 Crystal structure of $Cs_2(UO_2)_2Si_8O_{19}$ by Babo and Albrecht-Schmitt.[165]

In a similar way zur Loye *et al.* report the structural analysis of two caesium uranium oxides (Figure 34), which also show a network of equatorially linked uranyl(VI) polyhedra forming cavities which are occupied by Cs^+ cations. However, neither of the structures contains an interaction of the Cs^+ with the uranyl moiety.[166]

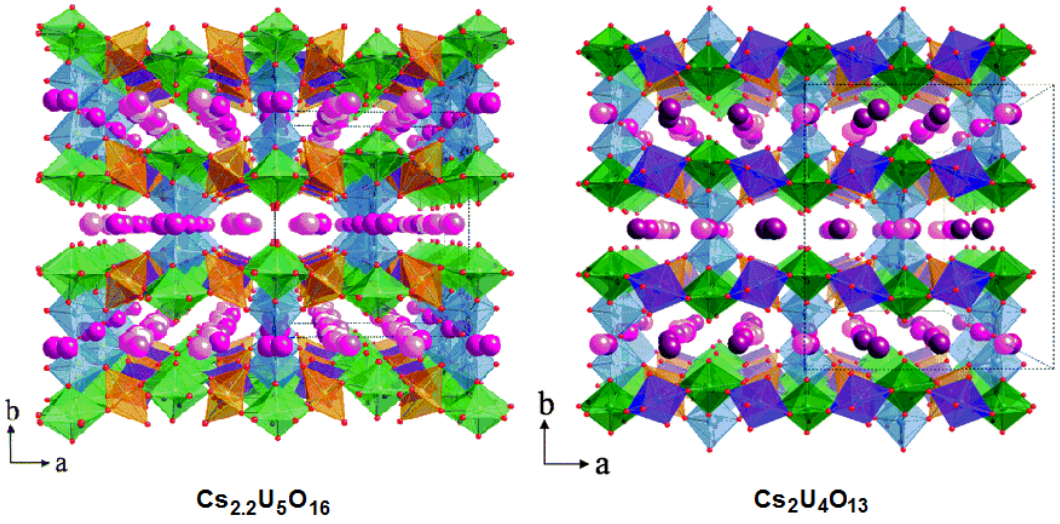

Figure 34 Crystal structure of $Cs_{2.2}U_5O_{16}$ (left) and $Cs_2U_4O_{13}$ (right). The differently coloured polyhedra represent crystallographically different uranyl polyhedra. Oxygen atoms are red, Cs atoms are pink (left) and purple (right).[166]

2.2.3 Reductive uranyl metalation using Ga

In an attempt to transform the reductive metalation seen for elemental rubidium and caesium it had been tried to use gallium to evaluate the overall reactivity of Group 13 metal reagents on uranyl(VI) Pacman. Using metallic Ga as the reducing agent in the presence of two equivalents of GaI_3 and three equivalents of **A** in pyridine was anticipated to generate $[(py)_x(I_2GaOUO)(py)(H_2L)]$ (Scheme 27).

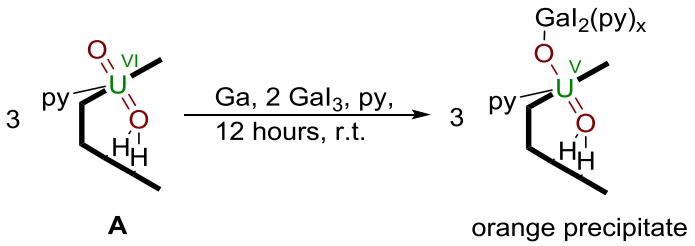

Scheme 27 Reduction of **A** using Ga and GaI_3, postulated to have formed a Ga^{III}-O-U^{V}=O motif.

Upon sonication the brown reaction mixture formed a red solution and an orange precipitate which was separated by centrifugation and analysed by ^{1}H-NMR spectroscopy (Figure 35).

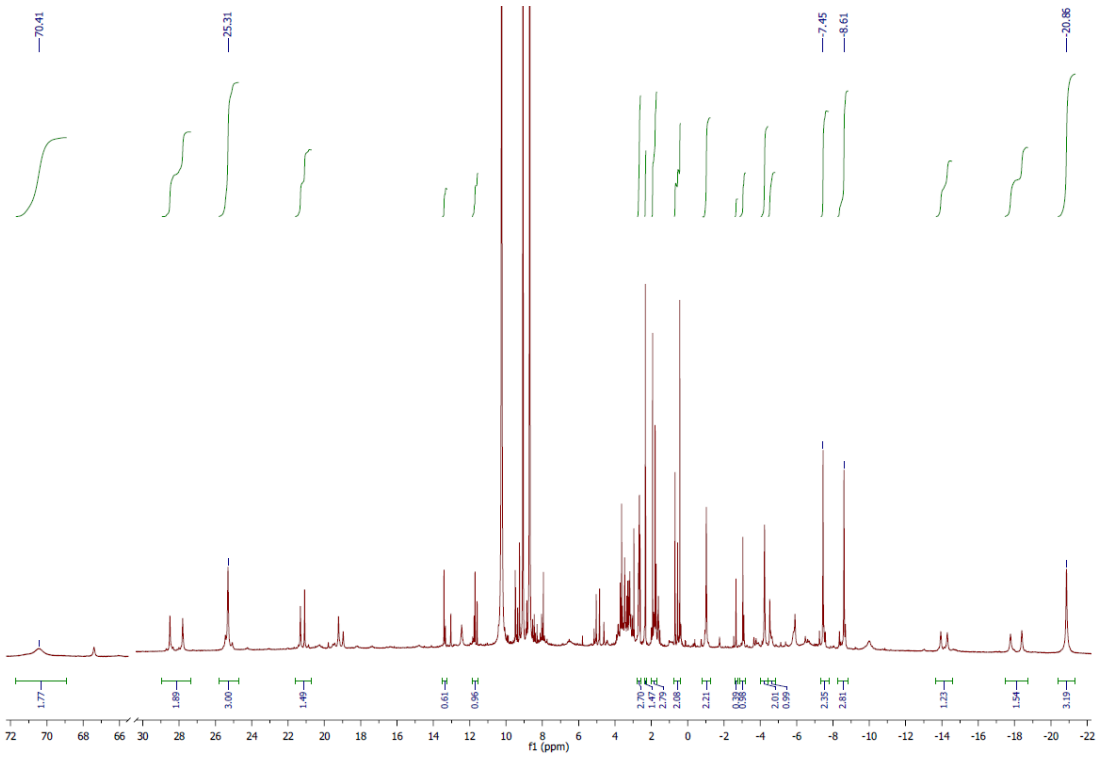

Figure 35 ^{1}H-NMR spectrum in C_5D_5N after treatment of **A** with Ga/GaI_3.

The spectrum showed the formation of paramagnetically shifted resonances, attributable to a uranyl(V) Pacman complex of the supposed formula $[(py)_x(I_2GaOUO)(py)(H_2L)]$. In particular, there are four resonances at -20.86, -8.61, -7.41 and 25.31 which can be attributed to the CH_3 groups of the dimethyl dipyrromethane moiety. Also a shift for the pyrrole N-H protons can be noted at 70.41 ppm. However, not all of the resonances of the remaining protons of the macrocycle can be properly assigned. The methyl resonances of the aromatic backbone cannot be found at all, and also the pyrrole C-H as well as imine =N-CH- and aromatic C-H resonances do not comply with the "classic" Pacman behaviour. Usually these have been found to integrate to two protons each in uranyl(V) Pacman, yet this spectrum shows a variety of different peaks integrating to one proton each, supposedly because the symmetry of the macrocycle is broken, maybe because of the formation of a dimeric complex. Any attempt to purify the material by recrystallisation remained unsuccessful and hence no further characterisation had been carried out.

2.3 Conclusion

The reported syntheses of the first reductive alumination of uranyl(VI) which enhance the basicity of the uranyl oxygen atoms has allowed the development of a catalytic route to the formation of exclusively mono-oxo metalated uranyl(V) alkali metal complexes. The acidity of the NH groups of the Pacman macrocycle is significantly decreased which allows these reactions to proceed with alkali metal hydrides. This catalytic functionalisation may provide an opportunity for new catalysed uranyl functionalisation reactions with other d- and f-Group metal cations, and may as well offer a general low-cost, one-pot route to the selective Group 1 cation metalation of d-block metal oxo complexes. It has been shown that the transmetalation of aluminated uranyl(V) can be driven to the formation of a dimeric cation-cation uranyl(V) complex by use of lithium alkyls in a non-coordinating environment. The reductive metalation by elemental alkali metals is exemplified in the synthesis of the first mono-metalated uranyl(V) complex coordinated to a Rb^+ cation as well as in the synthesis of a hexameric Cs(I)-uranyl(V) complex, completing the series of mono-metalated alkali metal uranyl(V) complexes.

3 Uranyl functionalisation with Group IV organometallic compounds, Group II metals and Zn metal

3.1 Uranyl functionalisation using Group IV organometallic compounds

The oxophilic character of the di-valent metallocene complexes of titanium and zirconium has been demonstrated in a variety of reactions by Uwe Rosenthal and co-workers, for instance in the activation of C-H, C-C and C-heteroatom bonds by bis(trimethylsilylacetylene) complexes of Group IV metals.[167,168] An example of a tandem C-H and C-Si bond activation in a decamethylhafnocene bis(trimethylsilyl)acetylene complex is shown in Scheme 28.

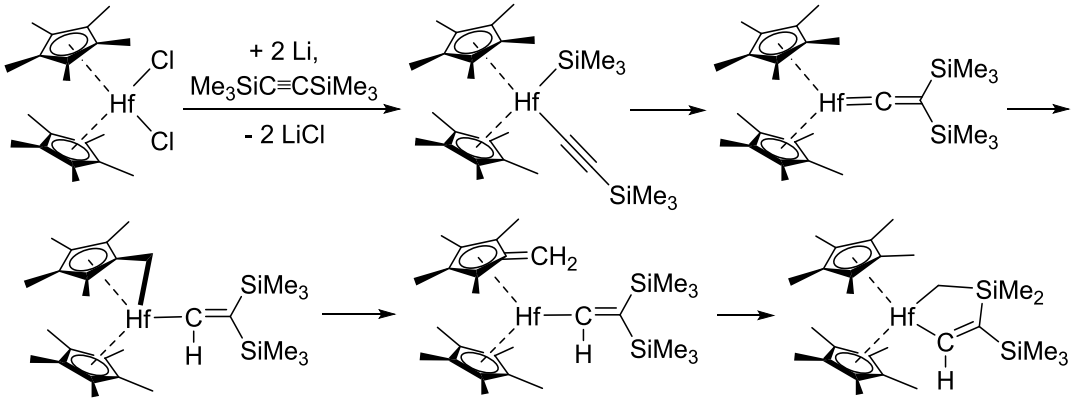

Scheme 28 Tandem C-H and C-Si bond activation in a decamethylhafnocene bis(trimethylsilyl)acetylene complex.[168]

It has been confirmed that the influence of the electronic nature of the cyclopentadienyl plays a vital role in the reactivity of these metallacyclopropanes upon reaction with water and carbon dioxide.[169] For example permethylated titanocene bis(trimethylsilylacetylene) complex reacts with water to form $Cp^*_2Ti^{IV}(OH)_2$, whereas the non-methylated complex yields the titanoxane $Cp_2Ti^{III}OTi^{III}Cp_2$ as the only product. In a similar way a reaction with CO_2 with permethylated titanocene bis(trimethylsilylacetylene) activates carbon dioxide and yields a mixture of $Cp^*_2Ti^{II}(CO)_2$ and $Cp^*_2Ti^{III}OCO_2TiCp^*_2$. Similarly, the slightly bigger permethylated zirconium complex results in carbon dioxide insertion into the cyclopropane moiety to

yield a zirconafuranone complex. The less sterically hindered non-methylated Zr complex reacts to the dimeric zirconafuranone.

Given the oxophilic nature of the titanium as well as the possibility of generating magnetic coupling between a d^1(Ti) and f^1(U) centre *via* a uranyl oxygen atom in a Ti^{III}-O-U^{V}=O motif the single electron reduction of uranyl(VI) to uranyl(V) by oxidation of Ti(II) to Ti(III) is an interesting target.

In this context the syntheses of the relevant Ti and Zr starting materials ($Cp_2Ti(\eta^2\text{-}C_2(SiMe_3)_2)$, $[Cp_2TiCl]_2$ and $Cp_2Zr(\eta^2\text{-}C_2(SiMe_3)_2)\cdot py$) were carried out by Dr. Johann A. Hlina. VT magnetic analysis was performed by Dr. Alessandro Prescimone and the relevant data evaluation was carried out by Dr. Nicola Magnani at the Institute for Transuranium Elements in Karlsruhe, Germany.

3.1.1 Uranyl functionalisation with Ti(II) and Ti(III)

Treatment of **A** with one equivalent of $Cp_2Ti(\eta^2\text{-}C_2(SiMe_3)_2)$ in benzene at room temperature results in the formation of a pale brown solution which affords upon work-up the red Ti(III)-uranyl(V) complex [(py)(Cp_2TiOUO)(py)(H_2L)] **9**, in 73 % yield (Scheme 29). Similarly the combination of a benzene suspension of **A** with 0.5 equivalents of $[Cp_2TiCl]_2$ resulted, after sonication at 70 °C for 20 minutes in the formation of an orange-yellow solution which afforded after slow solvent evaporation dark red crystals of the new Ti(IV)-uranyl(V) complex [((Cl)Cp_2TiOUO)(py)(H_2L)] **10** in 72 % yield, suitable for X-ray structural analysis.

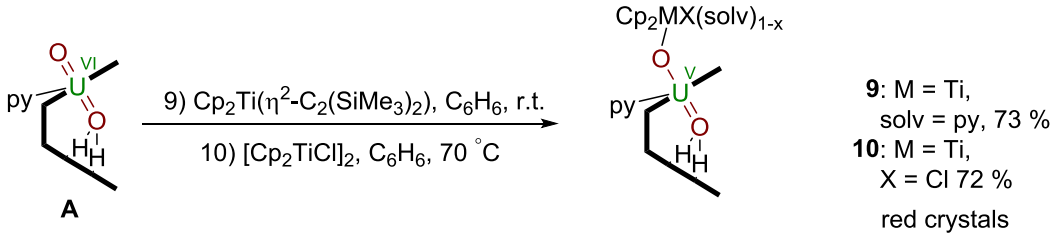

Scheme 29 Metalation of uranyl(VI) using low-valent titanium reagents.

Complex **9** represents to our knowledge the first f^1-d^1 system, so the potential for oxo-mediated electron-coupling between the f^1 centre of the uranyl(V) and the d^1 centre of the titanium(III) was investigated by VT SQUID magnetometry on this

material. The magnetic susceptibility χ and the inverse susceptibility 1/χ are shown as a function of temperature T in Figure 36. No clear sign of magnetic coupling between the uranyl(V) and the titanium(III) centre can be ascertained from the shape of this curve. A ligand-field analysis assuming a pure spin 1/2 for the d^1 electron of the Ti(III) and a total orbital moment of J = 5/2 for the f^1 electron of the uranyl(V) (carried out by Dr. Nicola Magnani, Institute for Transuranium Elements, Karlsruhe, Germany, *cf.* Section 6.2.10) shows that the antiferromagnetic exchange interaction is indeed relatively small.[170] As to why no slow magnetic relaxation can be seen in the ac measurements and therefore the molecule is not a single-molecule magnet it can be argued that the total magnetic moment of the molecule is too low and the weak antiferromagnetic coupling between Ti and U gives rise to an effective magnetic transition pathway allowing a very fast relaxation of the magnetisation of the molecule.

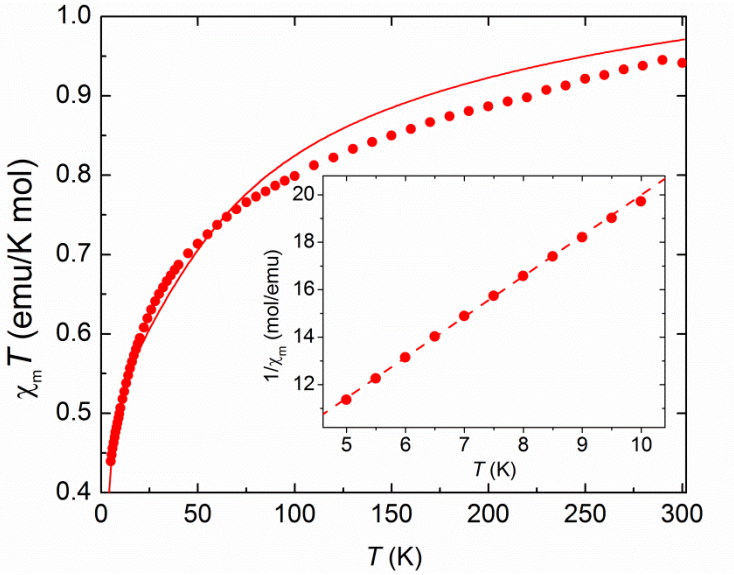

Figure 36 Magnetic susceptibility of complex **9** as a function of temperature, plotted as χT *vs.* T (main panel) and 1/χ *vs.* T (inset). Dots: experimental data. Solid line: ligand-field calculation. Dashed line: Curie-Weiss fit.

In addition to the successful reduction of uranyl(VI) with titanium(II) a similar reaction using Cp^*_2Co as the reductant, was taken to target a Co^{III}-O-U^{V}=O motif (Scheme 30).

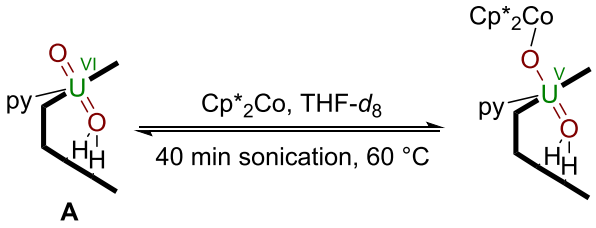

Scheme 30 Attempted reductive metalation of **A** using Cp^*_2Co.

A mixture of **A** and Cp^*_2Co in THF-d_8 was sonicated at 60 °C for 40 minutes to form a dark red-brown solution and a red-brown precipitate. After centrifugation the mother liquor was analysed by ^{1}H-NMR spectroscopy and showed the formation of paramagnetic resonances. The precipitate was dissolved in pyridine-d_5 and showed the clean formation of a paramagnetic product which was assigned to a uranyl(V) Pacman complex with Co^{III} coordination (Figure 37).

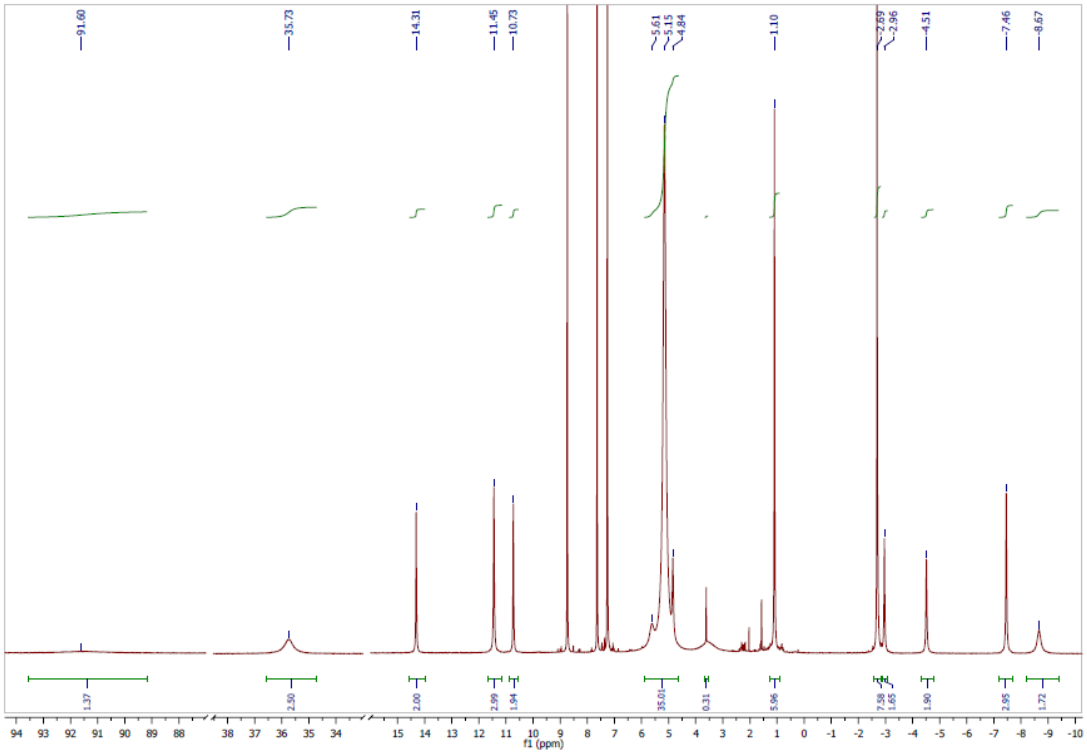

Figure 37 ^{1}H-NMR spectrum assigned to a Co(III) uranyl(V) Pacman complex.

The spectrum contains paramagnetic chemical shifts as would be expected for a uranyl(V) Pacman macrocycle complex, with NH resonances shifted to the high frequency of 91.60 ppm. At –2.69 ppm and 1.10 one finds two resonances ascribable to the methyl groups of the phenyl backbone of the macrocycle. The four methyl

groups of the dimethyl dipyrromethane moiety are shifted to low frequencies -8.67 ppm and -7.46 ppm as well as higher frequencies of 11.45 ppm and 35.73 ppm. At 5.15 ppm one finds one resonance that is attributable to the 30 hydrogen atoms of the pentamethyl cyclopentadienyl groups. It was attempted to isolate this material by crystallisation however, the only material that could be obtained was the starting material Cp^*_2Co and **A**, both verified by X-ray diffraction and ^{1}H-NMR spectroscopy. From this it can be concluded that Cp^*_2Co forms with uranyl(V) and outer sphere complex with no direct cation-cation interaction, most likely due to the steric congestion invoked by the pentamethyl cyclopentadienyl rings. Scheme 31 illustrates the observed reactivity of Cp^*_2Co and **A**. In tetrahydrofuran solution a Co(III)-uranyl(V) complex forms as a precipitate which can be isolated and redissolved in pyridine. In pyridine solution the complex can be observed spectroscopically, however, upon crystallisation the starting material is reformed.

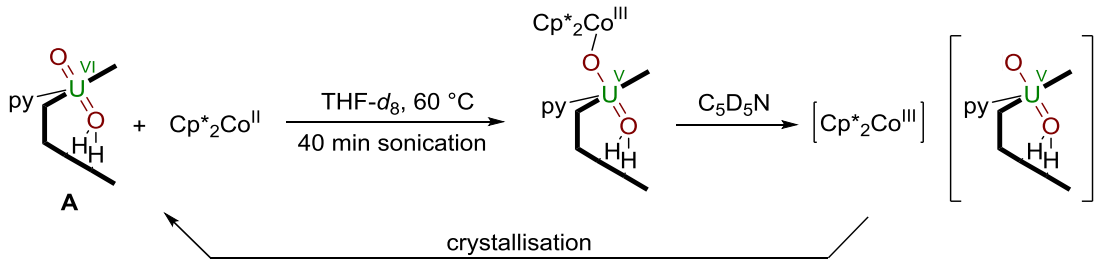

Scheme 31 Observed reactivity of Cp^*_2Co and **A**.

Similar reactivity of this kind had been previously observed by Hayton *et al*. in uranyl ^{Ar}acnac (Ar*N*C(Ph)CHC(Ph)*O*; Ar = 3,5-^{t}Bu$_2$C$_6$H$_3$) complexes and Cp_2Co as well as Cp^*_2Co have both been successfully used as a reductant to obtain outer sphere uranium(IV) and uranyl(V) complexes.[68,144,171] These results also speak for the formulation of an outer sphere complex which uranyl Pacman that could be written as $Cp^*_2Co^{III}[(OU^{V}O)(py)(H_2L)]$. It is thinkable that this results from the demanding sterics of the Cp^*_2Co, which does not allow the formation of a $Cp^*_2Co^{III}$-O-U^{V}=O motif.

3.1.2 Uranyl functionalisation using Zr(II) and Zr(IV)

The synthesis of Ti(III) complexes is relatively straightforward, and a number of low-valent titanium complexes have found applications as catalysts, for example in the McMurry reaction.[172,173] Because low-valent titanium compounds are readily accessible they can be used either as a molecular compound or prepared *in situ*.[174–177] In contrast, Zr(III) complexes remain relatively scarce, and only a few molecular Zr(III) complexes have been synthesised to date.[178–180] However, in light of the straightforward preparation of the Ti^{III}-O-U^{V}=O motif from $Cp_2Ti(\eta^2\text{-}C_2(SiMe_3)_2)$, it was anticipated that the reaction with the Zr congener $Cp_2Zr(\eta^2\text{-}C_2(SiMe_3)_2)\cdot py$ would give a similar result by forming a Zr^{III}-O-U^{V}=O bond. However, the treatment of uranyl Pacman **A** with the Zr(II) complex $Cp_2Zr(\eta^2\text{-}C_2(SiMe_3)_2)\cdot py$ remained unsuccessful, probably because of the formation of a rather unstable Zr(III) complex which prefers bulkier ligands for its stabilisation.[179,181] Eventually, $Cp_2Zr(\eta^2\text{-}C_2(SiMe_3)_2)\cdot py$ could be used as a Zr(II) starting material for the synthesis of the Zr^{IV}-O-U^{V}=O complex by *in situ* comproportionation with Cp_2ZrCl_2.

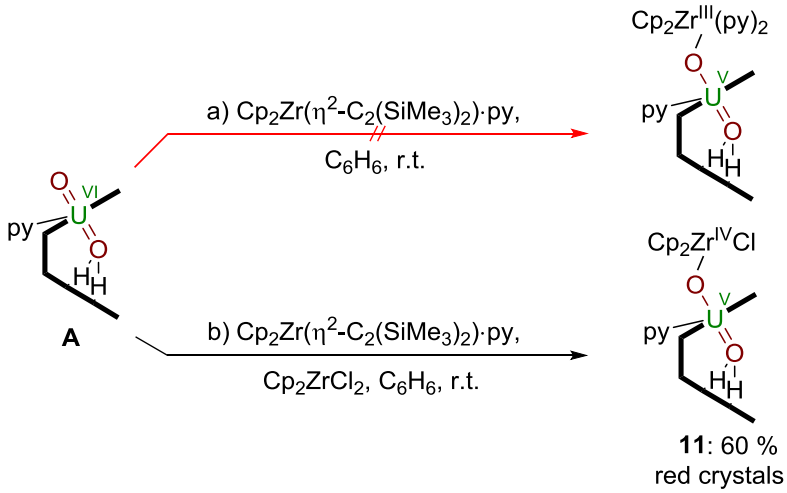

Scheme 32 Attempted reductive metalation of **A** using Zr(II) (a) and reductive metalation of **A** using Zr(II) and Zr(IV) (b).

The X-ray crystal structures of **9** and **10** were determined and show the expected coordination of Ti to the exogenous oxygen atom of the uranyl moiety in the classic wedge-shaped Pacman geometry (Figure 38). Complex **9** crystallises in a triclinic crystal system, and the structural solution was performed in space group *P*-1 with two molecules in the unit cell. Compound **10** crystallises in a monoclinic crystal system.

The structural solution was performed in space group $P2_1/c$ showing four molecules per unit cell. The uranyl oxo-groups adopt in both complexes a *trans* geometry, with an O1-U1-O2 angle of 175.3(3)° (**9**) and 177.43(9)° (**10**) and U1-O1 and U1-O2 bond lengths significantly elongated to 1.846(6) Å and 1.925(6) Å (**7**) as well as 1.841(2) Å and 1.979(3) Å (**10**) respectively, compared to the $O=U^{VI}=O$ bonds of 1.793(6) Å and 1.773(6) Å for **A**. Both Ti atoms in **9** and **10** are η^5 coordinated by two cyclopentadienyl rings, yet the Ti^{III} in **9** saturates its fourth coordination sphere by coordination of a pyridine molecule, which in **10** is occupied by chloride. Additionally, the Ti^{III}-O2 bond length of 2.155(6) Å in **9** is longer than the Ti^{IV}-O2 bond length of 1.952(3) Å in **10**, due to the higher formal charge of Ti^{IV} and its increased Lewis acidity compared to Ti^{III}. For comparison the Ti^{III}-O bond length in the reported $(Cp_2Ti]_2(\mu$-O) is 1.838(1) Å,[182] which is significantly shorter than in **9** and **10**, confirming that the uranyl oxygen acts towards the Ti as a donor and not like an oxide. More so the $Ti^{IV}=O$ double bond in $Cp^*_2Ti(O)$(4-phenylpyridine) has a distance of 1.665(3) Å, representing the Ti(IV) oxidation state and the Ti=O double bond character.[183]

The hydrogen-bonding interactions between the *endo*-oxo O1 and the two pyrrole protons in the vacant macrocyclic pocket, shown by O1···N4 3.09(1) Å and O1···N5 3.02(1) Å (**9**) and O1···N4 3.021(4) Å and O1···N5 3.099(3) Å (**10**) are slightly shorter than those in **A** (3.111(7) Å and 3.146(7) Å) and support again the enhanced oxo basicity of the f^1 cation.

The structural solution of the solid state structure of **11** was performed in the monoclinic crystal system $P2_1/c$ with four molecules in the unit cell, showing that this complex is isostructural to the Ti(IV) complex **10**. If the synthesis is carried out in the presence of Mg (*cf.* 3.1.3), compound **11-MgCl2** crystallises with one equivalent of $MgCl_2(py)_2$ in a monoclinic crystal system with space group $C2_1/c$ and eight molecules per unit cell. The uranyl oxo-groups adopt a *trans* geometry, with an O1-U1-O2 angle of 176.7(3)° and U1-O1 and U1-O2 bond lengths significantly elongated to 1.829(8) Å and 1.995(7) Å respectively, compared to the $O=U^{VI}=O$ bonds of 1.793(6) Å and 1.773(6) Å for **A**. The Zr atom in **11** is, as the Ti atom in **10** η^5-coordinated by two cyclopentadienyl rings, with the fourth coordination sphere occupied by chloride. Additionally, the Zr^{IV}-O2 bond length of 2.031(7) Å in **11** is longer than the Ti^{IV}-O2

bond length of 1.952(3) Å in **10**, due to the smaller ionic radius of Ti^{IV}. As for **9** and **10** the hydrogen-bonding interactions between the *endo*-oxo O1 and the two pyrrole protons in the vacant macrocyclic pocket of **11** are slightly shorter (O1···N4 3.09(1) Å and O1···N5 3.01(1) Å) than those in **A**.

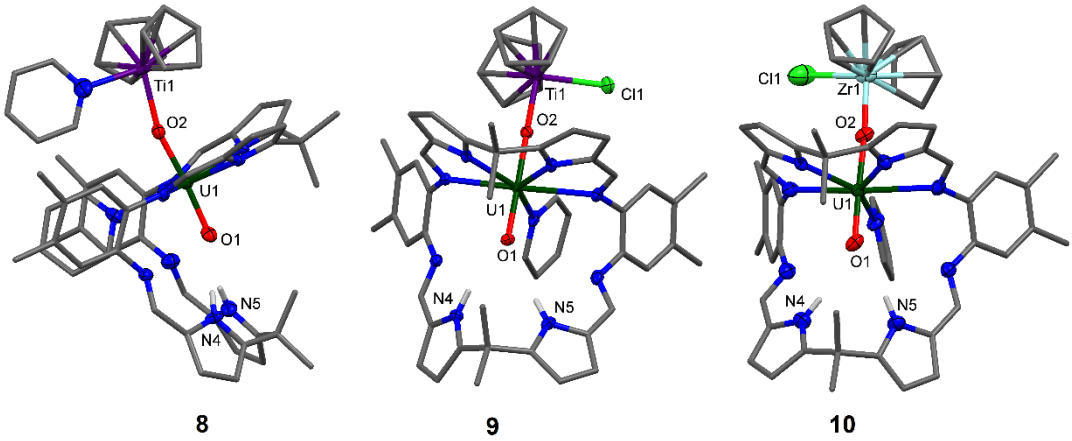

Figure 38 Solid state structures of **9** (side view), **10** and **11** (both front view). For clarity, all hydrogen atoms except pyrrole NHs and all solvent molecules are omitted (displacement ellipsoids are drawn at 50% probability). Selected bond lengths (Å) for **9**: U1-O1 1.846(6), U1-O2 1.925(6), O1-N4 3.09(1), O1-N5 3.02(1). O1-U1-O2 bond angle: 175.3(3)°. Selected bond lengths (Å) for **10**: U1-O1 1.841(2), U1-O2 1.979(3), O1-N4 3.021(4), O1-N5 3.099(3). O1-U1-O2 bond angle: 177.43(9)°. Selected bond lengths (Å) for **11**: U1-O1 1.829(8), U1-O2 1.995(7), O1-N4 3.09(1), O1-N5 3.01(1). O1-U1-O2 bond angle: 176.7(3)°.

Table 8 lists the characteristic bond distances and bond angles of the synthesised Group IV uranyl(V) complexes. Most notably the Ti^{III}-O2-U1 bond angle in **9** is slightly bent in comparison to **10** and **11**, as the slightly bulkier pyridine molecule pushes the Ti(III) away from linearity as it orientates itself in a π-stacking motif in alignment with the aromatic backbone of the macrocycle.

Table 8 Comparison of bond distances and angles of Group IV uranyl(V) complexes 9 – 11

Bond	Ti^{III}-O-U^{V}=O **9**	Ti^{IV}-O-U^{V}=O **10**	Zr^{IV}-O-U^{V}=O **11**
U1-O1 (Å)	1.846(6)	1.841(2)	1.829(8)
U1-O2 (Å)	1.925(6)	1.979(3)	1.995(7)
O1-N4 (Å)	3.09(1)	3.021(4)	3.09(1)
O1-N5 (Å)	3.02(1)	3.099(3)	3.01(1)
M1-O2 (Å)	2.155(6)	1.952(3)	2.031(7)
O1-U1-O2 (°)	175.3(3)	177.43(9)	176.7(3)
M1-O2-U1 (°)	165.2(4)	174.3(1)	172.4(3)

The similarities between **9**, **10** and **11** can also be observed spectroscopically. In particular the uranyl(V) complexes which show a coordination to the tetravalent Group(IV) metal Ti (**10**) and Zr (**11**) feature similar paramagnetic shifts in their respective ^{1}H-NMR spectrum (Figure 39).

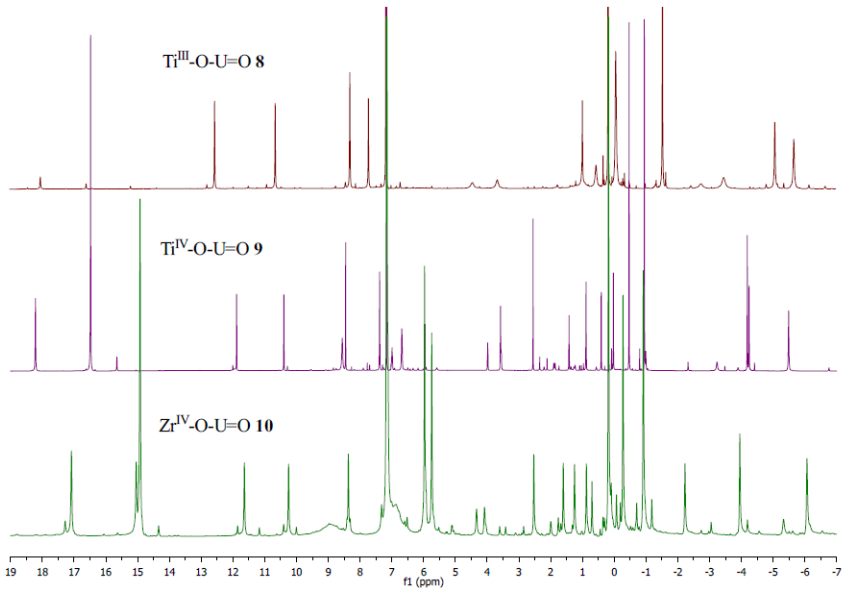

Figure 39 ^{1}H-NMR spectra of **9**, **10** and **11** in C_6D_6 in the range from 19 ppm to -7 ppm (high frequency resonances omitted for clarity).

The most significant difference between complex **9** with the Ti(III) coordination and **10** and **11** is the shift of the cyclopentadienyl protons at 0.16 ppm, resulting from

the influence of the paramagnetic d^1 centre on the Ti(III). In contrast to this the proton resonances of the Cp rings in **10** and **11** are shifted to 16.48 ppm (**10**) and 14.94 ppm (**11**). For comparison Table 9 lists characteristic shifts of the ^{1}H-NMR resonances of **9**, **10** and **11**.

Table 9 Characteristic ^{1}H-NMR shifts for complexes 9 – 11

Resonance	Ti^{III}-O-U^{V}=O **9**	Ti^{IV}-O-U^{V}=O **10**	Zr^{IV}-O-U^{V}=O **11**
(s, 3H, C*H*$_3$)	-5.71	-5.49	-6.14
(s, 3H, C*H*$_3$)	-5.09	-4.19	-3.92
(s, 6H, Ph-C*H*$_3$)	-1.53	-0.95	-0.85
(s, 6H, Ph-C*H*$_3$)	-0.07	-0.47	-0.26
(s, 10H, C$_5$*H*$_5$)	**0.16**	**16.48**	**14.94**
(s, 2H, pyrrole)	0.51	0.41	0.23
(s, 2H, pyrrole)	0.99	0.89	1.64
(d, 2H, pyrrole)	10.63	10.40	10.20
(d, 2H, pyrrole)	12.53	11.89	11.58
(s, 3H, C*H*$_3$)	21.24	18.21	16.96
(br, 2H, N*H*)	71.35	63.95	61.82

In order to better understand the interactions of the Lewis basic uranyl(V) oxygen to the coordinating metal quantum chemical calculations were carried out by Xiaobin Zhang and Prof. Dr. Georg Schreckenbach at the University of Manitoba, Canada (*cf.* 6.1 for details regarding the level of theory). For these studies the Quantum Theory of Atoms-in-Molecules (QTAIM)[184,185] has been used, which focuses on the electron density between two atoms rather than orbital overlap. This theory has already been successfully employed to determine major characteristics in the bonding in actinide complexes, for example actinide-nitrogen systems like $[AnX_3]_2(\mu\text{–}\eta^2\text{:}\eta^2\text{-}N_2)$ (An = Th–Pu; X = F, Cl, Br, Me, H, OPh).[186] This theory is also being used to compare the degree of covalency of actinide complexes to lanthanide system, which is crucial for nuclear waste separation, as this determines the selectivity of the ligand.[187,188]

Zhang and Schreckenbach carried out calculations to compare the uranyl(V) complexes **1**, **6**, **9**, **10**, **11** and the uranyl(VI) starting material **A**. Selected bond properties of the bond critical points of these complexes are given in Table 10 ($\nabla^2\rho$ – Laplacian of the electron density, ρ – electron density, η – eta index, H – total electronic energy density; all quantities given in atomic units (a. u.))

Table 10 Properties of bond critical points of the metalated uranyl oxo-groups in the gas phase

Complex	Parameter	$\nabla^2\rho$	ρ	η	H
1 (Al^{III}-O-U^{V}=O)	Al^{III}-O2	0.529	0.072	0.149	0.003
	O2-U^{V}	0.180	0.166	0.266	-0.074
	U^{V}=O1	0.419	0.230	0.321	-0.143
6 (K^{I}-O-U^{V}=O)	K^{I}-O2	0.067	0.013	0.131	0.004
	O2-U^{V}	0.433	0.233	0.319	-0.146
	U^{V}=O1	0.431	0.225	0.314	-0.137
9 (Ti^{III}-O-U^{V}=O)	Ti^{III}-O2	0.306	0.066	0.201	-0.003
	O2-U^{V}	0.431	0.174	0.266	-0.082
	U^{V}=O1	0.427	0.231	0.319	-0.145
10 (Ti^{IV}-O-U^{V}=O)	Ti^{IV}-O2	0.446	0.104	0.218	-0.016
	O2-U^{V}	0.410	0.154	0.259	-0.063
	U^{V}=O1	0.431	0.237	0.321	-0.152
11 (Zr^{IV}-O-U^{V}=O)	Zr^{IV}-O2	0.404	0.110	0.222	-0.025
	O2-U^{V}	0.381	0.147	0.263	-0.058
	U^{V}=O1	0.431	0.236	0.320	-0.150
A (O=U^{VI}=O)	O2=U^{VI}	0.439	0.277	0.342	-0.207
	U^{VI}=O1	0.450	0.252	0.325	-0.171

The data in Table 10 shows that the Laplacian of the electron density ($\nabla^2\rho$) is positive for all calculated bonds, suggesting a largely ionic character. However, a

comparison of the absolute values of the electron density (ρ) and the total electronic energy density (H) indicate the covalent character of these bonds. In particular the value of H suggest a tendency of decreasing covalency of the O2-U^{V} bond with **6** (K^{I}-O-U^{V}=O) > **9** (Ti^{III}-O-U^{V}=O) > **1** (Al^{III}-O-U^{V}=O) > **10** (Ti^{IV}-O-U^{V}=O) > **11** (Zr^{IV}-O-U^{V}=O). The tendency of η, which decreases with decreasing covalent character,[189,190] is in good agreement with ρ and H.

All U-O bonds show negative values of H, indicating their covalent character. This is also true for the metal-oxygen bonds of the coordinating metal except for complexes **1** and **6**, where H is slightly positive (0.003 and 0.004, respectively).

A contour plot of the calculated bond critical points for **1** is given in Figure 40.

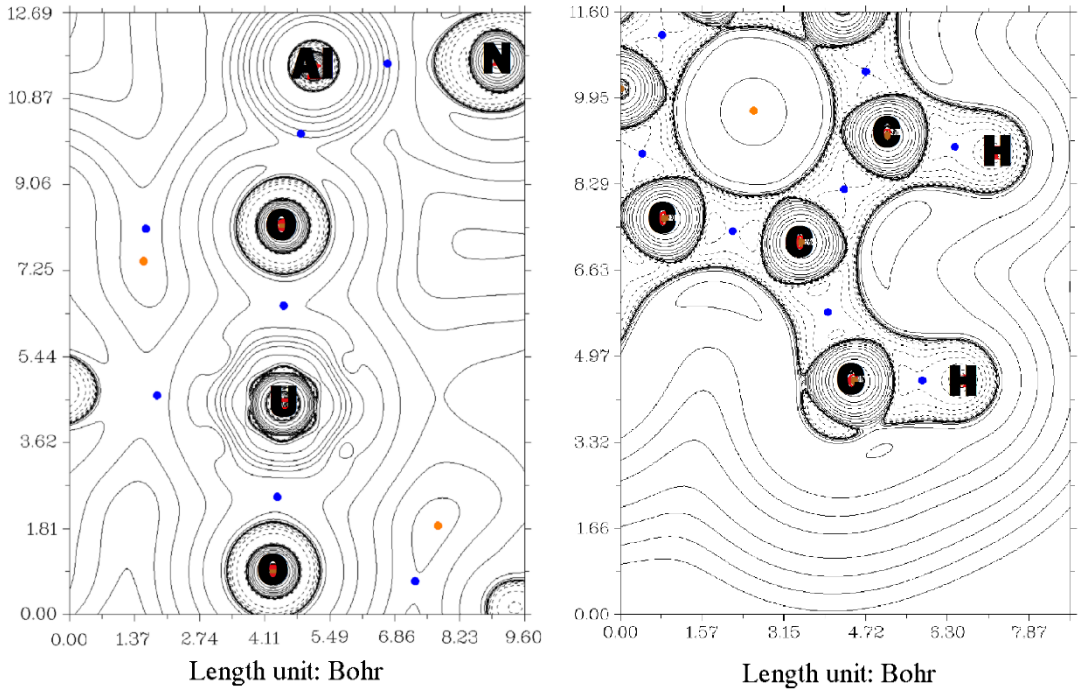

Figure 40 Laplacian contour line diagrams for **1**. Left: (py)N-Al^{III}-O-U^{V}=O moiety. Right: Phenyl backbone of the macrocycle displaying the C_6 ring with one aromatic hydrogen atom and one methyl-C atom and methyl-H atom. Solid lines represent areas of reduced electron density; dashed lines represent concentrated electron density. Blue spots indicate the calculated bond critical points.

It can be clearly seen from Figure 40 that the bond critical points (BCP) for the aluminium atom in the (py)N-Al^{III}-O-U^{V}=O motif (left) are located close to the nucleus, indicating the ionic character of the Al-O bond. In contrast the BCPs for the O-U^{V}=O motif lie within the bond, indicating its covalent character. This is

comparable to the contour plot of the C-C framework of the ligand (right), where the BCPs of the covalent C-C and C-H bonds are as well located in equal distance from the two nuclei.

Similarly Hirshfeld[191] charge analysis as well as Mulliken[192] population analysis agree with the experimental results and confirm the reduced formal charge on the uranium atom. The results are shown in Table 11.

Table 11 Partial atomic charges for the uranium atom in uranyl Pacman complexes in the gas phase derived from Hirshfeld and Mulliken analysis

Complex	Hirshfeld	Mulliken
1 (Al^{III}-O-U^{V}=O)	1.288	0.473
6 (K^{I}-O-U^{V}=O)	1.245	0.429
9 (Ti^{III}-O-U^{V}=O)	1.258	0.441
10 (Ti^{IV}-O-U^{V}=O)	1.298	0.481
11 (Zr^{IV}-O-U^{V}=O)	1.300	0.484
A (O=U^{VI}=O)	1.339	0.520

Natural bond order (NBO) calculations and Mayer NBO analysis which has found wide application in inorganic chemistry have been carried out to determine the bond order of the uranyl moiety.[193] The Wiberg[194] and Mayer[195] bond order analyses given in Table 12 confirm the reduction in the uranyl bond order for the synthesised uranyl(V) complexes. For comparison the uranyl(VI) bond order in **A** was calculated and show values for O2=U^{VI} of 2.128 (Wiberg) and 2.455 (Mayer) and for U^{VI}=O1 1.906 (Wiberg) and 2.188 (Mayer). In contrast to this all bond orders calculated for the reduced uranyl(V) complexes show with Wiberg calculations values below 2. The lowest O2-U^{V} bond order is thus calculated for the Zr(IV) complex **11** (1.116); the lowest bond order for U^{V}-O1 (1.714) is calculated for the Ti(III) complex **9**. Mayer analysis shows clearly a reduced bond order for the metalated O2-U^{V} bond with the lowest value (1.382) calculated for the Zr(IV) complex **11**. The endogenous uranyl-oxygen bond U^{V}-O1 shows in the Mayer analysis values above 2, with the lowest value

calculated for the K complex **6** (2.098). Both Wiberg and Mayer bond order analyses calculate for the K-O2 bond in complex **6** values of 0.015 and 0.083, respectively, indicating that this bond is rather ionic. The values for the other M-O2 bonds show values between 0.370 (Al^{III}-O2; Wiberg) and 0.897 (Zr^{IV}-O2, Mayer) and indicate a more covalent nature of these bonds.

Table 12 Bond orders in the gas phase of the M-O-U^{V}=O moieties derived from Wiberg and Mayer calculations

Complex	Parameter	Wiberg	Mayer
1 (Al^{III}-O-U^{V}=O)	Al^{III}-O2	0.370	0.829
	O2-U^{V}	1.299	1.465
	U^{V}=O1	1.777	2.159
6 (K^{I}-O-U^{V}=O)	K^{I}-O2	0.015	0.083
	O2-U^{V}	1.836	2.224
	U^{V}=O1	1.723	2.091
9 (Ti^{III}-O-U^{V}=O)	Ti^{III}-O2	0.486	0.655
	O2-U^{V}	1.334	1.668
	U^{V}=O1	1.714	2.197
10 (Ti^{IV}-O-U^{V}=O)	Ti^{IV}-O2	0.728	0.883
	O2-U^{V}	1.160	1.424
	U^{V}=O1	1.787	2.230
11 (Zr^{IV}-O-U^{V}=O)	Zr^{IV}-O2	0.623	0.897
	O2-U^{V}	1.116	1.382
	U^{V}=O1	1.788	2.220
A	O2=U^{VI}	2.128	2.455
	U^{VI}=O1	1.906	2.188

To elucidate the nature of the hydrogen bonding between the lower pocket pyrrole N-H atoms and the endogenous uranyl oxygen O1 the bond critical points of these bonds have been determined in the gas-phase using the QTAIM approach. Figure 41 illustrates the calculated hydrogen bonds in the lower macrocyclic pocket, taking into account the contribution of the methyl groups of the dimethyl dipyrromethane moiety.

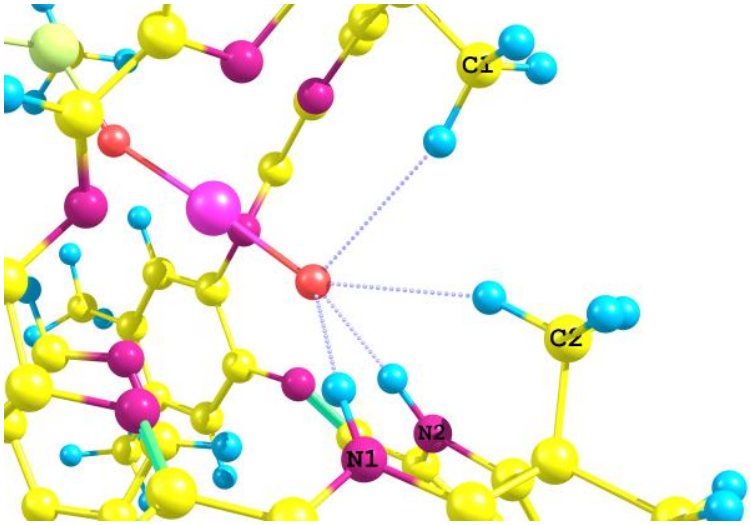

Figure 41 Illustration of the calculated hydrogen bonding interactions in the lower macrocyclic pocket (Optimised structure; U (pink), O (red), C (yellow), N (purple), H (light blue)).

The hydrogen bonds can be categorised as “strong” or “strongly covalent” (D···A 2.2 – 2.5 Å), “moderate” or “mostly electrostatic” (D···A 2.5 – 3.2 Å) and “weak” or electrostatic/dispersion (D···A 3.2 – 4.0 Å)[196] Based on the theory of “Atoms-in-Molecules” Popelier also suggested eight criteria to characterise the hydrogen bonding,[197] of which two can be directly applied here:

a) The electron density ρ at the bond critical point ranges from 0.002 – 0.035 a.u.

b) The Laplacian of the electron density $\nabla^2\rho$ at the bond critical point ranges from 0.024 – 0.139 a.u.

Table 13 lists the bond metrics derived for the hydrogen interactions in the lower macrocyclic pocket.

Table 13 Properties of selected bond critical points of hydrogen bonds in the gas-phase

Complex	Parameter	$\nabla^2\rho$	ρ	H	Bond length	
					H…A[a]	D…A[b]
1 (Al^{III}-O-U^{V}=O)	C1-H···O	0.0217	0.0064	0.0014	2.670	3.736
	C2-H···O	0.0361	0.0093	0.0022	2.435	3.475
	N1-H···O	0.0773	0.0218	0.0021	1.986	3.010
	N2-H···O	0.0806	0.0230	0.0019	1.964	2.991
6 (K^{I}-O-U^{V}=O)	C1-H···O	0.0227	0.0067	0.0015	2.646	3.727
	C2-H···O	0.0360	0.0092	0.0022	2.440	3.470
	N1-H···O	0.0856	0.0249	0.0015	1.906	2.935
	N2-H···O	0.0905	0.0268	0.0011	1.935	2.962
9 (Ti^{III}-O-U^{V}=O)	C1-H···O	–[c]	–	–	3.224	4.210
	C2-H···O	0.0342	0.0089	0.0021	2.450	3.510
	N1-H···O	0.0645	0.0176	0.0025	2.069	3.095
	N2-H···O	0.0685	0.0189	0.0024	2.041	3.066
10 (Ti^{IV}-O-U^{V}=O)	C1-H···O	0.0138	0.0044	0.0009	2.884	3.922
	C2-H···O	0.0282	0.0074	0.0018	2.542	3.591
	N1-H···O	0.0604	0.0158	0.0027	2.044	3.073
	N2-H···O	0.0682	0.0185	0.0025	2.107	3.128
11 (Zr^{IV}-O-U^{V}=O)	C1-H···O	0.0155	0.0040	0.0010	2.827	3.872
	C2-H···O	0.0297	0.0077	0.0019	2.521	3.567
	N1-H···O	0.0640	0.0170	0.0026	2.080	3.101
	N2-H···O	0.0710	0.0194	0.0024	2.025	3.054
A	C1-H···O	0.0176	0.0052	0.0011	2.767	3.818
	C2-H···O	0.0313	0.0079	0.0020	2.497	3.545
	N1-H···O	0.0669	0.0173	0.0027	2.065	3.086
	N2-H···O	0.0666	0.0172	0.0027	2.068	3.088

[a] H···A H = hydrogen, A = hydrogen acceptor (O)
[b] D···A D = hydrogen donor, A = hydrogen acceptor (O)
[c] QTAIM analysis does not locate a bond path of C1-H…O in **9**.

The data given in Table 13 show that both the electron density ρ and the Laplacian $\nabla^2\rho$ of the pyrrole N-H···O1 as well as of the methyl C-H···O1 lie within this range and the electron density of N-H···O1 is about one order of magnitude smaller than for

a covalent bond. Therefore both the N-H···O1 and C-H···O1 interactions can be classified as hydrogen bonds,[198] however, according to the bond distances the hydrogen bonds of the pyrrole rings to the uranyl oxygen (N-H···O1) belong to moderate hydrogen bonds whereas the coordination of the methyl hydrogen atoms (C-H···O1) belong to weak hydrogen-bonds. Thus both hydrogen bonds concomitantly "protect" the endogenous uranyl oxygen sterically and electronically and attenuate any reductive uranyl functionalisation in the lower macrocyclic pocket.

The results regarding the synthesis of Group(IV)-uranyl(V) has led to attempt the synthesis of a Hf(IV)-uranyl(V) complex.

From the observed reactivity it has been anticipated that also Hf should yield a similar uranyl(V) complex. In contrast to classic text-book chemistry which regards Zr and Hf to be chemically identical, the organometallic chemistry of these two metals is more unlike than one would expect. It has not only been shown that Hf complexes are capable of functionalising N_2 and of coupling CO_2 and N_2 to substituted hydrazine products[199,200] but also that the metallacyclopropene complex of decamethyl-hafnocene shows tandem Si-C and C-H bond activation which have been unprecedented with the similar Ti and Zr complexes. Additionally, the Hf-acetylene interaction in this complex is much stronger than in the analogous Ti and Zr complexes resulting from a larger s character in the C=C bonding giving shorter Hf-C than Zr-C bonds.[168] However, the hafnocene metallacyclopropene also reacts for instance with CO_2 to a hafnofuranone complex.[201]

Ultimately, **A** was treated with a twofold excess of hafnocene dichloride Cp_2HfCl_2 in the presence of Mg metal in pyridine. After sonication for 3 hours a cherry red solution and a light yellow precipitate ($MgCl_2$) had formed. After centrifugation the mother liquor was dried under vacuum and extracted with benzene. The extract was dried under vacuum and it was attempted to recrystallise the material from THF, from which also the ^{1}H-NMR spectrum was recorded. This showed clearly a paramagnetic shift which related to the resonances already known from the Zr(IV)-uranyl(V) complex. However, due to the presence of residual oxygen in the solvent the complex slowly disintegrated to uranyl(VI) Pacman and μ-oxo-bis(chlorohafnocene) $(Cp_2HfCl)_2O$.

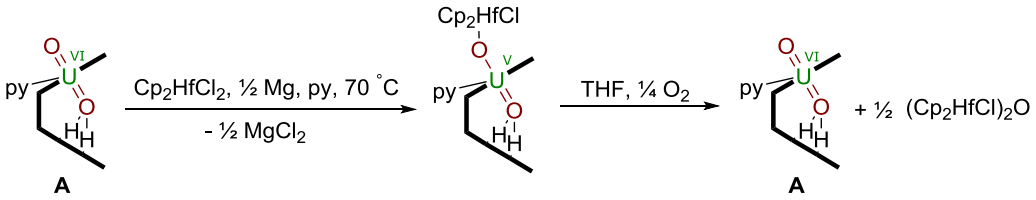

Scheme 33 *In situ* synthesis of Hf(IV)-uranyl Pacman with subsequent decomposition by oxygen.

The *in situ* synthesis of a Hf(IV)-uranyl(V) Pacman complex using Cp_2HfCl_2, Mg and **A** in pyridine is feasible, however, the formation of the target material is accompanied by the formation of a Mg(II)-uranyl(V) Pacman complex **11** as can be seen from its ^{1}H-NMR spectrum. Clearly the formation of paramagnetic resonances which are similarly shifted as the Zr homologue **11** allow the formulation of a Hf complex of uranyl Pacman. This is expected because of the similar ionic radii of Zr and Hf. Even though the reaction proceeds within three hours at 70 °C no pure material could be isolated as the contamination with **11** and $MgCl_2$ as the side products leave an inseparable mixture of these three components. Figure 42 shows a comparison between the pyridine spectra of the *in situ* prepared Hf complex with **11** and **12**.

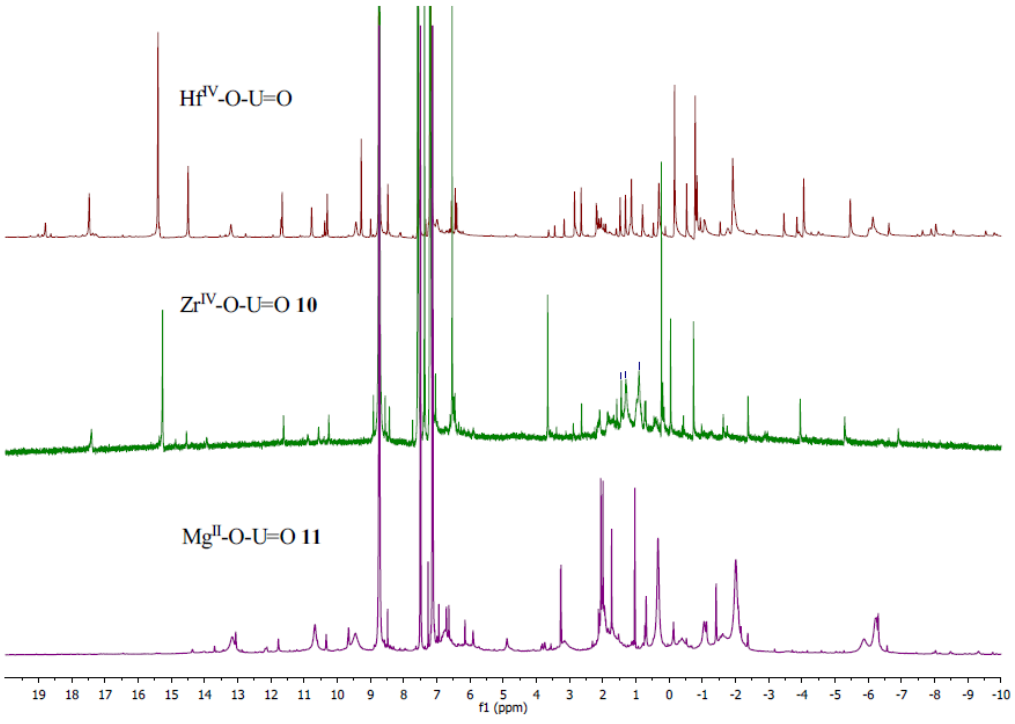

Figure 42 ^{1}H-NMR spectrum of *in situ* synthesised Hf(IV)-uranyl(V) Pacman complex in pyridine-d_5 from 20 to -10 ppm (top). For comparison, the pyridine spectra of the Zr(IV) complex **11** (centre) and the Mg(II) complex **12** (bottom) (high frequency resonances omitted for clarity).

3.1.3 Uranyl functionalisation *via in-situ* reduction using Group IV metallocene dichlorides and Mg

The synthesis of a Zr^{IV}-O-U^{V}=O complex can also be achieved by reducing **A** with metallic Mg in the presence of Cp_2ZrCl_2 in pyridine at room temperature (Scheme 34).

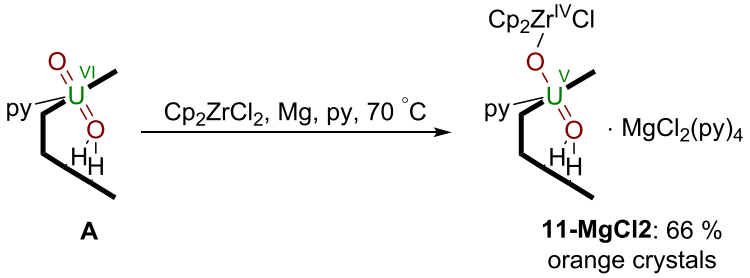

Scheme 34 Reductive metalation of **A** using Zr(IV) and Mg

As a side product $MgCl_2$ is formed which makes the work-up and isolation of sufficiently pure **11** rather tedious, however, ^{1}H-NMR spectroscopy showed the formation of **11** while X-ray crystallography confirmed that this material crystallises as the $MgCl_2(py)_4$ co-crystallisate **11-MgCl2**.

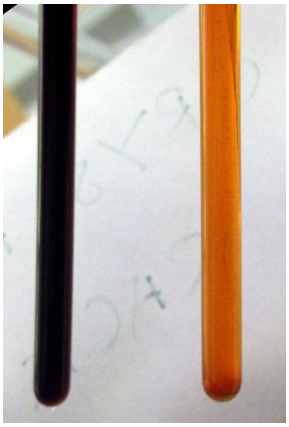

Figure 43 NMR samples of **A** (left) and **11** (right). (Photo: Max McMullon)

Therefore the synthesis of **10** was attempted from a similar reduction of **A** with metallic Mg in the presence of Cp_2TiCl_2, however, the desired product did not form, instead it was found that the Mg adduct is the sole product of this reaction (Scheme 35).

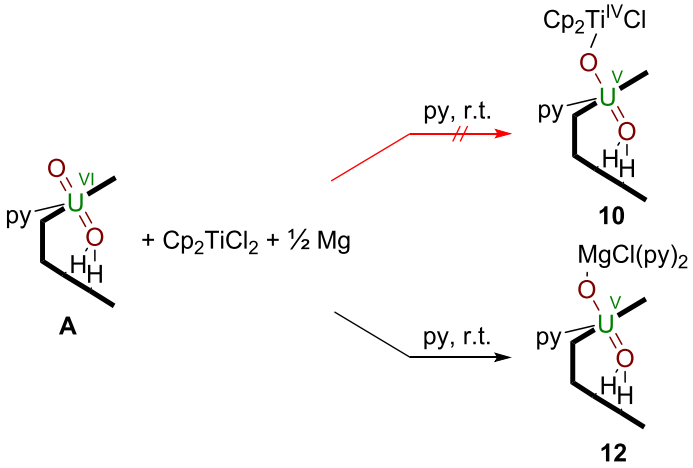

Scheme 35 Reductive metalation of **A** with Mg in the presence of Cp_2TiCl_2.

Comparing the standard bond dissociation enthalpies of the individual bonds involved, one finds that the bond dissociation enthalpy for the Ti-O bond is higher with ΔH_{diss} = 662 kJ/mol compared to the Mg-O bond with ΔH_{diss} = 394 kJ/mol. However, the formation of a Ti-N bond (ΔH_{diss} = 464 kJ/mol) with the solvent pyridine which is present in excess, which is therefore thermodynamically in favour of a Ti-O bond formation. However, the formation of a Ti-N bonds (ΔH_{diss} = 464 kJ/mol) with the solvent pyridine are favoured over the formation of Mg-N bonds (ΔH_{diss} = 201 kJ/mol).[44] A study carried out by Rodgers *et al.* on the periodic trends regarding the binding of M^+ metal ions to pyridine shows a bond energy of the Mg^+-py bond of 200.0 kJ/mol and for the Ti^+-py bond of 217.2 kJ/mol, which also shows the higher affinity of Ti-ions towards N-donors compared to Mg ions.[202] Therefore, there is a possibility that every titanium species that forms may be used up by the solvent during the reaction. Then any excess magnesium can coordinate to the uranyl oxygen.

3.2 Uranyl functionalisation using divalent metals

Having observed reduction of uranyl(VI) by addition of metallic Mg while attempting to synthesise **10** it was envisaged that the sole addition of a reducing metal should yield new uranyl(V) motifs. Thus Mg metal and Ca metal were used in the presence of their corresponding metal halides, $MgCl_2$ and CaI_2, respectively, to give the first Group(II)-uranyl(V) complexes. Similarly Zn metal has been tried as a reducing agent, and both comproportionation reactions with $ZnCl_2$ as well as ZnI_2 have led to isolable mono-oxo functionalised Zn(II)-uranyl(V) complexes.

3.2.1 Uranyl functionalisation using Mg metal

The divalent (Mg) and transition metal (Mn, Fe, Co, Ni) chemistry of uranium remains relatively restricted to only a few examples, of which most importantly some natural uranyl(VI) minerals are known to incorporate these ions into their structures, such as $Mg[(UO_2)(AsO_4)]_2(H_2O)_{12}$ (nováčekite-I), $Mg[(UO_2)(PO_4)]_2(H_2O)_{10}$ (saléeite), $Fe[(UO_2)(AsO_4)]_2(H_2O)_8$ (metakahlerite) and $Co[(UO_2)(AsO_4)]_2(H_2O)_{12}$ (kirchheimerite) to name but a few. However, these minerals only consist of uranyl phosphate and uranyl arsenate sheets of the autunite-type, incorporating the divalent and transition metals in their interlayers in form of octahedrally hydrated cations. Therefore no direct interaction of the metal with the uranyl(VI) moiety can be observed.[203]

Synthesis of **12** was thus performed by suspending **A** and 0.5 equivalents $MgCl_2$ and 0.5 equivalents metallic Mg in pyridine with subsequent sonication and stirring for 72 hours at room temperature to form a cherry red solution which affords upon standing beige crystals of $[(py)_2(ClMgOUO)(py)(H_2L)]$ **12** in 69 % yield (Scheme 36).

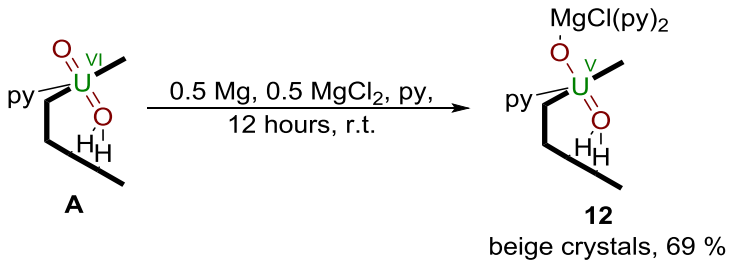

Scheme 36 Reductive metalation of **A** using Mg and $MgCl_2$.

Recrystallisation of **12** from a concentrated pyridine solution afforded suitable crystals for X-ray diffraction. The solid state structure is shown in Figure 46 and is described in comparison with its Ca analogue in Section 3.2.2.

The synthesis of **12** can be described either with the supposed formation of a Mg^{I}-Cl complex in solution[204] which functions as a one-electron reductant or assuming the formation of a magnesium-bridged bis(uranyl(V) Pacman) complex (Scheme 37).

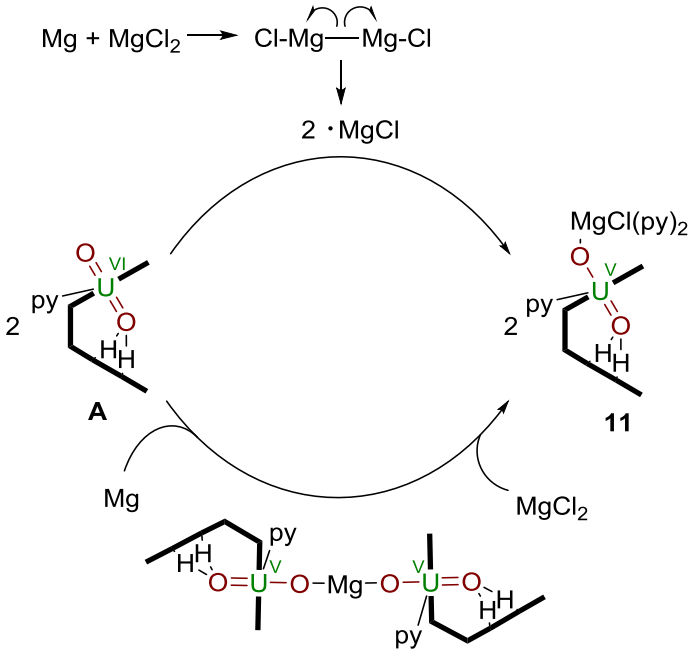

Scheme 37 Formation of magnesium uranyl(V) Pacman proposing two different reaction mechanisms. Top: Uranyl(VI) reduction *via* Mg^{I} Bottom: Uranyl(VI) reduction *via* formation of a magnesium-bridged bis(uranyl(V) Pacman) complex.

The formation of Mg^{I} complexes has a long history of investigations since the discovery of the first Grignard reaction[205] and the Schlenk equilibrium.[206] Cameron Jones and co-workers have shown that Mg^{I} complexes with Mg-Mg bonds are thermally stable[207] and can be used as facile two centre/two electron reductants[208] or in the synthesis of unusual low-valent main Group metal complexes.[209] It can thus be hypothesised that in a pyridine solution magnesium metal inserts into a magnesium chloride bond in $MgCl_2$ to form Cl-Mg-Mg-Cl, which upon Mg-Mg bond homolysis yields two ·MgCl, which reductively metalate uranyl Pacman to give **12**. However, it could also be possible that in a Schlenk-like equilibrium the magnesium acts as a two electron reductant, forming a magnesium bridged bis(uranyl(V) Pacman) complex,

which then reacts with the present $MgCl_2$ to the monomeric complex **12**. It is well known that the "classic" Schlenk equilibrium between $MgCl_2$, RMgCl and R_2Mg (with R = alkyl, aryl) is strongly solvent dependent and theoretical calculations show that the formation of R_2Mg and $MgCl_2$ is favoured in highly coordinating solvents.[210] If this model be transferred onto the uranyl reduction (with R = O=U-O) it is likely that a dimeric complex may form in solution. To support this hypothesis an experiment was carried out reaction two equivalents of uranyl(VI) Pacman **A** with one equivalent of Mg metal in pyridine to react overnight at room temperature to an orange-red suspension. The suspension was filtered and the ^{1}H-NMR spectrum recorded (Figure 44). The spectrum showed the formation of paramagnetic resonances which can be attributed to a uranyl(V) complex, but whether this complex is monomeric or dimeric cannot be stated from this data.

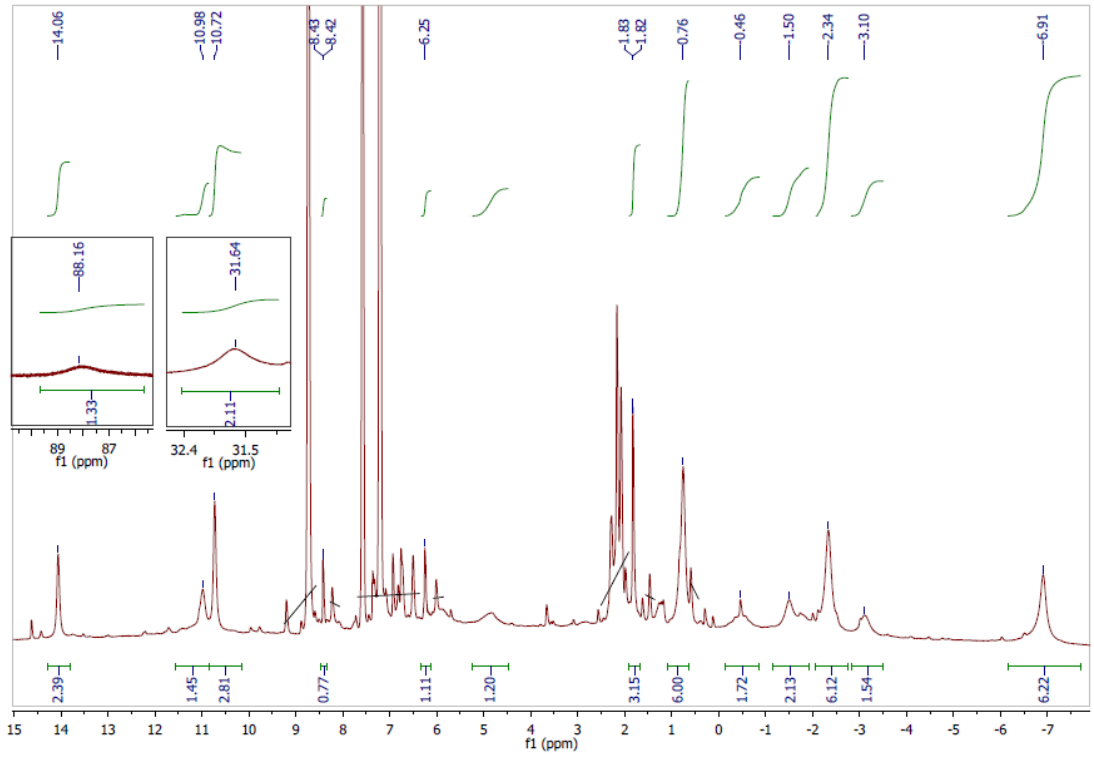

Figure 44 ^{1}H-NMR spectrum after treatment of **A** with Mg metal in pyridine, showing the formation of paramagnetic resonances.

The spectrum shows resonances shifted from -6.91 ppm to 88.16 ppm. Small amounts (≈ 7 %) of uranyl(VI) Pacman remain present. The resonance at 88.16 ppm can be attributed to the pyrrole NH protons. The resonances at 0.76 ppm and -3.10 can

be attributed to the methyl groups of the pyrrole backbone. The resonances at 31.64 ppm, 1.82 ppm and -6.91 ppm can be attributed to the methyl groups of the dimethyl dipyrromethane moiety. The resonances at 14.06, 10.98, 10.72, 8.43, 6.25, -0.46, -1.50 and -2.34 ppm can tentatively be assigned to the phenyl-H (2x), pyrrole-H (4x) and =N-CH- (2x) atoms of the Pacman macrocycle.

All attempts to isolate this complex have failed. The filtrate was evaporated to dryness to yield a thick red viscous material. Recrystallisation had been attempted by cooling to -35 ºC and hexane diffusion, but failed to give any isolable material.

Currently no final conclusion can be given as to whether the above reaction proceeds *via* Mg^{I} or *via* a bis(uranyl(V)) complex as an intermediate.

3.2.2 Uranyl functionalisation using Ca metal

In addition to the reduction of uranyl(VI) with Mg treatment of **A** in a similar way with Ca by suspending **A** in pyridine with 0.5 equivalents of CaI_2 and 0.5 equivalents of metallic Ca followed by 60 minutes sonication at 50 °C followed by stirring at room temperature for 48 hours afforded a red solution, which after evaporation of the solvent and recrystallisation from THF resulted in the formation of pale red translucent plates of $[(py)_2(thf)_2(ICaOUO)(py)(H_2L)]$ **13** in 69 % yield (Scheme 38).

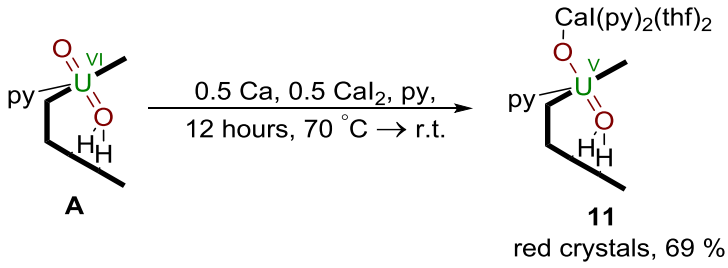

Scheme 38 Reductive metalation of **A** using Ca and CaI_2.

Recrystallisation of **13** from a concentrated tetrahydrofuran solution yielded red tabular crystals suitable for X-ray structural analysis, of which the solid state structure is shown in Figure 46.

Unlike Mg and divalent transition metals, Ca coordination to uranyl(VI) has been known from nature for many years. For instance, the two polymorphs of the common uranyl silicate uranophane $Ca[(UO_2)(SiO_3OH)]_2(H_2O)_5$ crystallise by coordination of

Ca^{2+} ions to the apices of uranyl(VI) pentagonal bipyramids, thus linking the layers of the uranyl silicate.[211,212] However, to date no Ca(II)-uranyl(V) coordination has been reported neither from natural sources nor by synthetic approaches.

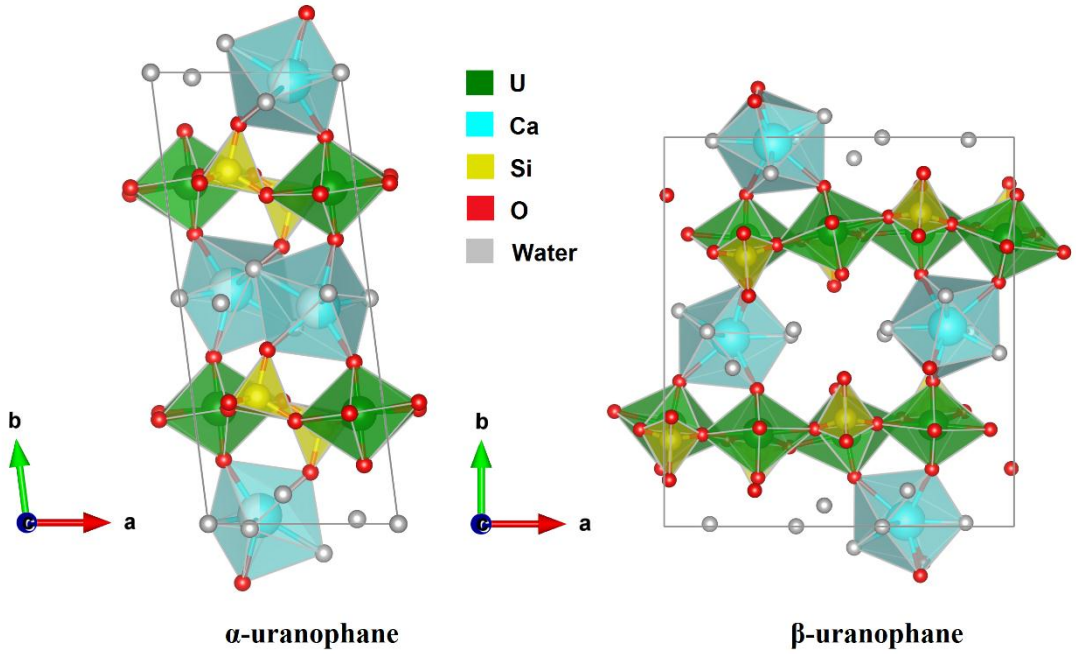

Figure 45 Unit cell crystal structures of α-uranophane and β-uranophane in the direction of the crystallographic c-axis.[211,212]

For comparison, the Ca···O=U^{VI}=O distances in α-uranophane range from 2.38(1) Å to 2.439(9) Å and in β-uranophane from 2.471(6) Å to 2.685(6) Å, which are of mere electrostatic nature and therefore longer than in **13** due to its more ionic character. The O=U^{VI}=O distances range from 1.76 Å to 1.81 Å as expected for uranyl(VI), whereas in **13** it is significantly elongated to U1-O1 1.864(2), U1-O2 1.909(2) as seen for uranyl(V).

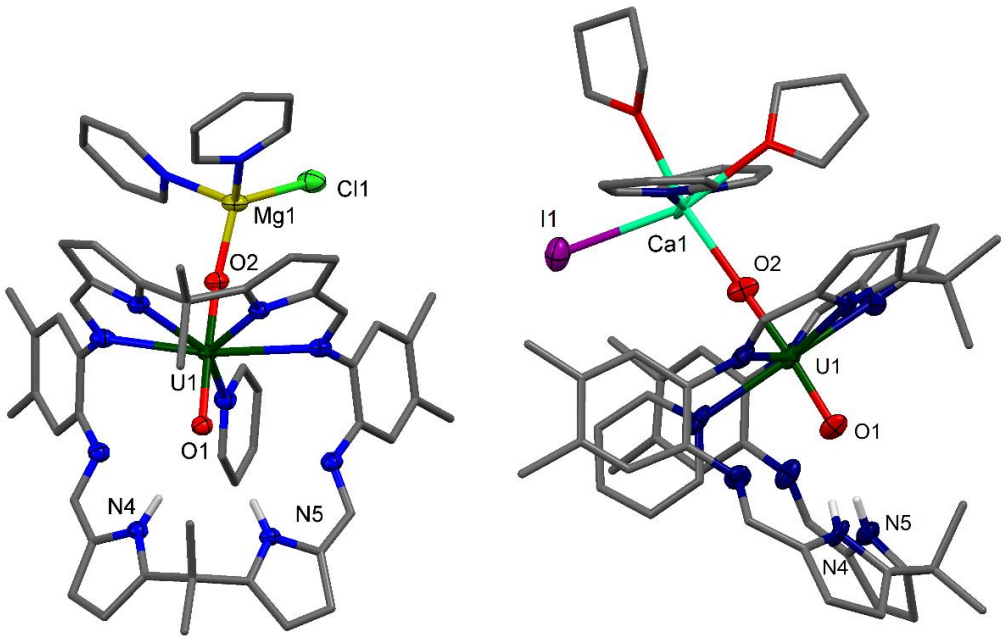

11 **12**

Figure 46 Solid state structures of **12** (front view) and **13** (side view). For clarity, all hydrogen atoms except the pyrrole NHs and all solvent molecules are omitted (displacement ellipsoids are drawn at 50% probability). Selected bond lengths (Å) for **12**: U1-O1 1.864(2), U1-O2 1.909(2), O1-N4 2.889(3), O1-N5 3.040(3). O1-U1-O2 bond angle: 174.21(9)°. Selected bond lengths for **13**: U1-O1 1.88(1), U1-O2 1.90(1), O1-N4 2.95(2), O1-N5 2.92(2). O1-U1-O2 bond angle: 176.0(6)°.

The two compounds **12** and **13** crystallise in a monoclinic crystal system, and the structural solution was performed in space group *I*2/*a* with four molecules per unit cell (**12**) and in space group $P2_1/c$ with four molecules in the unit cell (**13**). Both complexes show a coordination of the alkaline earth metal to the exogenous uranyl oxygen. Both complexes show similar bond metrics. The distances of the uranium atom to the endogenous oxygen atom U1-O1 measure 1.864(2) Å (**12**) and 1.88(1) Å (**13**), and the distances of the uranium atom to the exogenous metalated oxygen U1-O2 show values of 1.909(2) Å (**12**) and 1.90(1) Å (**13**) and represent the +5 oxidation state of the uranium atom. The O1-$N_{pyrrole}$ bond distances behave similarly and show values of O1-N4 2.889(3) Å and O1-N5 3.040(3) Å for **12** and O1-N4 2.95(2) Å and O1-N5 2.92(2) Å for **13**. The O1-U1-O2 bond angles deviate only slightly from linearity with 174.21(9)° (**12**) and 176.0(6)° (**13**).

3.2.3 Uranyl functionalisation using Zn metal

To further probe the reductive potential of other metal/metal salt systems Zn was used to generate singly reduced uranyl(V) Pacman complexes by adding stoichiometric amounts of Zn and ZnX_2 (X = Cl (**14**), I (**15**)) to a pyridine solution of **A**. After 30 minutes agitation using ultrasonication a red solution is formed which after 12 hours stirring results in the formation of a lemon yellow suspension. These mixtures were centrifuged and the resulting yellow precipitate extracted with fresh pyridine, which results upon standing in the formation of yellow translucent prisms of $[(py)_2(ClZnOUO)(py)(H_2L)]$ **14** and $[(py)_2(IZnOUO)(py)(H_2L)]$ **15**, respectively.

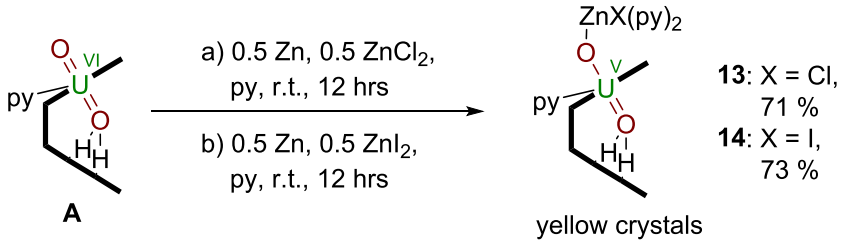

Scheme 39 Reductive metalation of **A** using Zn and $ZnCl_2$ (a) or ZnI_2 (b).

The solid state structures of both compounds are shown in Figure 47.

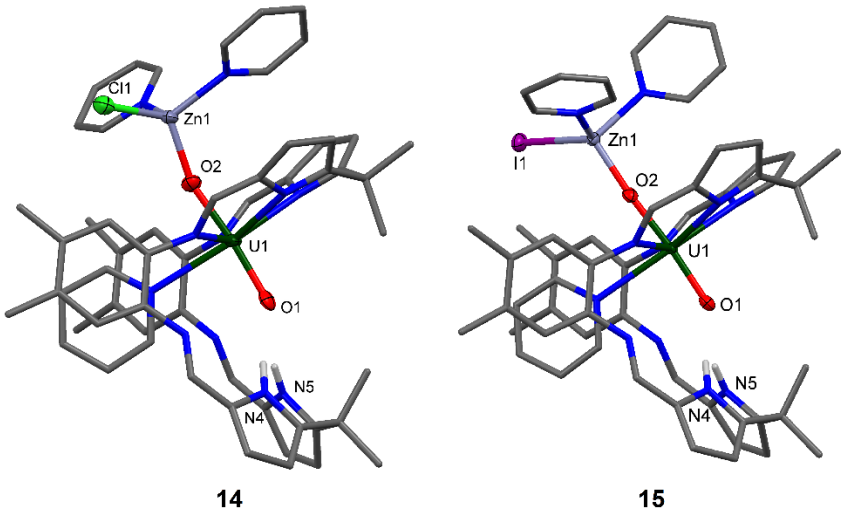

14 **15**

Figure 47 Solid state structures of **14** (left) and **15** (right). For clarity, all hydrogen atoms except the pyrrole NHs and all solvent molecules are omitted (displacement ellipsoids drawn at 50% probability). Selected bond lengths (Å) for **14**: U1-O1 1.872(9), U1-O2 1.917(9), O2-Zn1 1.898(9), O1-N4 3.04(1), O1-N5 2.91(1). Selected bond angles: O1-U1-O2 174.6(4)°, U1-O2-Zn1 159.9(5)°. Selected bond lengths for **15**: U1-O1 1.867(2), U1-O2 1.909(2), O2-Zn1 1.930(2), O1-N4 2.895(4), O1-N5 2.982(4). Selected bond angles: O1-U1-O2 175.7(1)°, U1-O2-Zn1 175.1(1)°.

Compound **14** crystallises in a monoclinic crystal system, and the structural solution was performed in space group *I*2/*a* with eight molecules in the unit cell. **15** crystallises in an orthorhombic crystal system and the structural solution was performed in space group $P2_12_12_1$ with four molecules in the unit cell. Both complexes exhibit a uranyl(V) centre with similar bond distances of 1.87 Å for U1-O1 and 1.91 Å for U1-O2. The Zn1-O2 distances vary slightly, showing values of 1.898(9) Å in complex **14** and 1.930(2) Å in complex **15**. The distances between the N atoms of the lower pocket pyrrole rings and the uranyl oxygen O1 are similar, showing a slight asymmetry between N4-O1 and N5-O1 of about 0.1 Å (O1-N4 3.04(1), O1-N5 2.91(1) (**14**) vs. O1-N4 2.895(4), O1-N5 2.982(4) (**15**)). The O1-U1-O2 bond angle in both complexes is identical, showing a value of 175°, however, the Zn1-O2-U1 bond angle differs from complex **14** with a value of 159.9(5)° to complex **15** with a value of 175.1(1)°.

The similarity of the two compounds can also be seen in the ^{1}H-NMR spectra, which practically overlay, apart from the pyrrole N-H resonances, which are shifted towards 75.37 ppm for **14** and 74.52 ppm for **15** (Figure 48).

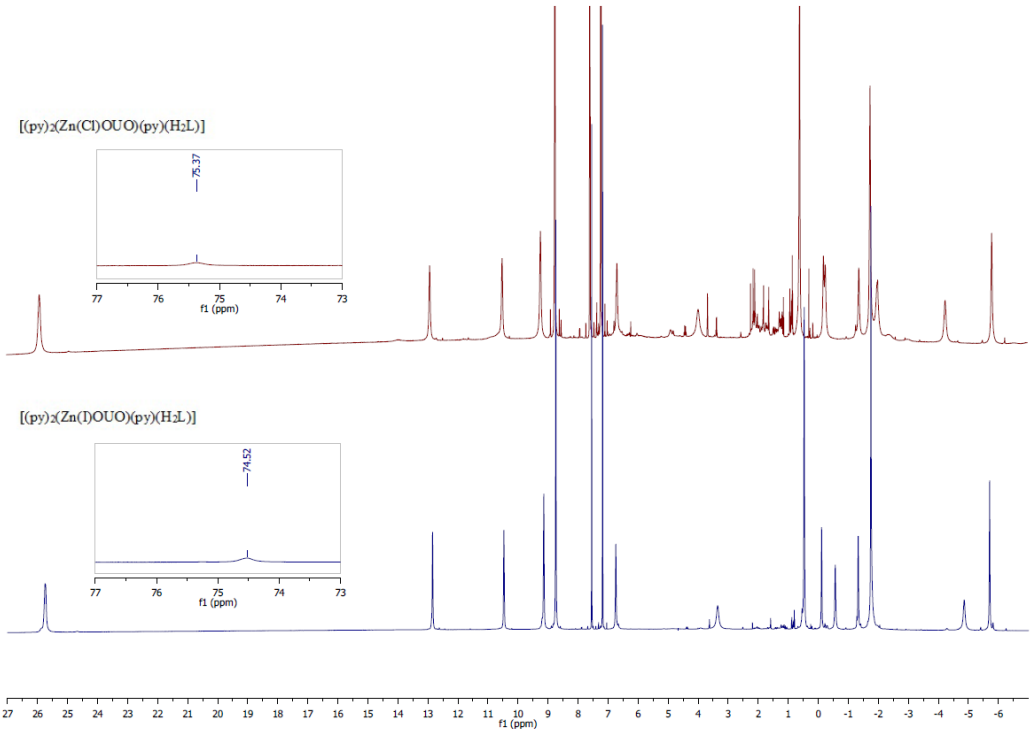

Figure 48 ^{1}H-NMR spectra of **14** (top) and **15** (bottom), showing significant shifts in the pyrrole N-H resonances and similar shifts for the remaining macrocyclic framework.

In Table 14 the characteristic bond features of the Group II and Group XII uranyl(V) Pacman complexes are listed. The coordination of a divalent metal to the exogenous uranyl oxygen leads to a uranyl(V) moiety with similar bond lengths within the standard deviation. The endogenous U1-O1 bond distances average to 1.87 Å and the exogenous U1-O2 distances average to 1.91 Å. Similarly the N-H···O1 interactions with the lower macrocyclic pocket average to 2.944 Å and 2.963 Å, respectively. The uranyl O1-U1-O2 bond angle is essentially linear with 175º. The major difference between the four structures is the distance Ca1-O2 distance with 2.33(1) Å, which is significantly longer than the Zn1-O2 and Mg1-O2 distances and results from the bigger ionic radius of 1.14 Å for Ca, compared to 0.71 Å for Mg and 0.74 Å for Zn.[136] Interesting to note is that the M1-O2-U1 bond angle differs depending in the nature of the halide attached to the divalent metal. In the complexes which bind the smaller chloride the angle is bent with 158.0(1)º (**12**) and 159.9(5)º (**14**), whereas the bigger iodide results in a more linear angle 176.7(7)º (**13**) 175.1(1)º (**15**).

Table 14 Comparison of bond distances and angles of the M(II)-uranyl(V) complexes 12 – 15

Entry	Mg-O-U^V=O	Ca-O-U^V=O	(Cl)Zn-O-U^V=O	(I)Zn-O-U^V=O
	12	**13**	**14**	**15**
U1-O1 (Å)	1.864(2)	1.88(1)	1.872(9)	1.867(2)
U1-O2 (Å)	1.909(2)	1.90(1)	1.917(9)	1.909(2)
O1-N4 (Å)	2.889(3)	2.95(2)	3.04(1)	2.895(4)
O1-N5 (Å)	3.040(3)	2.92(2)	2.91(1)	2.982(4)
M1-O2 (Å)	1.901(2)	2.33(1)	1.898(9)	1.930(2)
O1-U1-O2 (°)	174.21(9)	176.0(6)	174.6(4)	175.7(1)
M1-O2-U1 (°)	158.0(1)	176.7(7)	159.9(5)	175.1(1)

Another attempt of using metallic Zn in the presence of $FeBr_2$ as well as in the presence of $NiCl_2$ in order to yield BrFe-O-U^V=O or ClNi-O-U^V=O motifs has not yet

been successful (Scheme 40). These reactions, using stoichiometric amounts of **A**, Zn and the respective metal halide have formed red solutions upon stirring in pyridine, however, no pure material could be isolated and the NMR spectra remain inconclusive, although paramagnetic resonances were visible, which may result from a mixture of different reduced transition metal uranyl(V) complexes.

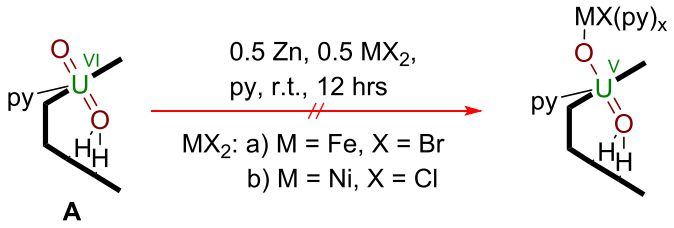

Scheme 40 Attempted reduction of **A** using Zn metal in the presence of $FeBr_2$ (a) and $NiCl_2$ (b).

As expected, the attempt of a homometallic reduction using the systems $Fe/FeBr_2$ and $Ni/NiCl_2$ were not successful due to the relatively high reduction potential of metallic Fe and Ni (Scheme 41).

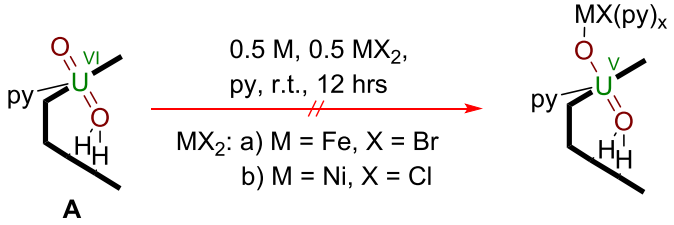

Scheme 41 Attempted homometallic reduction of **A** using $Fe/FeBr_2$ (a) and $Ni/NiCl_2$ (b).

3.3 Conclusion

It has been shown that the synthesis of mono-metalated Group(IV) uranyl(V) complexes is feasible using low-valent Ti and Zr starting materials. The use of Ti(II) results in a single electron uranyl reduction and the first Ti(III)-uranyl(V) complex. The use of trivalent Ti or Zr both as a solid material or prepared *in-situ* results also in single electron uranyl(V) reduction to the mono-metalated Ti(IV)- or Zr(IV)-uranyl(V) complex. Single electron uranyl reduction is also accomplishable when mixtures of divalent metals (Mg, Ca, Zn) are used with their respective halide salts (Cl, I) to generate the M(II)-uranyl(V) complexes. It is possible that this reaction proceeds *via*

the formation of a dimeric, metal-bridged uranyl(V)-uranyl(V) complex, however, further work is needed to verify this hypothesis. For example by using the heavier homologues of the alkaline earth metals Sr and Ba which possess bigger ionic radii, or by attempting the reaction at lower temperatures over a prolonged period of time. Theoretical calculation in comparison with complexes presented in Chapter 2 of this thesis support the formulation of the uranyl(V) complexes and propose a moderately strong endogenous NH-O interaction which prevents further reactivity.

4 Uranyl functionalisation using f-elements

4.1 Uranyl functionalisation using lanthanides

The lanthanide ions are an important component of nuclear waste in the nuclear fuel cycle, because they are permanently generated in nuclear fission reactions. As such, they contribute to the aging of nuclear fuel due to their high neutron cross sections and form a major component of nuclear waste.[213] Their chemical behaviour is similar to the trivalent transuranium elements americium and curium which require highly selective ligands and demanding processes like SANEX (**S**elective **A**cti**n**ide **Ex**traction),[214–216] TALSPEAK (**T**rivalent **A**ctinide **L**anthanide **S**eparation by **P**hosphorus Reagent **E**xtraction from **A**queous **K**omplexes)[217–219] or TRUEX (**Tr**ans**u**ranic **Ex**traction)[220] in order to separate them from the nuclear waste stream. However, not much is known about the chemical behaviour and the solution or solid state structures of mixed actinide-lanthanide materials. Moreover, actinyl-lanthanide complex may be of importance for the development of new single molecule magnets (SMMs).[98,221] These are molecules whose intrinsic magnetic properties show the characteristics known from bulk magnets. As such, these molecules can be magnetised and retain their magnetisation below a certain temperature.[222] In particular some lanthanide complexes employing Tb^{3+} and Dy^{3+} ions have recently been synthesised and show high blocking temperatures of 50 K and 10 K, respectively, proving the suitability of these elements for molecular magnetism.[223]

4.1.1 Uranyl functionalisation using $SmI_2(thf)_2$

Attempts were made to reductively functionalise uranyl Pacman **A** by addition of one equivalents of $SmI_2(thf)_2$. This reaction was carried out in pyridine at room temperature, however, analysis showed that the product was not the desired adduct $[(solv)_x(I_2Sm^{III}OUO)(py)(H_2L)]$. Instead, dark blue translucent crystals of **A** and pale red translucent crystals of $[OU(py)_5OSm(I_4)OU(py)_5{=}O]^+[I]^-$ **16** were isolated in crystallographic yield.

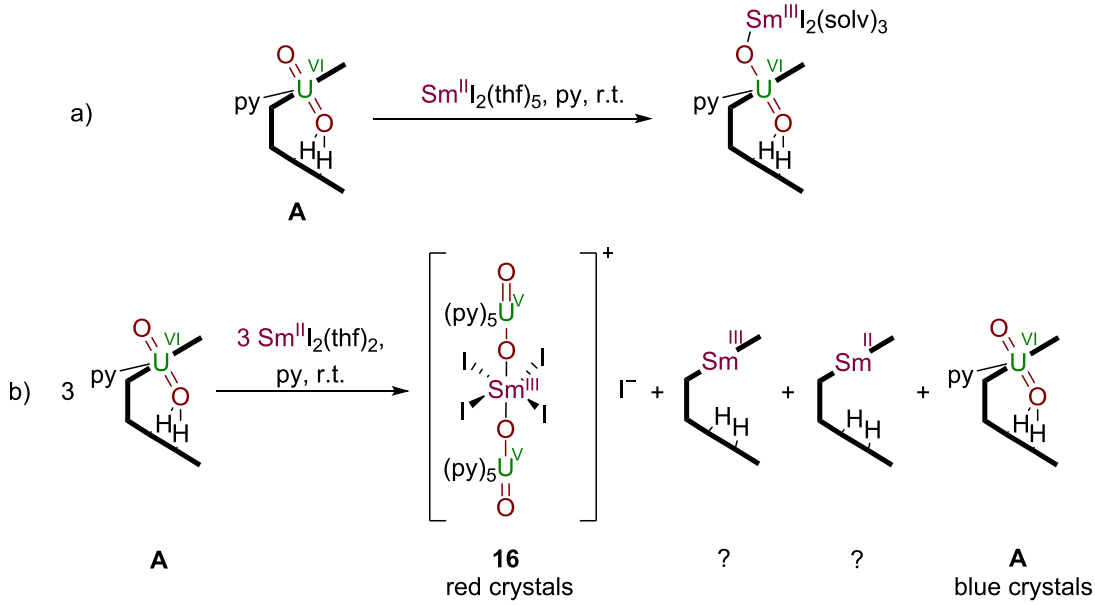

Scheme 42 Attempted reductive metalation of **A**; a) shows the desired product on addition of Sm(II) and b) shows the actual products identified and postulated materials formed.

This reaction is counter-intuitive and previously unprecedented in uranyl Pacman chemistry. It is the first example of a postulated transmetalation of the Pacman ligand, deduced from absent resonances of the free ligand. However, the formation of $[Sm^{III}(H_2L)]$ and $[Sm^{II}(H_2L)]$ remains questionable, as no attributable resonances were observed in the ^{1}H-NMR spectrum of the reaction mixture. This reaction was repeated using the correct stoichiometry yielding **16** with no starting material **A** remaining (Scheme 43).

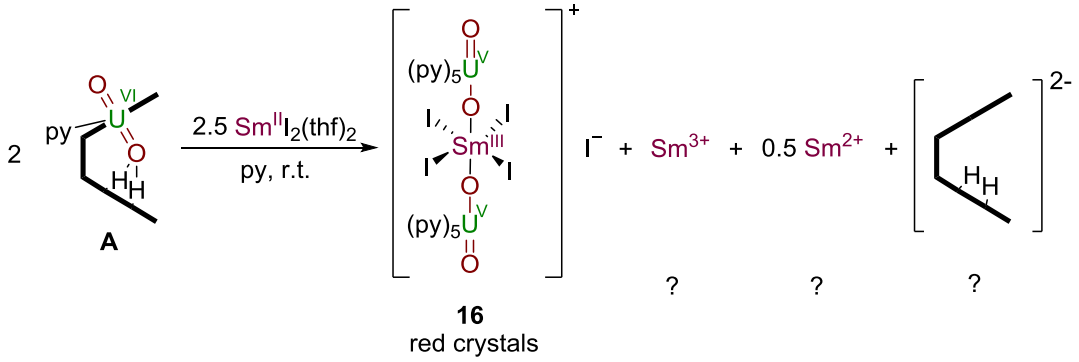

Scheme 43 Stoichiometric reaction of **A** with $SmI_2(thf)_2$ leading to the formation of **16** and unidentified side products.

The molecular structure of **16** is given in Figure 49. The compound crystallises in a monoclinic crystal system and the structural solution was performed in space group $P2_1/n$ with two molecules in the asymmetric unit.

Complex **16** consists of two uranyl(V) moieties, which in their equatorial plane are coordinated by five neutral pyridine molecules. This plane is usually occupied by a charged ligand to compensate the positive charge on the uranium atom, making this a rather unusual binding mode for uranyl, and only few examples of that kind have been reported so far, namely $\{[U^{V}O_2(py)_5][KI_2(py)_2]\}_\infty$, independently reported by Ephritikhine *et al.*[94] and Mazzanti *et al.*[95], and their Li and Tl derivatives.[224]

The two uranyl moieties in **16** are linked *via* one oxygen atoms to a Sm^{III} cation. The Sm itself coordinates four iodide anions in its equatorial plane. The overall charge is ultimately balanced by one outer sphere iodide anion – crystallographically disordered over two sites in the lattice (Figure 49).

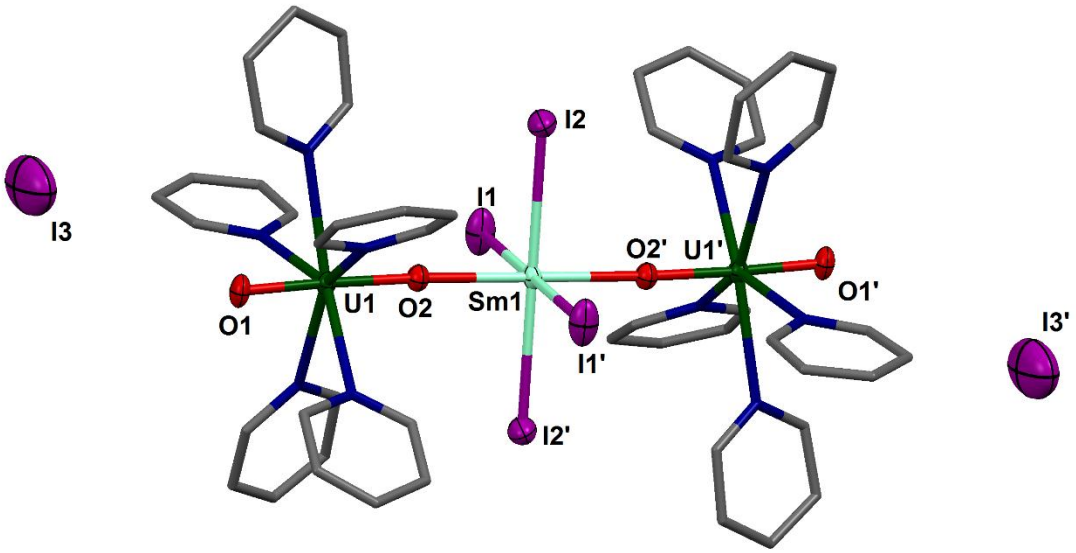

Figure 49 Crystal structure of **16**. For clarity, all hydrogen atoms and all solvent molecules are omitted (displacement ellipsoids are drawn at 50% probability). Selected bond lengths (Å): U1-O1 1.810(4), U1-O2 1.911(4), O2-Sm1 2.34(1), Sm1-I1 3.0659(5), Sm1-I2 3.1077(3). Bond angles: O1-U1-O2 177.8(4)°, U1-O2-Sm1 176.3(4)°, O2-Sm1-O2' 180.0(3)°.

This molecule is entirely linear with bond angles of O1-U1-O2 177.8(2)°, U1-O2-Sm1 176.3(2)° and O2-Sm1-O2' 180.0(1)°. In contrast to the previously described uranyl(V) Pacman complexes the bond length U1-O1 (1.810(4) Å) shows

practically no elongation which would be expected for a reduced uranyl. However, U1-O2 has a bond length of 1.911(4) Å and is drastically effected by the coordination of Sm. The Sm-I bond distances of 3.0659(5) Å (Sm1-I1) and 3.1077(3) Å (Sm1-I2) reflect the oxidation state +3 for the samarium atom. As well as the Sm1-O2 distance of 2.342(4) Å these values are in accord with reported bond distances for Sm(III) compounds. For example, cyclopentadienyl samarium(III) diiodide $CpSmI_2(thf)_3$ shows bond lengths of 3.143 Å for Sm^{III}-I and 2.415 for Sm^{III}-O(thf)[225] and the seven coordinate cationic samarium complex $[(thf)_5SmI_2]^+[Co(CO)_4]^-$ has bond lengths of 3.010 Å for Sm^{III}-I and 2.459 Å for Sm^{III}-O(thf).[226] In contrast, iodide complexes of divalent samarium show slightly longer bond distances due to the reduced charge on the metal centre. For instance, the dimeric pentamethyl cyclopentadienyl samarium iodide complex $[Cp^*SmI(thf)_2]_2$ shows Sm^{II}-I distances of 3.356 Å and Sm^{II}-O(thf) distances of 2.670 Å.[227] Similarly, bond lengths of 3.317 Å for Sm^{II}-I and 2.542 Å for Sm^{II}-O(thf) were observed for the samarium diiodide tetramethylurea adduct $[SmI_2(thf)_2(CO(N(Me_2)_2)_2]$.[228]

Figure 50 shows the unit cell of **16** in the direction of the crystallographic *a*- and *c*-axis with the non-H,C atoms drawn as polyhedra. This figure illustrates the packing motif of **16** in the solid state, in particular the propeller-type packing of this linear molecule.

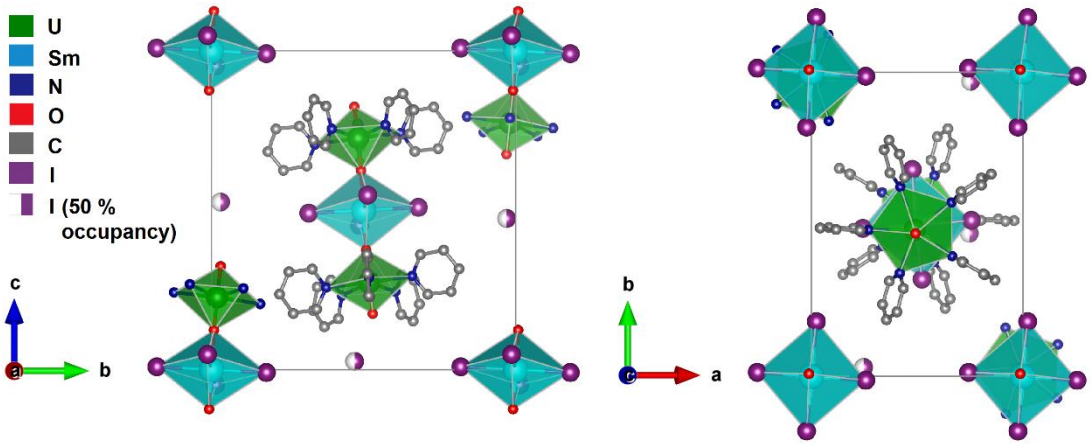

Figure 50 Unit cell of **16** in the direction of the crystallographic *a*- and c-axis.

The ^{1}H-NMR spectrum (Figure 51), recorded immediately after mixing **A** and $SmI_2(thf)_2$, shows the formation of new resonances which are attributable to a

Sm^{III}-O-U^{V}=O type complex within the Pacman framework. An NH resonance is observed at 68.78 ppm which can be assigned to the pyrrole protons in the lower macrocyclic pocket of the Pacman complex. Also, the methyl groups of the dimethyl dipyrromethane moiety are shifted to resonances of 20.62, 10.74, 1.83 and -5.29 ppm. These appear to be in the same region as the other oxo-metalated uranyl complexes which are described in this thesis. Additionally there are eight resonances which integrate to two hydrogen atoms each, and two resonances which integrate to six hydrogen atoms. These resonances can all be assigned to the symmetric Pacman scaffold that has been observed in mono-metalated uranyl(V) complexes. Therefore it appears that the Sm(III)-uranyl(V) Pacman complex may be a potentially isolable intermediate which subsequently undergoes transmetalation to **16**.

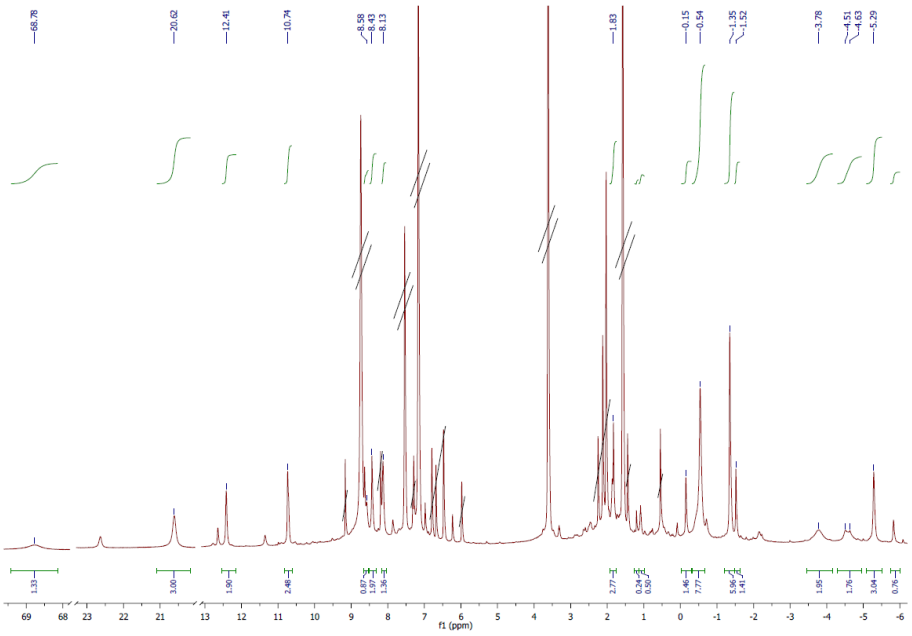

Figure 51 ^{1}H-NMR spectrum of the initial solution formed by adding $SmI_2(thf)_3$ to **A**. Crossed-out resonances are identified as uranyl(VI) Pacman (**A**); doubly crossed-out resonances are identified as pyridine and tetrahydrofuran.

The synthesis of a mixed halide analogue of **16** was targetted by treating $UO_2Cl_2(thf)_3$ in the presence of $SmI_2(thf)_2$ with metallic Sm (Scheme 44). The reaction was carried out in pyridine at room temperature and gave an instant colour change from yellow to red. However, after filtration of the red solution the only isolable was $UO_2I_2(py)_3$, which was confirmed by single crystal X-ray diffraction.[229]

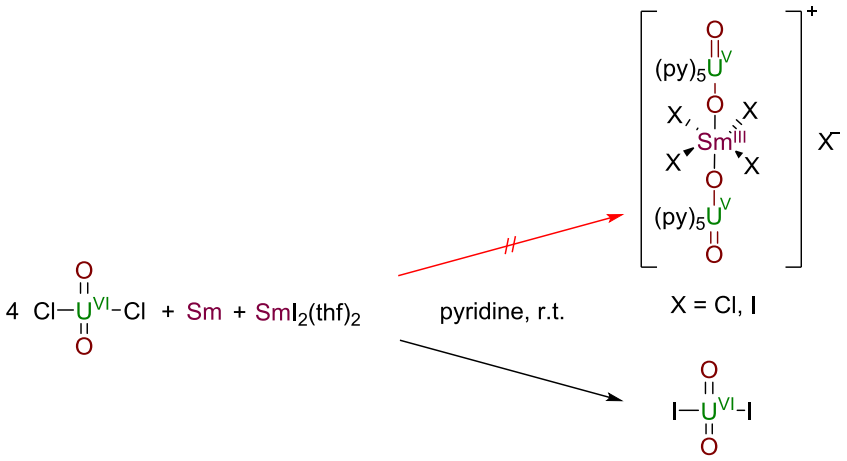

Scheme 44 Attempted reduction of uranyl chloride using Sm and SmI_2, forming uranyl iodide.

Similarly, synthesis of **16** was attempted by treatment of a brown suspension of two equivalents of uranium dioxide and samarium metal in pyridine by addition of 2.5 equivalents of I_2 (Scheme 45). The mixture was heated for 14 days at 80 °C to give a dark red solution, which lead only to the formation of $SmI_3(py)$. This is most likely due to the extremely poor solubility of UO_2.

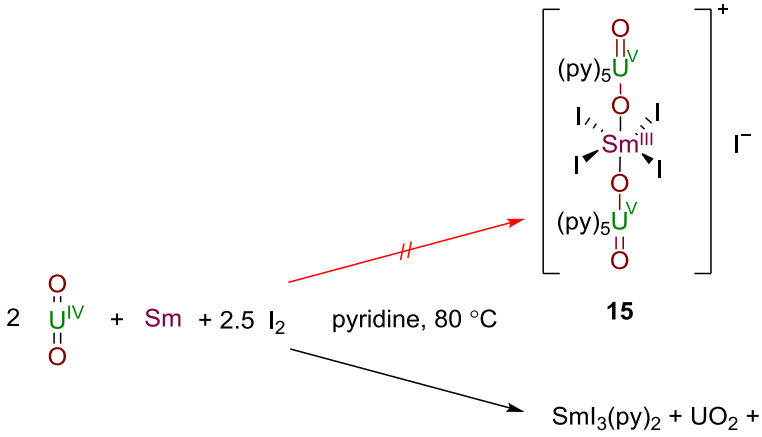

Scheme 45 Attempted oxidation of uranium dioxide and samarium metal with iodine in pyridine to **16** leading to the formation of $SmI_3(py)_2$.

Complex **16** appears to be a promising candidate for the study of mixed f-block complexes with potentially interesting magnetic properties, especially in the light of recent investigations by Mazzanti and co-workers who have successfully synthesised a uranyl(V) complex with a uranyl oxo capped by a manganese(II) ion. This complex shows the highest relaxation barrier reported for a mono-uranium system at 81 ± 0.5 K (Figure 52).[230]

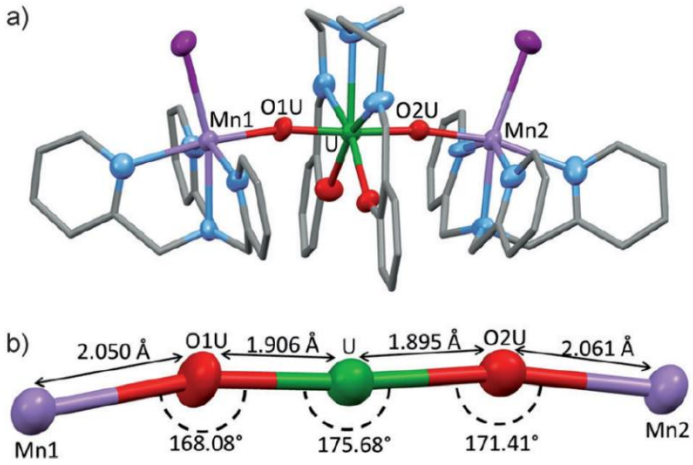

Figure 52 Depiction of the [UO_2Mn_2] complex synthesised by Mazzanti *et al.* a) Molecular structure of [UO_2Mn_2] (H atoms and solvent molecules omitted for clarity) b) View of the linear Mn-O-U-O-Mn core (C = grey, O = red, Mn = violet, N = light blue, I = purple, U = green.[230]

The linearity of **16** compared to that of the [UO_2Mn_2] complex and the combination of the [Xe] $4f^5$ electron configuration of the Sm(III) with the [Rn] $5f^1$ electron configuration of the uranyl(V) linked *via* the uranyl oxygen atoms may represent a good pathway for strong magnetic superexchange.

Currently a large scale synthesis of **16** is being developed with the aim of clarifying the reaction mechanism, identifying the side products and investigating the compound's magnetic properties.

4.1.2 Uranyl functionalisation using Yb and Dy

Since complex **16** has shown that the formation of Ln(III)-uranyl(V) complexes does occur and may result in uranyl oxo metalation the use of the reduction potential of the lanthanide metals in combination with their halide salts was envisaged to form Ln(III) uranyl(V) Pacman complexes (Scheme 46).

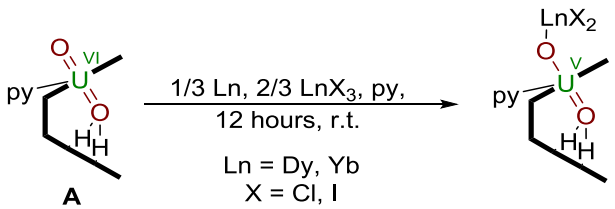

Scheme 46 Attempted synthesis of lanthanide functionalised uranyl(V) Pacman complexes.

Attempts were made to reductively functionalise **A** by addition of dysprosium metal chunks (0.33 eq) to a brown mixture of $DyCl_3$ (0.66 eq) and **A** (1 eq) in pyridine. The reaction was stirred at room temperature for 12 hours, resulting in a red solution. The solution was filtered and allowed to crystallise *via* solvent evaporation, yielding dark brown crystals of **A**.

Similarly, ytterbium metal (0.33 eq) was added to a solution of $YbCl_3$ (0.66) and **A** (1 eq) in pyridine. The mixture was stirred at room temperature for 12 hours, resulting in a red solution. After syringe filtration the obtained solution was allowed to crystallise by solvent evaporation After 48 hours a dark brown precipitate was obtained and after analysis by ^{1}H-NMR spectroscopy showed resonances that could only be assigned to that of **A**.

An *in-situ* NMR spectrum could not be obtained for the previously discussed reactions, possibly due to presence of unpaired f-electrons whose relaxation times are too fast to be measured on the NMR timescale, and perhaps also due to fast chemical exchange processes. This could result from either presence of Dy^{3+} ([Xe] $4f^9$) or Yb^{3+} ([Xe] $4f^{13}$) along with the possible formation of uranyl(V) ([Rn] $5f^1$).[231]

Additionally, an equimolar mixture of **A**, ytterbium metal and I_2 was stirred at room temperature in pyridine overnight. This was an attempt to either form YbI_2 *in-situ* or a reduced uranyl Pacman complex that subsequently undergoes oxidation by I_2. However, the only product that could be isolated from the red mixture were crystals of YbI_2. (Scheme 47).

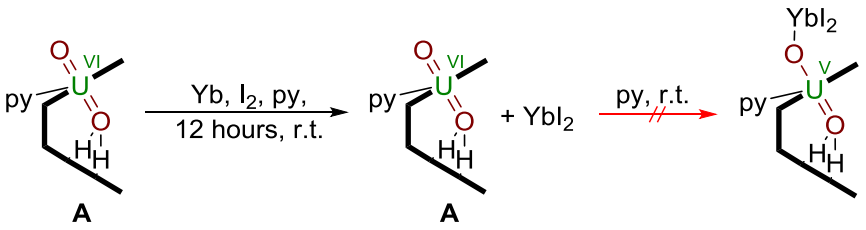

Scheme 47 Attempted synthesis of Yb-funtionalised uranyl Pacman by combined oxidation-reduction.

In the light of the previously described exogenous uranyl oxo-metalation using Group I, Group II, Group IV, Group XII and Group XIII metals and organometallic reagents similar Ln-uranyl(V) complexes could not be obtained.

4.2 Uranyl functionalisation using organometallic uranium compounds

In contrast to the lanthanides the chemical behaviour of the early actinides Th – Pu differs greatly and shows a wide range of different oxidation states.

In an attempt to synthesise the first homobimetallic U(IV)-uranyl(V) complex different uranium(III) starting materials had been chosen to reductively functionalise uranyl(VI) in the Pacman complex. The material used for the syntheses described in paragraph 4.2.1 and 4.3 were prepared in collaboration with Michał S. Dutkiewicz at the Institute for Transuranium Elements in Karlsruhe, Germany; uranyl(VI) tetraethyl Pacman $\mathbf{A^{Et}}$ was synthesised with the tetraethyl macrocycle H_4L^{Et} and purified by pentane extraction. The reagent Cp_3U was synthesised *via* reduction of Cp_3UCl with sodium amalgam and purified by pentane extraction. All other syntheses and characterisations were carried out at the University of Edinburgh.

4.2.1 Uranyl functionalisation using Cp_3U

Treatment of $\mathbf{A^{Et}}$ with Cp_3U in THF-d_8 at -96 °C resulted in the formation of brown plates of $[Cp_3UOUO(thf)(H_2L^{Et})]$ **17**, the first homobimetallic uranium complex containing both uranium(IV) and uranyl(V) (Scheme 48).

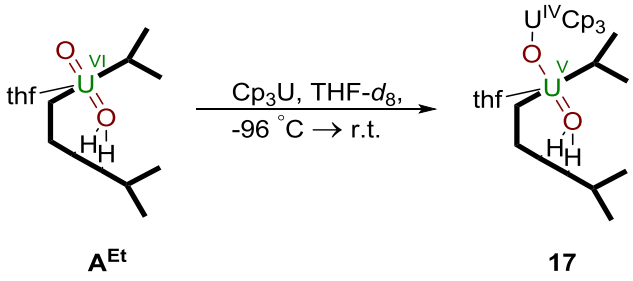

$\mathbf{A^{Et}}$ **17**

Scheme 48 Reductive metalation of $\mathbf{A^{Et}}$ with Cp_3U.

The solid state structure of **17** is shown in Figure 53. **17** crystallises as thin brown plates in a triclinic crystal system, and the structural solution was performed in space group *P*-1 with two molecules per unit cell.

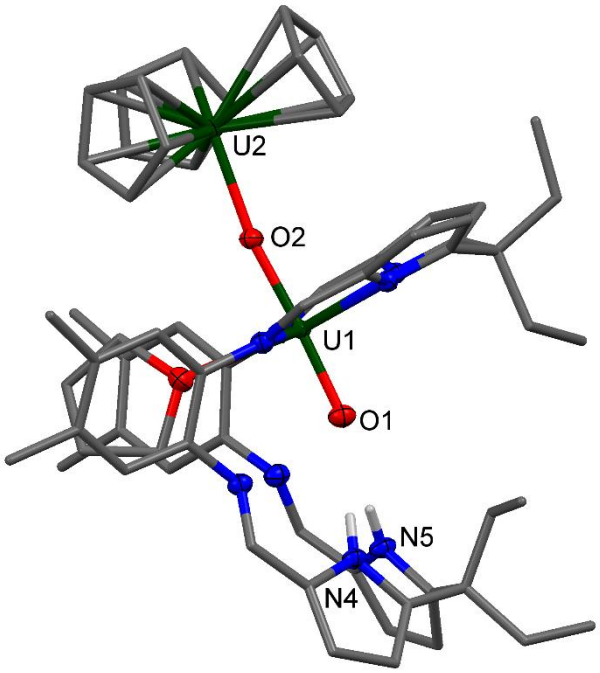

Figure 53 Solid state structure of **17** (side view). For clarity, all hydrogen atoms except the pyrrole NHs and all solvent molecules are omitted (displacement ellipsoids are drawn at 50% probability). Selected bond lengths (Å): U1-O1 1.844(3), U1-O2 1.986(3), U2-O2 2.245(3), O1-N4 3.137(4), O1-N5 3.070(4). Bond angles: O1-U1-O2 176.9(1)°, U1-O2-U2 171.3(1)°.

The solid state structure of **17** represents a uranyl(V) Pacman complex with bond distances of 1.844(3) Å for U1-O1 and 1.986(3) Å for U1-O2, characteristic of the +5 oxidation state for the uranyl. The bond distance of 2.245(3) Å for U2-O2 represents the +4 oxidation state for the capped oxo atom. This is consistent with other U(IV) complexes containing oxo-groups[232][233] an makes this complex an f^1-f^2system. The uranyl (O1-U1-O2) remains practically linear with a bond angle of 176.9(1)°, and the capped oxo uranium bond angle (U1-O2-U2) only slightly out of linearity with an angle of 171.3(1)°.

^{1}H-NMR analysis shows that this material has a high tendency to disproportionate in THF-d_8 solution showing, showing the resonances of **17**, the presence of the starting material $\mathbf{A^{Et}}$ and an unidentified compound. The ^{1}H-NMR resonances of **17** show clearly the resonances of $\mathbf{A^{Et}}$ (Figure 54). ^{1}H-DOSY showed the presence of two major products of comparable size, which were ascribed to **17** and $\mathbf{A^{Et}}$.

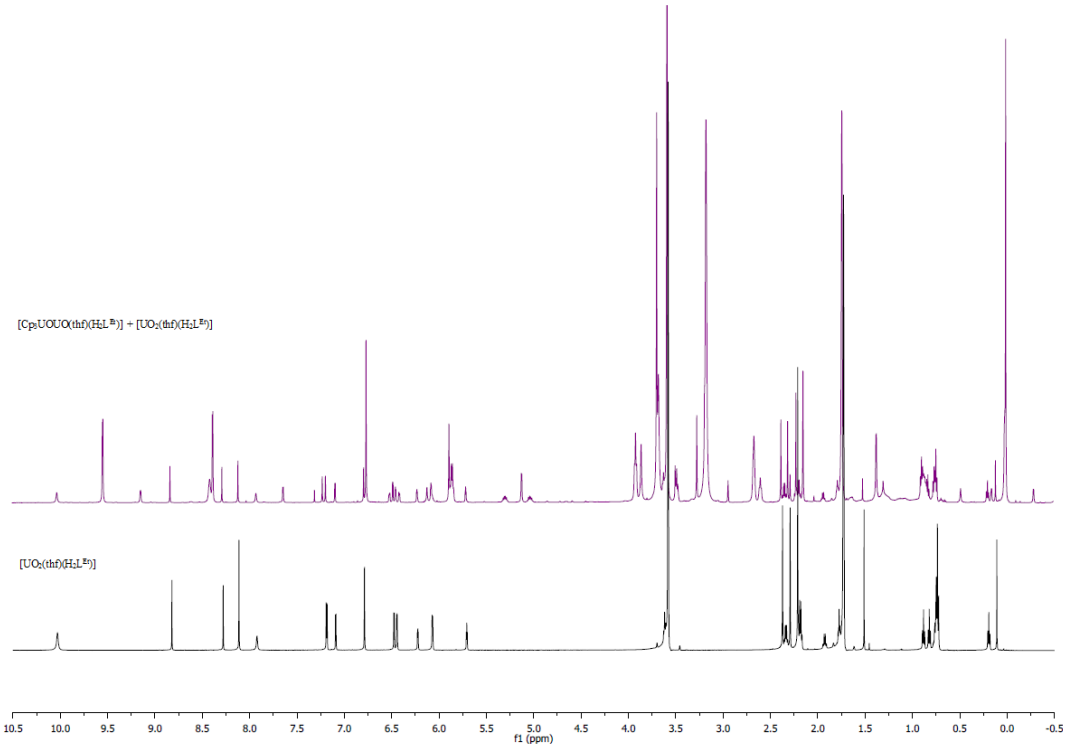

Figure 54 ^{1}H-NMR spectrum of crystalline **17** (top) and $[UO_2(thf)(H_2L^{Et})]$ $\mathbf{A^{Et}}$ (bottom) from 10.5 to -0.5 ppm in THF-d_8, showing the presence of $\mathbf{A^{Et}}$, indicating the tendency of **17** to decompose to give uranyl(VI) (high frequency resonances in **17** omitted for clarity).

Similarly, the synthesis of **17** was attempted by adding Cp_3UCl to a tetrahydrofuran solution of potassium uranyl(V) Pacman **6** at room temperature (Scheme 49).

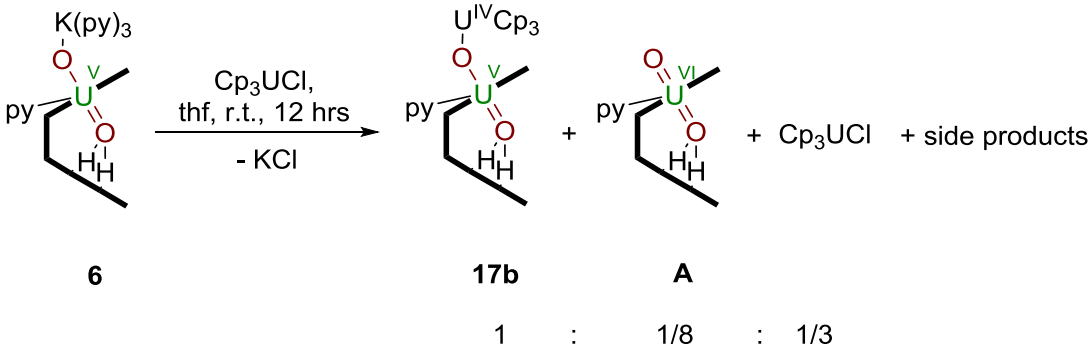

Scheme 49 Salt metathesis of **6** with Cp_3UCl to form **17b**.

After 12 hours at room temperature a white precipitate formed and the ^{1}H-NMR spectrum showed the formation of a new product which was assigned to **17b**. However, also the formation of uranyl(VI) Pacman **A** (12 % with respect to the

resonances assigned to **17b**) was observed; in addition resonances were observed which could not be ascribed to any known component that may be expected to form in this mixture. Similarly, unreacted Cp_3UCl remained present and accounted for 33 % with respect to **17b**. The ^{1}H-NMR showed no resonances for the starting material **6**, $Cp_3U{\cdot}thf$ (-15.35 ppm) or Cp_4U (20.20 ppm)[234] could be observed. Heating of this mixture to 70 ºC for three hours gave an increase of the amount of **A** from 12 % to 25 %. This indicates a high tendency for disproportionation as already observed for **17**. Hence no pure material of **17b** could be isolated from this reaction.

In order to investigate whether the above salt metathesis reaction gives isolable products two reactions of **6** with UCl_4 and $ThCl_4(dme)_2$ in pyridine were attempted. However, both reactions have not shown any formation of a complex that could be assigned to either $[(solv)_x(Cl_3UOU^VO)(py)(H_2L)]$ or $[(solv)_x(Cl_3ThOU^VO)(py)(H_2L)]$. The ^{1}H-NMR spectrum showed in both cases the re-formation of **A**, possibly attributable to a fast disproportionation of uranyl(V) induced by the addition of an actinide halide.

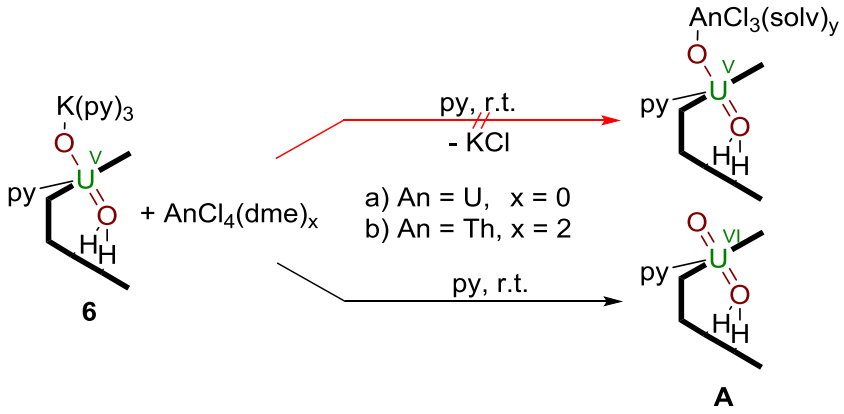

Scheme 50 Attempted salt metathesis of **6** using UCl_4 (a) and $ThCl_4(dme)_2$.

4.2.2 Uranyl functionalisation using $U(N(SiMe_3)_2)_3$

4.2.2.1 Reduction of $[(U^{VI}O_2)(py)(Zn)(py)(L)]$ with $U(N(SiMe_3)_2)_3$

Treatment of one equivalent of uranyl(VI)-Zn(II) Pacman complex $[(U^{VI}O_2)(py)(Zn)(py)(L)]$ $\mathbf{A^{Zn}}$ with one equivalent of uranium tris(hexamethyl-disilylamide) $U(N(SiMe_3)_2)_3$ in pyridine at -35 °C gave a dark red solution. Upon standing red crystals of the singly reduced complex $[(U^{V}O_2)(py)(Zn)(py)(L)]$ **18** suitable for X-ray structural analysis were obtained in a 70 % yield (Scheme 51).

The fate of the uranium(III) trisamide[235] remains unclear in this reaction. It is assumed that it reacts to the uranium(IV) metallacycle,[236] however, no resonances attributable to that product could be found in the *in-situ* ^{1}H-NMR spectrum.

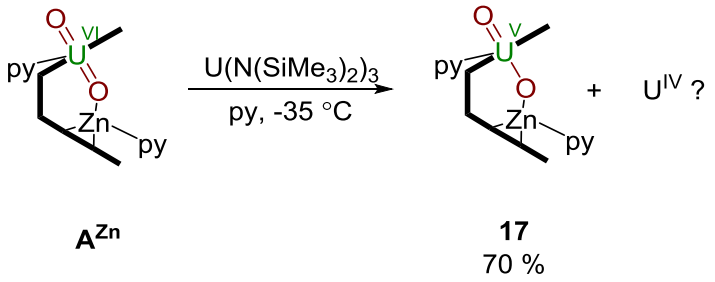

$\mathbf{A^{Zn}}$ **17** 70 %

Scheme 51 Synthesis of a uranyl(V)-Zn Pacman complex with no exogenous oxo-metalation.

18 crystallises in an orthorhombic cell, and the structural solution was performed in space group *Pnnm* with four molecules per unit cell. The solid state structure is shown in Figure 55. It shows that the molecule adopts the Pacman geometry with the zinc atom being crystallographically disordered. The disorder shows that 69 % of the zinc (Zn1A) is coordinated between the pyrrole-N and the imine group. In addition the Zn1A is coordinated by a pyridine solvent molecule and hence obtains a tetrahedral coordination environment. Also, 31% of the zinc (Zn1B, not shown for clarity) is sitting on the mirror plane between the two pyrrole-N and the *endo*-oxygen atom O1.

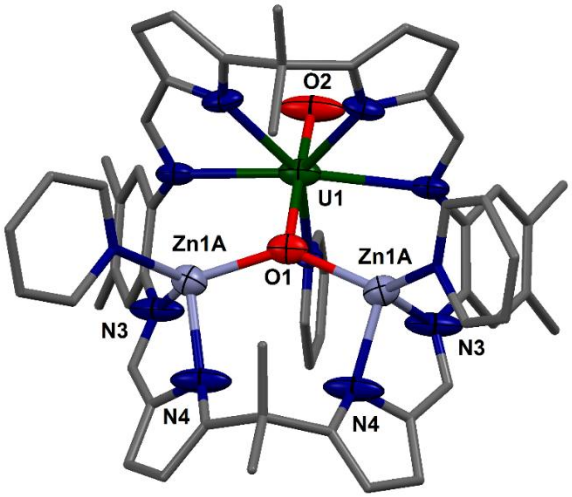

Figure 55 Solid state structure of **18**. For clarity only the major component is shown and all hydrogen atoms and all solvent molecules are omitted (displacement ellipsoids at 50% probability). Selected bond lengths (Å): U1-O1 1.92(2), U1-O2 1.82(2), O1-Zn1A 2.081(7), Zn1A-N3 2.00(2), Zn1A-N4 2.06(2). Bond angles: O1-U1-O2 172.4(7)°, U1-O1-Zn1A 107.3(7)°

The bond angle of 172.4(7)º for the O1-U1-O1 bond is representative of a *trans* oxo configuration. As observed in the previously described uranyl Pacman complexes the U-O bond distance that coordinates the metal atom is slightly longer than the uncoordinated one. In this case however it affects the endogenous U1-O1 distance, giving a bond length of 1.92(2) Å, whereas the exogenous U1-O2 bond distance has a value of 1.82(2) Å. This elongation of the bond lengths is significant for the +5 oxidation state of **18** when compared to the uranyl(VI) $O=U^{VI}=O$ bonds of 1.793(6) Å and 1.773(6) Å as reported for **A**.[125]

This reaction exemplifies that uranyl(V) compounds of the Pacman complex can be accessed by previous complexation of the lower macrocyclic pocket in uranyl(VI) Pacman with an oxophilic metal that subsequently helps to stabilise the uranyl(V) oxidation state. In contrast to the Zn(II)-uranyl(V) complexes **14** and **15** which show an exogenous oxo-coordination and which have been obtained *via* reduction using elemental zinc this complex is not reduced by the coordinating zinc but by the non-coordinating reducing agent $U(N(SiMe_3)_2)_3$. It can be hypothesised that uranyl(V) oxo-metal complexes may be obtained regardless of the oxophilicity of the reducing agent when a suitable coordination environment is provided.

4.2.2.2 Synthesis of $[(py)_3(KOUO)(py)(H_2L)]$ 6 *via* reduction of A using $K[U^{III}(N(SiMe_3)_2)_4]$

Attempts to use $U^{III}(N(SiMe_3)_2)_3$ as a reducing agent for uranyl(VI) Pacman **A** has serendipitously led to the synthesis of $U^{IV}(N(SiMe_3)_2)_4$. The addition of $K(py)_6[U^{III}(N(SiMe_3)_2)_4]$,[237] prepared by combining pyridine solutions of $KN(SiMe_3)_2$ with $U^{III}(N(SiMe_3)_2)_3$, to **A** led to the formation of the previously described uranyl(V) alkali metal complex **6** (*cf.* 2.1.2). ^{1}H-NMR spectroscopy confirmed the formation of $U^{IV}(N(SiMe_3)_2)_4$ **B** as the side product in essentially quantitative yield (Scheme 52).

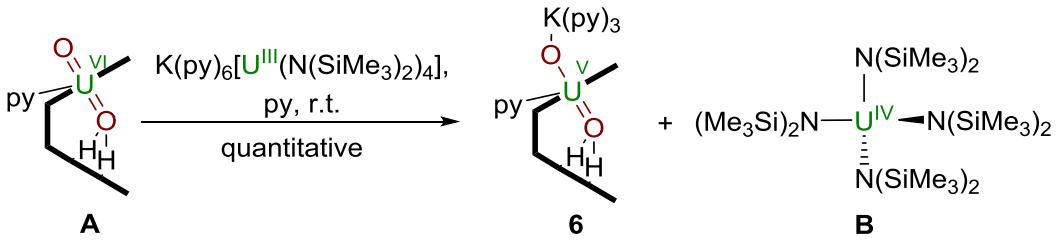

Scheme 52 Synthesis of **6** and **C** by reduction of **A** using $K(py)_6[U^{III}(N(SiMe_3)_2)_4]$.

The formation of $U^{IV}(N(SiMe_3)_2)_4$ can easily be observed by its ^{1}H-NMR resonance at -3.23 ppm in pyridine-d_5 as shown in Figure 56. Subsequent hexane extraction of this material allows the isolation of both pure metalated uranyl Pacman **6** and **B**.

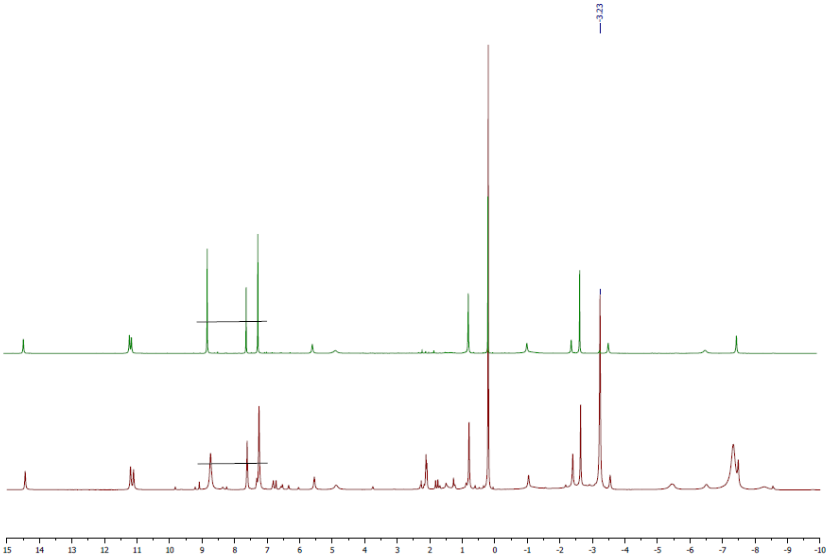

Figure 56 ^{1}H-NMR spectrum from 15 to -10 ppm in C_5D_5N of pure **6** (top) and of a reaction between **A** and $K(py)_6[U^{III}(N(SiMe_3)_2)_4]$ yielding a 1:1 mixture of **6** and **B** (-3.23 ppm) (bottom).

At the same time that this work was being carried out the uranium(IV) tetrakisamide complex **B** was synthesised independently by Schelter and co-workers in 2013 by controlled single electron oxidation of $U^{III}(N(SiMe_3)_2)_3$ using oxidising agents such as [TEMPO][BF_4] or $FcPF_6$ in THF.[238] This method gave low yields which was later improved by oxidation of $K(thf)_6[U^{III}(N(SiMe_3)_2)_4]$ with CuI, resulting in the formation of $U^{IV}(N(SiMe_3)_2)_4$ quantitatively. The crystallographic characterisation of this material is identical to the material described in this thesis.[238]

The synthesis of this uranium(IV) compound has been quite a difficult task for many years, with Andersen and co-workers only report the formation of $HU^{IV}(N(SiMe_3)_2)_3$ by addition of four equivalents of $NaN(SiMe_3)_2$ to a THF suspension of UCl_4, assuming THF to be the source of hydrogen, which reacts upon heating to 140 °C for 45 minutes to the uranium(IV) metallacycle in 85 % yield.[236][239]

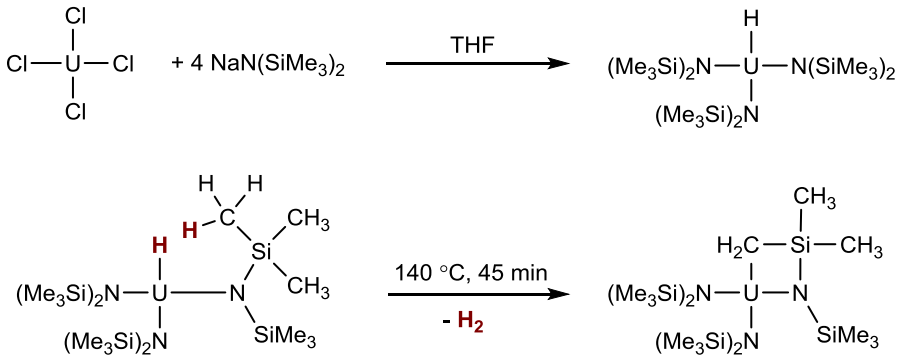

Scheme 53 Synthesis of the uranium(IV) metallacycle.

Notably, the comproportionation reaction of **A** and $K(py)_6[U^{III}(N(SiMe_3)_2)_4]$ described here features all four common oxidation states of uranium in a one-pot synthesis. It yields quantitatively the alkali metal uranyl(V) complex and the sterically congested, yet stable uranium(IV) tetrakis(hexamethyldisilylamide), both of which may be used as versatile starting materials for uranyl(V) and uranium(IV) chemistry.

4.3 Uranyl functionalisation using transuranium elements

The functionalisation of uranyl(VI) with transuranium elements is, not only in the light of air- and moisture-sensitive materials, a very demanding task. When undertaking transuranic research one encounters scarce availability of these materials, high radiotoxicity and also very high bureaucratic barriers, leading to a very limited number of places worldwide in which one is allowed to handle these elements in higher quantities. Regarding the specific requirements in synthesis, analysis and radiologic safety these materials can only be handled in designated research institutes. The following experiments were therefore undertaken at the Institute for Transuranium Elements (ITU) in Karlsruhe, Germany, a Joint Research Centre of the European Commission. This institute is a high-security area equipped with low-pressure glove-boxes and hot cells, designed for the safe handling, manipulation and analysis of nuclear power plant reactor core material, highly enriched nuclear fuel and highly radioactive isotopes for α-immunotherapy (^{213}Bi, ^{225}Ac). In particular, the ITU is one of the few places where one can handle and study the early transuranium elements neptunium, plutonium, americium and curium. An outstanding fact is that the ITU is worldwide the only institute which can provide elemental neptunium metal for synthetic chemistry (Figure 57).

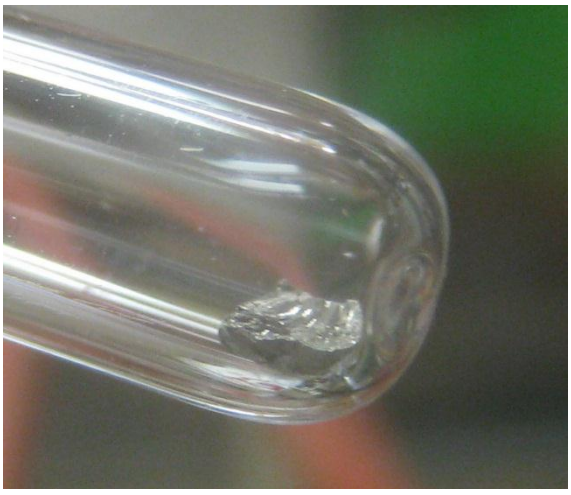

Figure 57 114 mg of metallic ^{237}Np used for the synthesis of low-valent organometallic neptunium starting material. The size of this material is approximately 5 mm × 3 mm × 3 mm. The activity is about 3 MBq. At the time of usage this material provided roughly 50 % of the world stock in elemental neptunium metal.

The EU Actinet-I3-AC3-JRP-02 and Talisman-JRPL-C02-07 programs granted altogether nine weeks of laboratory work in the Actinide User Labs of the ITU. The work was supervised by Prof. Dr. Roberto Caciuffo, Dr. Christos Apostolidis and Dr. Olaf Walter and carried out in close collaboration with Michał S. Dutkiewicz. During this time the syntheses of a variety of low-valent organometallic neptunium starting materials were undertaken (of which the description is subject to the doctoral thesis of Michał S. Dutkiewicz). The main focus was to target uranyl functionalisation, and it was envisaged to specifically compare the chemistry of trivalent uranium and neptunium complexes and their reductive potential towards uranyl(VI) Pacman.

4.3.1 Uranyl functionalisation using $Cp_3^{237}Np$

Treatment of $\mathbf{A^{Et}}$ with one equivalent of $Cp_3{}^{237}Np$ in tetrahydrofuran at -78 °C lead to the formation of a red solution. Filtration of this solution and recrystallisation by hexane diffusion led to the isolation of the first transuranium uranyl(V) Pacman complex $[Cp_3NpOUO(thf)(H_2L^{Et})]$ **19** (Scheme 54).

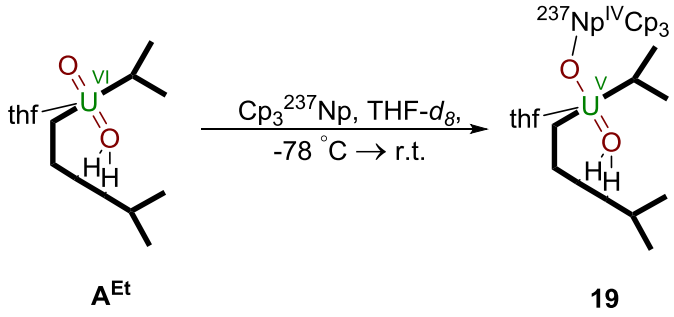

Scheme 54 Reductive metalation of $\mathbf{A^{Et}}$ with $Cp_3{}^{237}Np$.

The reaction between Cp_3Np and $\mathbf{A^{Et}}$ led to the formation of crystalline material suitable for X-ray diffraction. The solid state structure of **19** is shown in Figure 58. **19** crystallises as dark brown plates in a triclinic crystal system and the structural solution was performed in space group *P*-1 with two molecules in the unit cell. It is isostructural to its uranium congener $[Cp_3UOUO(thf)(H_2L^{Et})]$ **17**.

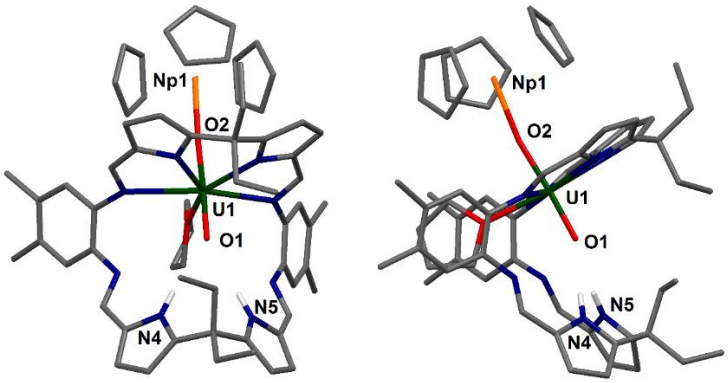

Figure 58 Solid state structure of the first heterobimetallic transuranium-uranyl(V) complex **19** in front view (left) and side view (right). For clarity, all hydrogen atoms except the pyrrole NHs and all solvent molecules are omitted (displacement ellipsoids are drawn at 50% probability). Selected bond lengths (Å): U1-O1 1.826(8), U1-O2 1.973(7), Np1-O1 2.251(7), O1-N4 3.15(1), O1-N5 3.09(1). Bond angles: O1-U1-O2 176.9(3)°, Np1-O1-U1 170.6(4)°.

Complex **19** is the Np analogue of complex **17**. The uranyl moiety shows a similar elongation for U1-O1 and U1-O2 in **19** (1.826(8) Å and 1.973(7) Å) as in **17** (1.844(3) Å and 1.986(3) Å). The same behaviour can be observed in the O1-$N_{pyrrole}$ distances (3.15(1) Å/3.09(1) Å (**19**) and 3.137(4) Å/3.070(4) Å (**17**)). Both the coordination of neptunium(IV) and uranium(IV) to the uranyl moiety are essentially linear (An^{IV}-O2-U1: 170.6(4)° (**19**) and 171.3(1)° (**17**)). Table 15 lists the main characteristics of the two actinide(IV)-uranyl(V) complexes. The bond distances are comparable in both complexes, with all values within the experimental error.

Table 15 Comparison of bond distances and angles of complexes 17 and 19

Entry	U^{IV}-O-U^{V}=O **17**	Np^{IV}-O-U^{V}=O **19**
U1-O1 (Å)	1.844(3)	1.826(8)
U1-O2 (Å)	1.986(3)	1.973(7)
O1···N (Å)	3.137(4)/3.070(4)	3.15(1)/3.09(1)
An^{IV}-O2 (Å)	2.245(3)	2.251(7)
O1-U1-O2 (°)	176.9(1)	176.9(3)
An^{IV}-O2-U1 (°)	171.3(1)	170.6(4)

The similarity of the two materials **17** and **19** exemplifies the proximity of the solid state behaviour of low-valent neptunium complexes to low-valent uranium complexes. It demonstrates the crucial role of An^{4+} ions in nuclear material.[240] Compounds like these may represent an important bonding motif of nuclear waste, since nuclear fuel is mainly formed of UO_2 pellets, which in a nuclear reaction can be transformed to NpO_2 with the metal in the oxidation state +4. Similarly dissolved nuclear fuel rods contain mainly UO_2^{2+} as well as NpO_2^{+} with the actinide metals in their higher oxidation states. During the nuclear fuel cycle and waste disposal these ions change their oxidation states in a similar manner. Hence neptunium can be seen as a hazardous substitute for uranium in nuclear fuel, nuclear waste and in nuclear accidents.

Additionally, an experiment that originally targeted the functionalisation of $\mathbf{A^{Et}}$ with $Cp_3{}^{237}Np$ has led to a new transuranium oxo-complex Treatment of $\mathbf{A^{Et}}$ with Cp_3Np in THF has resulted in the formation of a red solution, from which crystals of $[Cp_3NpONp(Cp_2)ONpCp_3]$ **20**. However, at the time of writing it is not clear from which particular reaction this product might stem, and current attempts to reproduce this material by the co-workers at ITU (Michał S. Dutkiewicz *et al.*) have failed.

It is conceivable that this material may have formed due to a simple contamination of the reaction vessel with molecular oxygen, however, in the absence of oxygen this compound may have formed in a successive deoxygenation of the THF solvent[241,242] or uranyl (Scheme 55).

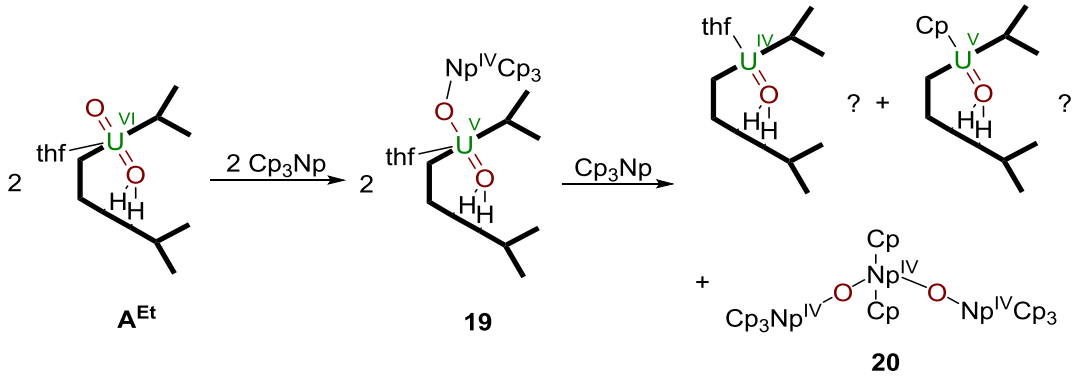

Scheme 55 Proposed reaction of $\mathbf{A^{Et}}$ with Cp_3Np leading to the formation of **19**.

As a preliminary result the crystallographic *.res file (courtesy to Dr. Olaf Walter) is used in Figure 59 to displaying the connectivity in **20**.

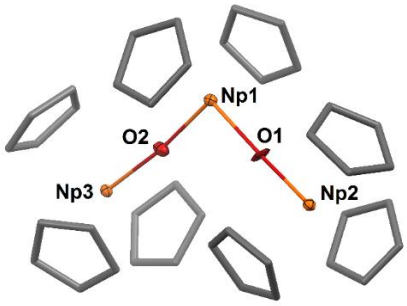

Figure 59 Solid state structure of the **20** based on the crystallographic *.res file. For clarity, all hydrogen atoms are omitted (displacement ellipsoids are drawn at 50% probability). Selected bond lengths (Å): Np-O1 2.0834, Np1-O2 2.0843, Np2-O1 2.0947, Np3-O2 2.0915. Bond angles: O1-Np1-O2 100.94°, Np1-O1-Np2 172.82°, Np1-O2-Np3 173.44°.

The solid state structure of **20** shows three Np(IV) centres, linked by two oxygen atoms. The Np-O distances are similar and average to 2.088 Å, representing the Np(IV) oxidation state.[243] The structure of the molecule is bent, and the main angle is represented by O1-Np1-O2 with 100.94°. The two Np-O-Np angles are essentially linear with 172.82° (Np1-O1-Np2) and 173.44° (Np1-O2-Np3). The geometry around the Np atoms is pseudo-tetrahedral. The angles on Np1 are with 121.58° largest for the Cp-Np1-Cp angle because of the steric demand of the Cp groups, but close to the ideal tetrahedral angle of 109.5° for the Cp-Np1-O angles (Cp-Np1-O2: 104.32° and 108.58°; Cp-Np1-O1: 109.86° and 109.45°). The six bond angles around Np2 fluctuate slightly around 109.5° (100.64°, 101.54°, 101.61°, 115.74°, 116.02° and 117.08°) as do the six angles around Np3 (99.86°, 101.40°, 102.60°, 116.01°, 116.26° and 116.51°).

4.3.2 Uranyl functionalisation using $Cp_3^{239}Pu$

The chemistry of the transneptunium element plutonium has recently lead to the first plutonium based $5f^5$ single molecule magnet in form of a Pu(III) [tris-(tri-1-pyrazolylborato)] complex.[244]

Here we attempted to generate the first heterobimetallic transneptunium uranyl(V) complex in a Pu^{IV}-O-U^{V}=O motif in a $5f^4 – 5f^1$ electron combination.

Olive green $\mathbf{A^{Et}}$ was mixed with dark green $Cp_3{}^{239}Pu$ in a Schlenk vessel and cooled the mixture with dry ice pellets. To this THF-d_8 was added and the dark green mixture was allowed to stir and warm to room temperature, and no colour change was observed. The material was dried and attempted to be recrystallised from this THF-d_8 solution by hexane diffusion but only microcrystalline material could be isolated which was tested for X-ray structural analysis but showed no diffraction. Because of poor quality of the obtained material and because of the handling difficulties regarding ^{239}Pu and the larger quantities of material needed for UV-vis or NMR spectroscopy this material was put aside and not considered for any further chemical analysis.

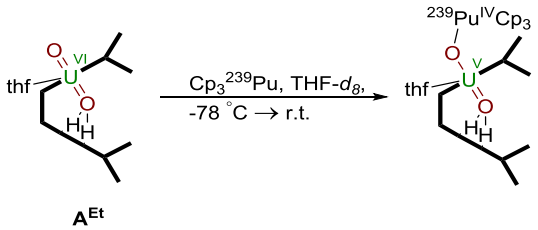

Scheme 56 Attempted reductive metalation of $\mathbf{A^{Et}}$ with $Cp_3{}^{239}Pu$

4.4 Conclusion

It has been shown in this chapter that the synthesis of lanthanide-actinyl and actinide-actinyl cation-cation complexes results in shows some inherent difficulties. The reductive metalation of uranyl(VI) with lanthanides and their respective metal halides is likely to happen in analogy with the previously described reactivity regarding Group I (Chapter 2) and Group II or Group XII (Chapter 0) metals. However, the presence of unpaired f-electrons inhibits their spectroscopic characterisation and it has not been possible to isolate a mono-metalated Ln(III)-uranyl(V) complex. In contrast to this results the treatment of uranyl(VI) Pacman with $SmI_2(thf)_2$ to a transamination and the formation of a bis(uranyl(V))-Sm(III) complex.

The reductive uranyl functionalisation has been demonstrated using Cp_3U to generate the first U(IV)-uranyl(V) CCI complex. This chemistry could be repeated successfully using a transuranium element, to generate the first heterobimetallic actinide(IV)-actinyl(V) complex with tetravalent neptunium. Both complexes are isostructural and prove that under reducing conditions the formation of actinide-actinyl CCIs is possible.

5 Uranyl functionalisation in redox active dipyrrole ligands

The chemistry of the Pacman ligand in Pacman porphyrins, heteroditopic pyrroles and calix[n]pyrroles has allowed for a wide variety of new bimetallic cobalt, palladium, nickel, copper, manganese and chromium complexes to be isolated.[132,245,246] Such complexes have demonstrated their reactivity towards photocatalytic oxidation of hydrocarbons,[247] their ability to serve as oxygen reduction catalysts[248–250] and their use as single molecule magnets.[60] This chemistry is limited with respect to the rigid ligand framework, which, if altered, can potentially affect the structural and electronic properties of some of these metal complexes, and hence lead to unexpected and novel reactivity modes.

One approach to functionalise the Pacman framework is the substitution of the methyl groups on the dimethyl dipyrromethane moiety for an electron withdrawing pentafluorophenyl Group and a hydrogen atom (Figure 60). This results in the dipyrromethane (sp^3) moiety to become redox active, and to oxidise readily to a dipyrromethene (sp^2) (also referred to as "*dipyrrin*"). Upon deprotonation the ligand formally changes from an L^{-2} ligand in the dipyrromethane to an L^{-1} ligand in the dipyrromethene. These dipyrromethenes have recently seen significant development, particularly with respect to applications regarding fluorescence and other optical properties.[251] In particular, the boron dipyrromethene BODIPY (Figure 60) has been studied intensively because of its intense colour and fluorescence,[252] photosensitivity with application to photodynamic therapy,[253] stability[254] and ease of access.[255]

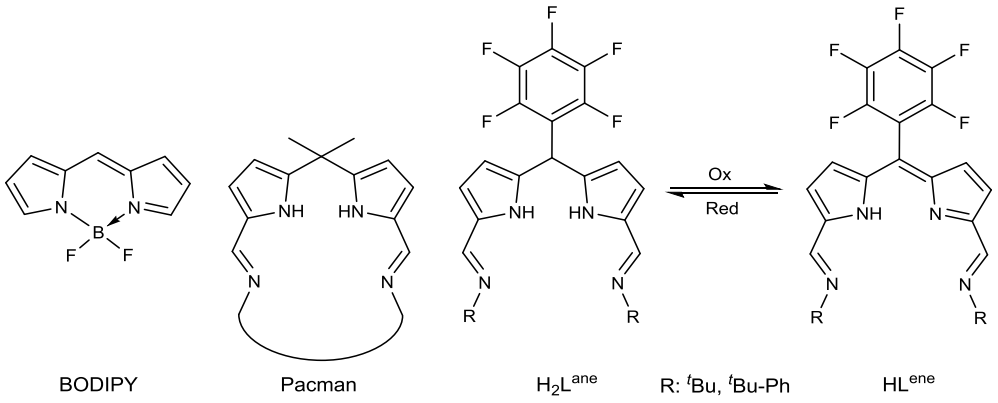

Figure 60 BODIPY and modification of the 'classic' Pacman dipyrromethane moiety by substitution of methyl for pentafluorophenyl and hydrogen, resulting in a redox-active ligand.

These ligands have been recently made in our labs[256] and their complexation studies were carried out along with Lucy N. Platts, James R. Pankhurst (synthesis and characterisation of uranyl(VI) (**21**) and uranium(IV) (**22**) dipyrrin complexes) and Dr. Daniel Betz (reductive silylation of uranyl dipyrromethane complexes (**23**)). This collaborative work is described in the following section.

5.1 Uranyl functionalisation in dipyrromethene ligand

5.1.1 Synthesis of uranyl(VI) dipyrromethene complex

The newly developed 4*N*-donor ligand H_2L^{ane}, consisting of a pentafluorophenyl dipyrromethane moiety readily oxidises on air[256] to give the corresponding purple dipyrromethene HL^{ene}. Treatment of the latter with one equivalent of uranyl bis(hexamethyldisilylamide) at room temperature in pyridine or tetrahydrofuran and subsequent substitution of the remaining silylamide group by treatment with one equivalent of pyridine hydrochloride yield the blue dipyrromethene uranyl(VI) chloride complex $[UO_2(Cl)(L^{ene})]$ **21** in 76 % yield (Scheme 57).

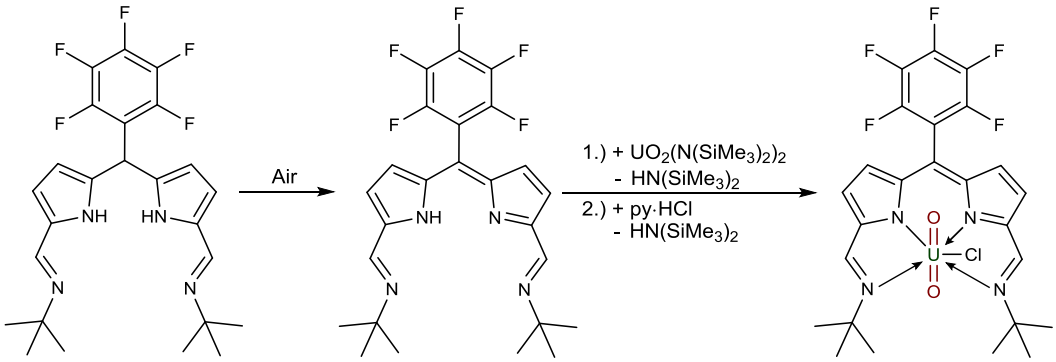

Scheme 57 Synthesis of uranyl(VI) dipyrromethene complex $[UO_2(Cl)(L^{ene})]$ **21**.

Single red pleochroic prisms of **21** which appear blue under transmitted light were obtained after recrystallisation from a concentrated benzene solution and were suitable for X-ray crystallographic analysis. **21** crystallises in a monoclinic crystal system and the structural solution was performed in space group *Cc* with four molecules per unit cell. The molecular structure is shown in Figure 61.

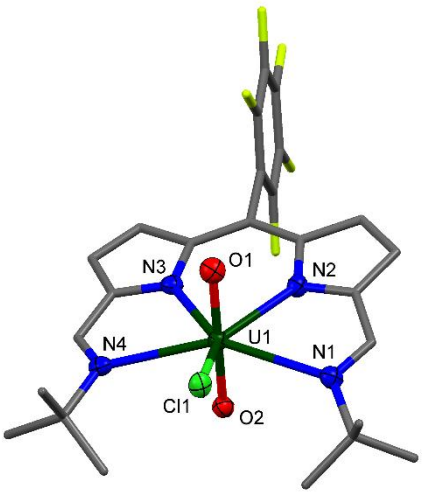

Figure 61 Solid state structure of **21**. For clarity, all hydrogen atoms and all solvent molecules are omitted (displacement ellipsoids are drawn at 50% probability). Selected bond lengths (Å): U1-O1 1.766(4), U1-O2 1.763(4). Bond angles: O1-U1-O2 175.5(2)°.

The solid state structure of **21** exhibits a pentagonal-bipyramidal uranyl(VI) moiety with bond distances for U1-O1 of 1.766(4) Å and U1-O2 of 1.763(4) Å, with an O1-U1-O2 bond angle of 175.5(2)°. The uranyl is coordinated in its equatorial plane by one chloride atom and by the four nitrogen atoms of the ligand with a U-N_{imine} bond length of 2.683 Å and a U-$N_{pyrrole}$ bond length of 2.474 Å. The C-C bond distances from the methene carbon to the pyrrole rings have values of 1.404(7) Å (C10-C9) and 1.387(7) Å (C10-C17), which are shorter than the average C-C single bonds of 1.54 Å and longer than the average C=C double bonds of 1.33 Å, representing the mesomeric stabilisation of the dipyrromethene (Figure 62).

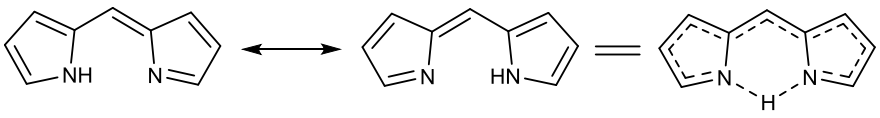

Figure 62 Mesomeric stabilisation of dipyrromethene.

Compound **21** has been tested for its stability in benzene, toluene, hexane, tetrahydrofuran and pyridine. It was found that the compound is unstable in the latter if left standing for a prolonged period of time. The ^{1}H-NMR spectrum was recorded straight after dissolving **21** in C_5D_5N, and after 12 and 36 hours. A dominant feature that could be observed is an increase in the resonance of the *tert*-butyl group of the

tert-butyl amine at 1.16 ppm (#). After 12 hours at room temperature the ratio of **21** to free *tert*-butyl amine is 70 % to 30 %, which rises to a ratio of 55 % to 45 % after 36 hours. Similarly, the imine resonance at 9.65 ppm (*) decreases with the same ratio (Figure 63). This suggests that the compound disintegrates by a bond-breakage of the imine-bond.

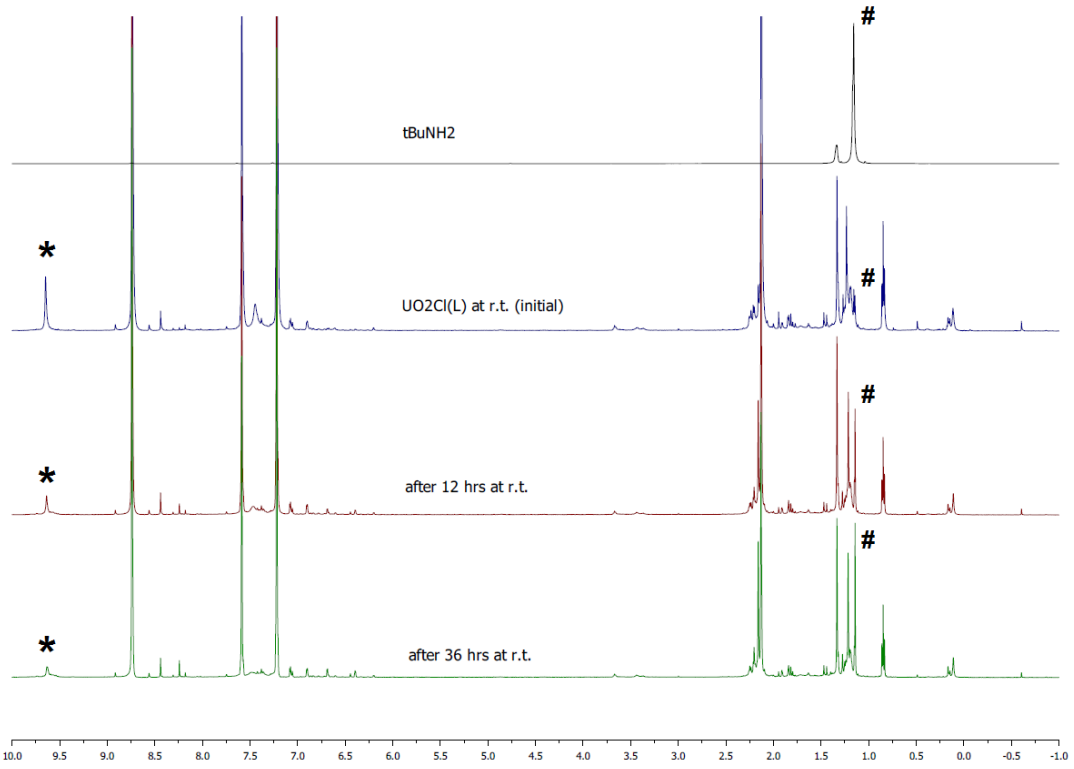

Figure 63 ^{1}H-NMR of **21** in pyridine at room temperature over 36 hours. The compound disintegrates by imine bond break. The imine resonance at 9.65 ppm (*) decreases as the *tert*-butyl resonance of free *tert*-butyl amine at 1.16 ppm (#) increases over time.

The redox chemistry of complex **21** was investigated using cyclic voltammetry and Figure 64 shows the cyclic voltammogram obtained from a 5 mM THF solution of **21** using 0.01 M [^{n}Bu$_4$N][PF$_4$] as the supporting electrolyte at a scan rate of 100 mVs^{-1}. All values are reference against Fc/Fc^{+}.

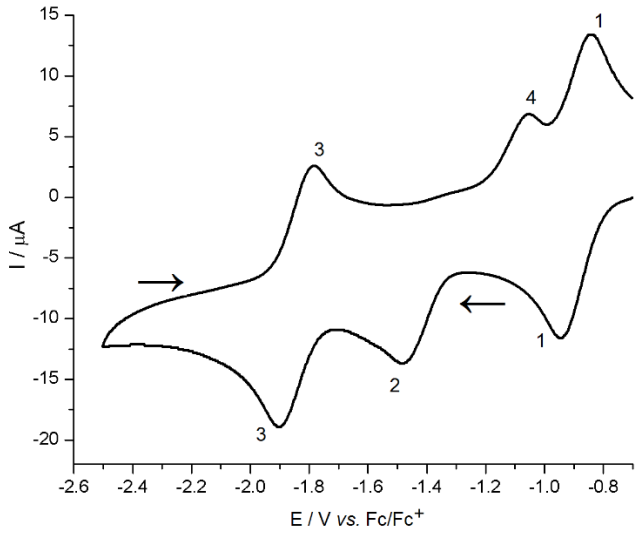

Figure 64 Cyclic voltammogram of **21** in a 5 mM THF solution using 0.01 M [$^{n}Bu_4N$][PF_6] at a scan rate of 100 mV s^{-1}.

The cyclic voltammogram of **21** shows two quasi-reversible reduction features assigned to the U(VI)/U(V) couple and the U(V)/U(IV) couple, respectively. One reductive feature is assigned to free ligand reduction. A small oxidation wave is assigned to an oxidative decomposition. The relevant processes and assignments are given in Table 16:

Table 16 Electrochemical processes observed by cyclic voltammetry of 21

Process	E_{pc} / V	E_{pa} / V	ΔE_p / V	Couple	Reversibility
1	-0.95	-0.85	-0.80	U(VI)/U(V)	quasi-reversible
2	-1.48	—	—	Ligand reduction	irreversible
3	-1.90	-1.80	-1.85	U(V)/U(IV)	quasi-reversible
4	—	-1.05	—	Oxidative decomposition	irreversible

The uranyl reduction features (1 and 3) are assigned as quasi-reversible because of the observed strong scan-rate dependence and large peak separation of about 100 mV each, which increase with increasing scan-rate. The ligand reduction at -1.48 V (2) was assigned by comparison of the cyclic voltammogram of the free ligand HL^{ene}. It is attributed to the first ligand reduction to the radical anion, which appears at the same potential.[256] The assignment of the U(VI)/U(V) couple (1) is in accord with

previously measured redox couples for multi-dentate, Schiff-base ligands in the range from -0.85 V to -1.09 V *vs*. Fc/Fc^+.[257,258] The U(V)/U(IV) (3) reduction potential is lower in comparison with other uranium(V) complexes with potentials in the range between -1.21 V and -1.89 V *vs*. Fc/Fc^+,[35,141,259,260] but is less negative than for previously reported uranyl Pacman complexes with values between -2.60 V and -2.88 V.[133] There is a small oxidative wave in the voltammogram at -1.05 V (2), which only appears after sweeping past the U(V)/U(IV) reduction process and is thus assigned to an oxidative decomposition because no corresponding reduction wave was detected by differential pulse voltammetry.

5.1.2 Synthesis of uranyl(IV) dipyrromethene complex

The uranyl(VI) dipyrromethene complex **21** has further been used to investigate its potential to undergo reductive metalation as previously demonstrated for the uranyl Pacman complexes.

At first, potassium metal was chosen as a reducing agent. Compound **21** was treated with two equivalents of K in pyridine and the mixture was allowed to stir at room temperature overnight, targeting the uranium(IV) complex $[(py)_3KOUOK(py)_3(L^{ene})]$ (Scheme 58).

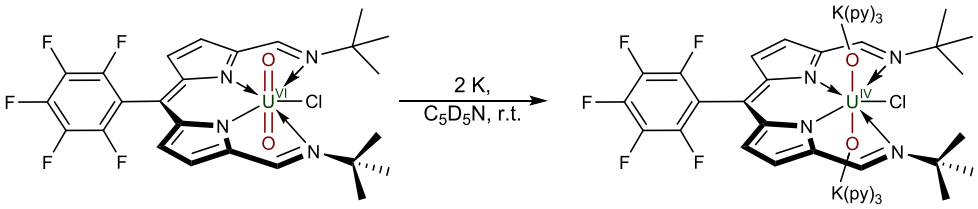

Scheme 58 Attempted reduction of **21** using K metal in pyridine.

The ^{1}H-NMR spectrum was recorded after 12 hours, and showed six resonances shifted paramagnetically from -10 to -50 ppm and two resonances shifted to 38.5 ppm and 50 ppm, respectively. Several inseparable resonances were found between 0 ppm and 10 ppm, and could not be fully identified. The paramagnetic resonances may be attributed to a reductive metalation of the uranyl, possibly to a mixture of singly and doubly metalated product. It is possible that dehalogenation may have occurred as a side-reaction. A product of such a dehalogenation could be a uranyl(V) which may

form cation-cation complexes in solution as demonstrated for uranyl(V) systems by Liddle and co-workers, who observed the formation of both dimeric and trimeric mixed valence uranyl(V)-uranyl(VI) complexes in solution and in the solid state.[261] Ultimately the redox activity of the dipyrromethene ligand itself may play a vital role, and, given the right reducing agent may be reduced to the dipyrromethane, thus complicating the feasibility of isolating defined products. Taking all this into account no further characterisation was carried out regarding reduction with K metal.

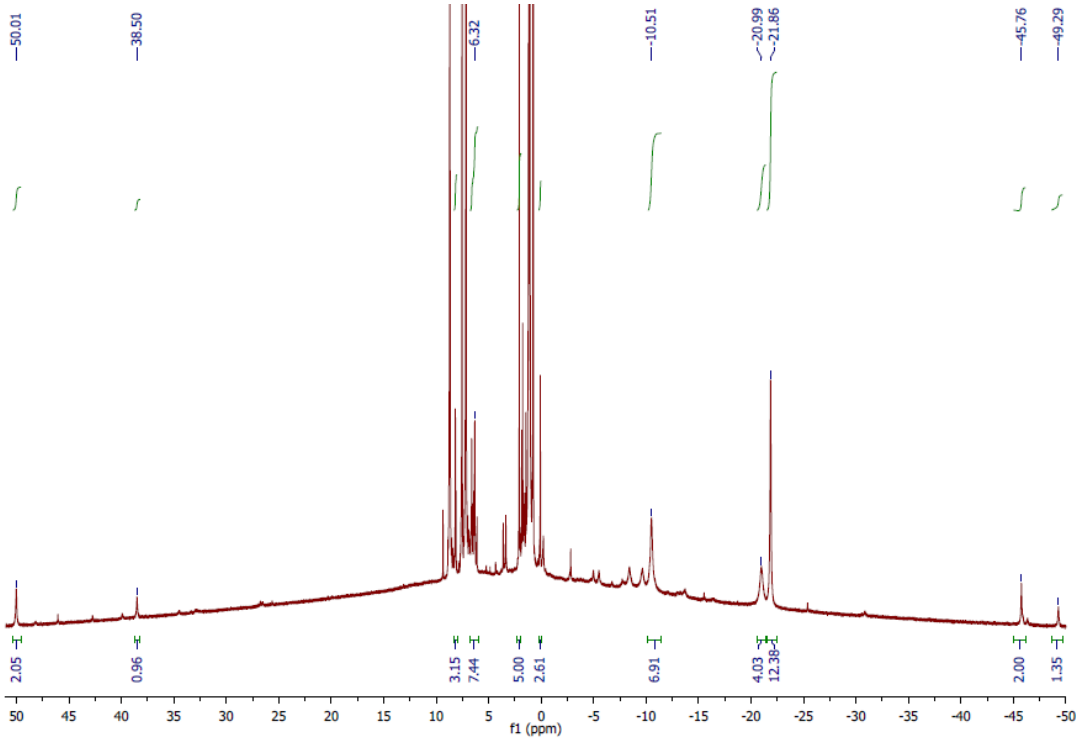

Figure 65 ^{1}H-NMR spectrum after treatment of **21** with 2 equivalents of metallic K in pyridine showing paramagnetic resonances indicating the formation of reduced uranyl/uranium species.

Given the relatively complex chemistry of **21** as demonstrated above, bis(cyclopentadienyl)titanium(III) chloride $[Cp_2TiCl]_2$ was chosen as a mild reducing agent. The oxophilicity of Ti is characterised by the bond dissociation enthalpy of the Ti-O bond of ΔH_{diss} = 662 kJ/mol, and as a single electron reductant it forms titanium(IV) as the thermodynamically most stable form of titanium.

Treatment of **21** with one equivalent of $[Cp_2TiCl]_2$ in benzene at room temperature lead to the straightforward formation of the first doubly titanated uranyl(IV) complex $[(Cp_2TiCl)OUO(Cp_2TiCl)(Cl)(L^{ene})]$ **22** known to date in 37 % yield (Scheme 59).

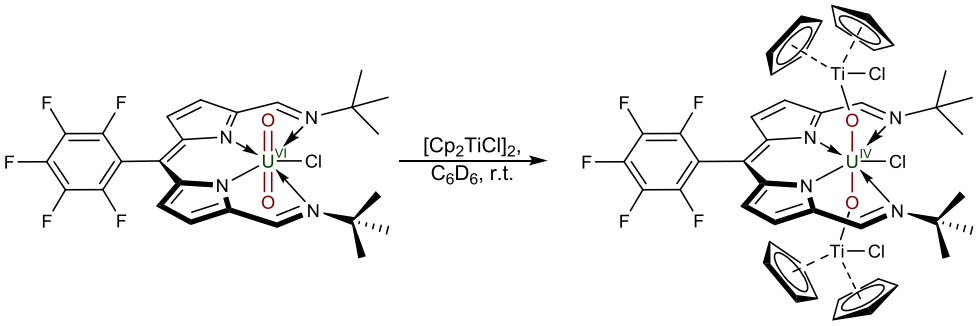

Scheme 59 Two electron reduction of **21** by $[Cp_2TiCl]_2$ to yield the uranium(IV) complex **22**.

Blue crystals suitable for X-ray diffraction could be obtained after recrystallisation of **22** from a concentrated benzene solution. **22** crystallises in a monoclinic crystal system, and the structural solution was performed in space group $P2_1/c$ with four molecules in the unit cell. The solid state structure of **22** is shown in Figure 66.

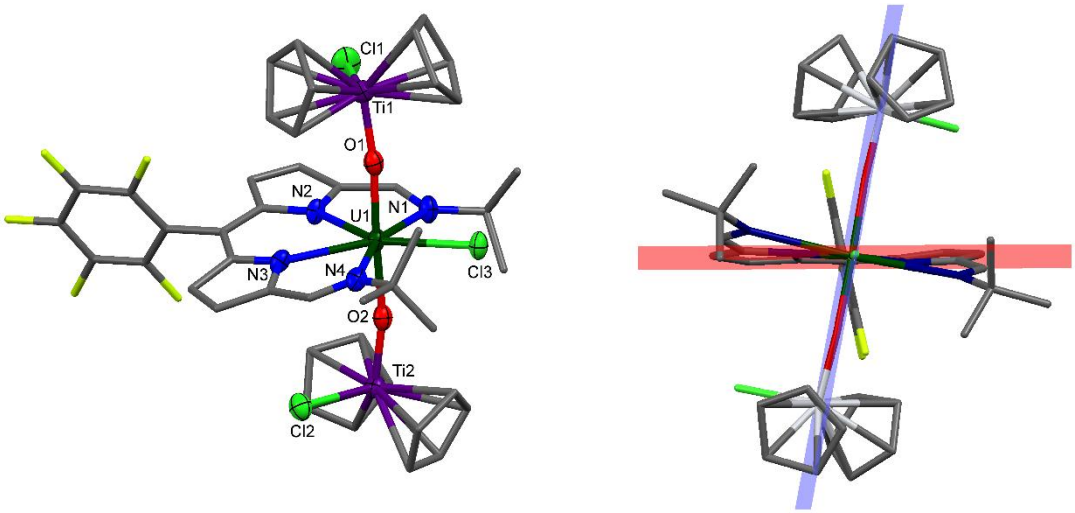

Figure 66 Solid state structure of **22**, in side view (left) and front view (right) showing the O-U-O plane (light blue) and the plane for the sp^2-hybridised *meso*-C atom (light red). For clarity, all hydrogen atoms and all solvent molecules are omitted (displacement ellipsoids are drawn at 50% probability). Selected bond lengths (Å): U1-O1 2.066(7), U1-O2 2.062(7), Ti1-O1 1.841(7), Ti2-O2 1.842(7). Bond angles: O1-U1-O2 177.0(2)°, Ti1-O1-U1 170.9(4)°, Ti2-O2-U1 169.2(3)°.

The solid state structure exhibits long U-O distances of 2.066(7) Å for U1-O1 and 2.062(7) Å for U1-O2, representing the U(IV) oxidation state.[262,263] The Ti-O bond distances show identical values of 1.841(7) Å for Ti1-O1 and 1.842(7) Å for Ti2-O2. The O1-U1-O2 bond angles is linear with 177.0(2)°, the U1-O1-Ti1 bond angle is

slightly bent with a value of 170.9(4)°, similar to the U1-O2-Ti2 angle (169.2(3)°). The C-C bond distances of the methene carbon to the pyrrole rings show values of 1.40(1) Å (C10-C9) and 1.39(1) (C10-C17) Å, similar to those seen in the uranyl(VI) complex **21** and representing the dipyrromethene moiety. The U-$N_{pyrrole}$ bond lengths are elongated from 2.474 Å in **20** to 2.531 Å in **21**. The X-ray diffraction data shows that the molecule is asymmetric, with the pentafluorophenyl group being rotated away from the O-U-O plane by 20.2° (Figure 66). Additionally, the *tert*-butyl groups point in opposite directions away from the plane along the methene carbon, which is similarly affecting the imine nitrogen atoms as well as the pyrrole rings. The twisting of the molecule can also be seen in the ^{1}H and ^{19}F-NMR spectra for this compound, which show individual environments for the protons as well as five individual fluorine resonances.

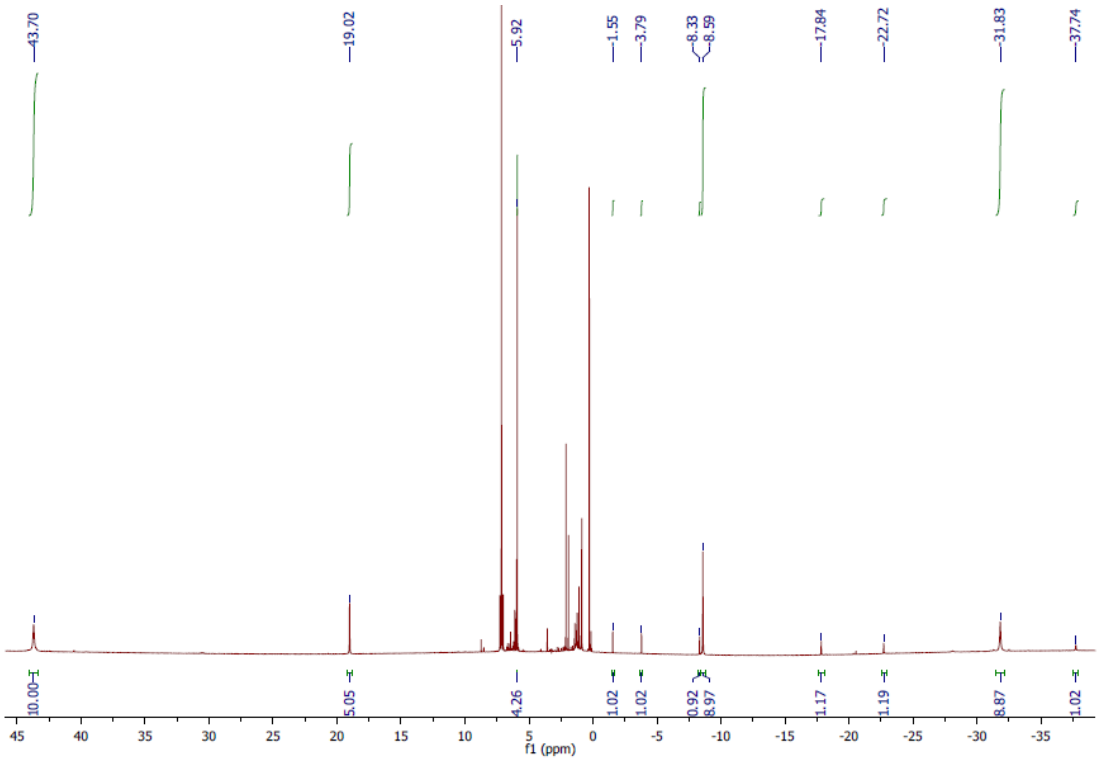

Figure 67 ^{1}H-NMR spectrum in C_6D_6 of **22** showing individual resonances for all protons confirming the complex' asymmetry in solution. The resonances from 0 ppm to 2.5 ppm are attributed to residual hexane and silicon grease introduced from freshly recrystallised $[Cp_2TiCl]_2$.

The ^{1}H-NMR spectrum of **22** shows the formation of a paramagnetic product within the range from -40 ppm to +45 ppm. The *tert*-butyl groups are observed as separate resonances at -31.83 ppm and -8.59 ppm representing the molecule's asymmetry. Similarly the imine protons resonate individually at -37.74 ppm and -8.33 ppm. The cyclopentadienyl rings however show three individual resonances, with two of them at 5.92 ppm and 19.02 ppm representing 5 protons each and the third one at 43.70, representing 10 protons of two cyclopentadienyl rings. This suggests that the asymmetry of the complex has a less strong effect on these two groups and allows them to rotate freely and are equivalent.

The C-H hydrogen atoms of the two pyrrole rings have been identified at -22.72 ppm and -17.84 ppm corresponding to one ring and at -3.79 ppm and -1.55 ppm corresponding to the other ring. Correlation spectroscopy was used to identify the coupling between these hydrogen atoms and revealed a coupling constant of 5 Hz for the latter two. However, we were not able to determine the coupling constant of the second pyrrole ring. Figure 68 shows the coupling of the pyrrole protons.

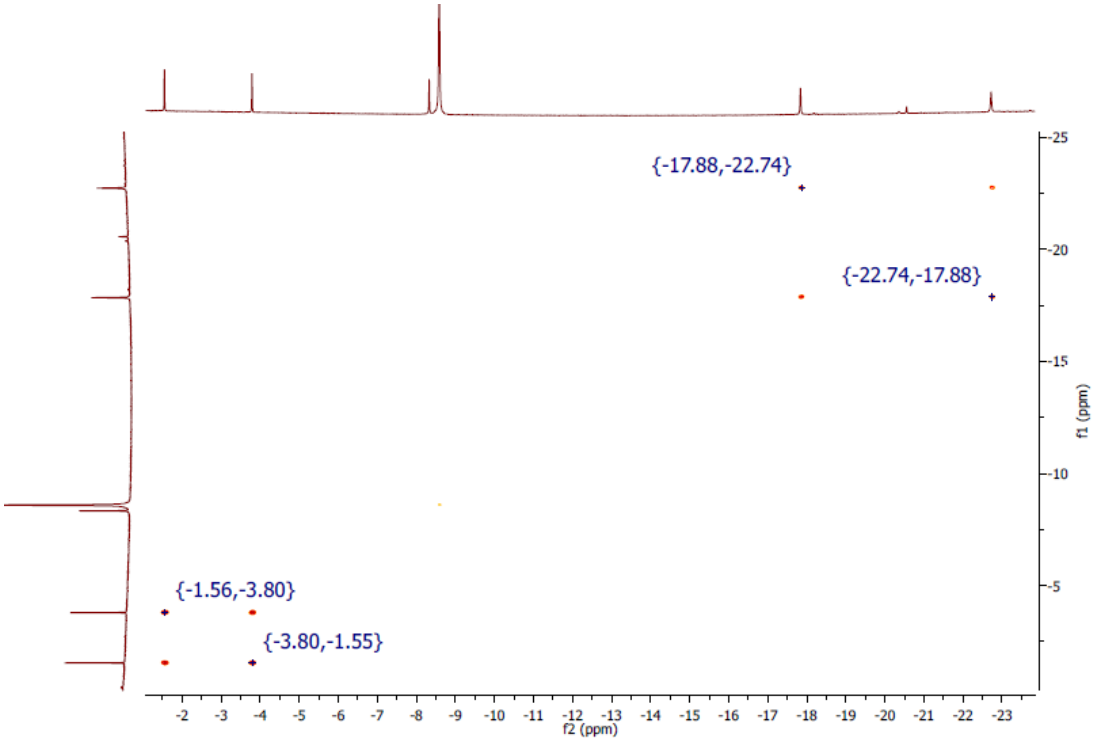

Figure 68 ^{1}H-^{1}H-COSY experiment on **22** revealing the coupling of the pyrrolic protons.

The asymmetry of complex **22** is also reflected in its ^{19}F-NMR spectrum, which shows five individual fluorine resonances at δ_F -139.81 (d, F_{ortho}), -143.92 (d, F_{ortho}), -154.29 (t, F_{meta}), -156.49 (t, F_{meta}), -163.09 (m, F_{para}) ppm.

Additionally we attempted the synthesis of the uranyl(V) intermediate with a mono-oxo-metalated uranyl, however, this hypothetic complex was not accessible in our hands (Scheme 60). Treatment of **21** with 0.5 equivalents of $[Cp_2TiCl]_2$ in benzene has led to the formation of the uranyl(IV) complex **22** and the uranyl(VI) complex **21**, resulting either from a two electron reduction or a disproportionation of uranyl(V) to uranyl(IV) and uranyl(VI).

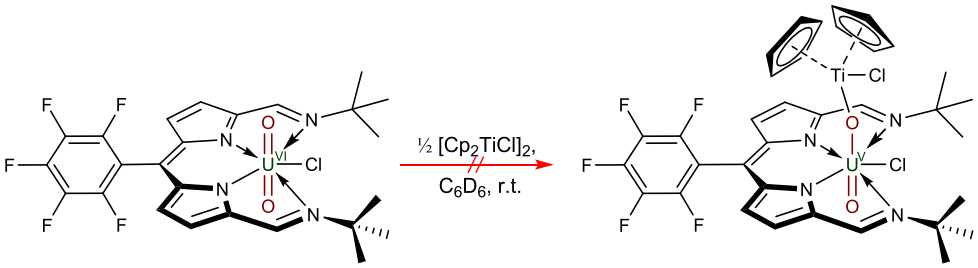

Scheme 60 Attempted single electron reduction of **21** to a Ti(IV)-uranyl(V) complex

This instability of uranyl(V) intermediates however is a well-known aspect of uranyl(VI) functionalisation (*cf.* Chapter 1.2.1). In similar approaches Hayton and co-workers have observed that a that the addition of $B(C_6F_5)_3$ to a uranyl(V) complex also yields a doubly metalated uranium(IV) moiety, along with the uranyl(VI) starting material and other products.[171]

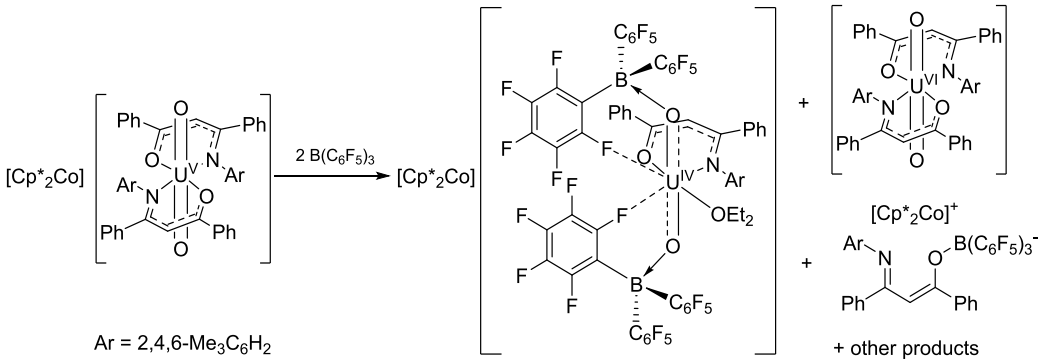

Scheme 61 Uranyl(V) disproportionation observed by Hayton *et al.*[171]

To date we have not been able to measure the cyclic voltammogram of **22** which should give further insight into the redox processes of this material. However, the reduction chemistry of $[Cp_2TiCl]_2$ has been investigated by Daasbjerg *et al.*[264,265] and shows a reductive potential between -0.41 V and -1.27 V. This is not negative enough for the second reduction feature of -1.85 V seen for **21** (Table 16). Quite possibly this is because the coordination of a Lewis acid to one uranyl oxo-group enhances the Lewis basicity of the other oxo-group and alters the second reduction potential, favouring a concerted two-electron reduction. To support this theory computational studies are currently being carried out by Laurent Maron and co-workers in Toulouse, France.

In order to gain deeper insight into the electronic nature of complex **22** this material was further investigated using UV-vis spectroscopy. The spectrum of **22** is compared with the starting material **21** and with the free ligand HL in Figure 69.

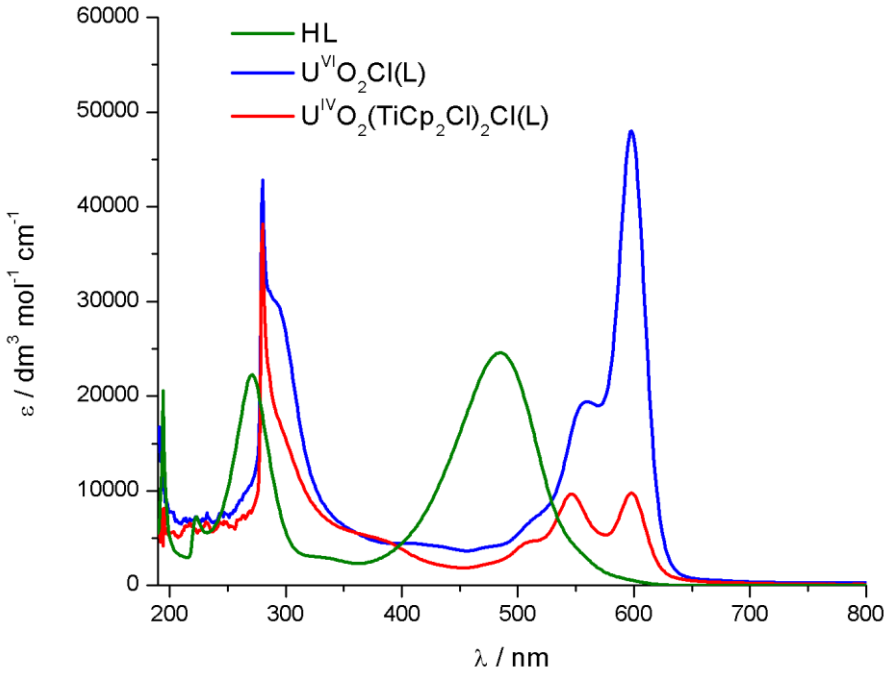

Figure 69 UV-vis spectra for the protonated ligand HL (green, hexane solution), $U^{VI}O_2Cl(L)$ **21** (blue) and $U^{IV}O_2(TiCp_2Cl)_2Cl(L)$ **22** (red) (both toluene solutions).

The spectrum of the free ligand HL^{ene} shows a strong absorption at 486 nm which corresponds to its orange-red colour in solution, as well as a smaller absorption in the UV region at 270 nm. The transition at 486 nm can be assigned to a ligand based $\pi - \pi^*$

transition from HOMO (H) to LUMO (L), whereas the latter can be assigned to a H−(L+1) transition as reported for similar ligands.[256] In comparison the uranyl(VI) complex **21** and the uranium(IV) complex **22** show a strong red-shift, with complex **21** absorbing at 597 nm with an extinction coefficient of ε = 47,924 M^{-1} cm^{-1} and a shoulder at 550 nm. In contrast to this complex **22** shows two absorption bands at 595 nm and 546 nm with extinction coefficients of ε = 7,869 M^{-1} cm^{-1} and 9,673 M^{-1} cm^{-1} respectively. Both complexes show an additional absorption at 280 nm. These values correspond to their blue to purple colour in solution and in the solid state. The large values of the extinction coefficients may suggest that these transitions are either $\pi - \pi^*$ or charge-transfer (CT) transitions. However, this is speculative and further work is needed to confirm this. Currently these complexes are under investigation using computational chemistry in order to determine the nature of their UV-vis behaviour and to assign if the excitation is ligand or metal based.

Compared to the well-studied BODIPY systems with extinction coefficients of above 80,000 M^{-1} [266] cm^{-1} and up to 120,000 M^{-1} cm^{-1} [267] the extinction coefficients for **21** and **22** are rather small. However, they are quite similar to pyridomethane-BF_2 complexes, in which the pyrrole rings are substituted for pyridine rings.[268] For comparison Table 17 lists the obtained ε-values for the obtained complexes.

Table 17 Extinction coefficients for HL^{ene}, U(VI) (21) and U(IV) (22)

Compound	λ (nm)	ε (M^{-1} cm^{-1})	Error (M^{-1} cm^{-1})
HL	486	24, 329	1262
U(VI)	597	47, 924	5887
U(VI)	280	38, 432	4953
U(IV)	595	7, 869	4554
U(IV)	546	9, 673	4646
U(IV)	280	18, 288	4373

The table shows that the extinction coefficient for the uranium(IV) complex has dropped to about one fourth of the value for the uranyl(VI) complex, whereas the value at 280 nm is merely reduced to one half. This absorption is even lower than the one determined for the free ligand. Currently no sufficient explanation can be given as to why these values show a tendency in absorption of U(VI) > HL > U(IV).

5.2 Uranyl functionalisation in a dipyrromethane ligand

In an attempt to synthesise a uranyl(VI) dipyrromethane complex by a simple acid-base reaction between $UO_2(N(SiMe_3)_2)_2$ and the pentafluorophenyl dipyrromethane ligand H_2L^{aneAr} in pyridine at room temperature the desired complex could not be isolated (Scheme 62).

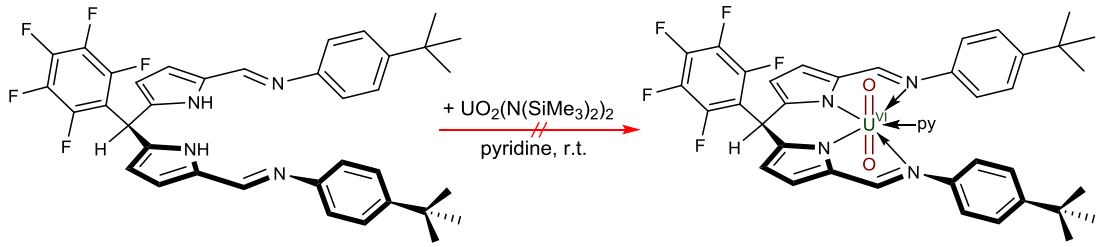

Scheme 62 Intended reaction by treatment of H_2L^{aneAr} with $UO_2(N(SiMe_3)_2)_2$.

Instead, upon heating a mixture of the purple pentafluorophenyl dipyrromethane ligand (H_2L^{eneAr}) with one equivalent of uranyl(VI) silylamide at 70 °C in pyridine reductive silylation was observed in both the ^{1}H-NMR spectrum and X-ray crystallography. The results of the diffraction studies show that **23** is a mixture of two products forming superimposed crystals of a uranium(IV) dipyrromethane complex (29 %) and a uranium(III) dipyrromethene complex (71 %) which results from the oxidation of the ligand (Scheme 63).

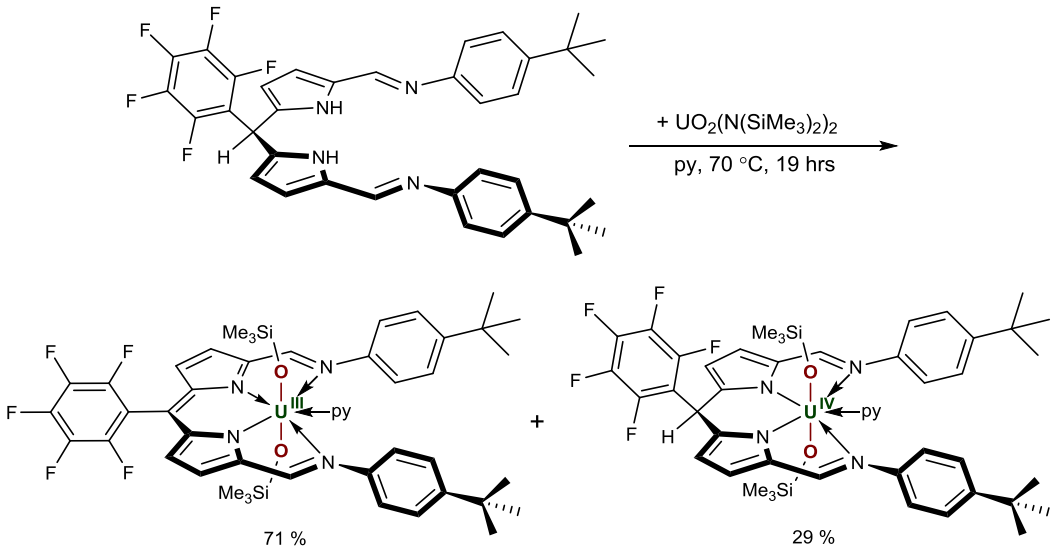

Scheme 63 Treatment of H_2L yielding a U(III) and a U(IV) siloxide.

Figure 70 shows the ^{1}H-NMR spectrum of an inseparable mixture of **23**, showing resonances within a range of -14 ppm to +40 ppm. The paramagnetic resonances which were observed can be assigned to both a reductively silylated uranium(III) and a reductively silylated uranium(IV) complex, however, four resonances at -0.05 ppm, 0.30 ppm, 1.13ppm and 1.37 ppm could not be assigned and quite possibly suggest the formation of one or more side-products which were not isolated upon work-up.

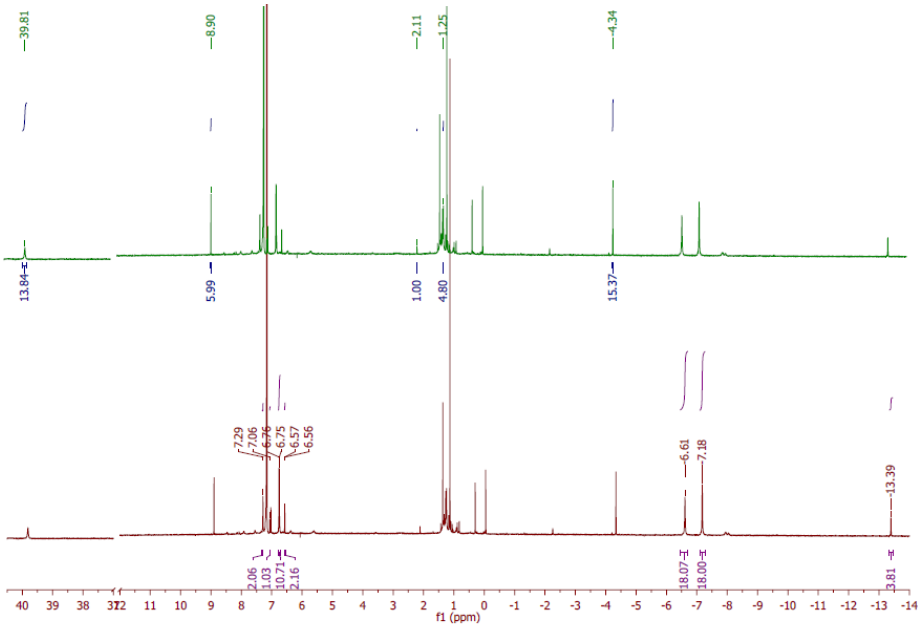

Figure 70 ^{1}H-NMR spectrum of the inseparable mixture of **23** in C_6D_6. The green spectrum (top) is assigned to the U(IV) complex, the red spectrum (bottom) is assigned to the U(III) complex.

Dark blue single crystals were obtained by solvent evaporation of the reaction mixture, which crystallises in a triclinic crystal system. The structural solution was performed in space group *P*-1 with two formula units per unit cell. The solid state structure of the major component of **23** in shown in Figure 71. The ligand coordinates in the equatorial plane of the O-U-O moiety with its four N-donor atoms. Additionally the uranium atom coordinates a pyridine solvent molecule at its fifth coordination site between the two aryl groups of the ligand orientated in a π-stacking motif. The coordination environment of the uranium is hence pentagonal-bipyramidal. Both oxo-groups of the uranium are capped by a trimethylsilyl group, resulting from a bond cleavage of the N-Si bond of the hexamethyldisilylamide group during the reaction.

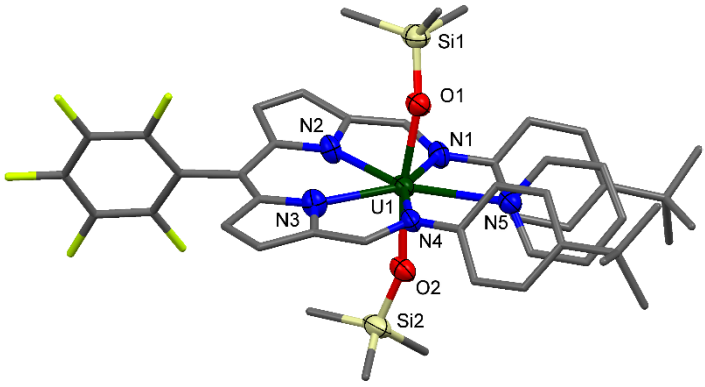

Figure 71 Solid state structure of the major component of **23**. For clarity, all hydrogen atoms, all atoms of the minor component and all solvent molecules are omitted (displacement ellipsoids are drawn at 50% probability). Selected bond lengths (Å): U1-O1 2.114(4), U1-O2 2.113(4), Si1-O1 1.638(5), Si2-O2 1.631(4), U1-N1 2.561(6), U1-N2 2.437(5), U1-N3 2.417(6), U1-N4 2.590(6). Bond angles: O1-U1-O2 170.1(2)°, Si1-O1-U1 158.7(3)°, Si2-O2-U1 157.2(3)°.

The structural analysis revealed two superimposed molecules (Figure 72), 71 % of which shows a doubly silylated uranyl motif in an oxidised ligand, making it formally a uranium(III) dipyrromethene complex, and 29 % show a doubly silylated uranyl in the reduced form of the ligand, making it a uranium(IV) dipyrromethane complex.

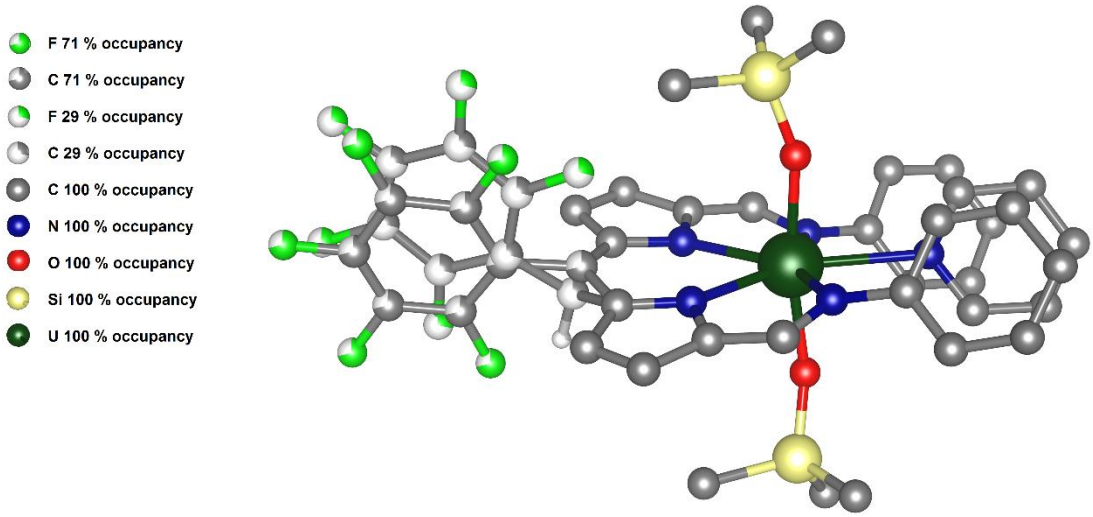

Figure 72 Crystallographically superimposed U(III) and U(IV) complex, indicated by the occupancy of the F and C atoms of the pentafluorophenyl ring.

A discussion of the bond distances and angles must therefore remain rather unspecific as the Solid state structure represents the average of two components. Likewise all bond parameters average between the characteristic values of U(III) and U(IV).

The uranium-oxygen distances U1-O1 and U1-O2 (2.114(4) Å and 2.113(4) Å) are longer than the uranyl(VI) bond distances of 1.78 Å and also longer than any uranyl(V)-oxygen bond distances reported in this thesis of which the longest appears in compound **10** with a U-O distance of 1.979(3) Å, indicating the formation of a uranium oxidation state below +5.

The U-O bond lengths in U(IV) bis(benzopinacolate) U($Ph_4C_2O_2$)($thf)_2$ complexes deviate from 2.131(4), 2.158(3), 2.159(3) and 2.162(4) Å,[269] which are in the same range as the observed values for complex **22**, whereas the U-O bond lengths in uranium(III)-aryl oxide U($ODtbp)_3$ (ODtbp – 2,6-di-*tert*-butyl phenolate) complexes range from 2.149(4) to 2.165(3), averaging to 2.159 Å.[270] The analogous uranium(IV) complex shows bond distances 2.135(4) Å.[271] Uranium(III) tris(aryloxide) complexes reported by Meyer *et al.* with an average U-O distance of 2.679 Å.[272]

A uranium(IV) siloxide complex synthesised by Hayton *et al.*[144] is shown in Figure 73.

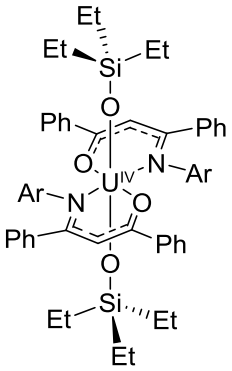

Figure 73 Uranium(IV) siloxide complex by Hayton *et al.*[144]

The U-O bond distances for this complex measure 2.129(2) Å and are similar to other reported uranium siloxides,[141] and resemble those as $[Cp_2Co][U(OSiPh_3)(OB\{C_6F_5\}_3)(Aracnac)_2]$ (2.173(8) Å)[68] and $Cp_3U(OSiPh_3)$ (2.135(8) Å).[273] The authors report that the U-N bond distances (2.484(3) Å) and the $U\text{-}O_{Aracnac}$ (2.268(2) Å) bond lengths are consistent with the uranium(IV) oxidation state.

In order to gain more extensive analysis on compound **23** a qualitative UV-vis spectrum was recorded on the mixture of oxidation states. Figure 74 shows the spectrum of a 0.2 mM toluene solution of **23**.

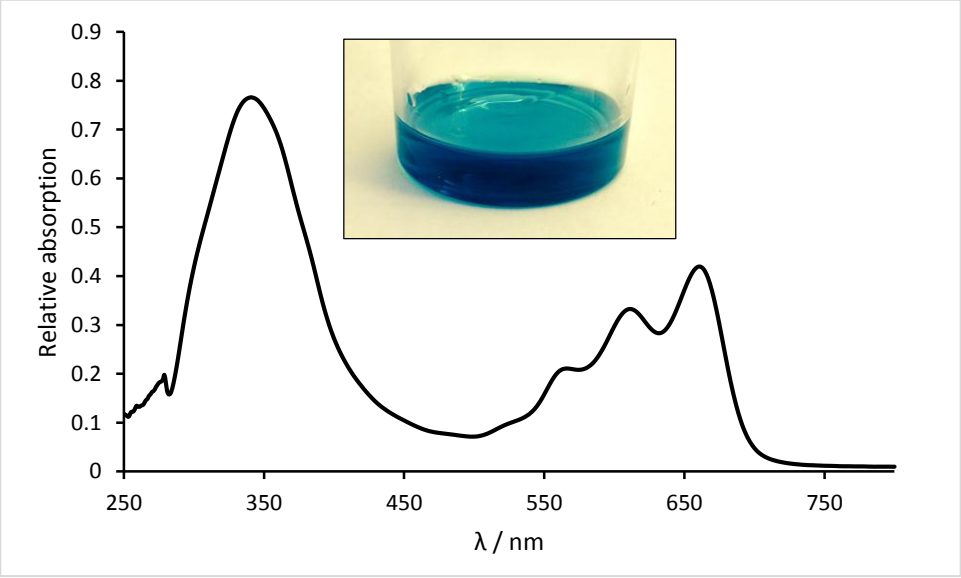

Figure 74 Qualitative UV-vis spectrum of a 0.2 mM toluene solution of **23** (inset). (Photo: Max McMullon)

Pankhurst *et al.*[256] report the dominant absorption band for the free dipyrromethane ligand H_2L^{aneAr} at 373 nm and assign the observed absorption to a mixture of HOMO (H) to LUMO H–(L+1) (59%) and (H−1)–L (32%) transitions, with the H–L transition appearing as a shoulder at 413 nm. The oxidation of H_2L^{aneAr} to the dipyrrin HL^{eneAr} results in a red-shift of both the (H−1)–L and H–L transitions to be red-shifted to 520 nm and 540 nm, respectively, while the H–(L+1) transition remains in the UV-region at 290 nm. This change in electronic structure is typical for dipyrromethene compounds[274] and reflects a 1.6 eV stabilisation of the LUMO upon oxidation.

Compound **23** shows a strong absorption at 665 nm, with two shoulders appearing at 619 nm and 566 nm, corresponding to the light blue colour of the solution. This red-shift is stronger than the absorption reported for the free dipyrrin, and these values are assigned to a ligand based $\pi - \pi^*$ transition from HOMO to LUMO. Another strong absorption appears at 341 nm. The obtained values are comparable to those measured for complex **21** and **22** (*cf.* Section 5.1.2), however, due to the mix of oxidation states a full assignment cannot be given at this stage.

To our surprise the light blue solution did not change its colour when exposed to air and the UV-vis spectrum showed no change in absorption. Only after the sample was exposed to air for a week a change in colour back to purple (= free ligand H_2L^{aneAr}) could be observed, suggesting a relative inertness of the uranium siloxide complex to oxygen and moisture.

Most likely the observed reaction results from a bond cleavage of the Si-N bond in $HN(SiMe_3)_2$, as previously observed in reductive uranyl silylation.[102,134] Quite possibly this is enhanced *via* a formation of a cation-cation complex between two uranyl moieties which may form in solution (Scheme 64).

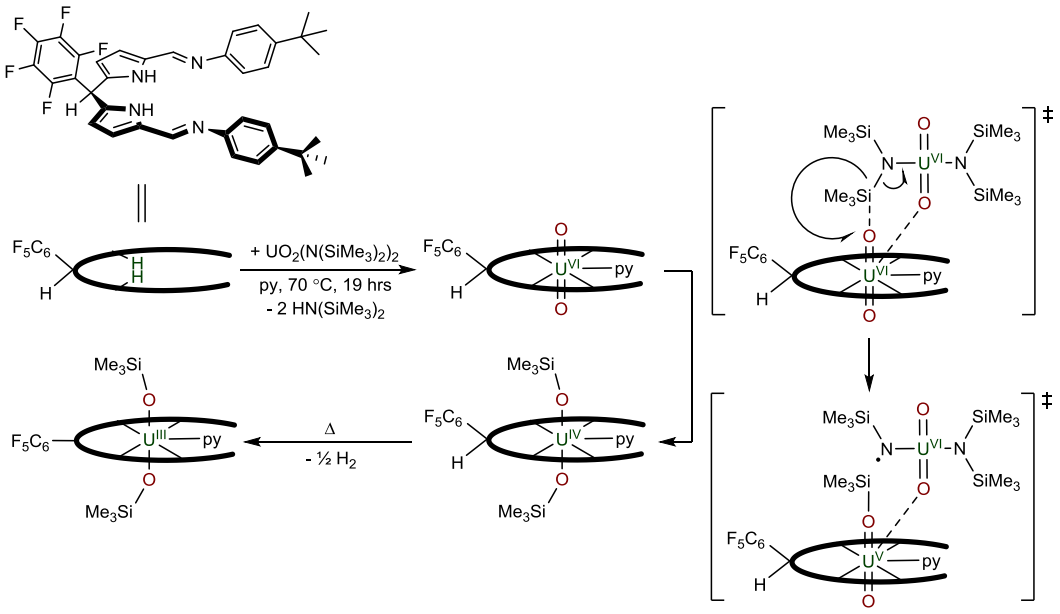

Scheme 64 Proposed reaction mechanism of uranyl(VI) complexation and reduction in dipyrromethane complexes.

It can be hypothesised that the reduction from the U(IV) complex to the U(III) complex could also proceed in the solid state. This could possibly be verified by careful isolation of the U(IV) complex at temperatures below 70 °C and subsequent gentle heating of the isolated material (Scheme 65).

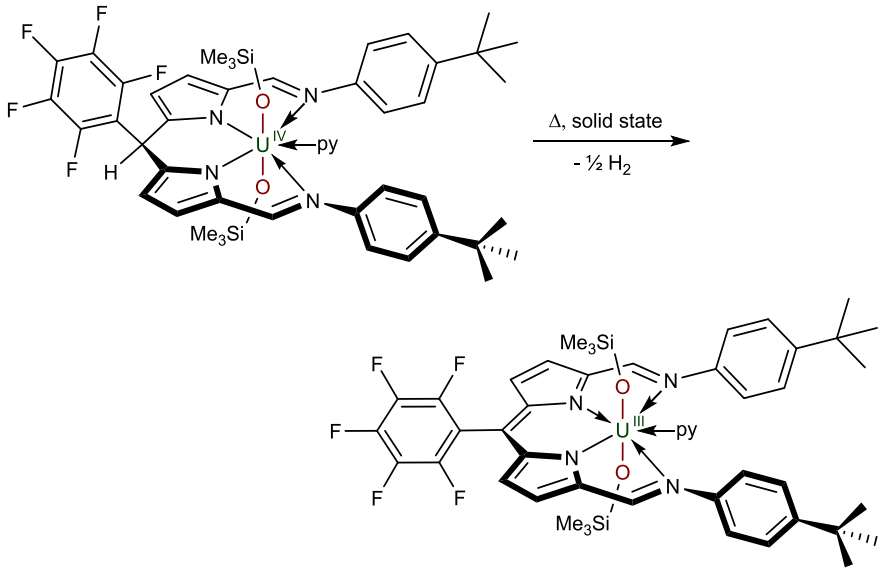

Scheme 65 Proposed solid state synthesis of U(III) siloxide complex.

The described reactions show a potential to successively access all oxidation states of uranium in one ligand system, if the proposed products have been correctly identified. However, so far it was not possible to reproduce this work or to isolate pure material. Further work needs to be carried out to precisely determine all reaction products and to accurately synthesise pure material. Further spectroscopic studies like ^{19}F and ^{29}Si NMR, UV-vis-NIR and cyclic voltammetry are needed to confirm these preliminary results. This may be supported by computational studies to gain insight into the electronic structure of this material.

5.3 Conclusion

It has been shown in this chapter that the use of redox active dipyrromethane and dipyrromethene ligands offers new modes of reactivity regarding uranyl oxo functionalisation. The successful synthesis of a new uranyl(VI) dipyrromethene complex is presented. The reduction of this complex with Ti(III) leads to the two-electron reduction of the uranyl and to a doubly titanated uranium(IV) complex. UV-vis spectra and cyclic voltammetry support the assignment of the oxidation state.

The reductive silylation of uranyl(VI) in a dipyrromethane complex has been exemplified in the isolation of crystalline material, that suggests the formulation of a mixed uranium(III)/uranium(IV) complex. This material is currently still being investigated.

6 Experimental section

6.1 General methods and instrumentation

All manipulations were carried out under dry, oxygen-free dinitrogen atmosphere using standard Schlenk techniques or an MBraun Unilab glove-box. Deuterated pyridine, deuterated tetrahydrofuran and deuterated benzene were boiled over potassium, distilled and three times freeze-pump-thaw degassed prior to use. All other solvents were nitrogen purged and dried via passage through Vacuum Atmosphere drying towers. Pyridine was degassed and distilled over potassium.

All reactions involving ^{237}Np and ^{239}Pu were carried out using standard Schlenk techniques under argon atmosphere inside low-pressure nitrogen-filled glove-boxes at the Institute for Transuranium Elements in Karlsruhe, Germany.

^{1}H, ^{13}C{^{1}H}, ^{7}Li{^{1}H}, ^{19}F{^{1}H} and ^{29}Si-NMR spectra were recorded on a Bruker ava400 at 298 K at 400 MHz, Bruker ava500 at 298 K at 500 MHz, Bruker pro500 at 298 K at 500 MHz and Bruker ava600 at 298 K at 600 MHz. Chemical shifts are given in parts per million and referenced to residual proton resonances of the respective solvent.

Single crystal X-Ray diffraction data was collected using an Oxford Diffraction Supernova instrument at 120 K, fitted with a CCD area detector using CuKα radiation (λ = 1.5418 Å) or MoKα radiation (λ = 0.7107 Å) or using an Eos Excalibur instrument at 170 K using MoKα radiation (λ = 0.7107 Å). Structural solution and refinement was carried out using either SHEL-XS-97 direct methods,[275] SHEL-XS-97 Patterson methods,[275] *SIR*92[276] or the SUPERFLIP charge-flipping program[277] and refined using a full-matrix least square refinement on $|F|^2$ using SHELXL-97.[275] All programs were used either within the *WinGx* suite[278] or *OLEX*2.[279]

Elemental analysis was carried out by Mr. Stephen Boyer, London Metropolitan University.

Infrared spectra were recorded on a Jasco 410 spectrophotometer as a nujol mull between NaCl disks. Intensities are assigned as: w = weak, m = medium, s = strong. UV/Vis/NIR spectra were recorded on a Jasco V-670 spectrophotometer in a 10 mm quartz cuvette fitted with a Teflon tap.

Cyclic voltammograms were recorded using an Autolab 302 potentiostat and the data processed using GPES Manager version 4.9. Experiments were undertaken at room temperature in a glove-box in a 15 ml glass vial as the cell with a platinum wire embedded in

glass as the working electrode, a platinum gauze as the counter electrode and a silver wire as the pseudo-reference electrode. The solution employed was 5.0 mM of the compound with 0.2 M $[NBu_4][PF_6]$ as the supporting electrolyte and scan rates between 100–1000 mVs^{-1}. All potentials were referenced against $[Cp_2Fe]^{0/+}$ (i.e. $Fc/Fc^+ = 0.0$ V).

Variable temperature magnetic susceptibility (dc and ac) measurements were carried out by Dr. Alessandro Prescimone at the University of Edinburgh and made on a Quantum Design Magnetic Property Measurement System (SQUID magnetometer) equipped with a 7T magnet operating in the 350±2 K temperature range. Diamagnetic corrections were applied using Pascal's constants. The sample was placed in a gelatine capsule and fitted inside a plastic straw. The data analysis was carried out by Dr. Nicola Magnani at the Institute for Transuranium Elements in Karlsruhe, Germany.

Theoretical calculations were performed by Xiaobin Zhang and Prof. Dr. Georg Schreckenbach at the University of Manitoba, Canada. All geometries were fully optimised at the Density Functional Theory (DFT) level using the Perdew-Burke-Ernzerhof (PBE) functional[280,281] with correlation consistent all-electron cc-pVDZ basis sets for the large component and corresponding kinetically balanced basis sets for the small component,[282] using the Priroda code, version 13.[283] Priroda applies the full Dirac equation but with spin-orbit projected out and neglected.[284] Vibrational frequency calculations were performed at the same level of theory in order to verify that the geometries are real minima on the potential energy surfaces. QTAIM analysis was performed with the MultiWFN code.[285] The NBO 6.0 program[286] as interfaced with Amsterdam Density Functional (ADF)[287–289] was used for NBO analysis. ADF calculations were performed using the PBE functional and the scalar zeroth order regular approximation (ZORA) method[290–294] with corresponding double zeta polarised (DZP) basis set for light elements and triple zeta polarised (TZP) for uranium.

6.2 Synthetic procedures for isolated compounds

$[(UO_2)(py)(H_2L)]$[125] **A**, Tebbe's reagent[295], H_4L(Pacman),[132] $UO_2Cl_2(thf)_3$,[296] UI_3,[297] $UO_2(N(SiMe_3)_2)_2(py)_3$,[298], HL,[256] H_2L,[256] $Cp_2Ti(\eta^2\text{-}C_2(SiMe_3)_2$[299], $[Cp_2TiCl]_2$[300] and $Cp_2Zr(\eta^2\text{-}C_2(SiMe_3)_2)\cdot py$[301] were synthesised according to literature procedures. $\mathbf{A^{Zn}}$ was synthesised according to a modified literature procedure, using $Zn(N(SiMe_3)_2)_2$.[302] $U(N(SiMe_3)_2)_3$ was synthesised according to a modified literature procedure using UI_3 as the starting material.[303] All other reagents were used as received.

6.2.1 Synthesis of [(py)(Me$_2$AlOUO)(py)(H$_2$L)] 1

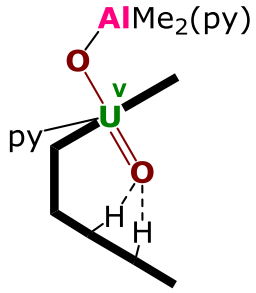

A brown suspension of [(UO$_2$)(py)(H$_2$L)] **A** (150 mg, 0.1035 mmol) in C_6D_6 (1.0 ml plus 0.1 ml pyridine) was combined with $Cp_2TiCH_2ClAlMe_2$ **(**0.15 ml, 0.1035 mmol) (Tebbe's reagent) at room temperature to form a dark brown solution. The solvent was reduced to *ca.* 0.5 ml under vacuum to afford [(py)(Me$_2$AlOUO)(py)(H$_2$L)] **1** as yellow crystals. The product was isolated by filtration and washed with cold toluene (3 x 0.5 ml, -35 ºC). Recrystallisation of **1** from toluene at -35 °C afforded yellow crystals suitable for X-ray diffraction. Yield: 79 mg (67%).

^{1}H-NMR (C_6D_6): δ_H -5.11 (s, 3H, C*H*$_3$), -4.96 (s, 3H, C*H*$_3$), -2.04 (s, 2H), -1.35 (s, 6H, Ph-C*H*$_3$), 0.12 (s, 2H), 0.29 (s, 6H, Ph-C*H*$_3$), 0.85 (s, 2H), 0.87 (s, 2H), 3.02 (s, 2H), 7.19 (s, 2H), 8.10 (s, 3H, C*H*$_3$), 10.21 (d, 2H, pyrrole, $^3J_{H\text{-}H}$ = 4 Hz), 12.18 (d, 2H, pyrrole, $^3J_{H\text{-}H}$ = 4 Hz), 14.51 (s, 6H, Al-C*H*$_3$), 21.25 (s, 3H, C*H*$_3$), 68.65 (br, 2H, N*H*); ^{13}C{^{1}H}-NMR (C_6D_6): δ_C 15.74, 15.92, 16.34, 16.90, 17.56, 18.69, 21.04, 21.76, 34.10, 52.23, 77.29, 101.99, 108.06, 109.35, 112.11, 115.90, 119.93, 120.40, 122.79, 126.03, 126.33, 126.77, 128.90, 129.66, 138.22, 145.22, 148.97, 162.64; Analysis. Found: C, 56.58; H, 4.99; N, 12.17 % $C_{54}H_{60}AlN_{10}O_2U$ requires: C, 56.59; H, 5.28; N, 12.22 %; FTIR (nujol, cm^{-1}): ν 2927 (w, NH/ nujol), 2854 (w, nujol), 1581 (w, imine), 1462 (s, nujol), 1377 (s, nujol), 1285 (m, L), 1261 (m, L), 1084 (w, L), 1044 (m, L), 1019 (m, L), 893 (w, asymm. UO stretch), 865 (w, L), 800 (s, L), 722 (w, nujol). L = stretches attributed to the Pacman ligand.

6.2.2 Synthesis of [(py)(*i*Bu$_2$AlOUO)(py)(H$_2$L)] 2

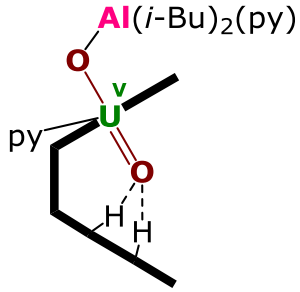

A solution of di(*iso*-butyl)aluminium hydride in hexane (1.0 M, 3.5 ml, 3.53 mmol) was added to a stirred brown solution of **A** (2.30 g, 1.77 mmol) in toluene (40 ml) in a Teflon-tapped ampoule and the resulting mixture heated to 70 °C for 24 h. The pale brown reaction mixture was filtered hot, concentrated to a volume of 20 ml and cooled to -35 °C upon which a dark-yellow solid of [(py){(*i*-Bu)$_2$AlOUO}(py)(H$_2$L)] **2** precipitated. The product was isolated by filtration and washed with cold toluene (3 x 0.5 ml, -35 ºC). Recrystallisation of **2** from benzene-THF at -35 °C yielded yellow needles suitable for X-ray diffraction. Yield: 1.10 g (51%).

^{1}H-NMR (C_6D_6): δ_H -5.29 (s, 3H, CH_3), -5.22 (s, 3H, CH_3), -2.50 (s, 2H), -0.01 (d, 2H, pyrrole, $^{3}J_{H\text{-}H}$ = 4 Hz), 0.16 (s, 6H, Ph-CH_3), 0.67 (d, 2H, pyrrole, $^{3}J_{H\text{-}H}$ = 4 Hz), 1.09 (s, 2H), 2.42 (s, 2H), 6.08 (d, 6H, Al-CH_2CH(CH_3)$_2$, $^{3}J_{H\text{-}H}$ = 8 Hz), 6.66 (d, 6H, Al-CH(CH_3)$_2$, $^{3}J_{H\text{-}H}$ = 8 Hz), 7.43 (s, 2H), 8.05 (d, 4H, $^{3}J_{H\text{-}H}$ = 4 Hz), 8.61 (m, 2H), 10.33 (d, 2H, pyrrole, $^{3}J_{H\text{-}H}$ = 4 Hz), 11.29 (br, 2H, Al-CH_2CH(CH_3)$_2$), 12.23 (d, 2H, pyrrole, $^{3}J_{H\text{-}H}$ = 4 Hz), 16.30 (d, 2H, Al-CH_2CH(CH_3)$_2$, $^{3}J_{H\text{-}H}$ = 8 Hz), 16.78 (d, 2H, Al-CH_2CH(CH_3)$_2$, $^{3}J_{H\text{-}H}$ = 8 Hz), 20.71 (s, 3H, CH_3), 22.35 (s, 2H), 69.12 (br, 2H, NH); ^{13}C{^{1}H}-NMR (C_6D_6): δ_C 1.75, 2.98, 15.72, 16.73, 20.71, 25.17, 30.55, 36.41, 39.25, 52.12, 76.27, 101.97, 107.83, 109.51, 111.58, 113.65, 115.88, 118.70, 120.49, 122.93, 123.27, 126.02, 127.19, 130.67, 142.91, 145.53, 149.59, 162.74; Analysis. Found: C, 58.57; H, 5.85; N, 11.26 % $C_{60}H_{70}AlN_{10}O_2U$ requires: C, 58.67; H, 5.74, N, 11.40 %; FTIR (nujol, cm^{-1}): ν 2924 (w, NH), 2853 (w, NH), 1581 (w, imine), 1461 (s, L), 1377 (s, L), 1284 (m, L), 1262 (m, L), 1217 (m, L), 1070 (m, L), 1043 (m, L), 1019 (m, L), 892 (w, asymm. UO stretch), 867 (w, L), 796 (s, L), 722 (w, L). L = stretches attributed to the Pacman ligand; CV: $i_{p/c}$ = -1.65 V; $i_{p/a}$ = -1.31 V; $E_{1/2}$ = -1.42 V uranium(IV)/uranyl(V).

6.2.3 Synthesis of [{(UO$_2$)Li(py)(H$_2$L)}$_2$] 3

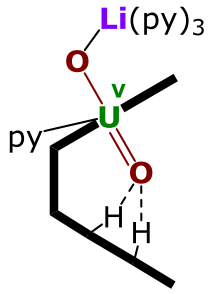

With MeLi (1eq): A solution of MeLi in Et_2O (0.23 ml, 0.036 mmol, 0.16 mM) was added by micro-syringe to a yellow solution of [(py){(*i*-Bu)$_2$AlOUO}(py)(H$_2$L)] **2** (45.0 mg, 0.036 mmol) in C_6D_6 (0.5 ml) in a Teflon-tapped NMR tube. The resulting brown solution was separated from a small amount of precipitate by centrifugation (4500 rpm/10 min). This clear brown solution afforded red-brown crystals of [{(UO$_2$)Li(py)(H$_2$L)}$_2$] **3** suitable for X-ray structural analysis. The solvent was decanted off and the product dried under vacuum. Yield: 7.4 mg (40 %).

With MeLi (2eq): A solution of MeLi in Et_2O (0.46 ml, 0.072 mmol, 0.16 mM) was added by micro-syringe to a yellow solution of [(py){(i-Bu)$_2$AlOUO}(py)(H$_2$L)] **2** (45.0 mg, 0.036 mmol) in C_6D_6 (0.5 ml) in a Teflon-tapped NMR tube. The resulting brown solution was separated from a small amount of precipitate by centrifugation (4500 rpm/10 min). The brown solution afforded a red-brown precipitate of [{(UO$_2$)Li(py)(H$_2$L)}$_2$] **3**. The supernatant was decanted off and dried under vacuum. Yield: 8.3 mg (45 %).

With LiCH$_2$(TMS): Solid LiCH$_2$(TMS) (1.6 mg, 0.016 mmol) was added to a yellow solution of **2** (20.0 mg, 0.016 mmol) in C_6D_6 (0.5 ml) in a Teflon-tapped NMR tube and the mixture heated at 50 °C for 12 h. The resulting brown solution afforded dark red crystals of **3**

suitable for an X-ray crystallographic cell check. The product was decanted and dried under vacuum. Yield: 3.3 mg (40 %).

With $LiCH(TMS)_2$: Solid $LiCH(TMS)_2$ (2.7 mg, 0.016 mmol) was added to a yellow solution of **2** (20.0 mg, 0.016 mmol) in C_6D_6 (0.5 ml) in a Teflon-tapped NMR tube and the mixture allowed to react at room temperature for 48 h. The resulting brown solution afforded dark red crystals of **3** suitable for an X-ray crystallographic cell check. The product was decanted and dried under vacuum. Yield: 3.6 mg (44%).

^{1}H-NMR (C_6D_6): δ_H -4.50 (s, 3H, C*H*$_3$), -1.07 (s, 3H, C*H*$_3$), -1.03 (s, 3H, C*H*$_3$), -0.75 (s, 6H, Ph-C*H*$_3$), -0.35 (s, 2H), 1.77 (s, 6H, Ph-C*H*$_3$), 2.12 (s, 2H), 7.44 (s, 2H), 7.60 (s, 2H), 9.89 (s, 2H), 10.69 (s, 2H), 11.24 (s, 2H), 11.92 (s, 2H), 10.09 (s, 3H, C*H*$_3$), 19.56 (br, 2H, N*H*); ^{13}C{^{1}H}-NMR (C_5D_5N): δ_C 1.48, 3.42, 15.38, 16.54, 17.94, 25.90, 38.70, 67.93, 106.00, 107.24, 107.38, 109.41, 111.42, 115.73, 120.42, 149.18; Analysis. Found: C, 55.80; H, 4.46; N, 12.57% $C_{94}H_{94}Li_2N_{18}O_4U_2$ requires: C, 55.62; H, 4.67, N, 12.42 %; FTIR (nujol, cm^{-1}): ν 2952 (w, NH), 2854 (w, nujol), 1578 (w, imine), 1462 (s, nujol), 1377 (s, nujol), 1279 (m, L), 1262 (m, L), 1047 (m, L), 1019 (w), 894 (w, asymm. UO stretch), 796 (w, L), 722 (m, nujol). L = stretches attributed to the Pacman ligand.

Rearrangement of **3** *to* **4***:* Solid **3** (7 mg, 3.5 μmol) was dissolved in C_5D_5N at room temperature and the ^{1}H-NMR spectrum was recorded. The spectrum shows resonances that support the formation of complex **4**.

6.2.4 Synthesis of $[(py)_3(LiOUO)(py)(\{Li(py)\}_2L)]$ A^{3Li}

An excess of solid LiH (2.0 mg, 0.251 mmol) was added to an orange solution of **2** (6.0 mg, 4.79 μmol) in C_5D_5N (0.5 ml) in a Teflon-tapped NMR tube and the resulting dark red mixture was heated at 40 °C for 12 h. The reaction mixture was then centrifuged (7000 rpm/1 min) to remove any unreacted LiH. The resulting clear red solution afforded orange crystals of $[(py)_3(LiOUO)(py)$ $(\{Li(py)\}_2L)]$ $\mathbf{A^{3Li}}$ suitable for X-ray diffraction. The crystals were decanted and dried under vacuum. Yield: 2.3 mg (34%).

^{1}H-NMR (C_5D_5N): δ_H -8.34 (s, 2H), -4.92 (s, 3H, C*H*$_3$), -2.40 (s, 2H), -2.31 (s, 2H), -1.87 (s, 6H, Ph-C*H*$_3$), -1.19 (s, 2H), 0.33 (s, 6H, Ph-C*H*$_3$), 1.10 (s, 2H), 1.33 (s, 3H, C*H*$_3$), 7.10 (s, 2H), 7.90 (s, 3H, C*H*$_3$), 9.60 (s, 2H), 11.30 (s, 2H), 20.98 (s, 3H, C*H*$_3$); Analysis. Found: C, 60.63; H, 5.02; N, 13.67 % $C_{72}H_{70}Li_3N_{14}O_2U$ requires: C, 60.80; H, 4.96, N, 13.79 %; FTIR (nujol, cm^{-1}): ν 1594 (w, imine), 1463 (s, nujol), 1376 (s, nujol), 1305 (m, L), 1261 (m, L),

1089 (m, L), 1041 (m, L), 968 (w), 894 (w, asymm. UO stretch), 804 (w, L), 722 (m, nujol). L = stretches attributed to the Pacman ligand.

6.2.5 Synthesis of [(py)$_3$(LiOUO)(py)(H$_2$L)] 4

A solution of DIBAL (0.1 M, 0.05 ml, 5.4 μmol) in hexane was added to a mixture of **A** (60.0 mg, 54.0 μmol) and LiH (2.1 mg, 0.27 mmol) in toluene (3 ml) at room temperature. The suspension was stirred at 65 °C for 72 h after which an orange suspension had formed. All volatiles were removed under vacuum and the residues were dissolved in C_5D_5N (0.5 ml) to give a red solution. This solution was centrifuged (7000 rpm/min) to remove excess LiH. Analysis of the ^{1}H-NMR and ^{7}Li-NMR spectra showed the sole formation of **4**. On standing at room temperature, crystalline **4** formed and was isolated by decanting the supernatant and drying under vacuum. Isolated yield: 16 mg (24%).

^{1}H-NMR (C_5D_5N): δ_H -8.57 (s, 2H), -6.90 (s, 2H), -6.44 (s, 2H), -3.55 (s, 2H), -2.33 (s, 6H, Ph-C*H*$_3$), -1.79 (s, 2H), -0.47 (s, 3H, C*H*$_3$), 0.52 (s, 6H, Ph-C*H*$_3$), 1.75 (s, 3H, C*H*$_3$), 5.70 (s, 2H), 9.10 (s, 2H), 13.87 (s, 2H), 26.35 (s, 3H, C*H*$_3$), 32.13 (s, 3H, C*H*$_3$), 85.48 (br, 2H, N*H*); ^{7}Li-NMR (C_5D_5N): δ_{Li} 88.48; ^{13}C{^{1}H}-NMR (C_5D_5N): δ_C 15.27, 16.95, 18.27, 18.67, 35.12, 37.40, 93.93, 95.86, 106.43, 106.65, 107.34, 107.78, 110.86, 111.41, 112.32, 115.50, 117.81, 118.87, 120.11, 120.97, 122.92, 125.96, 126.95, 129.17, 144.13, 146.46, 146.99, 153.86, 167.64, 174.28; Analysis. Found: C, 59.51; H, 4.86; N, 13.46 % $C_{62}H_{62}LiN_{12}O_2U$ requires: C, 59.47; H, 4.99, N, 13.42 %; FTIR (nujol, cm^{-1}): ν 2923 (w, NH/ nujol), 2854 (w, nujol), 1580 (w, imine), 1462 (s, L), 1377 (s, nujol), 1287 (m, L), 1215 (w, L), 1181 (w, L), 1040 (m, L), 969 (s), 891 (w, asymm. UO stretch), 823 (w, L), 722 (s, nujol). L = stretches attributed to the Pacman ligand.

6.2.6 Synthesis of [(py)$_3$(NaOUO)(py)(H$_2$L)] 5

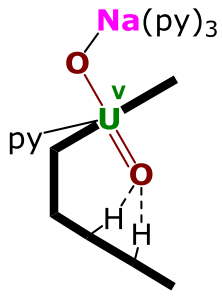

Solid NaH (1.0 mg, 0.040 mmol) was added to an orange solution of **2** (50.0 mg, 0.040 mmol) in C_5D_5N (0.4 ml) in a Teflon-tapped NMR tube and the mixture was allowed to react at room temperature for 1 h. The resulting dark red solution was allowed to crystallise for two weeks, affording dark red crystals of [(py)$_3$(NaOUO)(py)(H$_2$L)] **5** suitable for X-ray structural analysis. The product was decanted and dried under vacuum. Yield: 20.0 mg (40%).

Catalytic synthesis of **5***:*

A solution of DIBAL (0.01 M, 0.90 ml, 9.00 µmol) in hexane was added to a mixture of **A** (89.6 mg, 90.0 µmol) and NaH (10.7 mg, 0.45 mmol) in toluene (3 ml) at room temperature. The suspension was stirred at 70 °C for 72 h after which an orange precipitate had formed. All volatiles were removed under vacuum and the residues were dissolved in C_5D_5N (0.5 ml) to give a red solution. This solution was centrifuged (7000 rpm/ min) to remove excess NaH. Analysis of the ^{1}H-NMR spectrum showed the sole formation of **5**. On standing at room temperature, crystalline **5** formed and was isolated by decanting the supernatant and drying under vacuum. Yield: 70 mg (62%).

^{1}H-NMR (C_5D_5N): δ_H -7.59 (s, 3H, C*H*$_3$), -7.44 (s, 3H, C*H*$_3$), -3.44 (s, 2H), -2.62 (s, 6H, Ph-C*H*$_3$), -2.07 (s, 2H), -1.87 (s, 3H, C*H*$_3$), 0.45 (s, 6H, Ph-C*H*$_3$), 0.72 (s, 2H), 0.74 (s, 2H), 5.78 (s, 2H), 10.83 (s, 2H), 11.01 (s, 2H), 14.18 (s, 2H), 31.79 (s, 3H, C*H*$_3$), 91.11 (br, 2H, N*H*); ^{13}C{^{1}H}-NMR (C_5D_5N): δ_C 15.20, 16.80, 19.60, 19.73, 19.94, 24.98, 25.15, 27.11, 28.58, 29.04, 35.22, 36.51, 40.45, 41.71, 106.29, 109.61, 112.72, 114.95, 119.49, 121.32, 132.83, 134.00, 135.53, 141.11, 144.64, 145.40, 149.49, 159.67, 165.07; Analysis. Found: C, 57.82; H, 6.32; N, 12.97 % $C_{62}H_{42}D_{20}N_{12}NaO_2U$ requires: C, 57.80; H, 6.41, N, 13.05 %; FTIR (nujol, cm^{-1}): ν 2928 (w, NH/ nujol), 2854 (w, nujol), 1579 (w, imine), 1462 (s, nujol), 1377 (s, nujol), 1289 (m, L), 1214 (w, L), 1181 (w, L), 1041 (m, L), 967 (s), 891 (w, asymm. UO stretch), 823 (w, L), 761 (m, L), 722 (s, nujol). L = stretches attributed to the Pacman ligand.

6.2.7 Synthesis of [(py)$_3$(KOUO)(py)(H$_2$L)] 6

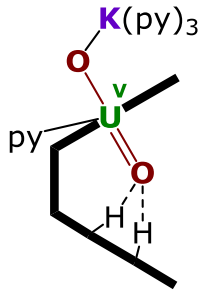

Solid KH (0.8 mg, 0.020 mmol) was added to an orange solution of **2** (25.0 mg, 0.020 mmol) in C_5D_5N (0.4 ml) in a Teflon-tapped NMR tube and the mixture was allowed to react at room temperature for 2 h. The resulting dark red solution was stored at room temperature for three days to afford block-shaped red crystals of [(py)$_3$(KOUO)(py)(H$_2$L)] **6** suitable for X-ray diffraction. The crystals were decanted and dried under vacuum. Yield: 34.0 mg (34%).

^{1}H-NMR (C_5D_5N): δ_H -7.53 (s, 3H, C*H*$_3$), -6.57 (s, 3H, C*H*$_3$), -3.59 (s, 2H), -2.71 (s, 6H, Ph-C*H*$_3$), -2.45 (s, 2H), -1.09 (s, 3H, C*H*$_3$), 0.11 (s, 2H), 0.71 (s, 6H, Ph-C*H*$_3$), 4.80 (s, 2H), 5.51 (s, 2H), 11.07 (s, 2H), 11.13 (s, 2H), 14.39 (s, 2H), 32.73 (s, 3H, C*H*$_3$), 93.06 (br, 2H, N*H*); ^{13}C{^{1}H}-NMR (C_5D_5N): δ_C 14.88, 16.56, 19.27, 91.53, 106.05, 109.08, 110.02, 112.35, 114.76, 115.22, 118.59, 118.86, 120.71, 122.03, 123.28, 125.88, 128.76, 129.51, 146.44,

146.70, 148.44, 159.28, 161.10, 161.52; Analysis. Found: C, 52.93; H, 4.82; N, 11.40 % $C_{42}H_{42}KN_8O_2U$ requires: C, 52.11; H, 4.37, N, 11.58 %; FTIR (nujol, cm^{-1}): ν 2927 (w, nujol), 2854 (w, nujol), 1581 (w, imine), 1462 (s, nujol), 1377 (s, nujol), 1283 (m, L), 1214 (w, L), 1042 (m, L), 1018 (w, L), 907 (s), 894 (w, asymm. UO stretch), 771 (m, L), 722 (s, nujol). L = stretches attributed to the Pacman ligand.

6.2.7.1 Synthesis of 6 and $U(N(SiMe_3)_2)_4$ *via* reduction of A with $K[U^{III}(N(SiMe_3)_2)_4]$

To a purple solution of $U(N(SiMe_3)_2)_3$ (500.0 mg, 0.69 mmol) in C_5H_5N (3 ml) a colourless solution of $KN(SiMe_3)_2$ (138.7 mg, 0.69 mmol) in C_5H_5N (2 ml) was added. This mixture was added to a brown suspension of **A** (920.7 mg, 0.69 mmol) in C_5H_5N (3 ml) at room temperature and the mixture allowed to stir for 15 minutes. The solvent was removed und vacuum and the dried material extracted with toluene (3 × 15 ml). The residue was recrystallised from C_5H_5N to yield **6** (600 mg, η = 67 %). The toluene washings were combined, dried under vacuum and the dried material re-extracted with hexane (3 × 3 ml) to give $U(N(SiMe_3)_2)_4$ **B**. Yield: 270 mg (44 %).

6.2.7.2 Catalysis

General procedures:

Small scale reactions (entries 1, 2, 5, 6):

A solution of DIBAL (see Table 18 for quantities) was added to a suspension of $[(UO_2)(py)(H_2L)]$ **A** (see table) and KH in C_6D_6 (0.5 ml) and heated to 70 ˚C. After a certain time period (Table 1), the mixture was filtered, the filtrate evaporated to dryness under reduced pressure, and the residues dissolved in C_5D_5N and analysed by ^{1}H-NMR spectroscopy.

Table 18 DIBAL concentrations

Entry	Mol% $HAl(i\text{-}Bu)_2$	Time/h	Ratio **6**/**A**
1	5	24	20/80
2	5	60	20/80
3	10	96	100/0
4	0	96	50/50
5	0	240	80/20

Large scale reaction (entry 3):

A solution of DIBAL in hexane (0.01 M, 90.0 µL, 9.00 µmol) was added to a suspension of [(UO_2)(py)(H_2L)] **A** (100 mg, 90.00 µmol) and KH (18.0 mg, 0.45 mmol) in toluene (15 ml) at room temperature and stirred at 70 °C for 96 h. The mixture was filtered and the filtrate dried under reduced pressure and redissolved in C_5D_5N. Analysis of the ^{1}H-NMR spectrum showed the sole formation of **6**. On standing, crystals of **6** formed, and were isolated by decanting the supernatant liquors and drying under vacuum. Yield: 60 mg (52%).

6.2.8 Synthesis of [(py)$_3$(RbOUO)(py)(H_2L)] 7

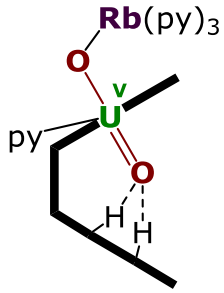

Rb metal (6.6 mg, 0.077 mmol) was added to a dark brown solution of **A** (82.9 mg, 0.076 mmol) in C_5D_5N (1.0 ml) in a Teflon-tapped reaction ampoule and allowed to react at room temperature for 3 h to form an intensely dark red solution. The solution was centrifuged (6000 rpm/ 1 min) and syringe filtered (0.45 µm PTFE filter) into a Teflon-tapped NMR tube. The volume was concentrated by removing the solvent under vacuum to a volume of ca. 0.3 ml to afford intensely dark red prismatic crystals of [(py)$_3$(RbOUO)(py)(H_2L)] **7** suitable for X-ray diffraction. The crystals were decanted and dried under vacuum. Yield: 66.0 mg (64%).

^{1}H-NMR (C_5D_5N): δ_H -7.36 (s, 3H, C*H*$_3$), -6.15 (s, 3H, C*H*$_3$), -3.60 (s, 2H), -2.63 (s, 6H, Ph-C*H*$_3$), -2.47 (s, 2H), -0.94 (s, 2H), 0.05 (s, 2H), 0.84 (s, 6H, Ph-C*H*$_3$), 5.20 (s, 2H), 5.38 (s, 2H), 10.98 (s, 2H), 11.12 (s, 3H, C*H*$_3$), 14.32 (s, 2H), 32.82 (s, 3H, C*H*$_3$), 92.37 (br, 2H, N*H*); ^{13}C{^{1}H}-NMR (C_5D_5N): δ_C 15.30, 16.98, 19.67, 19.69, 19.72, 20.11, 106.15, 106.43, 108.28, 109.32, 112.88, 115.06, 115.10, 115.18, 115.57, 118.22, 118.48, 118.94, 120.47, 120.86, 122.38, 122.86, 126.54, 133.10, 133.21, 134.03, 134.74, 135.06, 140.51, 141.29, 141.81, 142.85, 144.37, 144.76, 146.44, 147.04, 148.33, 152.42, 159.49; Analysis. Found: C, 56.12; H, 4.63; N, 12.70 % $C_{62}H_{62}N_{12}O_2RbU$ requires: C, 55.96; H, 4.70, N, 12.63 %; FTIR (nujol, cm^{-1}): ν 3368 (w, NH) 2927 (nujol), 2854 (w, nujol), 1582 (w, imine), 1462 (s, nujol), 1377 (s, nujol), 1290 (m, L), 1214 (w, L), 1039 (m, L), 1000 (w, L), 963 (s), 892 (w, asymm. UO stretch), 771 (m, L), 722 (s, nujol). L = stretches attributed to the Pacman ligand.

6.2.9 Synthesis of [(CsOUO)(py)(H$_2$L)]$_6$ 8

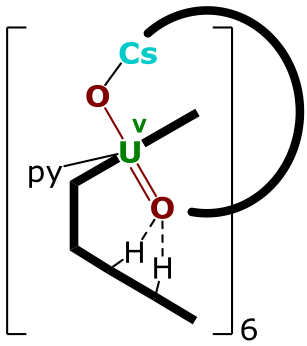

Cs metal (24.7 mg, 0.186 mmol) was added to a dark brown solution of **A** (202 mg, 0.186 mmol) in C_5D_5N (1.0 ml) in a Teflon-tapped reaction ampoule and allowed to react at room temperature for 30 minutes to form an intensely dark red solution. The solution was syringe filtered (0.45 µm PTFE filter) into a Teflon-tapped NMR tube. The volume was concentrated by removing the solvent under vacuum to a volume of ca. 0.3 ml to afford after three weeks small rectangular red crystals of [(CsOUO)(py)(H$_2$L)]$_6$ **8** suitable for X-ray diffraction. The crystals were decanted and dried under vacuum. Yield: 144.0 mg (68 %).

^{1}H-NMR (C_5D_5N): δ_H -7.01 (s, 3H, C*H*$_3$), -5.73 (s, 3H, C*H*$_3$), -3.46 (s, 2H), -2.65 (s, 6H, Ph-C*H*$_3$), -0.82 (s, 2H), 0.98 (s, 6H, Ph-C*H*$_3$), 2.05 (br, 4H), 5.42 (br, 2H), 5.69 (br, 2H), 11.06 (s, 2H), 11.37 (s, 3H, C*H*$_3$), 14.48 (s, 2H), 33.78 (s, 3H, C*H*$_3$), 92.21 (br, 2H, N*H*); Analysis. Found: C, 49.56; H, 4.26; N, 11.02 % $C_{47}H_{47}CsN_9O_2U$ requires: C, 49.48; H, 4.15, N, 11.05 %; FTIR (nujol, cm^{-1}): ν 3368 (w, NH) 2906 (nujol), 1582 (s, imine), 1461 (s, nujol), 1377 (s, nujol), 1289 (m, L), 1213 (w, L), 1041 (m, L), 1017 (w, L), 960 (w), 892 (m, asymm. UO stretch), 775 (m, L), 721 (s, nujol). L = stretches attributed to the Pacman ligand.

6.2.10 Synthesis of [(py)(Cp$_2$TiOUO)(py)(H$_2$L)] 9

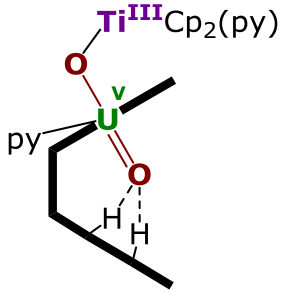

A brown suspension of [(UO$_2$)(py)(H$_2$L)] **A** (300 mg, 0.226 mmol) in C_6H_6 (5.0 ml) was combined with Cp$_2$Ti(η^2-C$_2$(SiMe$_3$)$_2$ (78.9 mg, 0.226 mmol) at room temperature to form a light brown solution. The solvent was reduced to *ca*. 1.5 ml under vacuum to afford [(py)(Cp$_2$TiOUO)(py)(H$_2$L)] **9** as a beige powder. The mother liquor was filtered off and the powder recrystallised from pyridine to afford red crystals suitable for X-ray diffraction. The pyridine was decanted off and the crystals were isolated and dried under vacuum. Yield: 230 mg (73%).

^{1}H-NMR (C_6D_6, 400 MHz): δ_H -5.71 (s, 3H, C*H*$_3$), -5.09 (s, 3H, C*H*$_3$), -3.57 (s, 2H), -1.53 (s, 6H, Ph-C*H*$_3$), -0.07 (s, 6H, Ph-C*H*$_3$), 0.16 (s, 10H, C_5H_5), 0.51 (s, 2H, pyrrole), 0.99 (s, 2H, pyrrole), 7.70 (s, 2H), 8.27 (s, 3H, C*H*$_3$), 10.63 (d, 2H, pyrrole, $^3J_{H\text{-}H}$ = 4 Hz), 12.53 (d, 2H, pyrrole, $^3J_{H\text{-}H}$ = 4 Hz), 21.24 (s, 3H, C*H*$_3$), 71.35 (br, 2H, N*H*); ^{1}H-NMR (C_5D_5N, 400 MHz):

δ_H -11.09 (s, 3H, CH_3), -5.95 (s, 3H, CH_3), -3.02 (s, 2H), -2.38 (br, 6H, Ph-CH_3), -1.64 (s, 10H, C$_5H_5$), -0.62 (s, 6H, Ph-CH_3), 1.13 (s, 2H), 8.21 (s, 2H), 9.10 (s, 2H), 11.08 (s, 3H, CH_3), 13.18 (s, 2H), 25.54 (s, 3H, CH_3), 75.40 (br, 2H, N*H*); $^{13}C\{^1H\}$-NMR (C_6D_6): δ_C 10.06, 15.92, 18.15, 20.80, 34.23, 52.63, 106.46, 109.15, 114.54, 116.34, 122.54, 123.17, 123.42, 125.90, 126.47, 146.04, 149.26, 163.54; Analysis. Found: C, 59.71; H, 5.12; N, 11.53 % $C_{67}H_{67}N_{11}O_2TiU$ requires: C, 59.86; H, 5.02; N, 11.46 %; FTIR (nujol, cm^{-1}): ν 2925 (w, NH), 2854 (w, NH), 1581 (w, imine), 1461 (s, L), 1377 (s, L), 1288 (m, L), 1268 (m, L), 1181 (w, L), 1044 (m, L), 1019 (m, L), 893 (w, asymm. UO stretch), 865 (w, L), 800 (s, L), 722 (w, L). L = stretches attributed to the Pacman ligand.

SQUID: Variable temperature magnetic susceptibility (dc and ac) measurements were carried out by Alessandro Prescimone and performed on a Quantum Design Magnetic Property Measurement System (SQUID magnetometer) equipped with a 7 T magnet operating in the 350±2 K temperature range. Diamagnetic corrections were applied using Pascal's constants.

The magnetic properties were modelled by Nicola Magnani, Institute for Transuranium Elements, Karlsruhe Germany, stating the following: "The magnetic properties of the Ti(III)-U(V) complex **9** were modelled assuming that the former $3d^1$ ion is represented by a pure-spin moment S = 1/2 and the latter 5 f^1 ion by a total (orbital+spin) moment J = 5/2. The Hamiltonian which describes the quantum states of the U-Ti pair in an external magnetic field **B** can then be written as $-2J_{ex}\mathbf{S}\cdot\mathbf{J} + B_2^0O_2^0(\mathbf{J}) + B_4^0O_4^0(\mathbf{J}) - \mu_B\mathbf{B}\cdot\left(g_S\mathbf{S} + g_J\mathbf{J}\right)$, where J_{ex} is the exchange coupling constant, the B_k^q's (O_k^q's) are the ligand-field parameters (operators) for the U(V) ion, and the g's are the gyromagnetic factors. No ligand-field parameters has been explicitly considered for the Ti(III) sites because its orbital moment is expected to be quenched; for the same reason, we can safely assume that g_S = 2. The choice of a purely axial ligand-field potential for U(V) was made assuming that the two linearly arranged O atoms account for the large majority of it, and that the five N's in the equatorial plane mostly contribute with a term proportional to $O_6^5(\mathbf{J})$ which, however, does not affect a J = 5/2 moment (the Stevens factor γ is equal to zero). Mixing of the ground state with the excited J = 7/2 spin-orbit multiplet was not investigated in detail, but it was effectively taken into account by using g_J as a variable fitting parameter instead of fixing its value to the usual Landé factor (6/7 for the f^1 configuration); this can also account for covalency, to the extent where it can be described by an orbital reduction factor k_L defined so that $g_J\mathbf{J} = k_L\mathbf{L} + 2\mathbf{S}$. The best fit of the susceptibility curve, shown in the main panel of Fig. X as χT-vs-T, was found with the parameters g_J = 0.80, $B_2^0 = -30$ cm^{-1}, B_4^0 = 1.9 cm^{-1}, and $J_{ex} = -0.97$ cm^{-1}. The relatively small

value of the coupling constant explains why no clear antiferromagnetic behaviour is visible above 5 K, for example as a maximum in the χ-*vs*.-T curve. The signs of B_2^0 and B_4^0 are the same as for the Stevens factors α and β for the f^1 configuration, which means that their geometrical factor is positive in both cases, as expected for two O ligands coordinated at an angle close to 180°.

According to the above calculations, the single-ion ground state of U(V) is the J_z = ±3/2 doublet, separated from the ±5/2 level by 95 cm^{-1} and from the ±1/2 level by 760 cm^{-1}. Indeed, the dc susceptibility plotted as $1/\chi$ vs T (Figure 36, inset) follows almost precisely a straight line in the low-temperature region, where only the ground state is thermally populated. The best fit to a Curie-Weiss behaviour $1/\chi = (T - \theta)/C$ gives $\theta = -1.7$ K and $C = 0.585$ emu K/mol. The sum of the contribution to C of a pure-spin S_z = ±1/2 doublet (0.375 emu K/mol) and of a J_z = ±3/2 ligand-field doublet (0.207 emu K/mol) gives 0.574 emu K/mol, in excellent agreement with the experimental value, and the small negative value of θ confirms that the U and Ti ions are weakly antiferromagnetically coupled."

6.2.11 Synthesis of [((Cl)Cp$_2$TiOUO)(py)(H$_2$L)] 10

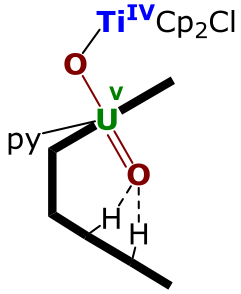

A brown suspension of [(UO$_2$)(py)(H$_2$L)] **A** (40.6 mg, 0.033 mmol) in C$_6$D$_6$ (0.5 ml) was combined with [Cp$_2$TiCl]$_2$ (7.1 mg, 0.0165 mmol) to form a light orange-brown solution. The suspension was sonicated at 70 °C for 70 minutes to afford an orange-yellow solution. The mixture was centrifuged and allowed to crystallise by solvent evaporation to afford [(Cp$_2$Ti(Cl)OUO)(py)(H$_2$L)] **10** as dark red crystals suitable for X-ray diffraction. The crystals were isolated by decanting off the mother liquor and dried under vacuum. Yield: 29 mg (72%).

^{1}H-NMR (C$_6$D$_6$): δ_H -5.49 (s, 3H, C*H*$_3$), -4.24 (s, 2H), -4.19 (s, 3H, C*H*$_3$), -0.95 (s, 6H, Ph-C*H*$_3$), -0.47 (s, 6H, Ph-C*H*$_3$), 0.03 (s, 2H), 0.41 (s, 2H, pyrrole), 0.89 (s, 2H, pyrrole), 2.55 (s, 2H), 6.68 (br, 2H, pyridine), 6.99 (br, 1H, pyridine), 7.38 (s, 3H, C*H*$_3$), 8.45 (s, 2H), 8.56 (s, 2H, pyridine), 10.40 (d, 2H, pyrrole, $^3J_{H\text{-}H}$ = 4 Hz), 11.89 (d, 2H, pyrrole, $^3J_{H\text{-}H}$ = 4 Hz), 16.48 (s, 10H, C$_5$*H*$_5$), 18.21 (s, 3H, C*H*$_3$), 63.95 (s, 2H, N*H*); ^{13}C{^{1}H}-NMR (C$_6$D$_6$): δ_C 15.94, 16.35, 16.78, 22.88, 32.99, 50.46, 50.57, 68.16, 73.35, 107.03, 108.14, 110.65, 112.84, 113.48, 115.34, 119.12, 121.76, 122.75, 123.91, 124.75, 125.81, 127.20, 127.49, 131.12, 135.60, 137.48, 145.38, 151.98, 161.52; Analysis. Found: C, 55.66; H, 4.52; N, 10.18 % C$_{57}$H$_{57}$ClN$_9$O$_2$TiU requires: C, 56.05; H, 4.70, N, 10.32 %; FTIR (nujol, cm^{-1}): ν 2926, (w,

NH/nujol), 2854 (w, nujol), 1580 (w, imine), 1462 (s, nujol), 1377 (s, nujol), 1288 (m, L), 1265 (m, L), 1216 (m, L), 1076 (m, L), 1038 (m, L), 1018 (m, L), 893 (w, asymm. UO stretch), 811 (w, L), 766 (s, L), 722 (w, nujol). L = stretches attributed to the Pacman ligand.

6.2.12 Synthesis of [((Cl)Cp$_2$ZrOUO)(py)(H$_2$L)] 11

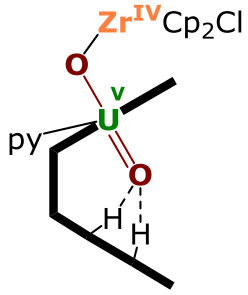

In situ reduction with Mg: A brown suspension of [(UO$_2$)(py)(H$_2$L)] **A** (100 mg, 0.076 mmol) in C$_5$D$_5$N (0.5 ml) was combined with Cp$_2$ZrCl$_2$ (22.0 mg, 0.076 mmol) and one piece of Mg turnings at room temperature to form a light brown suspension. The suspension was sonicated at 70 °C for 70 minutes to afford an orange-yellow solution. The mixture was centrifuged and allowed to crystallise by solvent evaporation to afford [(Cp$_2$Zr(Cl)OUO)(py)(H$_2$L)]·MgCl$_2$ **11-MgCl2** as beige crystals suitable for X-ray diffraction. The crystals were isolated by decanting off the mother liquor and dried under vacuum. Yield: 63 mg (66%).

In situ reduction with Zr(II): A mixture of Cp$_2$ZrCl$_2$ (200 mg, 0.69 mmol) and Cp$_2$Zr(η^2-C$_2$(SiMe$_3$)$_2$)·py (324.6 mg, 0.69 mmol) in pyridine was added to a brown suspension of [(UO$_2$)(py)(H$_2$L)] **A** (383 mg, 0.35 mmol) in benzene (3 ml) at room temperature and allowed to stir for 24 hours. The resulting red solution was evaporated to 1 ml and the yellow precipitated isolated by centrifugation (2 min, 6000 rpm). The mother liquor was removed and the precipitate was recrystallised from THF to afford light red crystals of [(Cp$_2$Zr(Cl)OUO)(py)(H$_2$L)] **11** suitable for X-ray diffraction. The crystals were isolated by decanting off the mother liquor and dried under vacuum. Yield: 260 mg (60%).

^{1}H-NMR (C$_6$D$_6$, 600MHz): δ_H -6.14 (s, 3H, C*H*$_3$), -3.92 (s, 3H, C*H*$_3$), -2.31 (s, 3H, C*H*$_3$), -0.85 (s, 6H, Ph-C*H*$_3$), -0.67 (s, 2H), -0.26 (s, 6H, Ph-C*H*$_3$), 0.23 (s (br), 2H, pyrrole), 1.64 (s (br), 2H, pyrrole), 2.58 (s, 2H), 7.05 (s, 2H), 8.35 (s, 2H), 10.20 (s, 2H, pyrrole), 11.58 (s, 2H, pyrrole), 14.94 (s, 10H, C$_5$*H*$_5$), 16.96 (s, 3H, C*H*$_3$), 61.82 (br, 2H, N*H*); ^{1}H-NMR (C$_5$D$_5$N, 400 MHz): δ_H -5.65 (s, 3H, C*H*$_3$), -4.18 (s, 3H, C*H*$_3$), -1.92 (s, 3H, C*H*$_3$), -0.85 (s, 6H, Ph-C*H*$_3$), -0.15 (s, 6H, Ph-C*H*$_3$), 1.30 (d, 2H, pyrrole, $^3J_{H\text{-}H}$ = 4 Hz), 1.41 (d, 2H, pyrrole, $^3J_{H\text{-}H}$ = 4 Hz), 2.50 (s, 2H), 7.35 (s, 2H), 8.44 (s, 2H), 10.38 (d, 2H, pyrrole, $^3J_{H\text{-}H}$ = 4 Hz), 11.80 (d, 2H, pyrrole, $^3J_{H\text{-}H}$ = 4 Hz), 15.57 (s, 10H, C$_5$*H*$_5$), 17.87 (s, 3H, C*H*$_3$), 63.32 (br, 2H, N*H*); ^{1}H-NMR (THF-d_8, 500 MHz): δ_H -5.54 (s, 3H, C*H*$_3$), -3.86 (s, 3H, C*H*$_3$), -1.89 (s, 2H), -0.66 (s, 6H, Ph-C*H*$_3$), -0.03 (s, 6H, Ph-C*H*$_3$), 1.30 (d, 2H, pyrrole, $^3J_{H\text{-}H}$ = 5 Hz), 1.54 (d, 2H, pyrrole, $^3J_{H\text{-}H}$ = 5 Hz), 2.71 (s, 2H), 7.29 (s, 2H), 8.48 (s, 2H), 10.24 (d, 2H, pyrrole, $^3J_{H\text{-}H}$ = 5 Hz),

11.61 (d, 2H, pyrrole, $^{3}J_{H\text{-}H}$ = 5 Hz), 15.10 (s, 10H, C_5H_5), 17.26 (s, 3H, CH_3), 61.37 (br, 2H, N*H*); $^{13}C\{^{1}H\}$-NMR (THF-d_8): δ_C 0.33, 16.01, 16.53, 23.90, 32.94, 42.74, 50.02, 78.11, 107.48, 111.06, 111.22, 114.52, 114.98, 115.05, 116.77, 120.72, 122.35, 122.53, 126.77, 131.06, 136.18, 145.16, 150.81, 151.22, 160.53 Analysis. Found: C, 54.26; H, 4.63; N, 9.86% $C_{57}H_{57}ClN_9O_2ZrU$ requires: C, 54.13; H, 4.54, N, 9.97 %; FTIR (nujol, cm^{-1}): ν 2924 (w, nujol), 2854 (w, nujol), 1580 (w, imine), 1462 (s, nujol), 1377 (s, nujol), 1286 (m, L), 1263 (m, L), 1046 (m, L), 1019 (w), 894 (w, asymm. UO stretch), 803 (w, L), 722 (m, nujol). L = stretches attributed to the Pacman ligand.

6.2.13 Synthesis of $[(py)_2(ClMgOUO)(py)(H_2L)]$ 12

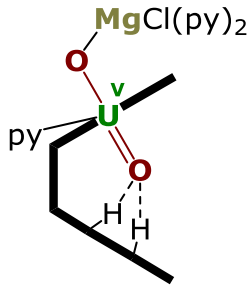

A mixture of **A** (274.2 mg, 0.246 mmol), $MgCl_2$ (11.7 mg, 0.123 mmol) and Mg (3.0 mg, 0.123 mmol) was suspended in pyridine (5 ml), sonicated for 160 minutes and stirred for 72 hours to form a cherry red solution. The mixture was dried and recrystallised from pyridine, affording beige crystals of $[(py)_2(ClMgOUO)(py)(H_2L)]$ **12** suitable for X-ray structural analysis. The crystals were decanted and dried under vacuum. Yield: 210.0 mg (69%).

From mixture with Cp_2TiCl_2: To a mixture of **A** (300.0 mg, 0.18 mmol), Cp_2TiCl_2 (45.5 mg, 0.18 mmol) and Mg (4.4 mg, 0.18 mmol) pyridine (2 ml) was added and the dark brown suspension was allowed to stir at room temperature for 48 hours to give a dark red solution. The solution was centrifuged (2 min, 6000 rpm) and the mother liquor was allowed to evaporate slowly to afford light beige crystals of $[(py)_2(ClMgOUO)(py)(H_2L)]$ **12** suitable for X-ray diffraction. The crystals were isolated by decanting off the mother liquor and dried under vacuum. Yield: 129 mg (58%).

^{1}H-NMR (C_5D_5N): δ_H -6.20 (s, 3H, CH_3), -5.99 (s, 3H, CH_3), -2.04 (s, 6H, Ph-CH_3), -1.76 (s, 3H, CH_3), -1.13 (s, 2H), -0.29 (s, 2H), 0.23 (s, 6H, Ph-CH_3), 0.99 (s, 2H), 2.83 (s, 2H), 6.85 (s, 2H), 9.32 (s, 3H, CH_3), 10.64 (s, 3H, CH_3), 13.08 (s, 2H), 77.28 (br, 2H, N*H*); $^{13}C\{^{1}H\}$-NMR (C_5D_5N): δ_C 12.32, 15.08, 16.23, 16.78, 17.62, 27.07, 36.81, 56.16, 67.03, 69.09, 94.29, 100.89, 106.05, 108.55, 112.93, 118.06, 119.72, 122.33, 127.19, 129.99, 141.38, 146.26, 147.64, 148.59, 165.89, 179.11 Analysis. Found: C, 55.68; H, 4.58; N, 12.46% $C_{57}H_{57}ClMgN_{11}O_2U$ requires: C, 55.84; H, 4.69, N, 12.57 %; FTIR (nujol, cm^{-1}): ν 2925 (w, NH/nujol), 2725 (w, NH), 1580 (w, imine), 1462 (s, nujol), 1377 (s, nujol), 1286 (m, L), 1213

(w, L), 1155 (w, L), 1041 (m, L), 973 (s), 891 (w, asymm. UO stretch), 827 (w, L), 722 (s, nujol). L = stretches attributed to the Pacman ligand.

6.2.14 Synthesis of [(py)$_2$(thf)$_2$(ICaOUO)(py)(H$_2$L)] 13

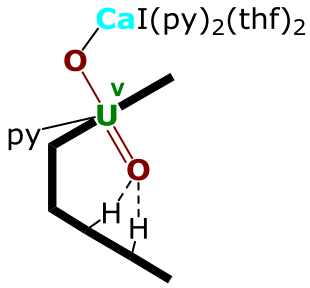

A mixture of **A** (200.0 mg, 0.180 mmol), CaI_2 (26.4 mg, 0.090 mmol) and Ca (3.6 mg, 0.090 mmol) was suspended in pyridine (3 ml), sonicated for 60 minutes at 50°C and stirred for 48 hours at room temperature to form a red solution. The mixture was dried and recrystallised from tetrahydrofuran, affording pale red translucent plates of [(py)$_2$(thf)$_2$(ICaOUO)(py)(H$_2$L)] **13** suitable for X-ray structural analysis. The crystals were decanted and dried under vacuum. Yield: 210.0 mg (69%).

^{1}H-NMR (C_5D_5N): δ_H -8.41 (s, 2H), -6.32 (s, 3H, C*H*$_3$), -2.65 (s, 2H), -2.17 (s, 6H, Ph-C*H*$_3$), -0.63 (s, 3H, C*H*$_3$), -1.36 (s, 2H), -1.23 (s, 2H), 0.23 (s, 6H, Ph-C*H*$_3$), 0.85 (s, 2H), 1.59 (s, 2H), 6.83 (s, 2H), 9.76 (s, 3H, C*H*$_3$), 10.80 (s, 2H), 13.38 (s, 2H), 28.16 (s, 3H, C*H*$_3$), 79.30 (br, 2H, N*H*); ^{13}C{^{1}H}-NMR (C_5D_5N): δ_C 13.80, 15.16, 16.34, 17.67, 22.14, 23.00, 26.02, 31.86, 36.15, 55.82, 60.71, 68.08, 89.47, 96.42, 106.99, 108.18, 112.91, 114.36, 117.05, 121.04, 125.86, 147.11, 165.55 Analysis. Found: C, 49.00; H, 4.35; N, 10.03% $C_{51}H_{55}CaIN_9O_3U$ requires: C, 49.12; H, 4.45, N, 10.11 %; FTIR (nujol, cm^{-1}): ν 2932 (w, nujol), 2725 (w, NH), 1552 (w, imine), 1462 (s, nujol), 1377 (s, nujol), 1272 (m, L), 1214 (w, L), 1179 (w, L), 1042 (m, L), 970 (s), 891 (w, asymm. UO stretch), 828 (w, L), 722 (s, nujol). L = stretches attributed to the Pacman ligand.

6.2.15 Synthesis of [(py)$_2$(ClZnOUO)(py)(H$_2$L)] 14

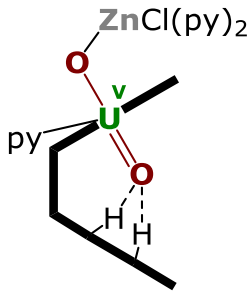

A mixture of **A** (100.0 mg, 0.092 mmol), $ZnCl_2$ (6.3 mg, 0.046 mmol) and Zn (3.0 mg, 0.046 mmol) was suspended in pyridine (3 ml), sonicated for 80 minutes to form a red solution which was left stirring overnight at room temperature to form a lemon yellow suspension. The mixture was centrifuged and the precipitate extracted with fresh pyridine, forming a yellow solution from which yellow, translucent plates of [(py)$_2$(ClZnOUO)(py)(H$_2$L)] **14** crystallised, which were suitable for X-ray structural analysis. The crystals were isolated by decanting the mother liquor off, followed by drying under vacuum. Yield: 83.0 mg (71%).

^{1}H-NMR (C_5D_5N): δ_H -5.83 (s, 3H, C*H*$_3$), -4.30 (s, 2H), -1.77 (s, 6H, Ph-C*H*$_3$), -1.41 (s, 2H), -0.29 (s, 2H), -0.22 (s, 2H), 0.58 (s, 6H, Ph-C*H*$_3$), 3.65 (s, 2H), 6.67 (s, 2H), 9.24 (s, 3H, C*H*$_3$), 10.51 (s, 2H), 12.93 (s, 2H), 25.98 (s, 3H, C*H*$_3$), 75.37 (br, 2H, N*H*); ^{13}C{^{1}H}-NMR (C_5D_5N): δ_C 9.61, 11.55, 14.66, 15.47, 16.96, 23.27, 24.51, 26.25, 32.14, 35.57, 39.52, 68.28, 95.12, 101.33, 108.09, 110.57, 116.86, 117.61, 126.79, 147.79, 164.28 Analysis. Found: C, 49.00; H, 4.35; N, 10.03% $C_{57}H_{57}ClN_{11}O_2UZn$ requires: C, 54.03; H, 4.53, N, 12.16 %; FTIR (nujol, cm^{-1}): ν 2954 (w, NH), 2723 (w, NH), 1563 (w, imine), 1462 (s, nujol), 1377 (s, nujol), 1287 (m, L), 1217 (w, L), 1154 (w, L), 1040 (m, L), 972 (s, L), 893 (w, asymm. UO stretch), 770 (w, L), 722 (s, nujol). L = stretches attributed to the Pacman ligand.

6.2.16 Synthesis of [(py)$_2$(IZnOUO)(py)(H$_2$L)] 15

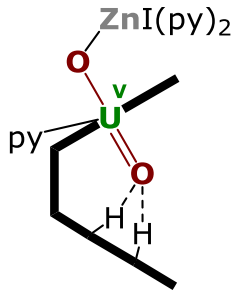

A mixture of **A** (100.0 mg, 0.092 mmol), ZnI_2 (14.6 mg, 0.046 mmol) and Zn (3.0 mg, 0.046 mmol) was suspended in pyridine (3 ml), sonicated for 30 minutes to form a red solution which was left stirring overnight at room temperature to form a lemon yellow suspension. The mixture was centrifuged and the precipitate extracted with fresh pyridine, forming a yellow solution from which yellow, translucent plates of [(py)$_2$(IZnOUO)(py)(H$_2$L)] **15** crystallised, which were suitable for X-ray structural analysis. The crystals were isolated by decanting the mother liquor off, followed by drying under vacuum. Yield: 91.2 mg (73%).

^{1}H-NMR (C_5D_5N): δ_H -5.71 (s, 3H, C*H*$_3$), -4.86 (s, 2H), -1.75 (s, 6H, Ph-C*H*$_3$), -1.33 (s, 2H), -0.57 (s, 2H), -0.11 (s, 2H), 0.47 (s, 6H, Ph-C*H*$_3$), 3.35 (s, 2H), 6.74 (s, 2H), 9.14 (s, 3H, C*H*$_3$), 10.47 (s, 2H), 12.84 (s, 2H), 25.75 (s, 3H, C*H*$_3$), 74.52 (br, 2H, N*H*); Analysis. Found: C, 50.51; H, 4.35; N, 11.31% $C_{57}H_{57}IN_{11}O_2UZn$ requires: C, 50.40; H, 4.23, N, 11.34 %; FTIR (nujol, cm^{-1}): ν 2928 (w, nujol), 2853 (w, nujol), 1559 (w, imine), 1462 (s, nujol), 1377 (s, nujol), 1287 (m, L), 1215 (w, L), 1182 (w, L), 1046 (m, L), 978 (s, L), 892 (w, asymm. UO stretch), 769 (w, L), 722 (s, nujol). L = stretches attributed to the Pacman ligand.

6.2.17 Synthesis of $[OU(py)_5OSm(I_4)OU(py)_5O]^+[I]^-$ 16

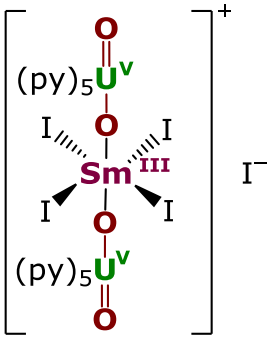

Synthetic route that led to the isolation of the first batch: To a brown solution of **A** (61.8 mg, 0.055 mmol) in pyridine-d_5 (0.5 ml) in a Teflon-tapped NMR tube $SmI_2(thf)_2$ (30.5 mg, 0.055 mmol) was added and the ^{1}H-NMR spectrum recorded. The resulting red reaction mixture was allowed to stand at room temperature. After four days the formation of several dark coloured crystals was observed. The crystalline material was examined under a microscope under Fomblin oil and found to exhibit two different kind of crystals, one of dark blue colour which revealed after X-ray structural analysis starting material **A** and another set of translucent pale red prisms of $[O=U(py)_5\text{-}O\text{-}Sm(I_4)\text{-}O\text{-}U(py)_5=O]^+$ I^- **16**. Since the isolated material **16** could not be separated from **A** no further characterisation could be carried out. The initial ^{1}H-NMR resonances recorded are not consistent with **16** and suggest the formation of a Sm(III) uranyl(V) Pacman complex.

Bulk scale synthesis: To a brown solution of **A** (97.4 mg, 0.089 mmol) in pyridine-d_5 (0.7 ml) in a Teflon-tapped ampoule $SmI_2(thf)_2$ (73.7 mg, 0.134 mmol) was added and vigorously stirred to form a red solution. An aliquot was taken and the initial ^{1}H-NMR spectrum recorded. The remaining solution was centrifuged (6000 rpm / 1 min) and syringe filtered (0.45 µm PTFE), the solvent removed under vacuum to a volume of ca. 0.3 ml and the mixture was allowed to crystallise at room temperature. After six days the formation of a few translucent pale red prisms of $[O=U(py)_5\text{-}O\text{-}Sm(I_4)\text{-}O\text{-}U(py)_5=O]^+$ I^- **16** was observed and the chemical identity confirmed by X-ray crystallography. Yield: Crystallographic.

The amount of material obtained was not sufficient for complete spectroscopic and elemental analysis.

6.2.18 Synthesis of $[Cp_3UOUO(thf)(H_2L^{Et})]$ 17

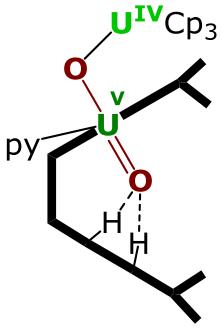

A mixture of $\mathbf{A^{Et}}$ (80.0 mg, 0.075 mmol) and Cp_3U (32.6 mg, 0.075 mmol) was cooled to -96 °C. To this mixture tetrahydrofuran (1.8 ml) was slowly added and the mixture left stirring and warm to room temperature overnight. The yellow brown suspension was centrifuged (1 min, 6000 rpm) and the amber-brown supernatant removed from the yellow precipitate. The precipitate was extracted with tetrahydrofuran to give a yellow-brown solution, from which yellow-brown plates of $[Cp_3UOUO(thf)(H_2L^{Et})]$ **17** formed, which were suitable for X-ray structural analysis. The

crystals were isolated by decanting the mother liquor off, followed by drying under vacuum. Yield: 36.0 mg (32 %).

^{1}H-NMR (THF-d_8): δ_H -9.43 (s, 2H), -7.88 (s, 2H), -5.92 (t, 3H, CH_3), -2.72 (q, 2H, CH_2), 0.00 (s, 6H, Ph-CH_3), 1.37 (q, 2H, CH_2), 2.14 (s, 2H), 2.66 (t, 3H, CH_3), 3.17 (s, 15H, Cp), 3.48 (q, 2H, CH_2), 3.69 (s, 6H, Ph-CH_3), 3.85 (s, 2H), 3.92 (t, 3H, CH_3), 5.86 (m, 3H, CH_3), 8.38 (s, 2H, pyrrole), 9.54 (s, 2H, pyrrole), 51.42 (br, 2H, N*H*); ^{13}C{^{1}H}-NMR (THF-d_8): δ_C 1.75, 2.11, 11.52, 11.96, 12.93, 16.47, 17.57, 21.58, 23.06, 30.07, 53.92, 109.23, 113.79, 120.15, 120.30, 127.73, 128.12, 128.59, 141.32, 145.10, 147.71, 155.79 Analysis. Found: C, 52.22; H, 5.07; N, 7.39 % $C_{65}H_{73}N_8O_3U_2$ requires: C, 52.38; H, 4.94, N, 7.52 %; FTIR (nujol, cm^{-1}): ν 3583 (w, NH), 1581 (w, imine), 1462 (s, nujol), 1377 (s, nujol), 1304 (m, L), 1286 (w, L), 1154 (w, L), 1049 (m, L), 973 (s), 893 (w, asymm. UO stretch), 770 (w, L), 722 (s, nujol). L = stretches attributed to the Pacman ligand.

6.2.19 Synthesis of [(U^{V}O$_2$)(py)(ZnL)] 18

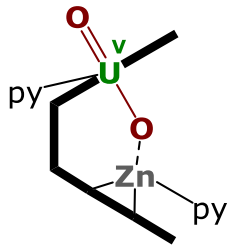

A pyridine solution of uranium tris(hexamethyldislylamide) (311 mg, 0.433 mmol) was added to a -35 °C pyridine solution of [(U^{VI}O$_2$)(py)(ZnL)] **A^{Zn}** (500 mg, 0.433 mmol) over 20 minutes. The mixtures was allowed to warm to room temperature overnight to form a slight suspension. The mixture was concentrated under vacuum to a volume of about 3 ml and centrifuged (4500 rpm/ 5 min) to remove any precipitate formed. The mother liquor was further concentrated under vacuum to yield red crystals of [(U^{V}O$_2$)(py)(ZnL)] **18** suitable for X-ray diffraction. Yield: 219 mg (44 %).

^{1}H-NMR (C_5D_5N): δ = -14.57 (s, 2H), -6.35 (s, 3H, CH_3), -4.82 (s, 2H), -4.74 (s, 2H), -3.54 (s, 2H), -3.06 (s, 2H), -2.70 (s, 2H), -2.34 (s, 2H), -2.04 (s, 3H, CH_3), -1.77 (s, 3H, CH_3), -0.27 (s, 3H, CH_3), -0.01 (s, 2H), 0.26 (s, 2H), 1.98 (s, 2H), 2.55 (s, 3H, CH_3), 5.23 (s, 3H, CH_3), 8.13 (s, 2H), 9.33 (s, 3H, CH_3), 10.30 (s, 2H), 11.69 (s, 2H), 12.55 (s, 2H), 12.79 (s, 2H), 29.55 (s, 3H, CH_3), 59.06 (s, 2H); ^{13}C{^{1}H}-NMR (C_6D_6): δ = 15.43, 15.61, 15.81, 19.04, 19.40, 21.35, 35.44, 55.27, 94.06, 105.80, 107.46, 112.76, 113.75, 118.53, 119.04, 120.50, 122.14, 125.33, 125.37, 125.48, 128.99, 130.40, 139.44, 142.67, 148.58, 151.64, 151.87, 161.84, 176.18 Analysis. Found: C, 54.18; H, 4.49; N, 12.16. $C_{52}H_{50}N_{10}O_2UZn$ requires: C, 54.29; H, 4.38; N, 12.18 %. FTIR (nujol, cm^{-1}): 1580 (w, imine), 1460 (s, L), 1377 (s, L), 1281 (m, L),

1262 (m, L), 1090 (w, L), 1048 (m, L), 1018 (m, L), 893 (w, asymm. UO stretch), 799 (s, L), 722 (w, L).

6.2.20 Synthesis of [$Cp_3NpOUO(thf)(H_2L^{Et})$] 19

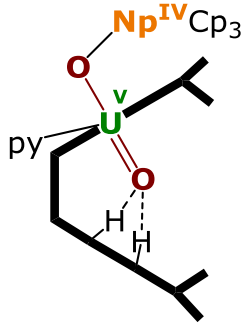

A mixture of $\mathbf{A^{Et}}$ (71 mg, 66.0 µmol) and Cp_3Np (42.8 mg, 99.0 µmol) was cooled to -78 °C. To this mixture tetrahydrofuran (5 ml) was slowly added and the mixture left stirring and warm to room temperature overnight to afford a red solution. The solution was concentrated under vacuum. Brown plates of [$Cp_3NpOUO(thf)(H_2L^{Et})$] **19** were grown by pentane diffusion into the concentrated mother liquor and were suitable for X-ray structural analysis. The crystals were isolated by decanting the mother liquor off, followed by drying under vacuum. Yield: 51.4 mg (46 %). The stability of **19** was checked *via* X-ray cell check after storage for 5 days at room temperature under Ar.

6.2.21 Synthesis of [$Cp_3NpONp(Cp_2)ONpCp_3$] 20

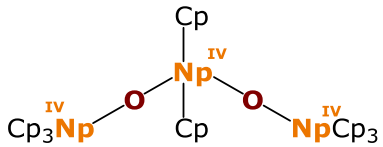

Olive green $\mathbf{A^{Et}}$ (42.8 mg, 39.8 µmol) and brown $Cp_3{}^{237}Np$ (17.2 mg, 39.8 µmol) were mixed and cooled with solid dry ice pellets. To this mixture THF-d_8 (4 ml) was added and the mixture was allowed to stir and warm to room temperature, forming a red solution within three hours. The material was dried and recrystallised from thf solution by hexane diffusion to yield big red needles of [$Cp_3NpONp(Cp_2)ONpCp_3$] **20**. Yield: Crystallographic.

6.2.22 Synthesis of [$UO_2(Cl)(L^{ene})$] 21

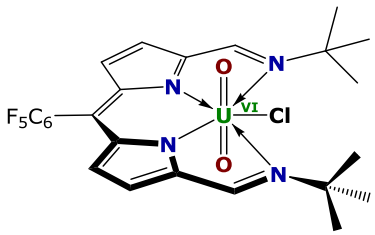

Dark purple HL^{ene}(pentafluorophenyl dipyrromethene) (0.40 g, 0.84 mmol) and red $UO_2\{N(SiMe_3)_2\}_2$ (0.63 g, 0.84 mmol) were weighed into a Schlenk flask, to which pyridine (15 ml) was added under cold conditions (-60 °C) forming a magenta purple solution. The solution was stirred at this temperature for two hours and was then stirred at room temperature for a further 12 hours, after which the solution had become a deep violet/blue colour. Pyridine hydrochloride (97.0 mg, 0.84 mmol) dissolved in pyridine (4 ml) was injected into the blue solution and

stirred for 12 hours. All volatiles were removed and the dried material was washed with hexane (2 x 20 ml) and dried under vacuum for 12 hours to yield [UO2(Cl)(L^{ene})] **21**. Purple-blue single crystals suitable for X-ray crystallography were obtained by recrystallisation from a concentrated benzene solution. Yield: 497 mg (76 %).

^{1}H-NMR (THF-d_8, 500 MHz): δ_H 2.00(s, 18H, C(CH_3)$_3$), 7.18 (d, 2H, pyrrole, , $^{3}J_{H\text{-}H}$ = 5 Hz) 7.25 (m, 2H, CH_{meta} pyridine), 7.29 (d, 2H, pyrrole, $^{3}J_{H\text{-}H}$ = 5 Hz), 7.65 (m, 1H, CH_{para} pyridine, 8.56 (m, 2H, CH_{ortho} pyridine), 9.52 (s, 2H, CH-N-C(CH$_3$)$_3$). ^{13}C{^{1}H}-NMR (THF-d_8, 500 MHz): δ_C 14.57, 23.67, 31.12, 32.68, 124.51, 124.91, 129.19, 135.17, 135.93, 136.44, 147.64, 150.97, 159.81, 160.93 ^{19}F-NMR (THF-d_8, 500 MHz): δ_F -163.34 (td, F_{meta}), -155.18 (t, F_{para}), -140.67 (F_{ortho}). Analysis. Found: C, 38.40; H, 3.25; N, 7.04 % $C_{25}H_{24}ClF_5N_4O_2U$ requires: C, 38.45; H, 3.10; N, 7.17 %; FTIR (nujol, cm^{-1}): υ 2925 (s, nujol), 2854 (s, nujol), 2726 (w, nujol), 1655 (w, L), 1607 (w, L), 1556 (m, imine), 1464 (s, nujol), 1408 (w, L), 1377 (s, nujol), 1266 (m, L), 1216 (m, L), 1188 (m, L), 1062 (m, L), 1004 (m, L), 952 (w, L), 932 (m, L), 879 (w, L), 847 (w, asymm. UO stretch), 819 (w, L), 773 (w, L), 756 (w, L), 722 (w, nujol). L = stretches attributed to the dipyrrin ligand.

6.2.23 Synthesis of [(Cp$_2$TiCl)OUO(Cp$_2$TiCl)(Cl)(L^{ene})] 22

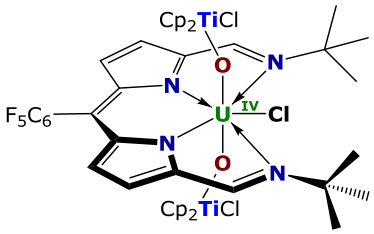

Purple-blue **21** [UO$_2$(L^{ene})(Cl)] (38.4 mg, 0.049 mmol) and [Cp$_2$TiCl]$_2$ (21.0 mg, 0.049 mmol) were measured into separate Teflon-tapped ampoules and dissolved in toluene (5 ml). The two solutions were combined and stirred for 12 hours at -40 °C, forming a dark blue solution which was allowed to warm to room temperature and allowed to stand for two days to afford blue crystals of [(Cp$_2$TiCl)OUO(Cp$_2$TiCl)(L^{ene})(Cl)] **22** suitable for X-ray diffraction. Yield: 115 mg (37 %).

^{1}H-NMR (C_6D_6, 500 MHz), δ_H -37.74 (s, 1H, CH-N-C(CH$_3$)$_3$), -31.83 (s, 9H, C(CH_3)$_3$), -22.72 (s, 1H, pyrrole), -17.84 (s, 1H, pyrrole), -8.59 (s, 9H, C(CH_3)$_3$), -8.33 (s, 1H, CH-N-C(CH$_3$)$_3$), -3.79 (d, 1H, pyrrole, $^{3}J_{H\text{-}H}$ = 5 Hz), -1.55 (d, 1H, pyrrole, $^{3}J_{H\text{-}H}$ = 5 Hz), 5.92 (s, 5H, C$_5H_5$TiCl), 19.02 (s, 5H, C$_5H_5$TiCl), 43.70 (s, 10H, C$_5H_5$TiCl). ^{19}F-NMR (C_6D_6, 500 MHz): δ_F -139.81 (d, F_{ortho}), -143.92 (d, F_{ortho}), -154.29 (t, F_{meta}), -156.49 (t, F_{meta}), -163.09 (m, F_{para}). Analysis. Found: C, 44.59; H, 3.69; N, 4.51 % $C_{45}H_{44}Cl_3F_5N_4O_2Ti_2U$ requires: C, 44.74;

H, 3.67; N, 4.64 %; %; FTIR (nujol, cm^{-1}): υ 2923 (s, nujol), 2856 (s, nujol), 2726 (w, nujol), 1659 (w, L), 1610 (m, L), 1560 (s, imine), 1521 (m, L), 1499 (s, L), 1463 (s, nujol), 1407 (m, L), 1377 (s, nujol), 1272 (s, L), 1220 (m, L), 1193 (s, L), 1156 (w, X), 1062 (s, L), 1001 (s, L), 982 (s, L), 962 (w, L), 948 (m, L), 898 (w, U-O_{asym}), 845 (m, X), 814 (s, X), 772 (m, L), 728 (m, nujol). L = stretches attributed to the dipyrrin ligand, X = stretches attributed to $TiCp_2Cl$.

6.2.24 Synthesis of [$Me_3SiOU^{III}OSiMe_3(py)(L^{eneAr})$] / [$Me_3SiOU^{IV}OSiMe_3(py)(L^{aneAr})$] 23

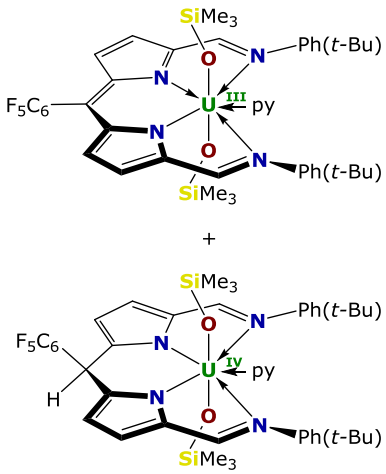

Red $UO_2(N(SiMe_3)_2)_2(py)_2$ (35.6 mg, 0.047 mmol) was added to a solution of bis-[4-((1*H*-pyrrol-2-yl) methylidene(4-(*tert*-butyl)tolyl)]imine)-yl] (pentafluoro-phenyl) methane (H_2L^{aneAr}) (30.0 mg, 0.047 mmol) in pyridine and heated for 41 hours at 70 °C to give a blue solution. All volatiles were removed *in vacuo* and the dried material redissolved in pyridine. From this solution blue crystals of superimposed [$Me_3SiOU^{III}OSiMe_3(L^{eneAr})$] / [$Me_3SiOU^{IV}OSiMe_3(L^{aneAr})$] **23** were grown. The mother liquor was decanted off and the crystals dried under vacuum. Yield: 32 mg (57 %).

^{1}H-NMR (C_6D_6, 600 MHz): **U^{III} component**: δ_H -7.18 (s, 18H, C(C*H*$_3$)$_3$), -6.61 (s, 18H, Si(C*H*$_3$)$_3$), 6.56 (d, 2H, pyrrole, $^3J_{H\text{-}H}$ = 6 Hz), 6.75 (m, 8H, Ar-*H*), 7.06 (s, 2H, N=C*H*), 7.29 (d, 2H, pyrrole, $^3J_{H\text{-}H}$ = 6 Hz). **U^{IV} component**: δ_H -4.34 (s, 18H, C(C*H*$_3$)$_3$), 1.25 (m, 4H, pyrrole), 1.27 (m, 8H, Ar-*H*), 2.11 (s, 1H, meso-*H*), 7.29 (s, 2H, N=C*H*), 39.81 (s, 18H, Si(C*H*$_3$)$_3$). Analysis. Found: C, 52.54; H, 5.38; N, 6.79 % $C_{53}H_{55}D_5F_5N_6O_2Si_2U$ (**U^{III}**) requires: C, 52.73; H, 5.43; N, 6.96 %; $C_{53}H_{56}D_5F_5N_6O_2Si_2U$ (**U^{IV}**) requires: C, 52.68; H, 5.51; N, 6.96 %; FTIR (nujol, cm^{-1}): υ 1583 (w, imine), 1462 (s, nujol), 1376 (s, nujol), 1290 (m, L), 1260 (m, L), 1051 (m, ν Si-O), 1000 (w, L), 946 (w, L), 923 (w, L), 878 (s, ν U-O), 836 (m, ν U-O), 722 (s, nujol). L = stretches attributed to the ligand.

6.3 Control reactions and others that did not yield the target product

6.3.1 Reactions to target functionalisation of [(py)(Me_2AlOUO)(py)(H_2L)] 1 and [(py)(^{i}Bu_2AlOUO)(py)(H_2L)] 2

6.3.1.1 Treatment of 1 and 2 with Rb metal

To a yellow solution of **1** (54.9 mg, 0.048 mmol) in C_6D_6 (0.5 ml) Rb metal (4.1 mg, 0.048 mmol) was added. The mixture was heated overnight at 80 ºC yet no change in the ^{1}H-NMR spectrum was observed. Naphthalene was added and the mixture heated for another 72 hours at 80 ºC, with the ^{1}H-NMR spectrum showing only the resonances of **1**.

A yellow solution of **2** (28.7 mg, 0.023 mmol) in C_6H_6 (0.4 ml) was layered with C_4H_8O (0.5 ml) and Rb metal (2.0 mg, 0.023 mmol) was added. The mixture was shaken and gave an orange solution, but no immediate reaction was observed. Heating this mixture at 80 °C overnight resulted in decomposition.

6.3.1.2 Treatment of 1 with HCl

To a yellow solution of **1** (28.6 mg, 0.025 mmol) in C_6D_6 (0.5 ml) HCl (0.25 M soln in Et_2O, 0.1 ml, 0.025 mmol) was added. The mixture was allowed to react for one hour to form a precipitate which was centrifuged off. The mother liquor was removed and the precipitate dried and redissolved in C_6D_6. The ^{1}H-NMR spectrum showed only the resonances of **1** and the formation of **A**.

6.3.1.3 Treatment of 1 with BH_3·SMe_2

To a yellow solution of **1** (22.9 mg, 0.020 mmol) in C_6D_6 (0.3 ml) an equivalent of BH_3·SMe_2 (0.2 M in thf, 0.1 ml, 0.020 mmol) was added *via* syringe. The mixture gave a clear red solution after 2 minutes. The ^{1}H-NMR spectrum showed a new set of resonances and no starting material could longer be seen. The mixture was dried under vacuum to remove all volatiles and redissolved in benzene. No pure and uniform material could be isolated from this synthesis.

6.3.1.4 Treatment of 1 with $BHCl_2$·dioxane

To a yellow solution of **1** (22.9 mg, 0.020 mmol) in C_6D_6 (0.3 ml) an equivalent of $BHCl_2$·dioxane (0.3 M in CH_2Cl_2, 0.067 ml, 0.020 mmol) was added *via* a syringe to give a brown precipitate immediately. The precipitate was separated from the mother liquor by centrifugation and dried under vacuum. The ^{1}H-NMR spectrum of the precipitate was recorded in a C_6D_6 solution. The material decomposed upon addition of pyridine and no pure and uniform material could be isolated from this synthesis.

6.3.1.5 Treatment of 1 with LiCl

To an orange-red solution of **1** (18.9 mg, 0.016 mmol) in C_5D_5N (0.4 ml) LiCl (0.7 mg, 0.016 mmol) was added and the mixture heated at 80 ºC. After 24 hours the ^{1}H-NMR spectrum showed mainly the formation of **A** along with minor amounts of indeterminable decomposition products.

6.3.1.6 Treatment of 1 with $LiNEt_2$

To a yellow solution of **1** (18.8 mg, 0.016 mmol) in C_6D_6 (0.4 ml) $LiNEt_2$ (1.3 mg, 0.016 mmol) was added. The mixture was heated at 80 ºC to solubilise the $LiNEt_2$. The ^{1}H-NMR spectrum resonances of **1**, **A** (relative ration 1 : 0.75) and a variety of paramagnetic resonances at low frequencies below -6 ppm as well as four individual resonances at high frequencies (39.02, 50.79, 64.43 and 68.51 ppm) with differing integral heights, indicating the probable formation of a mixture of mono- and doubly deprotonated species.

6.3.1.7 Treatment of 1 with MeOTf

To a yellow solution of **1** (30.3 mg, 0.026 mmol) in C_6D_6 (0.5 ml) methyl triflate (0.88 mmol in C_6D_6, 0.03 ml, 0.026 mmol) was added. The material decomposed instantly, forming a red, viscous oil. The ^{1}H-NMR spectrum showed no resonances attributable to any product.

6.3.1.8 Treatment of 1 with $[PPh_3CuH]_6$

To an orange-red solution of **1** (30.0 mg, 0.026 mmol) in C_5D_5N (0.4 ml) $[PPh_3CuH]_6$ (8.6 mg, 0.004 mmol) was added and the mixture was allowed to react at room temperature for three days. No reaction occurred and **1** was recovered as yellow crystals.

6.3.1.9 Treatment of 2 with Cp_2ZrHCl

To an orange-red solution of **2** (12.0 mg, 9.7 μmol) in C_6D_6 (0.4 ml) Cp_2ZrHCl (5.0 mg, 0.019 mmol) was added and the mixture heated at 80 °C for 21 days. No reaction was observed and **2** was recovered as yellow crystals.

To an orange-red solution of **2** (12.0 mg, 9.7 μmol) in C_6D_6 (0.4 ml) Cp_2ZrHCl (5.0 mg, 0.019 mmol) and two drops of THF was added and the mixture sonicated and allowed to stand for 2 days. No reaction was observed and **2** was recovered as yellow crystals.

To an orange-red solution of **2** (24.3 mg, 19.4 μmol) in C_6D_6 (0.4 ml) Cp_2ZrHCl (5.0 mg, 0.019 mmol) and one drop of THF was added. The mixture was sonicated for 10 minutes heated at 40 °C for 90 min. No reaction was observed and **2** was recovered as yellow crystals.

6.3.1.10 Treatment of 1 with Me_3OBF_4

To a yellow solution of **1** (10.0 mg, 0.008 mmol) in C_6D_6 (0.4 ml) Me_3OBF_4 (1.3 mg, 0.008 mmol) was added. The material decomposed instantly, forming a red, viscous oil. The ^{1}H-NMR spectrum showed no resonances attributable to any product.

6.3.2 Reactions to target further functionalisation of $[(py)_3(KOUO)(py)(H_2L)]$ 6

6.3.2.1 Treatment of 6 with Cp_3UCl

To a red solution of **6** (21.4 mg, 0.016 mmol) in C_5D_5N (0.4 ml) Cp_3UCl (7.8 mg, 0.016 mmol) was added and allowed to stand for one weak, forming a white precipitate. The ^{1}H-NMR spectrum of the supernatant showed the formation of a new product, as well as resonances attributed to Cp_3UCl, $Cp_3U{\cdot}py$, Cp_4U (relative ratio: 0.5:1:1) and uranyl(VI) Pacman A (12 %). Heating for three hours at 70 ºC increased the amount of **A** present to 25 %.

^{1}H-NMR (C_5D_5N): δ_H -8.94 (s, 2H), -8.57 (s, 20H, Cp_4U), -7.35 (s, 3H, C*H*$_3$), -3.25 (s, 15H, $Cp_3U{\cdot}py$), -2.61 (s, 15H, Cp_3UCl), -2.93 (s, 3H, C*H*$_3$), -0.59 (s, 6H, Ph-C*H*$_3$), 0.17 (s, 3H, C*H*$_3$), 0.45 (s, 2H), 0.52 (s, 2H), 3.26 (s, 2H), 3.60 (s, 6H, Ph-C*H*$_3$), 3.94 (s, 2H), 4.34 (s, 15H, Cp), 5.93 (s, 2H), 10.31 (s, 2H), 58.09 (br, 2H, N*H*)

6.3.2.2 Treatment of 6 with UCl_4

A red solution of **6** (50.0 mg, 0.039 mmol) in pyridine (30 ml) was mixed with a freshly prepared solution of olive green UCl_4 (14.8 mg, 0.039 mmol) in pyridine (30 ml) and allowed to stir for two hours. The volume was reduced to 2 ml under vacuum. The mixture was left to

settle overnight and centrifuged the next day to remove any undissolved material. The mother liquor was transferred to a Young's tap NMR tube, evaporated to dryness and replaced with fresh C_5D_5N. The ^{1}H-NMR spectrum showed only the resonances of **A**.

6.3.2.3 Treatment of 6 with $ThCl_4(dme)_2$

To a red solution of **6** (35.0 mg, 0.027 mmol) in C_5D_5N (0.4 ml) $ThCl_4$(dme)2 (15.0 mg, 0.027 mmol) was added and allowed to stand for three hours. The ^{1}H-NMR spectrum of the solution showed only the clean formation of **A**.

6.3.3 Further reductive metalations of $[(UO_2)(py)(H_2L)]$ A

6.3.3.1 A + Rb (excess)

To a brown suspension of **A** (31.1 mg, 0.029 mmol) in C_5D_5N (0.4 ml) Rb metal (7.0 mg, 0.082 mmol) was added and the mixture sonicated for 80 minutes to give an orange precipitate. The precipitate was centrifuged off (2 min/6000 rpm) and redissolved in C_5D_5N to give a ^{1}H-NMR spectrum similar to that of **7** and no pyrrole-NH resonances, indicating the formation of $[(py)_3(RbOUO)(py)(\{Rb(py)\}_2L)]$. Recrystallisation had been attempted by solvent evaporation, but remained unsuccessful.

6.3.3.2 A + Ga + GaI_3

To a brown suspension of **A** (53.8 mg, 0.049 mmol) in C_5D_5N (0.4 ml) a solution of GaI_3 (14.9 mg, 0.033 mmol) in C_5D_5N was added. To this Ga metal (1.4 mg, 0.020 mmol) was added and the mixture sonicate for 80 minutes and then left to stir at room temperature overnight to give an orange suspension. The suspension was centrifuged (2 min/6000 rpm) and the material redissolved in C_5D_5N. The ^{1}H-NMR showed the formation of multiple paramagnetic resonances, some of which could be attributed to a $[(py)_x(I_2GaOUO)(py)\ (H_2L)]$ complex. The material was split in half into two fractions. The first fraction was allowed to crystallise by solvent evaporation; the second fraction was dried under vacuum and redissolved in THF. It was not possible to isolate uniform material from these fractions.

^{1}H-NMR (C_5D_5N): -22.36 (s, 3H, C*H*$_3$), -19.91, -19.28, -15.80, -15.44, -10.11, -8.96, -6.02, -5.74, -4.54, -4.17, -1.07, -0.95, -0.81, 0.29, 0.43, 0.81, 0.82, 0.83, 1.12, 1.15, 1.17, 1.45, 1.96, 2.12, 2.13, 6.44, 10.20, 10.21, 11.91, 11.91, 17.46, 17.72, 19.59, 19.82, 23.81 (s, 3H, C*H*$_3$), 26.30, 27.00, 68.95 (br, 2H, N*H*).

6.3.3.3 A + Cp^*_2Co

To a brown suspension of **A** (50.0 mg, 0.037 mmol) in THF-d_8 (0.15 ml) a suspension of Cp^*_2Co in THF-d_8 (0.15 ml) was added and sonicated at 60 °C for 40 minutes to form a dark red-brown solution and precipitate. After centrifugation the mother liquor was analysed by ^{1}H-NMR spectroscopy and showed the formation of paramagnetic resonances. The precipitate was dissolved in pyridine-d_5 and showed the clean formation of a paramagnetic product which was assigned to a uranyl(V) Pacman complex with Co^{III} coordination. Upon crystallisation only the reformation of the starting material was observed.

^{1}H-NMR (C_5D_5N): δ_H -8.67 (s, 2H), -7.46 (s, 3H, C*H*$_3$), -4.51 (s, 2H), -2.96 (s, 2H), -2.69 (s, 6H, Ph-C*H*$_3$), 1.10 (s, 6H, Ph-C*H*$_3$), 4.84 (s, 2H), 5.15 (br, 30H, Cp*), 5.61 (br, 2H), 10.73 (s, 2H), 11.45 (s, 3H, C*H*$_3$), 14.31 (s, 2H), 35.73 (s, 3H, C*H*$_3$), 91.60 (br, 2H, N*H*)

6.3.3.4 A + Zr(II)

A mixture of brown **A** (150 mg, 0.122 mmol) and dark purple $Cp_2Zr(\eta^2\text{-}C_2(SiMe_3)_2\cdot py$ (57.4 mg, 0.122 mmol) in a Teflon-tapped ampoule was frozen in a Dewar flask filled with liquid N_2. To this mixture toluene (1.5 ml) was added slowly so that it immediately froze upon contact with the material and the glass of the ampoule. The temperature of the cold bath was slowly increased to -96 °C by careful addition of acetone. The brown suspension was allowed to stir at this temperature and allowed to warm to room temperature overnight to give a cherry-red suspension. The solvent was removed under vacuum. The ^{1}H-NMR spectrum was recorded in C_6D_6 and showed the formation of multiple paramagnetic resonances from 65 ppm to -45 ppm not attributable to a single product. No resonances of starting material **A** were observed.

6.3.3.5 A + Hf(IV) + Mg

a) equimolar: To a brown suspension of **A** (50.0 mg, 0.045 mmol) in C_5D_5N (0.4 ml) Cp_2HfCl_2 (17.0 mg, 0.045 mmol) and Mg metal (1.1 mg, 0.045 mmol) was added and the mixture was sonicated at room temperature for 2 hours with no colour change. The mixture was heated to 70 °C and sonicated for 80 minutes to give a red solution. The mixture was filtered *via* a syringe filter (0.45 μm PTFE). The ^{1}H-NMR spectrum in C_5D_5N showed the formation of paramagnetic resonances attributable to a [((Cl)Cp_2HfOUO)(py)(H_2L)] complex along with multiple resonances of inseparable side products.

b) excess Hf: To a brown suspension of **A** (73.1 mg, 0.065 mmol) in C_5H_5N (2.0 ml) Cp_2HfCl_2 (100.0 mg, 0.263 mmol) and Mg metal (1.6 mg, 0.065 mmol) was added and the

mixture was allowed to stir for six days until no Mg metal was left. The solvent was removed under vacuum and the dried material extracted with C_6D_6 to give an orange solution. The ^{1}H-NMR spectrum showed resonances attributable to a [((Cl)Cp_2HfOUO)(py)(H_2L)] complex. The solvent was removed and the material redissolved in C_4H_8O. Residual oxygen in the solvent resulted in the slow disintegration of the material to uranyl(VI) Pacman **A** and μ-oxo-bis(chlorohafnocene) (Cp_2HfCl).

^{1}H-NMR (C_6D_6, 600MHz): δ_H -6.09 (s, 3H, C*H*$_3$), -3.90 (s, 3H, C*H*$_3$), -2.44 (s, 3H, C*H*$_3$), -0.82 (s, 6H, Ph-C*H*$_3$), -0.65 (s, 2H), -0.29 (s, 6H, Ph-C*H*$_3$), 0.70 (s (br), 2H, pyrrole), 1.63 (s (br), 2H, pyrrole), 2.65 (s, 2H), 4.06 (s, 2H), 4.32 (s, 2H), 10.19 (s, 2H, pyrrole), 11.56 (s, 2H, pyrrole), 14.97 (s, 10H, C_5*H*$_5$), 16.87 (s, 3H, C*H*$_3$), 61.53 (br, 2H, N*H*);

6.3.3.6 A + Mg

To a brown suspension of **A** (84.0 mg, 0.074 mmol) in C_5H_5N (2 ml) Mg metal (0.89 mg, 0.037 mmol) was added and the mixture was allowed to stir for 24 hours at room temperature to form an orange-red suspension. The suspension was filtered and the ^{1}H-NMR spectrum. The spectrum showed the formation of paramagnetic resonances which can be attributed to a uranyl(V) complex. Any attempts to isolate this complex have failed. The solvent of the filtered solution was removed under vacuum to yield a thick red viscous material. Recrystallisation had been attempted by cooling to -35 ºC and hexane diffusion, but failed to give any isolable material.

^{1}H-NMR (C_5D_5N): δ_H -6.91 (s, 2H), -3.10 (s, 6H, Ph-C*H*$_3$), -2.34 (s, 3H, C*H*$_3$), -1.50 (s, 2H), -0.46 (s, 2H), 0.76 (s, 6H, Ph-C*H*$_3$), 1.83 (s, 3H, C*H*$_3$), 6.25 (s, 2H), 8.43 (s, 2H), 10.72 (s, 2H), 10.98 (s, 3H, C*H*$_3$), 14.06 (s, 2H), 31.64 (s, 3H, C*H*$_3$), 88.16 (br, 2H, N*H*)

6.3.3.7 A + Fe + $FeBr_2$

To a mixture of **A** (75.0 mg, 67.5 μmol) and $FeBr_2$ (7.3 mg, 33.7 μmol) in C_5D_5N (0.3 ml) Fe (1.9 mg, 33.7 μmol) was added and the suspension allowed to stir for 72 hours at 80 °C. The ^{1}H-NMR spectrum was recorded and showed only the resonances of **A**.

6.3.3.8 A + Ni + $NiCl_2$

To a mixture of **A** (48.0 mg, 43.2 μmol) and $NiCl_2$ (5.6 mg, 43.2 μmol) in C_5D_5N (0.3 ml) a Ni grain (excess) was added and the suspension allowed to stir for 72 hours at 80 °C. The ^{1}H-NMR spectrum was recorded and showed only the resonances of **A**.

6.3.3.9 A + Zn + $FeBr_2$

To a mixture of **A** (75.0 mg, 67.5 μmol) and $FeBr_2$ (7.3 mg, 33.7 μmol) in C_5D_5N (0.3 ml) Fe a Zn grain was added and the suspension allowed to stir for 72 hours at 80 °C. The ^{1}H-NMR spectrum was recorded and showed the formation of multiple paramagnetic resonances that could not be assigned to a single product.

6.3.3.10 A + Zn + $NiCl_2$

To a mixture of **A** (48.0 mg, 43.2 μmol) and $NiCl_2$ (5.6 mg, 43.2 μmol) in THF-d_8 (0.3 ml) a Zn grain (excess) was added and the suspension allowed to stir for 14 days at 80 °C. The ^{1}H-NMR spectrum was recorded and showed paramagnetically shifted resonances attributable to a uranyl(V) Pacman complex. Recrystallisation was attempted from a concentrated THF solution, but no defined material could be isolated.

6.3.4 Unsuccessful functionalisation of A^{Et} using $Cp_3{}^{239}Pu$

Olive green $\mathbf{A^{Et}}$ (49.3 mg, 45.9 μmol) and dark green $Cp_3{}^{239}Pu$ (23.2 mg, 45.9 μmol) were mixed and cooled with solid dry ice pellets. To this mixture THF-d_8 (4 ml) was added and the mixture was allowed to stir and warm to room temperature, without any colour change. The material was dried and attempted to be recrystallised from thf solution by hexane diffusion but no product could be isolated.

6.3.5 Further reductive metalations of $[UO_2(Cl)(L)]$ 21

6.3.5.1 Treatment of 21 with Me_3SiX (X = Cl, I)

Chlorotrimethylsilane (TMSCl) (0.01 ml, 0.076 mmol) was added dropwise to a blue solution of **21** (30.0mg, 0.038 mmol) in benzene (1.0 ml) in a Teflon-tapped NMR tube and the mixture was allowed to stir at room temperature for 2 hours and no colour change was observed. The mixture was subsequently heated for 12 hours at 90 °C. Paramagnetically shifted resonances in the ^{1}H-NMR in the range of δ_H 0 – 20 ppm indicated the slow formation of a reduced uranyl species. Excess iodotrimethylsilane (TMSI) was added dropwise to the mixture and an instant colour change was observed from blue to green. The ^{1}H-NMR spectrum showed paramagnetic resonances in the range of δ_H -25 to 50 ppm. ^{29}Si-NMR showed the

formation of two new Si resonances which were attributed to the doubly silylated uranyl moiety. From the oily green reaction mixture no isolable material could be obtained.

^{1}H-NMR (C_6D_6, 500 MHz), δ_H -18.04 (s, 18H), 0.07 (s, 0.5H), 0.14 (s, 6H), 0.16 (s, 1H), 0.19 (s, 1H), 0.24 (s, 0.5H), 0.31 (s, 2.5H), 0.61 (d, 1H), 2.17 (s, 6H), 4.03 (s, 1H), 53.98 (s, 9H). ^{19}F-NMR (C_6D_6, 500 MHz): δ_F, -160.07, -147.59, -140.53. ^{29}Si-NMR (C_6D_6, 500 MHz): δ_{Si} -21.85, 7.11.

6.3.5.2 Treatment of 21 with K

Metallic K (3.6 mg, 0.092 mmol) was added to a blue solution of **21** (36.0 mg, 0.046 mmol) in pyridine (1.0 ml) in a Teflon-tapped NMR tube. The mixture was allowed to react at room temperature under stirring for 24 hours. The ^{1}H-NMR spectrum of the reaction showed an unidentifiable mixture of products with paramagnetic resonances in the range of δ_H -50 – 50 ppm.

^{1}H-NMR (C_5D_5N): δ_H -49.24, -45.72, -21.81, -20.95, -10.47, -2.78, 0.12, 2.12, 38.54, 50.04

6.4 Crystallographic Data summary tables

	Crystal data		
Compound	**[(py)(Me$_2$AlOUO)(py)(H$_2$L)] 1**	**[(py){(*i*-Bu)$_2$AlOUO}(thf)(H$_2$L)] 2**	**[{(UO$_2$)Li(py)(H$_2$L)}$_2$] 3**
Chemical formula	$C_{93}H_{97}AlN_{10}O_2U$	$C_{74}H_{88}AlN_9O_3U$	$C_{124}H_{124}Li_2N_{18}O_4U_2$
MW	1651.82	1416.54	2420.35
Crystal system, space group	monoclinic, *P* 2$_1$/*c*	monoclinic, *P*2$_1$/*n*	triclinic, *P*-1
Temperature (K)	120	120	170
a, *b*, *c* (Å)	21.6483(2), 15.4318(2), 24.4807(2)	12.5004 (2), 40.0423 (6), 14.2199 (2)	11.963(5), 14.243(5), 17.926(5)
α, *β*, *γ* (º)	90.00, 98.4807, 90.00	90.00, 105.173 (2), 90.00	99.705(5), 90.311(5), 114.231
V (Å^3)	8086.50(14)	6869.57 (18)	2736.0(17)
Z	4	4	1
Radiation type	Cu *K*α	Mo *K*α	Mo *K*α
μ (mm^{-1})	6.182	2.43	3.019
Crystal size (mm)	0.1794 × 0.0864 × 0.167	0.30 × 0.12 × 0.09	0.3746 × 0.1856 × 0.1567
	Data collection		
Diffractometer	SuperNova, Dual, Cu at zero, Atlas	SuperNova, Dual, Cu at zero, Atlas	Xcalibur, Eos
Absorption correction	Gaussian	Gaussian	multi-scan
T_{min}, T_{max}	0.481, 0.895	0.648, 0.826	0.851, 1.000
No. of measured, independent and observed [$I > 2\sigma(I)$] reflections	96487, 16582, 13507	140222, 17029, 14619	21299, 21299, 16404
R_{int}	0.0700	0.079	0.0000
$(sin\ \theta/\lambda)_{max}$ (Å^{-1})	0.630	0.667	0.650
	Refinement		
$R[F^2 > 2\sigma(F^2)]$, $wR(F^2)$, S	0.039, 0.103, 1.03	0.046, 0.109, 0.95	0.040, 0.096, 1.05
No. of reflections	16582	17029	21299
No. of parameters	980	812	661

No. of restraints	0	87	0
H-atom treatment	mixed	mixed	constrained
$\Delta\rho_{max},\Delta\rho_{min}$(e Å^{-3})	2.17, -2.92	1.96, −2.22	4.26, -2.06

	Crystal data		
Compound	**[(py)$_3$(LiOUO)(py)(H$_2$L)] 4**	**[(py)$_3$(NaOUO)(py)(H$_2$L)] 5**	**[(py)$_3$(KOUO)(py)(H$_2$L)] 6**
Chemical formula	$C_{84.39}H_{84.39}Li_{0.87}N_{16.48}O_2U$	$C_{62}H_{62}N_{12}NaO_2U$	$C_{77}H_{76}KN_{15}O_2U$
MW	1606.79	1268.26	1520.66
Crystal system, space group	monoclinic, *Cc*	monoclinic, *Cc*	orthorhombic, P 2_1 2_1 2_1
Temperature (K)	170	170	170
a, *b*, *c* (Å)	14.7282 (5), 24.4176 (6), 22.8717 (7)	14.427 (5), 24.602 (5), 23.182 (5)	13.6930(3), 21.7419(5), 24.2382(4)
α, *β*, *γ* (º)	90.00, 90.634 (3), 90.00	90.00, 90.881 (5), 90.00	90.00, 90.00, 90.00
V (Å^3)	7973.5(4)	8227 (4)	7216.0(3)
Z	4	4	4
Radiation type	Mo *K*α	Mo *K*α	Mo *K*α
μ (mm^{-1})	2.09	2.02	2.364
Crystal size (mm)	0.92 × 0.58 × 0.35	0.93 × 0.40 × 0.23	1.2244 × 0.6915 × 0.4865
	Data collection		
Diffractometer	Xcalibur, Eos	Xcalibur, Eos	Xcalibur, Eos
Absorption correction	multi-scan	multi-scan	multi-scan
T_{min}, T_{max}	0.464, 1.000	0.530, 1.000	0.571, 1.000
No. of measured, independent and observed [$I > 2\sigma(I)$] reflections	41408, 18020, 14162	37697, 17997, 13051	46333, 16376, 14702
R_{int}	0.058	0.048	0.036
$(\sin\theta/\lambda)_{max}$ (Å^{-1})	0.649	0.649	0.649
	Refinement		
$R[F^2 > 2\sigma(F^2)]$, $wR(F^2)$, S	0.051, 0.103, 1.00	0.065, 0.170, 0.96	0.032, 0.076, 0.72

No. of reflections	18020	17997	16376
No. of parameters	960	581	874
No. of restraints	76	8	48
H-atom treatment	constrained	mixed	constrained
$\Delta\rho_{max}$, $\Delta\rho_{min}$ (e Å^{-3})	1.25, -0.68	4.51, −0.92	1.04, -0.95

	Crystal data		
Compound	**[(py)$_3$(RbOUO)(py)(H$_2$L)] 7**	**[(CsOUO)(py)(H$_2$L)]$_6$ 8**	**[(py)(Cp$_2$TiOUO)(py)(H$_2$L)] 9**
Chemical formula	$C_{62}H_{62}N_{12}O_2RbU\cdot3(C_5H_5N)$	$C_{282}H_{282}Cs_6N_{54}O_{12}U_6\cdot6(C_5H_5N)$	$C_{80}H_{80}N_{13}O_2TiU$
MW	1586.03	7319.84	1541.50
Crystal system, space group	Orthorhombic, $P2_12_12_1$	Trigonal, *R*-3	Triclinic, *P*-1
Temperature (K)	170	120	170
a, *b*, *c* (Å)	13.6821 (2), 21.8875 (3), 24.2440 (3)	27.7671 (4), 27.7671 (4) 35.7644 (5)	14.017 (5), 15.236 (5), 17.911 (5)
α, *β*, *γ* (º)	90.00, 90.00, 90.00	90.00, 90.00, 120.00	87.225 (5), 69.531 (5), 77.365 (5)
V (Å^3)	7260.27 (18)	23880.5 (8)	3495 (2)
Z	4	3	2
Radiation type	Mo *K*α	Cu *K*α	Mo *K*α
μ (mm^{-1})	2.09	14.25	2.49
Crystal size (mm)	1.26 × 0.86 × 0.52	0.05 × 0.04 × 0.03	0.12 × 0.11 × 0.07
	Data collection		
Diffractometer	Xcalibur, Eos	SuperNova, Dual, Cu at zero, Atlas	Xcalibur, Eos
Absorption correction	analytical	gaussian	multi-scan
T_{min}, T_{max}	0.425, 0.681	0.992, 0.995	0.926, 1.000
No. of measured, independent and observed [$I > 2\sigma(I)$] reflections	216174, 16642, 15775	123779, 11060, 9096	26501, 11901, 7334
R_{int}	0.076	0.096	0.122
$(\sin\theta/\lambda)_{max}$ (Å^{-1})	0.649	0.630	0.588

	Refinement		
$R[F^2 > 2\sigma(F^2)]$, $wR(F^2)$, S	0.025, 0.054, 1.05	0.066, 0.176, 1.03	0.080, 0.122, 0.99
No. of reflections	16642	11060	11901
No. of parameters	873	579	874
No. of restraints	76	21	58
H-atom treatment	constrained	constrained	mixed
$\Delta\rho_{max}$, $\Delta\rho_{min}$ (e Å^{-3})	1.24, −0.86	12.92, −1.91	0.98, −0.90

	Crystal data		
Compound	**[(Cl)(Cp$_2$TiOUO)(py)(H$_2$L)] 10**	**[(Cl)(Cp$_2$ZrOUO)(py)(H$_2$L)] 11**	**[(Cl)(Cp$_2$ZrOUO)(py)(H$_2$L)] × MgCl$_2$(py)$_4$ 11MgCl$_2$**
Chemical formula	$C_{87}H_{87}ClN_9O_2TiU$	$C_{82}H_{86}ClN_{12}O_3UZr$	$C_{86.48}H_{86.48}Cl_3MgN_{15}O_2UZr$
MW	1612.04	1652.33	1827.82
Crystal system, space group	Monoclinic, $P2_1/c$	Monoclinic, $P2_1/c$	Monoclinic, $C2/c$
Temperature (K)	120	170	170
a, b, c (Å)	20.517 (5), 21.431 (5), 19.018 (5)	20.2769 (12), 21.7767 (10), 18.5794 (11)	47.424 (5), 14.484 (5), 30.602 (5)
α, β, γ (º)	90.00, 117.115 (5), 90.00	90.00, 115.829 (7), 90.00	90.00, 127.576 (5), 90.00
V (Å^3)	7443 (3)	7384.4 (7)	16659 (7)
Z	4	4	8
Radiation type	Mo $K\alpha$	Mo $K\alpha$	Mo $K\alpha$
μ (mm^{-1})	2.37	2.43	2.23
Crystal size (mm)	0.21 × 0.10 × 0.07	0.53 × 0.23 × 0.17	0.30 × 0.06 × 0.02
	Data collection		
Diffractometer	SuperNova, Dual, Cu at zero, Atlas	Xcalibur, Eos	Xcalibur, Eos
Absorption correction	gaussian	multi-scan	Multi-scan
T_{min}, T_{max}	0.916, 0.965	0.626, 1.000	0.971, 1.000

No. of measured, independent and observed [$I > 2\sigma(I)$] reflections	156288, 18357, 15202	75846, 14015, 10516	49400, 14167, 7401
R_{int}	0.058	0.105	0.199
$(\sin\theta/\lambda)_{max}$ (Å^{-1})	0.680	0.610	0.588
	Refinement		
$R[F^2 > 2\sigma(F^2)]$, $wR(F^2)$, S	0.036, 0.080, 0.92	0.072, 0.178, 1.09	0.097, 0.203, 1.01
No. of reflections	18357	14015	14167
No. of parameters	910	901	979
No. of restraints	0	1	108
H-atom treatment	constrained	mixed	mixed
$\Delta\rho_{max}$, $\Delta\rho_{min}$ (e Å^{-3})	1.12, −0.59	5.64, −1.57	1.34, −1.08

	Crystal data		
Compound	**[(py)$_2$(ClMgOUO)(py)(H$_2$L)] 12**	**[(py)$_2$(thf)$_2$(ICaOUO)(py)(H$_2$L)] 13**	**[(py)$_2$(ClZnOUO)(py)(H$_2$L)] 14**
Chemical formula	$C_{175}H_{175}Cl_2Mg_2N_{33}O_4U_2$	$C_{65}H_{73}CaIN_{11}O_4U$	$C_{57}H_{57}ClN_{11}O_2UZn$
MW	3400.06	1477.35	1266.98
Crystal system, space group	Monoclinic, $I2/a$	Monoclinic, $P2_1/c$	Monoclinic, $I2/a$
Temperature (K)	120	170	120
a, b, c (Å)	24.852 (5), 23.010 (5), 28.754 (5)	17.4073 (7), 15.5310 (4), 33.3439 (15)	28.7327 (5), 22.9300 (3), 24.8036 (3)
α, β, γ (º)	90.00, 102.183 (5), 90.00	90.00, 114.157 (5), 90.00	90.00, 102.0775 (13), 90.00
V (Å^3)	16072 (6)	8225.2 (5)	15980.0 (4)
Z	4	4	8
Radiation type	Cu $K\alpha$	Mo $K\alpha$	Cu $K\alpha$
μ (mm^{-1})	6.53	2.45	6.62
Crystal size (mm)	0.17 × 0.04 × 0.04	0.66 × 0.54 × 0.24	0.13 × 0.08 × 0.05
	Data collection		

Diffractometer	SuperNova, Dual, Cu at zero, Atlas	Xcalibur, Eos	SuperNova, Dual, Cu at zero, Atlas
Absorption correction	gaussian	multi-scan	gaussian
T_{min}, T_{max}	0.893, 0.972	0.527, 1.000	0.889, 0.955
No. of measured, independent and observed [$I > 2\sigma(I)$] reflections	165331, 16761, 14608	130415, 11791, 10091	129575, 16675, 14839
R_{int}	0.058	0.121	0.081
$(sin\ \theta/\lambda)_{max}$ (Å^{-1})	0.630	0.555	0.630
	Refinement		
$R[F^2 > 2\sigma(F^2)]$, $wR(F^2)$, S	0.030, 0.074, 0.92	0.121, 0.282, 0.87	0.098, 0.237, 1.14
No. of reflections	16761	11791	16675
No. of parameters	984	724	660
No. of restraints	10	102	12
H-atom treatment	mixed	mixed	constrained
$\Delta\rho_{max}$, $\Delta\rho_{min}$ (e Å^{-3})	1.36, −0.96	3.22, −9.14	5.27, −3.70

	Crystal data		
Compound	**[(py)$_2$(IZnOUO)(py)(H$_2$L)] 15**	**[O=U(py)$_5$-O-Sm(I$_4$)-O-U(py)$_5$=O]$^+$ I$^-$ 16**	**[(Cp$_3$UOUO)(thf)(H$_2$L)] 17**
Chemical formula	$C_{62}H_{62}IN_{12}O_2UZn$	$C_{65}H_{65}I_5N_{13}O_4SmU_2$	$C_{77}H_{97}N_8O_6U_2$
MW	1437.54	2353.21	1706.69
Crystal system, space group	Orthorhombic, $P2_12_12_1$	Monoclinic, $P2_1/n$	Triclinic, P-1
Temperature (K)	120	170	120
a, b, c (Å)	13.2730 (1), 16.4368 (1), 27.8646 (2)	12.2775 (3), 17.1367 (3), 18.5315 (3)	12.6233 (2), 15.6060 (2), 18.6047 (2)
α, β, γ (º)	90.00, 90.00, 90.00	90.00, 104.174 (2), 90.00	93.935 (1), 100.005 (1), 105.575 (1)
V (Å^3)	6079.10 (7)	3780.25 (13)	3451.07 (8)

Z	4	2	2
Radiation type	Cu $K\alpha$	Mo $K\alpha$	Cu $K\alpha$
μ (mm^{-1})	12.32	7.13	13.57
Crystal size (mm)	0.12 × 0.06 × 0.03	0.29 × 0.26 × 0.23	0.09 × 0.08 × 0.04
	Data collection		
Diffractometer	SuperNova, Dual, Cu at zero, Atlas	Xcalibur, Eos	SuperNova, Dual, Cu at zero, Atlas
Absorption correction	multi-scan	multi-scan	gaussian
T_{min}, T_{max}	0.692, 1.000	0.638, 1.000	0.622, 0.783
No. of measured, independent and observed [$I > 2\sigma(I)$] reflections	99868, 12683, 12267	68099, 8655, 7615	85839, 14344, 13514
R_{int}	0.054	0.058	0.032
$(sin\ \theta/\lambda)_{max}$ ($Å^{-1}$)	0.631	0.649	0.630
	Refinement		
$R[F^2 > 2\sigma(F^2)]$, $wR(F^2)$, S	0.020, 0.047, 0.90	0.040, 0.075, 1.12	0.027, 0.062, 1.02
No. of reflections	12683	8655	14344
No. of parameters	720	439	867
No. of restraints	0	53	0
H-atom treatment	mixed	mixed	mixed
$\Delta\rho_{max}$, $\Delta\rho_{min}$ (e $Å^{-3}$)	0.46, −1.01	1.59, −1.46	2.83, −1.98

	Crystal data		
Compound	**[($OU^{V}O$)(py)(ZnL)] 18**	**[$Cp_3NpONp(Cp_2)ONpCp_3$] 19**	**[(Cp_3NpOUO)(thf)(H_2L)] 20**
Chemical formula	$C_{56.68}H_{55.84}N_{10.7}O_2UZn_{1.37}\cdot C_5H_6N\cdot C_5H_5N$		$C_{65}H_{73}N_8NpO_3U\cdot C_{4.46}H_{9.04}O\cdot 2(C_4H_8O)$
MW	1405.72		1712.28

Crystal system, space group	Orthorhombic, *Pnnm*	monoclinic, $P2_1/n$	Triclinic, *P*-1
Temperature (K)	170	100	100
a, *b*, *c* (Å)	19.8646 (4), 25.0270 (3), 13.5831 (5)	8.3268 27.6985 14.6706	12.6253 (15), 15.5437 (18), 18.576 (2)
α, *β*, *γ* (º)	90.00, 90.00, 90.00	90.000 90.748 90.000	93.830 (2), 100.069 (2), 105.514 (2)
V (Å^3)	6752.9 (3)	3383.34	3433.6 (7)
Z	4	4	2
Radiation type	Mo *K*α	Mo *K*α	Mo *K*α
μ (mm^{-1})	2.93		3.92
Crystal size (mm)	0.34 × 0.33 × 0.18		0.06 × 0.06 × 0.02
	Data collection		
Diffractometer	Xcalibur, Eos	Bruker APEX II Quazar diffractometer	Bruker APEX II Quazar diffractometer
Absorption correction	multi-scan		multi-scan
T_{min}, T_{max}	0.507, 1.000		0.649, 0.848
No. of measured, independent and observed [$I > 2\sigma(I)$] reflections	100156, 6461, 5694		29244, 15350, 7913
R_{int}	0.092		0.087
$(sin\ \theta/\lambda)_{max}$ (Å^{-1})	0.602		0.667
	Refinement		
$R[F^2 > 2\sigma(F^2)]$, $wR(F^2)$, *S*	0.137, 0.335, 1.21		0.068, 0.169, 0.95
No. of reflections	6461		15350
No. of parameters	419		831
No. of restraints	72		90
H-atom treatment	constrained		constrained
$\Delta\rho_{max}$, $\Delta\rho_{min}$ (e Å^{-3})	2.73, −6.28		2.77, −3.04

	Crystal data

Compound	**$[UO_2(Cl)(L^{ene})]$ 21**	**$[(Cp_2TiCl)OUO(Cp_2TiCl)(Cl)(L^{ene})]$ 22**	**$[Me_3SiOU^{III}OSiMe_3(py)(L^{ene}Ar)]$ / $[Me_3SiOU^{IV}O$-$SiMe_3(py)(L^{aneAr})]$ 23**
Chemical formula	$C_{37}H_{36}ClF_5N_4O_2U$	$C_{51}H_{50}Cl_3F_5N_4O_2Ti_2U$	$C_{53}H_{60.29}F_5N_6O_2Si_2U$
MW	937.18	1286.13	1202.57
Crystal system, space group	monoclinic, *Cc*	Monoclinic, $P2_1/c$	Triclinic, *P*-1
Temperature (K)	120	120	120
a, *b*, *c* (Å)	24.5647 (2), 8.4279 (1), 16.8859 (1)	14.486 (5), 30.377 (5), 12.092 (5)	10.9488 (3), 14.1061 (5), 18.1614 (7)
α, *β*, *γ* (º)	90.00, 91.172 (1), 90.00	90.00, 107.081 (5), 90.00	83.116 (3), 75.585 (3), 79.391 (3)
V (Å^3)	3495.14 (5)	5086 (3)	2662.11 (16)
Z	4	4	2
Radiation type	Cu *K*α	Cu *K*α	Cu *K*α
μ (mm^{-1})	14.35	13.44	9.53
Crystal size (mm)	0.11 × 0.05 × 0.04	0.12 × 0.04 × 0.02	0.09 × 0.05 × 0.03
	Data collection		
Diffractometer	SuperNova, Dual, Cu at zero, Atlas	SuperNova, Dual, Cu at zero, Atlas	SuperNova, Dual, Cu at zero, Atlas
Absorption correction	gaussian	gaussian	gaussian
T_{min}, T_{max}	0.743, 0.871	0.982, 0.996	0.722, 0.887
No. of measured, independent and observed [$I > 2\sigma(I)$] reflections	34748, 7244, 7139	75069, 9330, 7021	39293, 9731, 7223
R_{int}	0.033	0.158	0.098
$(\sin\theta/\lambda)_{max}$ (Å^{-1})	0.630	0.602	0.602
	Refinement		
$R[F^2 > 2\sigma(F^2)]$, $wR(F^2)$, *S*	0.027, 0.068, 1.04	0.056, 0.112, 1.06	0.043, 0.083, 0.97
No. of reflections	7244	9330	9731
No. of parameters	439	601	741
No. of restraints	2	0	29
H-atom treatment	mixed	mixed	mixed
$\Delta\rho_{max}$, $\Delta\rho_{min}$ (e Å^{-3})	3.81, −0.85	0.99, −1.59	1.08, −1.67

7 References

[1] H. W. Turnbull, Ed. , *The Correspondence of Isaac Newton*, University Press, London, **1959**.

[2] A. Meinrath, P. Schneider, G. Meinrath, *J. Environ. Radioact.* **2003**, *64*, 175–193.

[3] M. Betti, *J. Environ. Radioact.* **2003**, *64*, 113–119.

[4] D. R. Kindra, W. J. Evans, *Chem. Rev.* **2014**, *114*, 8865–8882.

[5] M. B. Andrews, C. L. Cahill, *Chem. Rev.* **2012**, *113*, 1121–1136.

[6] S. V. Krivovichev, I. G. Tananaev, V. Kahlenberg, R. Kaindl, B. F. Myasoedov, *Radiochemistry* **2005**, *47*, 525–536.

[7] S. Wu, S. Wang, J. Diwu, W. Depmeier, T. Malcherek, E. V. Alekseev, T. E. Albrecht-Schmitt, *Chem. Commun.* **2012**, *48*, 3479.

[8] L. Wang, R. Zhao, Z. Gu, Y. Zhao, Z. Chai, W. Shi, *Eur. J. Inorg. Chem.* **2014**, *2014*, 1158–1164.

[9] J. A. Pool, B. L. Scott, J. L. Kiplinger, *J. Am. Chem. Soc.* **2005**, *127*, 1338–1339.

[10] R. J. Baker, *Chem. - Eur. J.* **2012**, *18*, 16258–16271.

[11] T. Inoue, M. Sakata, H. Miyashiro, T. Matsumura, A. Sasahara, N. Yoshiki, *Nucl. Technol.* **1991**, *93 (2)*, 206–220.

[12] R. C. Ewing, *Nat. Mater.* **2015**, *14*, 252–257.

[13] IAEA, *IAEA Tech. Rep. Ser. No 435* **2004**.

[14] L. H. Baetsle, *Lecture at the Workshop on "Hybrid Nuclear Systems for Energy Production", Trieste*, **2001**.

[15] International Atomic Energy Agency, *Results Coord. Res. Proj. 1998-2004 IAEA-TECDOC-1563* **2007**, 1–36.

[16] International Atomic Energy Agency, *Proc. Spec. Meet. Held Vienna 18–22 June 2001 IAEA-TECDOC-1282* **2002**, 1–132.

[17] Bureau International des Poids et Mesures, *Table of Radionuclides*, **2006**.

[18] Nuclear Energy Agency, *OECD Publ.* **2006**.

[19] A. E. V. Gorden, J. Xu, K. N. Raymond, P. Durbin, *Chem. Rev.* **2003**, *103*, 4207–4282.

[20] F. Ménétrier, D. M. Taylor, A. Comte, *Appl. Radiat. Isot.* **2008**, *66*, 632–647.

[21] Y. Wang, M. Frutschi, E. Suvorova, V. Phrommavanh, M. Descostes, A. A. A. Osman, G. Geipel, R. Bernier-Latmani, *Nat. Commun.* **2013**, *4*, 1–9.

[22] T. P. McLaughlin, S. P. Monahan, N. L. Pruvost, V. V. Frolov, B. G. Ryazanov, V. I. Sviridov, *A Review of Criticality Accidents 2000 Revision*, Los Alamos National Lab., NM (US), **2000**.

[23] M. O. Mboulou, C. Hurtgen, K. Hofkens, C. Vandecasteele, *J. Environ. Radioact.* **1998**, *39*, 231–237.

[24] W. J. F. Standring, M. Dowdall, P. Strand, *Int. J. Environ. Res. Public. Health* **2009**, *6*, 174–199.

[25] R. W. Legget, K. F. Eckerman, V. F. Khokhryakov, K. G. Suslova, M. P. Krahenbuhl, S. C. Miller, *Radiat. Res.* **2005**, *164 (2)*, 111–122.

[26] M. E. Sokolnikov, E. S. Gilbert, D. L. Preston, E. Ron, N. S. Shilnikova, V. V. Khokhryakov, E. K. Vasilenko, N. A. Koshurnikova, *Int. J. Cancer* **2008**, *123*, 905–911.

[27] P. C. Burns, R. C. Ewing, A. Navrotsky, *Science* **2012**, *335*, 1184–1188.

[28] M. R. MacDonald, M. E. Fieser, J. E. Bates, J. W. Ziller, F. Furche, W. J. Evans, *J. Am. Chem. Soc.* **2013**, *135*, 13310–13313.

[29] H. S. La Pierre, H. Kameo, D. P. Halter, F. W. Heinemann, K. Meyer, *Angew. Chem. Int. Ed.* **2014**, *53*, 7154–7157.

[30] H. S. La Pierre, A. Scheurer, F. W. Heinemann, W. Hieringer, K. Meyer, *Angew. Chem. Int. Ed.* **2014**, *53*, 7158–7162.

[31] C. D. Carmichael, N. A. Jones, P. L. Arnold, *Inorg. Chem.* **2008**, *47*, 8577–8579.

[32] E. M. Matson, W. P. Forrest, P. E. Fanwick, S. C. Bart, *Organometallics* **2013**, *32*, 1484–1492.

[33] V. Brandel, N. Dacheux, M. Genet, *J. Solid State Chem.* **1996**, *121*, 467–472.

[34] K. Kvashnina, S. Butorin, P. Martin, P. Glatzel, *Phys. Rev. Lett.* **2013**, *111*, 3002.

[35] C. R. Graves, B. L. Scott, D. E. Morris, J. L. Kiplinger, *J. Am. Chem. Soc.* **2007**, *129*, 11914–11915.

[36] O. Hollóczki, *Inorg. Chem.* **2014**, *53*, 835–846.

[37] W. R. Wadt, *J. Am. Chem. Soc.* **1981**, *103*, 6053–6057.

[38] S. Berto, F. Crea, P. G. Daniele, A. Gianguzza, A. Pettignano, S. Sammartano, *Coord. Chem. Rev.* **2012**, *256*, 63–81.

[39] P. C. Burns, *Can. Mineral.* **2005**, *43*, 1839–1894.

[40] F. H. Kruse, *Acta Crystallogr.* **1961**, *14*, 1035–1041.

[41] P. L. Arnold, J. B. Love, D. Patel, *Coord. Chem. Rev.* **2009**, *253*, 1973–1978.

[42] G. Barea, A. Lledos, F. Maseras, Jean, Yves, *Inorg. Chem.* **1998**, *37*, 3321–3325.

[43] L. O. Atovmyan, M. A. Porai-Koshits, *J. Struct. Chem.* **1969**, *10*, 740–744.

[44] J. A. Dean, N. A. Lange, *Lange's Handbook of Chemistry*, McGraw-Hill, New York, **1999**.

[45] G. Gordon, H. Taube, *J. Inorg. Nucl. Chem.* **1961**, *19*, 189–191.

[46] R. G. Denning, *J. Phys. Chem. A* **2007**, *111*, 4125–4143.

[47] V. Vallet, T. Privalov, U. Wahlgren, I. Grenthe, *J. Am. Chem. Soc.* **2004**, *126*, 7766–7767.

[48] N. N. Krot, M. S. Grigoriev, *Russ. Chem. Rev.* **2004**, *73*, 89–100.

[49] J. C. Sullivan, J. C. Hindman, A. J. Zielen, *J. Am. Chem. Soc.* **1961**, *83*, 3373–3378.

[50] T. Z. Forbes, C. Wallace, P. C. Burns, *Can. Mineral.* **2008**, *46*, 1623–1645.

[51] I. A. Charushnikova, N. N. Krot, Z. A. Starikova, *Radiochim. Acta* **2009**, *95*, 495–499.

[52] J. C. Taylor, A. Ekstrom, C. H. Randall, *Inorg. Chem.* **1978**, *17*, 3285–3289.

[53] E. V. Alekseev, S. V. Krivovichev, W. Depmeier, O. I. Siidra, K. Knorr, E. V. Suleimanov, E. V. Chuprunov, *Angew. Chem. Int. Ed.* **2006**, *45*, 7233–7235.

[54] T. A. Sullens, R. A. Jensen, T. Y. Shvareva, T. E. Albrecht-Schmitt, *J. Am. Chem. Soc.* **2004**, *126*, 2676–2677.

[55] S. Tsushima, *Dalton Trans.* **2011**, *40*, 6732.

[56] J. C. Renshaw, L. J. C. Butchins, F. R. Livens, I. May, J. M. Charnock, J. R. Lloyd, *Environ. Sci. Technol.* **2005**, *39*, 5657–5660.

[57] M. Sundararajan, R. S. Assary, I. H. Hiller, D. J. Vaughan, *Dalton Trans.* **2011**, *40*, 11156–11163.

[58] P. L. Arnold, D. Patel, C. Wilson, J. B. Love, *Nature* **2008**, *451*, 315–317.

[59] M. Zegke, G. S. Nichol, P. L. Arnold, J. B. Love, *Chem. Commun.* **2015**, *51*, 5876–5879.

[60] P. L. Arnold, E. Hollis, F. J. White, N. Magnani, R. Caciuffo, J. B. Love, *Angew. Chem. Int. Ed.* **2011**, *50*, 887–890.

[61] L. Chatelain, V. Mougel, J. Pécaut, M. Mazzanti, *Chem. Sci.* **2012**, *3*, 1075.

[62] F. Burdet, J. Pécaut, M. Mazzanti, *J. Am. Chem. Soc.* **2006**, *128*, 16512–16513.

[63] V. Mougel, P. Horeglad, G. Nocton, J. Pécaut, M. Mazzanti, *Chem. - Eur. J.* **2010**, *16*, 14365–14377.

[64] G. B. Jin, *Inorg. Chem.* **2013**, *52*, 12317–12319.

[65] R. Copping, V. Mougel, C. Den Auwer, C. Berthon, P. Moisy, M. Mazzanti, *Dalton Trans.* **2012**, *41*, 10900–10902.

[66] P. Horeglad, G. Nocton, Y. Filinchuk, J. Pécaut, M. Mazzanti, *Chem. Commun.* **2009**, 1843.

[67] E. A. Pedrick, G. Wu, T. W. Hayton, *Inorg. Chem.* **2014**, *53*, 12237–12239.

[68] D. D. Schnaars, G. Wu, T. W. Hayton, *Inorg. Chem.* **2011**, *50*, 4695–4697.

[69] G. Nocton, J. Pécaut, Y. Filinchuk, M. Mazzanti, *Chem. Commun.* **2010**, *46*, 2757.

[70] E. A. Pedrick, G. Wu, N. Kaltsoyannis, T. W. Hayton, *Chem. Sci.* **2014**, *5*, 3204–3213.

[71] J. Selbin, J. D. Ortego, *Chem. Rev.* **1969**, *69*, 657–671.

[72] K. E. Knope, L. Soderholm, *Chem. Rev.* **2013**, *113*, 944–994.

[73] G. Gritzner, J. Selbin, *J. Inorg. Nucl. Chem.* **1968**, *30*, 1799–1804.

[74] T. Yamamura, K. Shirasaki, Y. Shiokawa, Y. Nakamura, S.-Y. Kim, *J. Alloys Compd.* **2004**, *374*, 349–353.

[75] K. Shirasaki, T. Yamamura, Y. Shiokawa, *J. Alloys Compd.* **2006**, *408-412*, 1296–1301.

[76] L. R. Morss, N. M. Edelstein, J. Fuger, Springer, Dordrecht, **2008**.

[77] M. C. F. Wander, K. L. Shuford, *Geochim. Cosmochim. Acta* **2012**, *84*, 177–185.

[78] I. Grenthe, J. Fuger, R. J. M. Konings, R. J. Lemire, A. B. Nuller, C. Nguyen-Trung, H. Wanner, *Chemical Thermodynamics of Uranium*, Nuclear Energy Agency/OECD, North Holland, **1992**.

[79] H. Steele, R. J. Taylor, *Inorg. Chem.* **2007**, *46*, 6311–6318.

[80] M. Bühl, G. Schreckenbach, *Inorg. Chem.* **2010**, *49*, 3821–3827.

[81] Z. Szabó, I. Grenthe, *Inorg. Chem.* **2010**, *49*, 4928–4933.

[82] V. Mougel, B. Biswas, J. Pécaut, M. Mazzanti, *Chem. Commun.* **2010**, *46*, 8648–8650.

[83] K. Takao, M. Kato, S. Takao, A. Nagasawa, A. C. Scheinost, G. Bernhard, C. Hennig, Y. Ikeda, *IOP Conf. Ser. Mater. Sci. Eng.* **2010**, *9*, 1–8.

[84] P. C. Burns, R. J. Finch, F. C. Hawthorne, M. L. Miller, R. C. Ewing, *J. Nucl. Mater.* **1997**, *249*, 199–206.

[85] A. L. Klingensmith, K. M. Deely, W. S. Kinman, V. Kelly, P. C. Burns, *Am. Mineral.* **2007**, *92*, 662–669.

[86] A. L. Klingensmith, P. C. Burns, *Am. Mineral.* **2007**, *92*, 1946–1951.

[87] P. C. Burns, R. J. Finch, *Am. Mineral.* **1999**, *84*, 1456–1460.

[88] F. C. Hawthorne, R. J. Finch, R. C. Ewing, *Can. Mineral.* **2006**, *44*, 1379–1385.

[89] J. R. Clark, **1960**, *45*, 200–208.

[90] K. Mizuoka, Y. Ikeda, *Inorg. Chem.* **2003**, *42*, 3396–3398.

[91] F. Quilès, A. Burneau, *Vib. Spectrosc.* **2000**, *23*, 231–241.

[92] J.-C. Berthet, M. Nierlich, M. Ephritikhine, *Angew. Chem. Int. Ed.* **2003**, *42*, 1952–1954.

[93] M. Ephritikhine, *Dalton Trans.* **2006**, 2501.

[94] J.-C. Berthet, G. Siffredi, P. Thuéry, M. Ephritikhine, *Chem. Commun.* **2006**, 3184–3186.

[95] L. Natrajan, F. Burdet, J. Pécaut, M. Mazzanti, *J. Am. Chem. Soc.* **2006**, *128*, 7152–7153.

[96] M. J. Sarsfield, M. Helliwell, *J. Am. Chem. Soc.* **2004**, *126*, 1036–1037.

[97] V. Mougel, J. Pécaut, M. Mazzanti, *Chem. Commun.* **2012**, *48*, 868.

[98] R. A. Layfield, *Organometallics* **2014**, *33*, 1084–1099.

[99] V. Mougel, L. Chatelain, J. Pécaut, R. Caciuffo, E. Colineau, J.-C. Griveau, M. Mazzanti, *Nat. Chem.* **2012**, *4*, 1011–1017.

[100] P. L. Arnold, A.-F. Pécharman, R. M. Lord, G. M. Jones, E. Hollis, G. S. Nichol, L. Maron, J. Fang, T. Davin, J. B. Love, *Inorg. Chem.* **2015**, *54*, 3702–3710.

[101] G. M. Jones, P. L. Arnold, J. B. Love, *Angew. Chem. Int. Ed.* **2012**, *51*, 12584–12587.

[102] P. L. Arnold, G. M. Jones, S. O. Odoh, G. Schreckenbach, N. Magnani, J. B. Love, *Nat. Chem.* **2012**, *4*, 221–227.

[103] G. Schreckenbach, P. J. Hay, R. L. Martin, *Inorg. Chem.* **1998**, *37*, 4442–4451.

[104] J. L. Brown, G. Wu, T. W. Hayton, *J. Am. Chem. Soc.* **2010**, *132*, 7248–7249.

[105] J.-C. Berthet, G. Siffredi, P. Thuéry, M. Ephritikhine, *Eur. J. Inorg. Chem.* **2007**, *2007*, 4017–4020.

[106] J.-M. Hur, S.-S. Hong, H. Lee, *J. Radioanal. Nucl. Chem.* **2010**, *284*, 7–11.

[107] E. Péligot, *J. Für Prakt. Chem.* **1841**, *24*, 442–451.

[108] R. D. Rieke, L. D. Rhyne, *J. Org. Chem.* **1979**, *44*, 3445–3446.

[109] T. Schleid, G. Meyer, L. R. Morss, *J. Common Met.* **1987**, *132*, 69–77.

[110] Bureau International des Poids et Mesures, *Table of Radionuclides*, **2006**.

[111] S. Wang, E. V. Alekseev, H. M. Miller, W. Depmeier, T. E. Albrecht-Schmitt, *Inorg. Chem.* **2010**, *49*, 9755–9757.

[112] P. C. Burns, A. L. Klingensmith, *Elements* **2006**, *2*, 351–356.

[113] B. Vlaisavljevich, P. Miró, D. Ma, G. E. Sigmon, P. C. Burns, C. J. Cramer, L. Gagliardi, *Chem. - Eur. J.* **2013**, *19*, 2937–2941.

[114] M. B. Jones, A. J. Gaunt, *Chem. Rev.* **2013**, *113*, 1137–1198.

[115] F. P. Brauer, R. W. Stromatt, J. D. Ludwick, F. P. Roberts, W. L. Lyon, *J. Inorg. Nucl. Chem.* **1960**, *12*, 234–235.

[116] A. C. Bean, B. L. Scott, T. E. Albrecht-Schmitt, W. Runde, *Inorg. Chem.* **2003**, *42*, 5632–5636.

[117] A.-G. D. Nelson, T. H. Bray, F. A. Stanley, T. E. Albrecht-Schmitt, *Inorg. Chem.* **2009**, *48*, 4530–4535.

[118] A.-G. D. Nelson, T. H. Bray, W. Zhan, R. G. Haire, T. S. Sayler, T. E. Albrecht-Schmitt, *Inorg. Chem.* **2008**, *47*, 4945–4951.

[119] M. Marquardt, "Californium May Show New Way to Recycle Radioactive Waste, Materials Research Society, 01.04.2014," can be found under http://www.materials360online.com/newsDetails/45412, **2014**.

[120] J. Ibers, *Nat. Chem.* **2010**, *2*, 996.

[121] G. A. Icopini, H. Boukhalfa, M. P. Neu, *Environ. Sci. Technol.* **2007**, *41*, 2764–2769.

[122] G. Givaja, A. J. Blake, C. Wilson, M. Schröder, J. B. Love, *Chem. Commun.* **2003**, 2508.

[123] J. L. Sessler, W.-S. Cho, S. P. Dudek, L. Hicks, V. M. Lynch, M. T. Huggins, *J. Porphyr. Phthalocyanines* **2003**, *01*, 97–104.

[124] J. B. Love, *Chem. Commun.* **2009**, 3154.

[125] P. L. Arnold, A. J. Blake, C. Wilson, J. B. Love, *Inorg. Chem.* **2004**, *43*, 8206–8208.

[126] J. W. Leeland, A. M. Z. Slawin, J. B. Love, *Organometallics* **2010**, *29*, 714–716.

[127] S. O. Odoh, G. Schreckenbach, *Inorg. Chem.* **2013**, *52*, 245–257.

[128] P. L. Arnold, A.-F. Pécharman, E. Hollis, A. Yahia, L. Maron, S. Parsons, J. B. Love, *Nat. Chem.* **2010**, *2*, 1056–1061.

[129] W. J. Evans, *J. Organomet. Chem.* **2002**, *647*, 2–11.

[130] T. S. Franczyk, K. R. Czerwinski, K. N. Raymond, *J. Am. Chem. Soc.* **1992**, *114*, 8138–8146.

[131] J. W. Leeland, F. J. White, J. B. Love, *J. Am. Chem. Soc.* **2011**, *133*, 7320–7323.

[132] G. Givaja, M. Volpe, J. W. Leeland, M. A. Edwards, T. K. Young, S. B. Darby, S. D. Reid, A. J. Blake, C. Wilson, J. Wolowska, et al., *Chem. - Eur. J.* **2007**, *13*, 3707–3723.

[133] P. L. Arnold, G. M. Jones, Q.-J. Pan, G. Schreckenbach, J. B. Love, *Dalton Trans.* **2012**, *41*, 6595–6597.

[134] P. L. Arnold, A.-F. Pécharman, J. B. Love, *Angew. Chem. Int. Ed.* **2011**, *50*, 9456–9458.

[135] P. L. Arnold, E. Hollis, G. S. Nichol, J. B. Love, J.-C. Griveau, R. Caciuffo, N. Magnani, L. Maron, L. Castro, A. Yahia, et al., *J. Am. Chem. Soc.* **2013**, *135*, 3841–3854.

[136] R. D. Shannon, *Acta Crystallogr. A* **1976**, *32*, 751–767.

[137] N. G. Connelly, W. E. Geiger, *Chem. Rev.* **1996**, *96*, 877–910.

[138] G. Nocton, P. Horeglad, V. Vetere, J. Pécaut, L. Dubois, P. Maldivi, N. M. Edelstein, M. Mazzanti, *J. Am. Chem. Soc.* **2010**, *132*, 495–508.

[139] K. Takao, M. Kato, S. Takao, A. Nagasawa, G. Bernhard, C. Hennig, Y. Ikeda, *Inorg. Chem.* **2010**, *49*, 2349–2359.

[140] K. Takao, S. Tsushima, T. Ogura, T. Tsubomura, Y. Ikeda, *Inorg. Chem.* **2014**, *53*, 5772–5780.

[141] J. L. Brown, C. C. Mokhtarzadeh, J. M. Lever, G. Wu, T. W. Hayton, *Inorg. Chem.* **2011**, *50*, 5105–5112.

[142] T. W. Hayton, G. Wu, *Inorg. Chem.* **2009**, *48*, 3065–3072.

[143] J. T. Spletstoser, J. M. White, A. R. Tunoori, G. I. Georg, *J. Am. Chem. Soc.* **2007**, *129*, 3408–3419.

[144] D. D. Schnaars, G. Wu, T. W. Hayton, *Inorg. Chem.* **2011**, *50*, 9642–9649.

[145] S. V. Krivovichev, V. Kahlenberg, *Z. Für Anorg. Allg. Chem.* **2005**, *631*, 739–744.

[146] S. V. Krivovichev, P. C. Burns, *J. Solid State Chem.* **2002**, *168*, 245–258.

[147] S. Wang, E. V. Alekseev, J. T. Stritzinger, W. Depmeier, T. E. Albrecht-Schmitt, *Inorg. Chem.* **2010**, *49*, 6690–6696.

[148] C. J. Pedersen, *J. Am. Chem. Soc.* **1967**, *89*, 7017–7036.

[149] J. D. Dunitz, P. Seiler, *Acta Crystallogr. Sect. B* **1974**, *30*, 2739–2741.

[150] J.-M. Lehn, *Angew. Chem. Int. Ed.* **1988**, *27*, 89–112.

[151] H. W. Kroto, J. R. Heath, S. C. O'Brien, R. F. Curl, R. E. Smalley, *Nature* **1985**, *318*, 162–163.

[152] A. R. Kennedy, J. G. MacLellan, R. E. Mulvey, *Acta Crystallogr. C* **2003**, *59*, m302–m303.

[153] D. V. Graham, A. R. Kennedy, R. E. Mulvey, C. T. O'Hara, *Acta Crystallogr. C* **2006**, *62*, m366–m368.

[154] A. R. Kennedy, J. Klett, R. E. Mulvey, S. Newton, D. S. Wright, *Chem. Commun.* **2008**, 308–310.

[155] M. Westerhausen, *Dalton Trans.* **2006**, 4755.

[156] D. K. Unruh, K. Gojdas, A. Libo, T. Z. Forbes, *J. Am. Chem. Soc.* **2013**, *135*, 7398–7401.

[157] G. M. Jones, Reduction and Functionalisation of Binuclear Uranium-Oxo Complexes, The University of Edinburgh, **2013**.

[158] J. T. Smith, N. A. Beresford, *Chernobyl - Catastrophe and Consequences*, Springer, Chichester, **2005**.

[159] M. P. Unterweger, *Appl. Radiat. Isot.* **2002**, *56*, 125–130.

[160] F. Brown, G. R. Hall, A. J. Walter, *J. Inorg. Nucl. Chem.* **1955**, *1*, 241–247.

[161] H. Nishita, D. Dixon, K. H. Larson, *Plant Soil* **1962**, *17*, 221–242.

[162] S. V. Avery, *J. Environ. Radioact.* **1996**, *30*, 139–171.

[163] P. Thuéry, B. Masci, *Dalton Trans.* **2003**, 2411–2417.

[164] B. Masci, P. Thuéry, *CrystEngComm* **2008**, *10*, 1082.

[165] J.-M. Babo, T. E. Albrecht-Schmitt, *J. Solid State Chem.* **2013**, *197*, 186–190.

[166] G. Morrison, C. M. Read, M. D. Smith, H.-C. zur Loye, *CrystEngComm* **2015**, *17*, 1968–1974.

[167] M. Haehnel, M. Ruhmann, O. Theilmann, S. Roy, T. Beweries, P. Arndt, A. Spannenberg, A. Villinger, E. D. Jemmis, A. Schulz, et al., *J. Am. Chem. Soc.* **2012**, *134*, 15979–15991.

[168] T. Beweries, V. V. Burlakov, M. A. Bach, S. Peitz, P. Arndt, W. Baumann, A. Spannenberg, U. Rosenthal, B. Pathak, E. D. Jemmis, *Angew. Chem. Int. Ed.* **2007**, *46*, 6907–6910.

[169] P.-M. Pellny, V. V. Burlakov, W. Baumann, A. Spannenberg, U. Rosenthal, *Z. Für Anorg. Allg. Chem.* **1999**, *625*, 910–918.

[170] Q. Ren, Z. Chen, J. Ren, H. Wei, W. Feng, L. Zhang, *J. Phys. Chem. A* **2002**, *106*, 6161–6166.

[171] D. D. Schnaars, G. Wu, T. W. Hayton, *J. Am. Chem. Soc.* **2009**, *131*, 17532–17533.

[172] J. E. McMurry, M. P. Fleming, *J. Am. Chem. Soc.* **1974**, *96*, 4708–4709.

[173] X.-F. Duan, J. Zeng, J.-W. Lü, Z.-B. Zhang, *J. Org. Chem.* **2006**, *71*, 9873–9876.

[174] M. Feurer, G. Frey, H.-T. Luu, D. Kratzert, J. Streuff, *Chem. Commun.* **2014**, *50*, 5370–5372.

[175] G. Frey, H.-T. Luu, P. Bichovski, M. Feurer, J. Streuff, *Angew. Chem. Int. Ed.* **2013**, *52*, 7131–7134.

[176] J. Li, C. Schulzke, S. Merkel, H. W. Roesky, P. P. Samuel, A. Döring, D. Stalke, *Z. Für Anorg. Allg. Chem.* **2010**, *636*, 511–514.

[177] Y. A. Min'ko, N. V. Belina, V. V. Sushev, G. K. Fukin, M. P. Bubnov, A. N. Kornev, *J. Organomet. Chem.* **2007**, *692*, 4157–4160.

[178] Z. E. Button, F. G. N. Cloke, N. A. Morley-Smith, M. P. Coles, P. B. Hitchcock, *J. Organomet. Chem.* **2010**, *695*, 2809–2813.

[179] G. Fochi, G. Guidi, C. Floriani, *J. Chem. Soc. Dalton Trans.* **1984**, 1253–1256.

[180] H. Helten, B. Dutta, J. R. Vance, M. E. Sloan, M. F. Haddow, S. Sproules, D. Collison, G. R. Whittell, G. C. Lloyd-Jones, I. Manners, *Angew. Chem. Int. Ed.* **2013**, *52*, 437–440.

[181] M. D. Fryzuk, L. Jafarpour, S. J. Rettig, *Organometallics* **1999**, *18*, 4050–4058.

[182] B. Honold, U. Thewalt, M. Herberhold, H. G. Alt, L. B. Kool, M. D. Rausch, *J. Organomet. Chem.* **1986**, *314*, 105–111.

[183] M. R. Smith III, P. T. Matsunaga, R. A. Andersen, *J. Am. Chem. Soc.* **1993**, *115*, 7049–7050.

[184] R. F. W. Bader, *Chem. Rev.* **1991**, *91*, 893–928.

[185] R. F. W. Bader, *Monatshefte Für Chem. - Chem. Mon.* **2005**, *136*, 819–854.

[186] Q.-R. Huang, J. R. Kingham, N. Kaltsoyannis, *Dalton Trans* **2015**, *44*, 2554–2566.

[187] N. Kaltsoyannis, *Inorg. Chem.* **2013**, *52*, 3407–3413.

[188] L. Petit, L. Joubert, P. Maldivi, C. Adamo, *J. Am. Chem. Soc.* **2006**, *128*, 2190–2191.

[189] D. Kratzert, D. Leusser, J. J. Holstein, B. Dittrich, K. Abersfelder, D. Scheschkewitz, D. Stalke, *Angew. Chem. Int. Ed.* **2013**, *52*, 4478–4482.

[190] B. Niepötter, R. Herbst-Irmer, D. Kratzert, P. P. Samuel, K. C. Mondal, H. W. Roesky, P. Jerabek, G. Frenking, D. Stalke, *Angew. Chem. Int. Ed.* **2014**, *53*, 2766–2770.

[191] F. L. Hirshfeld, *Theor. Chim. Acta* **1977**, *44*, 129–138.

[192] R. S. Mulliken, *J. Chem. Phys.* **1955**, *23*, 1833.

[193] A. J. Bridgeman, G. Cavigliasso, L. R. Ireland, J. Rothery, *J. Chem. Soc. Dalton Trans.* **2001**, 2095–2108.

[194] K. B. Wiberg, *Tetrahedron* **1968**, *24*, 1083–1096.

[195] I. Mayer, *Chem. Phys. Lett.* **1983**, *97*, 270–274.

[196] T. Steiner, *Angew. Chem. Int. Ed.* **2002**, *41*, 48–76.

[197] P. L. A. Popelier, *J. Phys. Chem. A* **1998**, *102*, 1873–1878.

[198] U. Koch, P. L. A. Popelier, *J. Phys. Chem.* **1995**, *99*, 9747–9754.

[199] W. H. Bernskoetter, A. V. Olmos, J. A. Pool, E. Lobkovsky, P. J. Chirik, *J. Am. Chem. Soc.* **2006**, *128*, 10696–10697.

[200] W. H. Bernskoetter, E. Lobkovsky, P. J. Chirik, *Angew. Chem. Int. Ed.* **2007**, *46*, 2858–2861.

[201] T. Beweries, V. V. Burlakov, S. Peitz, P. Arndt, W. Baumann, A. Spannenberg, U. Rosenthal, *Organometallics* **2008**, *27*, 3954–3959.

[202] M. T. Rodgers, J. R. Stanley, R. Amunugama, *J. Am. Chem. Soc.* **2000**, *122*, 10969–10978.

[203] A. J. Locock, P. C. Burns, T. M. Flynn, *Can. Mineral.* **2004**, *42*, 1699–1718.

[204] P. G. Jasien, C. E. Dykstra, *J. Am. Chem. Soc.* **1983**, *105*, 2089–2090.

[205] V. Grignard, *Comptes Rendus Hebd. Séances Académie Sci.* **1900**, *C*, 1322–1324.

[206] W. Schlenk, W. Schlenk jun., *Berichte Dtsch. Chem. Ges.* **1929**, *62*, 920–924.

[207] S. P. Green, C. Jones, A. Stasch, *Science* **2007**, *318*, 1754–1757.

[208] S. J. Bonyhady, S. P. Green, C. Jones, S. Nembenna, A. Stasch, *Angew. Chem. Int. Ed.* **2009**, *48*, 2973–2977.

[209] S. J. Bonyhady, D. Collis, G. Frenking, N. Holzmann, C. Jones, A. Stasch, *Nat. Chem.* **2010**, *2*, 856–869.

[210] J. Tammiku-Taul, P. Burk, A. Tuulmets, *J. Phys. Chem. A* **2004**, *108*, 133–139.

[211] A. V. Barinova, R. K. Rastsvetaeva, G. A. Sidorenko, D. Y. Pushcharovsky, *Dokl. Chem.* **2001**, *378*, 122–124.

[212] A. V. Barinova, R. K. Rastsvetaeva, G. A. Sidorenko, I. A. Verin, *Crystallogr. Rep.* **2003**, *48*, 12–15.

[213] M. Salvatores, G. Palmiotti, *Prog. Part. Nucl. Phys.* **2011**, *66*, 144–166.

[214] D. M. Whittaker, T. L. Griffiths, M. Helliwell, A. N. Swinburne, L. S. Natrajan, F. W. Lewis, L. M. Harwood, S. A. Parry, C. A. Sharrad, *Inorg. Chem.* **2013**, *52*, 3429–3444.

[215] S. Trumm, A. Geist, P. J. Panak, T. Fanghänel, *Solvent Extr. Ion Exch.* **2011**, *29*, 213–229.

[216] A. Geist, C. Hill, G. Modolo, M. R. S. J. Foreman, M. Weigl, K. Gompper, M. J. Hudson, *Solvent Extr. Ion Exch.* **2006**, *24*, 463–483.

[217] J. C. Braley, T. S. Grimes, K. L. Nash, *Ind. Eng. Chem. Res.* **2012**, *51*, 629–638.

[218] T. S. Grimes, R. D. Tillotson, L. R. Martin, *Solvent Extr. Ion Exch.* **2014**, *32*, 378–390.

[219] K. L. Nash, *Solvent Extr. Ion Exch.* **2015**, *33*, 1–55.

[220] B. J. Mincher, N. C. Schmitt, M. E. Case, *Solvent Extr. Ion Exch.* **2011**, *29*, 247–259.

[221] J. D. Rinehart, J. R. Long, *Chem. Sci.* **2011**, *2*, 2078.

[222] F. Neese, D. A. Pantazis, *Faraday Discuss* **2011**, *148*, 229–238.

[223] N. Giménez-Agulló, C. S. de Pipaón, L. Adriaenssens, M. Filibian, M. Martínez-Belmonte, E. C. Escudero-Adán, P. Carretta, P. Ballester, J. R. Galán-Mascarós, *Chem. - Eur. J.* **2014**, *20*, 12817–12825.

[224] J.-C. Berthet, G. Siffredi, P. Thuéry, M. Ephritikhine, *Dalton Trans.* **2009**, 3478.

[225] D. Stellfeldt, D. Meyer, G. B. Deacon, *Z. Für Anorg. Allg. Chem.* **1999**, *625*, 1252–1254.

[226] W. J. Evans, I. Bloom, J. W. Grate, L. A. Hughes, W. E. Hunter, J. L. Atwood, *Inorg. Chem.* **1985**, *24*, 4620–4623.

[227] W. J. Evans, I. Bloom, W. E. Hunter, J. L. Atwood, *J. Am. Chem. Soc.* **1985**, *107*, 941–946.

[228] M. Nishiura, K. Katagiri, T. Imamoto, *Bull. Chem. Soc. Jpn.* **2001**, *74*, 1417–1424.

[229] J.-C. Berthet, M. Nierlich, M. Ephritikhine, *Chem. Commun.* **2004**, 870.

[230] L. Chatelain, J. P. S. Walsh, J. Pécaut, F. Tuna, M. Mazzanti, *Angew. Chem. Int. Ed.* **2014**, *53*, 13434–13438.

[231] L. Aboshyan-Sorgho, H. Nozary, A. Aebischer, J.-C. G. Bünzli, P.-Y. Morgantini, K. R. Kittilstved, A. Hauser, S. V. Eliseeva, S. Petoud, C. Piguet, *J. Am. Chem. Soc.* **2012**, *134*, 12675–12684.

[232] L. Salmon, P. Thuéry, M. Ephritikhine, *Dalton Trans.* **2004**, 1635–1643.

[233] L. Salmon, P. Thuéry, M. Ephritikhine, *Chem. Commun.* **2006**, 856–858.

[234] R. von Ammon, B. Kanellakopulos, *Chem. Phys. Lett.* **1968**, *2*, 513–515.

[235] L. R. Avens, S. G. Bott, D. L. Clark, A. P. Sattelberger, J. G. Watkin, B. D. Zwick, *Inorg. Chem.* **1994**, *33*, 2248–2256.

[236] S. J. Simpson, R. A. Andersen, *J. Am. Chem. Soc.* **1981**, *103*, 4063–4066.

[237] W. J. Evans, D. S. Lee, D. B. Rego, J. M. Perotti, S. A. Kozimor, E. K. Moore, J. W. Ziller, *J. Am. Chem. Soc.* **2004**, *126*, 14574–14582.

[238] A. J. Lewis, U. J. Williams, P. J. Carroll, E. J. Schelter, *Inorg. Chem.* **2013**, *52*, 7326–7328.

[239] S. J. Simpson, H. W. Turner, R. A. Andersen, *Inorg. Chem.* **1981**, *20*, 2991–2995.

[240] L. S. Natrajan, A. N. Swinburne, M. B. Andrews, S. Randall, S. L. Heath, *Coord. Chem. Rev.* **2014**, *266-267*, 171–193.

[241] R. E. Mulvey, V. L. Blair, W. Clegg, A. R. Kennedy, J. Klett, L. Russo, *Nat. Chem.* **2010**, *2*, 588–591.

[242] J. Clayden, *Nat. Chem.* **2010**, *2*, 523–524.

[243] D. J. A. De Ridder, C. Apostolidis, J. Rebizant, B. Kanellakopulos, R. Maier, *Acta Crystallogr. Sect. C* **n.d.**, *52*, 1436–1438.

[244] N. Magnani, E. Colineau, J.-C. Griveau, C. Apostolidis, O. Walter, R. Caciuffo, *Chem. Commun.* **2014**, *50*, 8171.

[245] J. W. Leeland, C. Finn, B. Escuyer, H. Kawaguchi, G. S. Nichol, A. M. Z. Slawin, J. B. Love, *Dalton Trans.* **2012**, *41*, 13815–13831.

[246] C. J. Stevens, G. S. Nichol, P. L. Arnold, J. B. Love, *Organometallics* **2013**, *32*, 6879–6882.

[247] J. Rosenthal, T. D. Luckett, J. M. Hodgkiss, D. G. Nocera, *J. Am. Chem. Soc.* **2006**, *128*, 6546–6547.

[248] G. Givaja, M. Volpe, M. A. Edwards, A. J. Blake, C. Wilson, M. Schröder, J. B. Love, *Angew. Chem. Int. Ed.* **2007**, *46*, 584–586.

[249] A. M. J. Devoille, J. B. Love, *Dalton Trans.* **2012**, *41*, 65.

[250] C. J. Chang, Z.-H. Loh, C. Shi, F. C. Anson, D. G. Nocera, *J. Am. Chem. Soc.* **2004**, *126*, 10013–10020.

[251] A. Bessette, G. S. Hanan, *Chem. Soc. Rev.* **2014**, *43*, 3342.

[252] K. Tram, H. Yan, H. A. Jenkins, S. Vassiliev, D. Bruce, *Dyes Pigments* **2009**, *82*, 392–395.

[253] S. G. Awuah, Y. You, *RSC Adv.* **2012**, *2*, 11169–11183.

[254] I. J. Arroyo, R. Hu, G. Merino, B. Z. Tang, E. Peña-Cabrera, *J. Org. Chem.* **2009**, *74*, 5719–5722.

[255] A. Loudet, K. Burgess, *Chem. Rev.* **2007**, *107*, 4891–4932.

[256] J. R. Pankhurst, T. Cadenbach, D. Betz, C. Finn, J. B. Love, *Dalton Trans.* **2015**, *44*, 2066–2070.

[257] J. L. Sessler, T. D. Mody, M. T. Dulay, R. Espinoza, V. Lynch, *Inorganica Chim. Acta* **1996**, *246*, 23–30.

[258] A. R. Van Doorn, M. Bos, S. Harkema, J. Van Eerden, W. Verboom, D. N. Reinhoudt, *J. Org. Chem.* **1991**, *56*, 2371–2380.

[259] C. R. Graves, A. E. Vaughn, E. J. Schelter, B. L. Scott, J. D. Thompson, D. E. Morris, J. L. Kiplinger, *Inorg. Chem.* **2008**, *47*, 11879–11891.

[260] D. E. Morris, R. E. Da Re, K. C. Jantunen, I. Castro-Rodriguez, J. L. Kiplinger, *Organometallics* **2004**, *23*, 5142–5153.

[261] D. P. Mills, O. J. Cooper, F. Tuna, E. J. L. McInnes, E. S. Davies, J. McMaster, F. Moro, W. Lewis, A. J. Blake, S. T. Liddle, *J. Am. Chem. Soc.* **2012**, *134*, 10047–10054.

[262] P. B. Hitchcock, M. F. Lappert, A. Singh, R. G. Taylor, D. Brown, *J. Chem. Soc. Chem. Commun.* **1983**, *10*, 561–563.

[263] S. Fortier, G. Wu, T. W. Hayton, *Dalton Trans* **2010**, *39*, 352–354.

[264] R. J. Enemærke, J. Larsen, T. Skrydstrup, K. Daasbjerg, *J. Am. Chem. Soc.* **2004**, *126*, 7853–7864.

[265] R. J. Enemærke, J. Larsen, T. Skrydstrup, K. Daasbjerg, *Organometallics* **2004**, *23*, 1866–1874.

[266] T. Rousseau, A. Cravino, T. Bura, G. Ulrich, R. Ziessel, J. Roncali, *Chem. Commun.* **2009**, 1673.

[267] T. Yogo, Y. Urano, Y. Ishitsuka, F. Maniwa, T. Nagano, *J. Am. Chem. Soc.* **2005**, *127*, 12162–12163.

[268] Y.-D. Lin, T. J. Chow, *RSC Adv.* **2013**, *3*, 17924.

[269] C. Villiers, R. Adam, M. Lance, M. Nierlich, J. Vigner, M. Ephritikhine, *J. Chem. Soc. Chem. Commun.* **1991**, 1144–1145.

[270] S. M. Mansell, N. Kaltsoyannis, P. L. Arnold, *J. Am. Chem. Soc.* **2011**, *133*, 9036–9051.

[271] J. M. Berg, D. L. Clark, J. C. Huffman, D. E. Morris, A. P. Sattelberger, W. E. Streib, W. G. Van der Sluys, J. G. Watkin, *J. Am. Chem. Soc.* **1992**, *114*, 10811–10821.

[272] I. Castro-Rodriguez, H. Nakai, P. Gantzel, L. N. Zakharov, A. L. Rheingold, K. Meyer, *J. Am. Chem. Soc.* **2003**, *125*, 15734–15735.

[273] M. Porchia, N. Brianese, U. Casellato, F. Ossola, G. Rossetto, P. Zanella, R. Graziani, *J. Chem. Soc. Dalton Trans.* **1989**, 677–681.

[274] C. Bonnier, D. D. Machin, O. Abdi, B. D. Koivisto, *Org. Biomol. Chem.* **2013**, *11*, 3756.

[275] G. M. Sheldrick, *Acta Crystallogr. A* **2008**, *64*, 112–122.

[276] A. Altomare, G. Cascarano, C. Giacovazzo, A. Guagliardi, M. C. Burla, G. Polidori, M. Camalli, *J. Appl. Crystallogr.* **1994**, *27*, 435.

[277] L. Palatinus, G. Chapuis, *J. Appl. Crystallogr.* **2007**, *40*, 786–790.

[278] L. J. Farrugia, *J. Appl. Crystallogr.* **1999**, *32*, 837–838.

[279] O. V. Dolomanov, L. J. Bourhis, R. J. Gildea, J. A. K. Howard, H. Puschmann, *J. Appl. Crystallogr.* **2009**, *42*, 339–341.

[280] J. P. Perdew, K. Burke, M. Ernzerhof, *Phys. Rev. Lett.* **1996**, *77*, 3865–3868.

[281] J. P. Perdew, K. Burke, M. Ernzerhof, *Phys. Rev. Lett.* **1997**, *78*, 1396.

[282] D. N. Laikov, *Chem. Phys. Lett.* **1997**, *281*, 151–156.

[283] D. N. Laikov, Y. A. Ustynyuk, *Russ. Chem. Bull. Int. Ed.* **2005**, *54*, 820–826.

[284] K. G. Dyall, *J. Chem. Phys.* **1994**, *100*, 2118.

[285] T. Lu, F. Chen, *J. Comput. Chem.* **2012**, *33*, 580–592.

[286] E. D. Glendening, J. K. Badenhoop, A. E. Reed, J. E. Carpenter, J. A. Bohmann, C. M. Morales, C. R. Landis, F. Weinhold, **2013**.

[287] "ADF2010, SCM, Theoretical Chemistry, Vrije Universiteit, Amsterdam, The Netherlands, http://www.scm.com," can be found under http://www.scm.com/Doc/Doc2010/Background/References/page4.html, **n.d.**

[288] C. Fonseca Guerra, J. G. Snijders, G. te Velde, E. J. Baerends, *Theor. Chem. Acc.* **1998**, *99*, 391–403.

[289] G. te Velde, F. M. Bickelhaupt, E. J. Baerends, C. Fonseca Guerra, S. J. A. van Gisbergen, J. G. Snijders, T. Ziegler, *J. Comput. Chem.* **2001**, *22*, 931–967.

[290] E. van Lenthe, E.-J. Baerends, J. G. Snijders, *J. Chem. Phys.* **1993**, *99*, 4597.

[291] E. van Lenthe, E. J. Baerends, J. G. Snijders, *J. Chem. Phys.* **1994**, *101*, 9783.

[292] E. van Lenthe, A. Ehlers, E.-J. Baerends, *J. Chem. Phys.* **1999**, *110*, 8943.

[293] E. van Lenthe, J. G. Snijders, E. J. Baerends, *J. Chem. Phys.* **1996**, *105*, 6505.

[294] E. van Lenthe, R. van Leeuwen, E.-J. Baerends, J. G. Snijders, *Int. J. Quantum Chem.* **1996**, *57*, 281–293.

[295] W. A. Kinney, M. J. Coghlan, L. A. Paquette, *J. Am. Chem. Soc.* **1985**, *107*, 7352–7360.

[296] M. P. Wilkerson, C. J. Burns, R. T. Paine, B. L. Scott, *Inorg. Chem.* **1999**, *38*, 4156–4158.

[297] L. R. Avens, D. M. Barnhart, C. J. Burns, S. D. McKee, W. H. Smith, *Inorg. Chem.* **1994**, *33*, 4245–4254.

[298] D. M. Barnhart, C. J. Burns, N. N. Sauer, J. G. Watkin, *Inorg. Chem.* **n.d.**, *34*, 4079–4084.

[299] V. V. Burlakov, A. V. Polyakov, A. I. Yanovsky, Y. T. Struchkov, V. B. Shur, M. E. Vol'pin, U. Rosenthal, H. Görls, *J. Organomet. Chem.* **1994**, *476*, 197–206.

[300] H. Arp, M. Zirngast, C. Marschner, J. Baumgartner, K. Rasmussen, P. Zark, T. Müller, *Organometallics* **2012**, *31*, 4309–4319.

[301] U. Rosenthal, A. Ohff, M. Michalik, H. Görls, V. V. Burlakov, V. B. Shur, *Angew. Chem. Int. Ed.* **1993**, *32*, 1193–1195.

[302] P. L. Arnold, D. Patel, A. J. Blake, C. Wilson, J. B. Love, *J. Am. Chem. Soc.* **2006**, *128*, 9610–9611.

[303] R. A. Andersen, *Inorg. Chem.* **1979**, *18*, 1507–1509.

8 Publication related to this thesis

ChemComm

COMMUNICATION

View Article Online
View Journal | View Issue

Cite this: *Chem. Commun.*, 2015, **51**, 5876

Received 29th January 2015,
Accepted 23rd February 2015

DOI: 10.1039/c5cc00867k

www.rsc.org/chemcomm

Catalytic one-electron reduction of uranyl(VI) to Group 1 uranyl(V) complexes *via* Al(III) coordination†

Markus Zegke, Gary S. Nichol, Polly L. Arnold* and Jason B. Love*

Reactions between the uranyl(VI) Pacman complex $[(UO_2)(py)(H_2L)]$ of the Schiff-base polypyrrolic macrocycle L and Tebbe's reagent or DIBAL result in the first selective reductive functionalisation of the uranyl oxo by Al to form $[(py)(R_2AlOUO)(py)(H_2L)]$ (R = Me or ^{t}Bu). The clean displacement of the oxo-coordinated Al(III) by Group 1 cations has enabled the development of a one-pot, DIBAL-catalysed reduction of the U(VI) uranyl complexes to a series of new, mono-oxo alkali-metal-functionalised uranyl(V) complexes $[(py)_5(MOUO)(py)(H_2L)]$ (M = Li, Na, K).

The uranyl(VI) dication UO_2^{2+} is the most common form of uranium in the environment, and is reduced by minerals and microbes to the less stable uranyl(V) monocation UO_2^+, the chemistry of which has only recently been investigated in detail.[1–4] The [Rn] $5f^1$-electron configuration of uranyl(V) results in a variety of interesting properties such as cation–cation interactions (CCIs)[5] and single molecule magnetism (SMM),[6] and provides insight into often non-trivial 5f-electron behaviours.[7] Exploring the uranyl(V) oxidation state may help in understanding the fundamental uranium-based processes occurring in ground-water remediation and nuclear fuel corrosion.[8] Furthermore, due to the increased Lewis basicity of $U^VO_2^+$ compared to $U^{VI}O_2^{2+}$,[9] uranyl(V) complexes may also be employed to model the behaviour of highly radioactive neptunyl ions NpO_2^{2+} which are present in nuclear waste.[10] Studies by us,[11] and others,[12,13] on the reactions of uranyl(VI) complexes with silyl-containing reagents have led to new reductive oxo-functionalisation reactions being uncovered, forming stable silylated uranyl(V) complexes and a chemically inert and air-stable butterfly-shaped bimetallic uranium(V) dioxo complex.[14] As with reductive metalation reactions of the uranyl(VI) dication, the stability of uranyl(V) complexes against disproportionation is dramatically enhanced through the functionalisation of the more Lewis-basic oxo group of this f^1 cation.[15,16] Here, we report synthetic routes to the first oxo-aluminated uranyl(V) complexes, transmetalation reactions to the first mono-alkali metal uranyl(V) adducts supported by the Pacman ligand, and a new procedure to alkali-metal functionalised uranyl(V) complexes that is catalytic in the Al(III) reagent. Significantly, these complexes are exclusively *exo*-oxo metalated, and show high stability against disproportionation to uranyl(VI) and uranium(IV) compounds.[17,18]

We have studied a range of Al^{III} compounds that might behave as suitable electrophiles to the accessible oxo group of the uranyl ion in the uranyl(VI) Pacman complex $[(UO_2)(py)(H_2L)]$ **A**.[19] In particular, two compounds $[Cp_2Ti(\mu\text{-}Cl)(\mu\text{-}CH_2)AlMe_2]$ (Tebbe's reagent) and $[(^iBu)_2AlH]_2$ (DIBAL) have proven to be excellent sources of the oxophilic and Lewis acidic Al^{III} cation (Scheme 1).

The combination of benzene solutions of equimolar quantities of **A** and $[Cp_2Ti(\mu\text{-}Cl)(\mu\text{-}CH_2)AlMe_2]$, followed by the addition of 0.1 mL of pyridine at room temperature results in a clear orange solution from which yellow crystals form upon standing, characterised as $[(py)(Me_2AlOUO)(py)(H_2L)]$ **1**, and isolated in 67% yield. The X-ray crystal structure of **1** was determined and shows the expected wedge-shaped Pacman geometry of the parent complex with *exo*-oxo aluminium coordination (Fig. 1). The uranyl oxo groups adopt a *trans* geometry, with an O1–U1–O2 angle of 174.3(1)° and U1–O1 and U1–O2 bond lengths elongated to 1.857(3) Å and 1.962(3) Å respectively, compared to the O═U═O bonds of

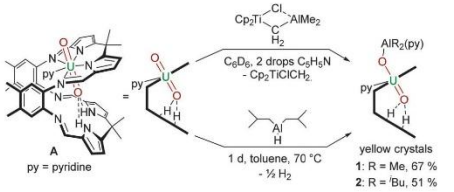

Scheme 1 Reductive alumination of $[(UO_2)(py)(H_2L)]$, **A** by Tebbe's reagent or DIBAL.

EaStCHEM School of Chemistry, The University of Edinburgh, David Brewster Road, Edinburgh EH9 3FJ, UK. E-mail: Polly.Arnold@ed.ac.uk, Jason.Love@ed.ac.uk; Fax: +44 (0) 130 650 6453; Tel: +44 (0) 130 650 5429

† Electronic supplementary information (ESI) available: Full synthetic and characterising data. CCDC 1046279–1046284. For ESI and crystallographic data in CIF or other electronic format see DOI: 10.1039/c5cc00867k

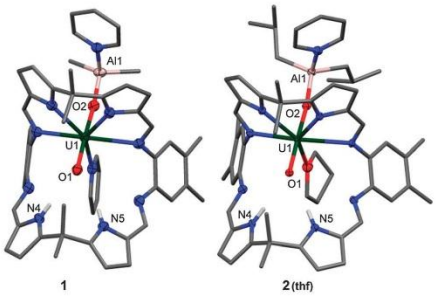

Fig. 1 Solid-state structures of **1** and **2(thf)**, front view. For clarity, all hydrogen atoms except the pyrrole NHs and all solvent molecules are omitted (displacement ellipsoids are drawn at 50% probability). Selected bond lengths (Å) and angles (°) for 1: U1–O1 1.857(3), U1–O2 1.962(3), O1–N4 2.964(5), O1–N5 3.068(5). O1–U1–O2 174.3(1); 2: U1–O1 1.855(2), U1–O2 1.962(2), O1–N4 3.033(4), O1–N5 3.027(4). O1–U1–O2 175.1(1).

1.793(6) Å and 1.773(6) Å for **A**.[19] This significant lengthening of these bonds is indicative of a decrease in the uranyl bond order and is similar to related experimental and calculated systems in which an increase of 0.151–0.242 Å in U–O bond lengths upon reduction of O=U^{VI}=O to O=U^{V}–O–M is seen.[20] Furthermore, the hydrogen-bonding interactions between the *endo*-oxo O1 and the two pyrrole protons in the vacant macrocyclic pocket, shown by O1···N1 2.964(5) Å and O1···N2 3.068(5) Å are slightly shorter than those in **A** (3.111(7) Å and 3.146(7) Å) and supports the enhanced oxo basicity of the f^1 cation. To our knowledge, this is the first reaction in which Tebbe's reagent is used as a source of aluminium.

A more atom-economic route to these heterobimetallic complexes is through the reaction between **A** and DIBAL in toluene at 70 °C for 24 h which results in the formation of yellow [(py)(^{i}Bu$_2$AlOUO)(py)(H$_2$L)] **2** in 51% yield. The solid state structure of **2** (Fig. 1) is very similar to **1**, once more exemplifying the formal U^{V} oxidation state through an elongation of the U1–O1 and U1–O2 bond distances. Mechanistically, it is likely that **1** and **2** are formed through Al–ligand bond homolysis (Al–H or Al–C) which provides the reducing electron. This process is similar to that suggested by us previously to be responsible for U^{VI} reduction in the formation of lithium-functionalised [(LiOUO)(py)(Li$_3$L)] and lanthanide-functionalised [UO$_2$(py)(Ln(py)L)]$_2$ that result from Li–C or Ln–N bond homolysis.[21]

The ^{1}H-NMR spectrum of **2** (see ESI†) shows contact-shifted and broadened resonances between −6 and +70 ppm due to the paramagnetism of the f^1 centre. Even so, the ^{i}Bu methyl hydrogens can be identified at 6.10 ppm and 6.67 ppm with $^{3}J_{H-H}$ coupling of 8 Hz, and the methine proton is a broad resonance at 11.31 ppm that couples with the methylene protons at 16.35 ppm and 16.81 ppm. The most contact-shifted resonance at +69 ppm is assigned to the pyrrole N–H protons. *In situ* measurements show the formation of gaseous H_2 at 4.49 ppm. Both $U^{V}O_2$–Al^{III} compounds **1** and **2** are stable in THF and pyridine solvents. A study of the redox chemistry of **2** by cyclic voltammetry in THF with 0.1 M

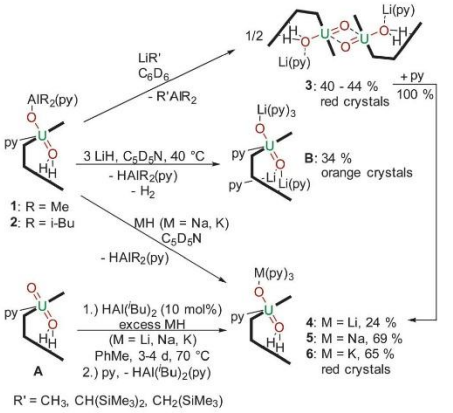

Scheme 2 Transmetalation reactions of **1** and **2** with R'Li, LiH, NaH and KH, and the HAl(^{i}-Bu)$_2$-catalysed reduction of [U^{VI}O$_2$(H$_2$L)] by MH.

[NBu$_4$][PF$_6$] as a supporting electrolyte at 500 mV s^{-1} reveals a quasi-reversible reduction at $E_{1/2}$ = −1.42 V (*vs.* Fc/Fc^{+}) which is tentatively ascribed to a uranyl(V)/uranium(IV) redox couple (see ESI†). A pre-reduction wave is also seen at E_{pc} = −1.45 V, implying that the redox chemistry of **1** and **2** is not straightforward, and as yet, in line with related U(V) complexes that we have studied, the chemical reduction of complex **1** or **2** has not yet been successful. However, we have found that the AlR$_2$ group is readily substituted by Group 1 metal cations by reaction with an alkyl or hydride reagent such as MeLi, NaH or KH (Scheme 2); these experiments had been anticipated to deprotonate the two, likely acidic, pyrrole NHs in **1** and **2**.

Reactions between benzene solutions of **1** with either one or two equivalents of the strong base MeLi affords solely [{(OUO)-Li(py)(H$_2$L)}$_2$] **3** in moderate isolated yield (40%), which remains U^{V} and doubly NH protonated. This contrasts with the reactions of the uranyl(VI) Pacman complex [UO$_2$(py)(H$_2$L)] **A** with single equivalents of LiR (R = H, NH$_2$, N^{i}Pr$_2$, N(SiMe$_3$)$_2$, CPh$_3$, C$_5$H$_5$) that simply result in pyrrole deprotonation to afford the uranyl(VI) complex [(UO$_2$)(py)(LiHL)],[22] and suggests that the hydrogen-bonding interaction between the f^1 uranyl oxo group and the pyrrole protons is significant enough to attenuate deprotonation. The X-ray crystal structure of **3** (Fig. 2) shows that the lithium cation is coordinated by the imine groups of the macrocycle and that the uranium centre has migrated from its usual N_4 donor pocket to an alternative pyrrole–imine–imine–pyrrole set. This results in the macrocycle folding at the *meso*-carbons and not the aryl groups, so resulting in a 'bowl-shaped' geometry.[23–25]

As above, the U1–O1 and U1–O2 bond lengths of 1.891(2) Å and 1.908(2) Å, respectively are elongated compared to those in **A**, supporting a U^{V} oxidation state, and the oxo groups are arranged in a *trans* disposition. The Li cation is thus sited within the cavity of the macrocycle, bound to the uranyl *endo*-oxo atom, the two imine groups, and a molecule of pyridine. As in the other complexes the

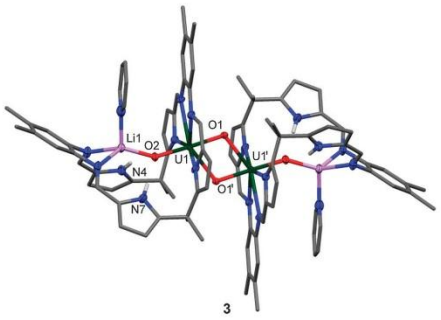

3

Fig. 2 Solid-state structure of **3**. For clarity, all hydrogen atoms except pyrrole NH and all solvent molecules are omitted (displacement ellipsoids are drawn at 50% probability). Selected bond lengths (Å) and angle (°): U1–O1 1.908(2), U1–O2 1.891(2), U1–O1′ 2.372(3), N4–O2 3.269(4), N7–O2 3.198(5). O1–U1–O2 177.7(1). U1···U1′: 3.5199(9).

uranyl is five-coordinate in the equatorial plane but the site which was occupied by the donor solvent is now filled by the *exo*-oxo group of its counterpart in the dimer, resulting in a diamond-shaped U_2O_4–cation–cation interaction.[1,2,16] The uranium–uranium separation in this dimer is short at 3.5199(9) Å, but similar to other complexes previously reported by us, for example 3.4487(4) Å in the uranyl(v) yttrium dimer $[\{UO_2Y(py)_2(L)\}_2]$.[26] Treatment of **2** with one equivalent of $LiCH_2SiMe_3$ or $LiCH(SiMe_3)_2$ in benzene also yielded **3**, and was verified by ^{1}H-NMR spectroscopy and crystal structure analysis (unit cell check). In contrast, reactions between **1** or **2** and an excess of LiH in the donor solvent pyridine at 40 °C results in the formation of the known, triply lithiated, uranyl(v) complex $[(py)_3(LiOUO)(py)(\{Li(py)\}_2L)]$ **B**.[21]

The difference in ability of the two types of Li reagents (LiR *vs.* LiH) to effect N–H deprotonation is likely due to the nature of the reaction solvent. The use of pyridine stabilises the exogenous coordination of the Li cation to the uranyl oxo group, whereas in benzene, the reorganization of the uranyl coordination pocket allows for maximum interaction of the Li cation with the macrocycle. In support of this, the addition of pyridine to a benzene solution of **3** shows a rearrangement from the bowl-shaped structure to **4**, possessing the classical Pacman structure (Fig. 3), suggesting that the bowl-shaped structure is only favoured in a non-coordinating solvent. Exogenous coordination of a Li cation was also seen in the cleavage products of the heterobimetallic lanthanide-uranyl(v) dimers $[\{(UO_2)Ln(py)_2(L)\}_2]$ (Ln = Sc, Y, Ce, Sm, Eu, Gd, Dy, Er, Yb, Lu) to yield $[(py)_3(LiOUO)Ln(py)_2(L)]$.[27]

Treatment of **1** or **2** with NaH or KH in pyridine at room temperature results exclusively in the exchange of the aluminium cation for the respective alkali metal to yield $[(py)_3(NaOUO)(py)(H_2L)]$ **5** and $[(py)_3(KOUO)(py)(H_2L)]$ **6** (Na: 69%, K: 65%); in both of these cases, the lower pocket remains protonated (Fig. 3). This is confirmed by the ^{1}H-NMR resonances of **4**, **5** and **6** in deuterated pyridine of which the pyrrole N–Hs show the most significant shifts to high frequencies at 85.48 ppm (**4**), 91.11 ppm (**5**) and 93.06 (**6**). Additionally the ^{7}Li-NMR of **4** shows

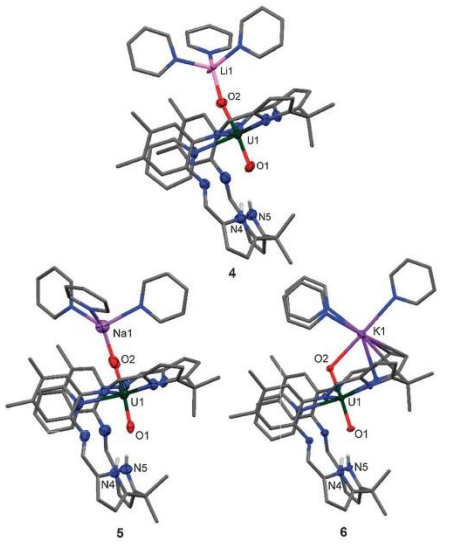

Fig. 3 Solid-state structures of **4**, **5** and **6** (side view). For clarity, all hydrogen atoms except pyrrole NHs and all solvent molecules are omitted (displacement ellipsoids are drawn at 50% probability). Selected bond lengths (Å) and angles (°) for 4: U1–O1 1.853(6), U1–O2 1.884(7), O1–N4 3.09(1), O1–N5 3.10(1), O1–U1–O2 173.8(3); 5: U1–O1 1.844(5), U1–O2 1.856(7), O1–N4 3.010(9), O1–N5 2.988(8). O1–U1–O2 174.2(3); 6: U1–O1 1.871(2), U1–O2 1.837(2), O1–N4 2.898(4), O1–N5 2.932(4). O1–U1–O2 176.1(1).

only one resonance at 88.48 ppm, supporting Li coordination to the paramagnet.

The solid state structures of **4**, **5** and **6** are very similar, and in contrast to **3** show the classic uranyl Pacman geometry. The main difference between the structures is that the U1–O2–M1 angle is nearly linear for the Li (**4**) (173.8(3)°) and Na (**5**) (174.7(6)°) complexes whereas the U1–O2–K1 angle is considerably bent (116.0(1)°). This is caused by an η^5-interaction between K and a U-bound pyrrolide ring due to the softness and size of K^+ (152 pm) compared to Na^+ (112 pm) and Li^+ (73 pm).[28]

It is clear from the above transmetalation reactions that the aluminium by-product is the alane or aluminium hydride. As such it was envisaged that formation of the reduced, alkali-metalated uranyl complexes **4–6** from **A** should be achievable using MH (M = Li, Na, K) and a catalytic amount of $AlH(^iBu)_2$, as this latter reagent should be regenerated during the transmetalation step. As such, reactions using 10 mol% of DIBAL and an excess of MH in toluene at 70 °C for 72 to 96 hours (Scheme 2) were carried out and are found to generate **4**, **5** or **6** in essentially quantitative yields (Table 1, showing reactions using KH only). Control reactions with no aluminium reagent formed 50% of **6** after 96 hours, and increasing the reaction time up to ten days afforded a **4**:1 mixture of **6** and **A**; as such, reactions that incorporate DIBAL are significantly accelerated.

Table 1 Example conditions for the HAl(i-Bu)$_2$-catalysed reduction of UO_2^{2+} with KH

Entry	mol% HAl(i-Bu)$_2$	Time/h	Ratio 6/A
1	5	24	20/80
2	5	60	20/80
3	10	96	100/0
4	0	96	50/50
5	0	240	80/20

Reaction conditions: 70 °C, toluene, 5 equivalents KH.

Treatment of **A** with 5 mol% of DIBAL only gave 20% of **6** with 80% of the starting material still present, even after a prolonged reaction time.

Additionally the redox chemistry of **6** was studied by cyclic voltammetry in THF with 0.2 M $[NBu_4][PF_6]$ as a supporting electrolyte at scan rates between 100 and 500 mV s^{-1} and reveals a quasi-reversible reduction at $E_{1/2} = -1.31$ V (*vs.* Fc/Fc$^+$) which is ascribed to a uranyl(v)/uranyl(vi) redox couple (see ESI†).

We report the first reductive alumination of the uranyl dication which results in a significant attenuation of the acidity of the pyrrole NHs through hydrogen bonding to the f^1 centre, such that reactions with Group 1 bases result in transmetalation instead of the deprotonation chemistry previously seen. This change in reactivity has allowed us to develop a new synthetic route to simple, Group 1 cation adducts of uranyl(v) Pacman complexes that is catalytic in aluminium reagent. This new Al-mediated route should provide opportunities for new catalysed uranyl functionalisation reactions with other d- and f-group metal cations, and could even offer a general low-cost, one-pot route to the selective Group-1 cation metalation of d-block metal oxo complexes.

The authors thank the EPSRC-UK, the University of Edinburgh, the EU Actinet-I3-AC3-JRP-02 and Talisman-JRPL-C02-07 programs, COST CM1006, and the Institute of Advanced Study, TU Munich for support. MZ thanks Dr Stephen M. Mansell for valuable advice.

Notes and references

1 P. L. Arnold, G. M. Jones, Q.-J. Pan, G. Schreckenbach and J. B. Love, *Dalton Trans.*, 2012, **41**, 6595–6597.
2 P. L. Arnold, J. B. Love and D. Patel, *Coord. Chem. Rev.*, 2009, **253**, 1973–1978.
3 D. D. Schnaars, G. Wu and T. W. Hayton, *Inorg. Chem.*, 2011, **50**, 9642–9649.
4 G. Nocton, P. Horeglad, V. Vetere, J. Pécaut, L. Dubois, P. Maldivi, N. M. Edelstein and M. Mazzanti, *J. Am. Chem. Soc.*, 2010, **132**, 495–508.
5 V. Mougel, J. Pécaut and M. Mazzanti, *Chem. Commun.*, 2012, **48**, 868.
6 V. Mougel, L. Chatelain, J. Pécaut, R. Caciuffo, E. Colineau, J.-C. Griveau and M. Mazzanti, *Nat. Chem.*, 2012, **4**, 1011–1017.
7 T. W. Hayton and G. Wu, *Inorg. Chem.*, 2009, **48**, 3065–3072.
8 P. C. Burns, R. C. Ewing and A. Navrotsky, *Science*, 2012, **335**, 1184–1188.
9 J.-C. Berthet, G. Siffredi, P. Thuéry and M. Ephritikhine, *Chem. Commun.*, 2006, 3184–3186.
10 R. Copping, V. Mougel, C. Den Auwer, C. Berthon, P. Moisy and M. Mazzanti, *Dalton Trans.*, 2012, **41**, 10900–10902.
11 P. L. Arnold, D. Patel, C. Wilson and J. B. Love, *Nature*, 2008, **451**, 315–317.
12 J. L. Brown, G. Wu and T. W. Hayton, *J. Am. Chem. Soc.*, 2010, **132**, 7248–7249.
13 J.-C. Berthet, G. Siffredi, P. Thuéry and M. Ephritikhine, *Eur. J. Inorg. Chem.*, 2007, 4017–4020.
14 P. L. Arnold, G. M. Jones, S. O. Odoh, G. Schreckenbach, N. Magnani and J. B. Love, *Nat. Chem.*, 2012, **4**, 221–227.
15 G. M. Jones, P. L. Arnold and J. B. Love, *Angew. Chem., Int. Ed.*, 2012, **51**, 12584–12587.
16 P. L. Arnold, A.-F. Pécharman and J. B. Love, *Angew. Chem., Int. Ed.*, 2011, **50**, 9456–9458.
17 A. Ekstrom, *Inorg. Chem.*, 1974, **13**(9), 2237–2241.
18 H. Steele and R. J. Taylor, *Inorg. Chem.*, 2007, **46**, 6311–6318.
19 P. L. Arnold, A. J. Blake, C. Wilson and J. B. Love, *Inorg. Chem.*, 2004, **43**, 8206–8208.
20 S. O. Odoh and G. Schreckenbach, *Inorg. Chem.*, 2013, **52**, 245–257.
21 P. L. Arnold, A.-F. Pécharman, E. Hollis, A. Yahia, L. Maron, S. Parsons and J. B. Love, *Nat. Chem.*, 2010, **2**, 1056–1061.
22 T. S. Franczyk, K. R. Czerwinski and K. N. Raymond, *J. Am. Chem. Soc.*, 1992, **114**, 8138–8146.
23 J. W. Leeland, F. J. White and J. B. Love, *J. Am. Chem. Soc.*, 2011, **133**, 7320–7323.
24 J. B. Love, *Chem. Commun.*, 2009, 3154.
25 G. Givaja, M. Volpe, J. W. Leeland, M. A. Edwards, T. K. Young, S. B. Darby, S. D. Reid, A. J. Blake, C. Wilson, J. Wolowska, E. J. L. McInnes, M. Schröder and J. B. Love, *Chem. – Eur. J.*, 2007, **13**, 3707–3723.
26 P. L. Arnold, E. Hollis, F. J. White, N. Magnani, R. Caciuffo and J. B. Love, *Angew. Chem., Int. Ed.*, 2011, **50**, 887–890.
27 P. L. Arnold, E. Hollis, G. S. Nichol, J. B. Love, J.-C. Griveau, R. Caciuffo, N. Magnani, L. Maron, L. Castro, A. Yahia, S. O. Odoh and G. Schreckenbach, *J. Am. Chem. Soc.*, 2013, **135**, 3841–3854.
28 R. D. Shannon, *Acta Crystallogr., Sect. A: Cryst. Phys., Diffr., Theor. Gen. Crystallogr.*, 1976, **32**, 751–767.

9 Table of complexes

Nr./ Formula	Molecular structure	Schematic drawing
A $[(UO_2)(py)(H_2L)]$	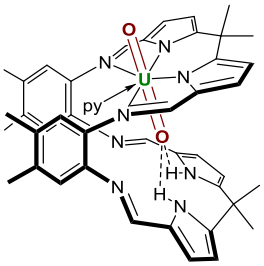	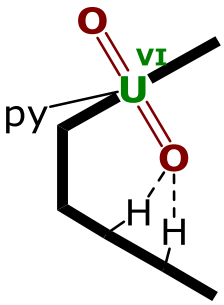
A^{Et} $[(UO_2)(thf)(H_2L)]$	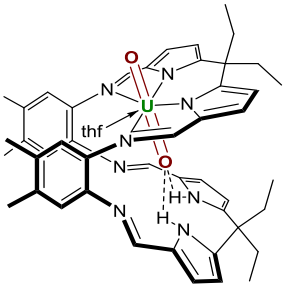	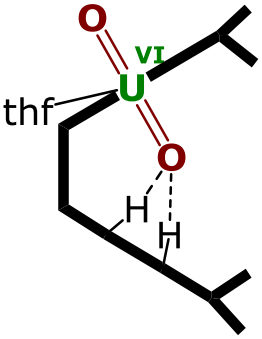
A^{3Li} $[(py)_3(LiOUO)(py)$ $(\{Li(py)\}_2L)]$	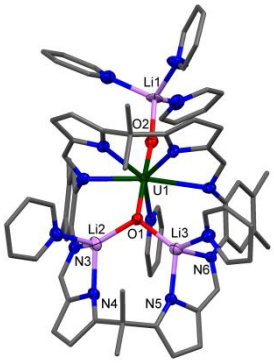	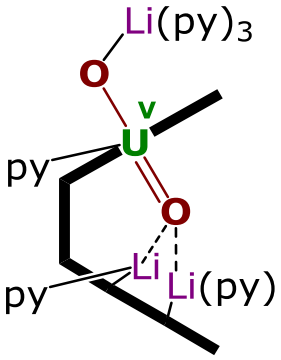
B $U(N(SiMe_3)_2)_4$	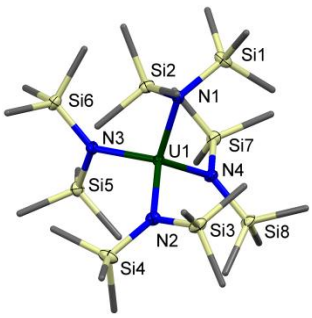	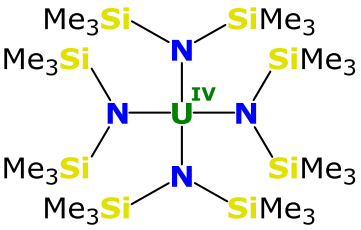

1 [(py)(Me_2AlOUO)(py)(H_2L)]	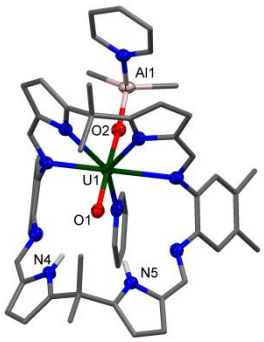	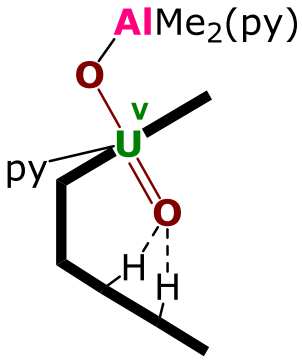
2 [(py)(^{i}Bu$_2$AlOUO)(py)(H_2L)]	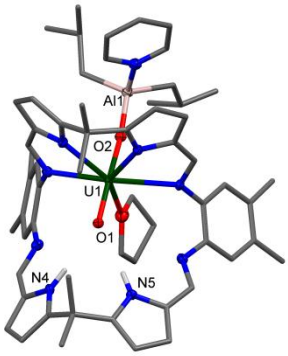	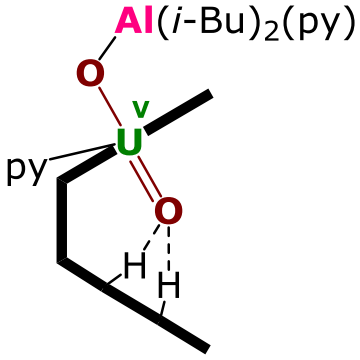
3 [{(OUO)Li(py)(H$_2$L)}$_2$]	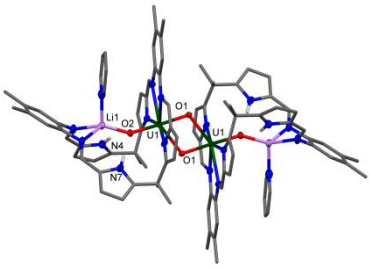	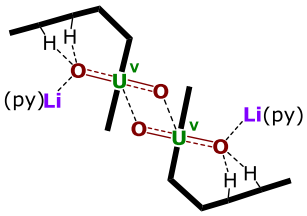
4 [(py)$_3$(LiOUO)(py)(H$_2$L)]	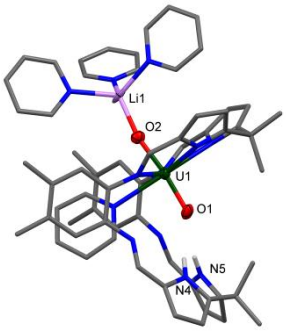	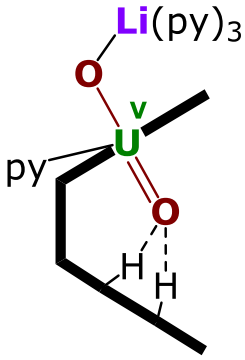

5 [(py)$_3$(NaOUO)(py)(H$_2$L)]	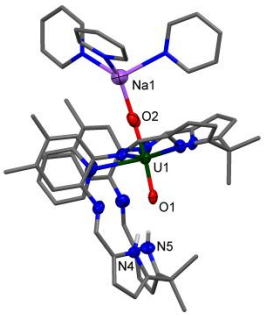	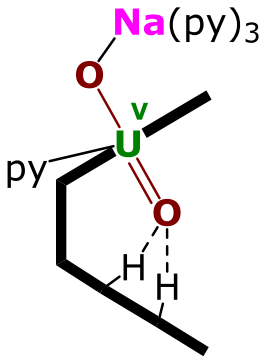
6 [(py)$_3$(KOUO)(py)(H$_2$L)]	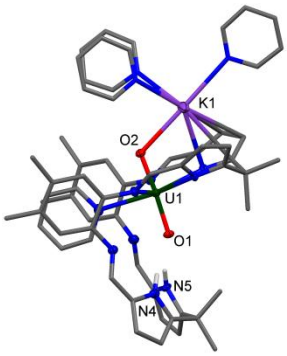	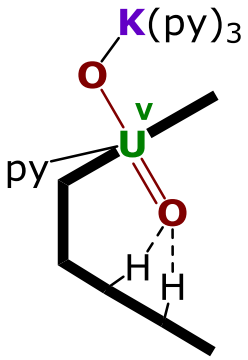
7 [(py)$_3$(RbOUO)(py)(H$_2$L)]	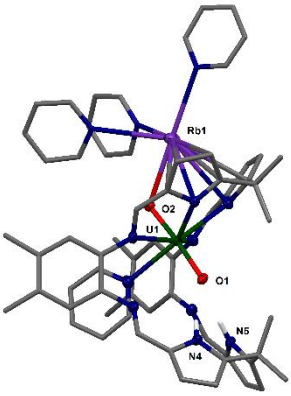	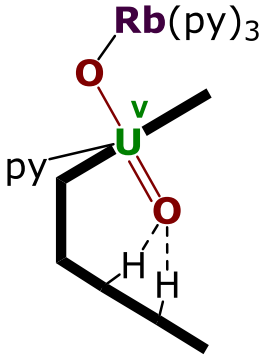

8

[(CsOUO)(py)(H$_2$L)]$_6$

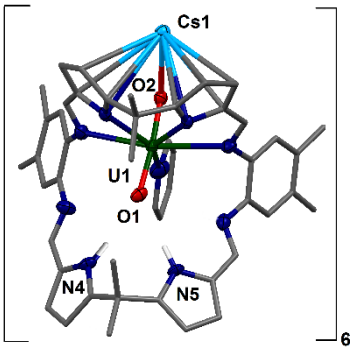

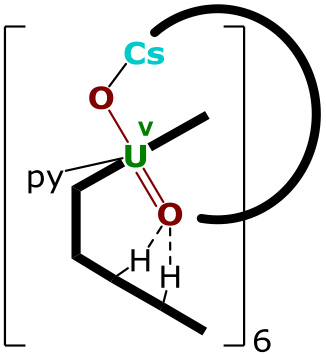

9

[(py)(Cp$_2$TiOUO)(py)(H$_2$L)]

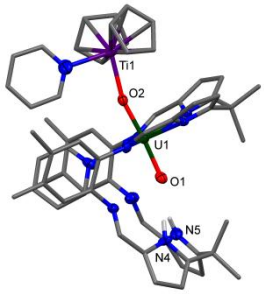

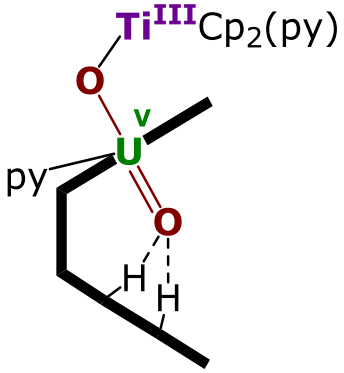

10

[((Cl)Cp$_2$TiOUO)(py)(H$_2$L)]

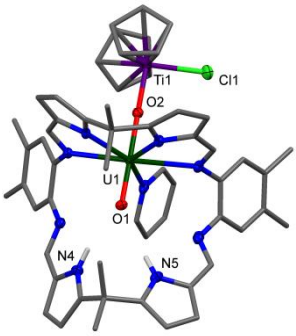

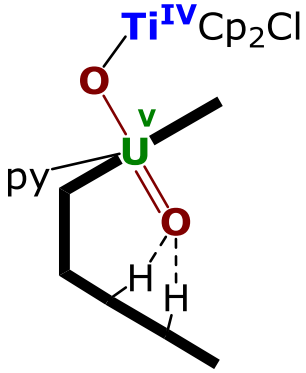

11

[((Cl)Cp$_2$ZrOUO)(py)(H$_2$L)]

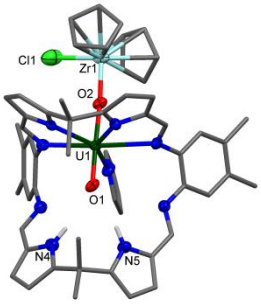

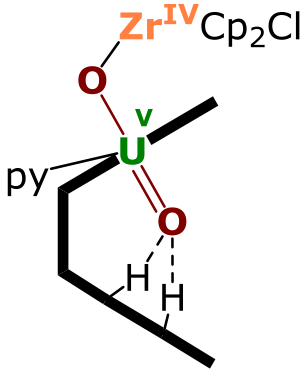

12

[(py)$_2$(ClMgOUO)(py)(H$_2$L)]

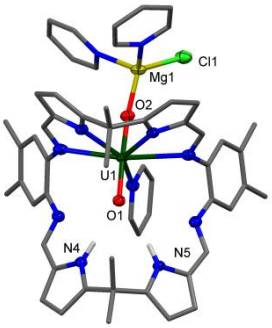

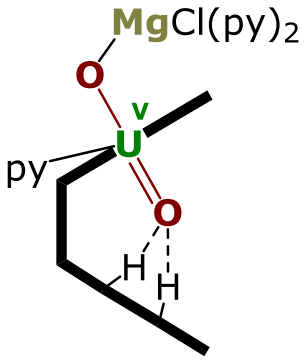

13

[(py)$_2$(thf)$_2$(ICaOUO)(py)(H$_2$L)]

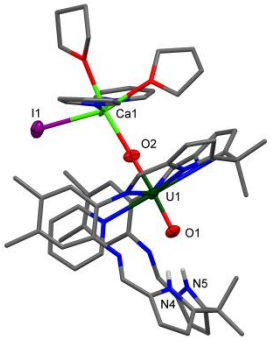

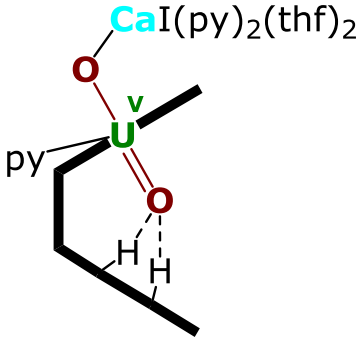

14

[(py)$_2$(ClZnOUO)(py)(H$_2$L)]

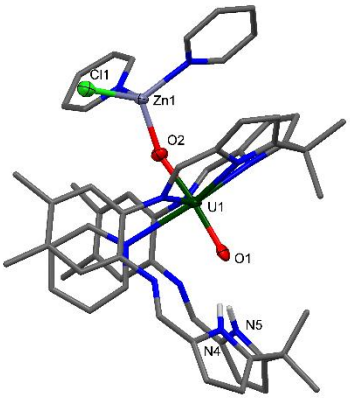

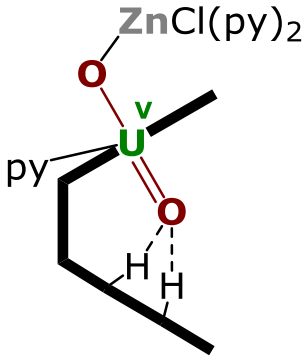

15

[(py)$_2$(IZnOUO)(py)(H$_2$L)]

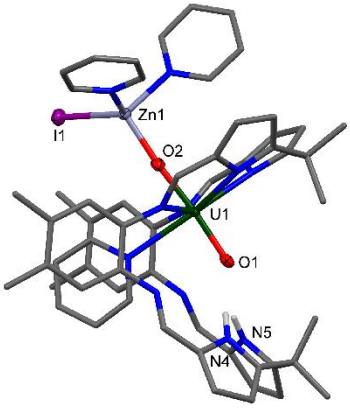

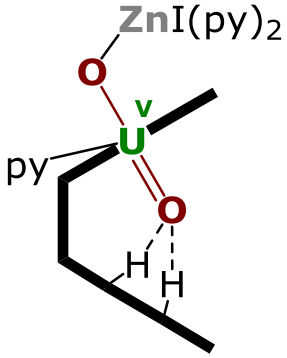

16

[O=U(py)$_5$-O-Sm(I$_4$)-O-U(py)$_5$=O]$^+$ I$^-$

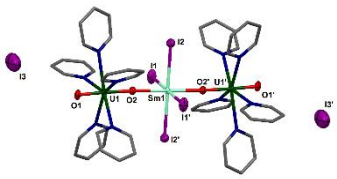

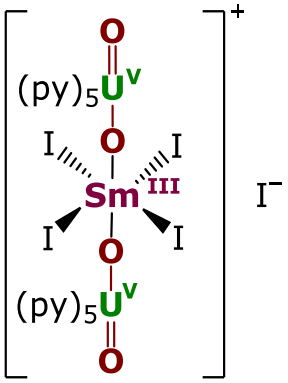

17

[Cp$_3$UOUO(thf)(H$_2$L^{Et})]

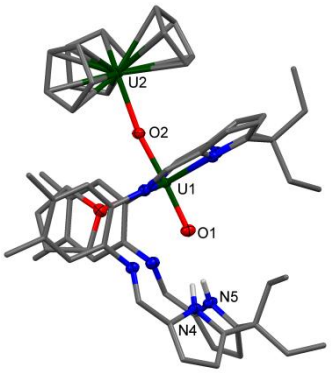

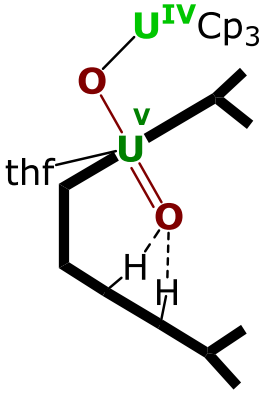

18

[(U^{V}O$_2$)(py)(ZnL)]

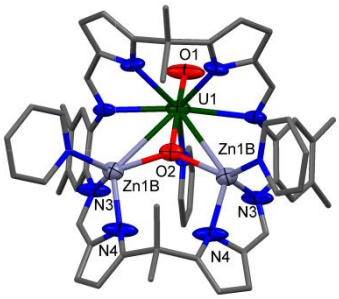

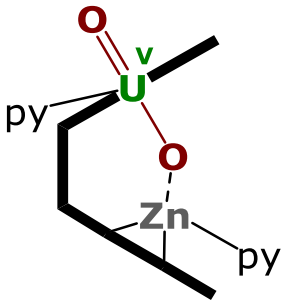

19

[Cp$_3$NpOUO(thf)(H$_2$L^{Et})]

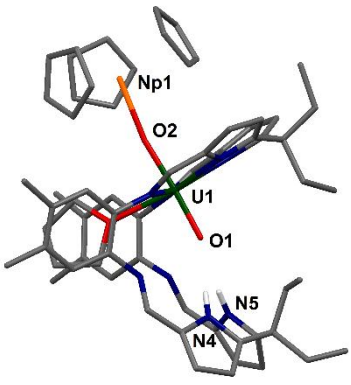

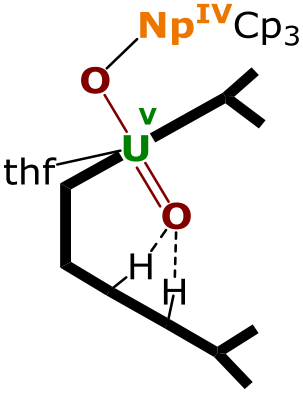

20

[$Cp_3NpONp(Cp_2)ONpCp_3$]

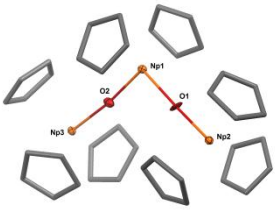

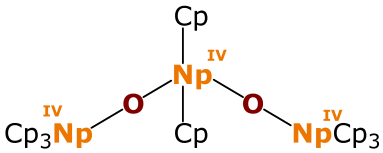

21

[$UO_2(Cl)(L^{ene})$]

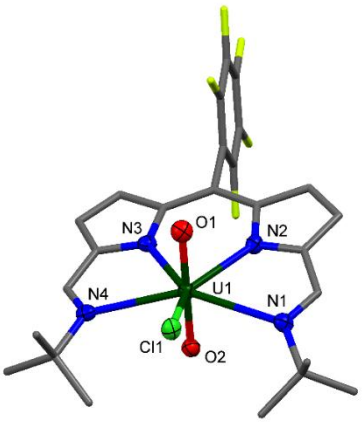

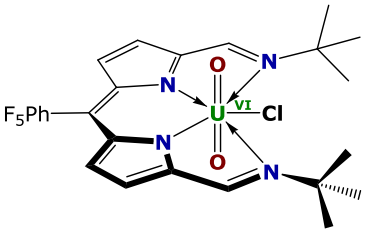

22

[$Cp_2TiCl)OUO(Cp_2TiCl)(Cl)(L^{ene})$]

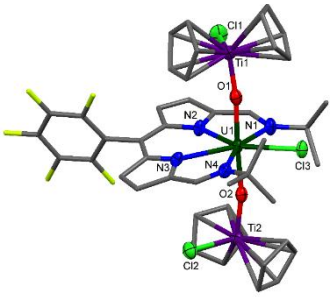

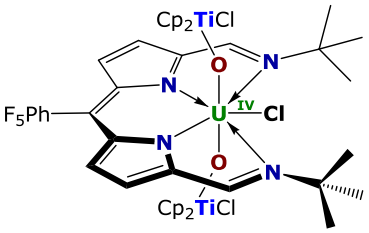

23

[$Me_3SiOUOSiMe_3(py)(L^{aneAr})$]